Quantum quenches and the holographic duality.

by

Anton van Niekerk

A thesis
presented to the University of Waterloo
in fulfillment of the
thesis requirement for the degree of
Doctor of Philosophy
in
Physics

Waterloo, Ontario, Canada, 2014

Author's Declaration

I hereby declare that I am the sole author of this thesis. This is a true copy of the thesis, including any required final revisions, as accepted by my examiners.

I understand that my thesis may be made electronically available to the public.

Abstract

We study quantum quenches in a strongly coupled conformal field theory, using the gauge/gravity duality. In the first part of the thesis, we consider a perturbative thermal quench of a field theory in four spacetime dimensions by a relevant operator of arbitrary dimension $2 \leq \Delta \leq 4$. This is done by numerically evolving the dual scalar field in five-dimensional asymptotically anti-de Sitter spacetime containing a large planar black hole, using a finite difference method. We holographically calculate the expectation values of the operator and of the field theory's stress-energy, as well its thermodynamic quantities. We find universal scaling behaviours of these quantities in the limits of both fast and slow quenches. Further, in the limit of fast quenches we find universal behaviour in the excitation and equilibration time of the operator expectation value. The excitation time scales to zero with the quenching time, while its equilibration time becomes constant and independent of the quenching rate.

In the second part of the thesis, we analytically derive the scaling observed during fast quenches in the first part. We work in the nonperturbative regime with a strongly coupled conformal field theory living in d spacetime dimensions, globally quenched by an operator $\mathcal{O}_\Delta$ of dimension $\frac{d}{2} \leq \Delta < d$. By taking the limit of very fast quenches, the dual gravity theory becomes linearized, as one needs only consider the near-boundary behaviour of the dual scalar field. For a given source for the scalar field, we analytically solve for the expectation value of the quenching operator, as well as the change in the energy density. We find that these quantities exhibit the scaling observed in the first part of the thesis, generalized to higher dimensions.

In the final part of the thesis, we again study quenches of a strongly coupled conformal field theory living in four spacetime dimensions, this time perturbatively quenched by a fermionic mass term. We focus on fast, global quenches of the thermal field theory by its holographic dual of a collapsing scalar field in five dimensional anti-de Sitter spacetime containing a black hole. Using an improved numerical method of Chebyshev pseudo-spectral methods, we evolve the profile of both the metric and scalar field. We calculate the time-evolution of the apparent and event horizons of the planar black hole, as well as the two-point function of a high-dimension operator, and the entanglement entropy of a strip on the boundary. These quantities probe thermalization of the field theory at different length scales. We find that the two-point function and entanglement entropy have longer thermalization times for wider separations, and that their thermalization times exhibit linear scalings with separation for wide surfaces. We also find that the thermalization times of the two-point function and entanglement entropy can exceed that of the operator expectation value.

iii

Acknowledgements

Dedication

To my parents, who have always encouraged me to follow my passion.

Table of Contents

List of Tables

List of Figures

xi

Chapter 1

Introduction

The holographic duality, or the AdS/CFT correspondence as it is more widely known, has become a powerful theoretical tool for studying strongly coupled quantum systems. It has given researchers in string theory insight into many phenomena that have been difficult to study with conventional quantum field theory techniques. The original formulation, as AdS_5 being dual (equivalent) to a supersymmetric conformal field theory (CFT) in four dimensions, is widely believed to extend to AdS in $d + 1$ dimensions and CFT's in d dimensions. Furthermore, it is also believed to be robust against large deformations of the theories on either side of the duality, such that many different physical situations in the field theory can be achieved, without supersymmetry or conformality. Examples of the types of systems in the field theory that may be modelled in this way include superconductors, particle collisions, hydrodynamics, and the main topic of this thesis, quantum quenches.

In the first part of this chapter, we will give a brief overview of the holographic duality, which will be used throughout this thesis, as well as some justification for some of its properties which will be assumed in later chapters. In the second part of this chapter, we will give a summary of studies of far-from-equilibrium systems in various fields, and justify the use of the duality for this purpose.

1.1 Constructing the holographic duality

1.1.1 Historical introduction

The holographic principle was first suggested by 't Hooft in 1993, arguing from the Bekenstein-Hawking black hole entropy formula [1]

$$S = \frac{A_{bh}}{4\,G_N},\tag{1.1}$$

that the information of a quantum field theory (QFT) in some volume could be stored on a surface in one fewer dimension [2]. This proposal was extended and linked to string theory by Susskind [3].
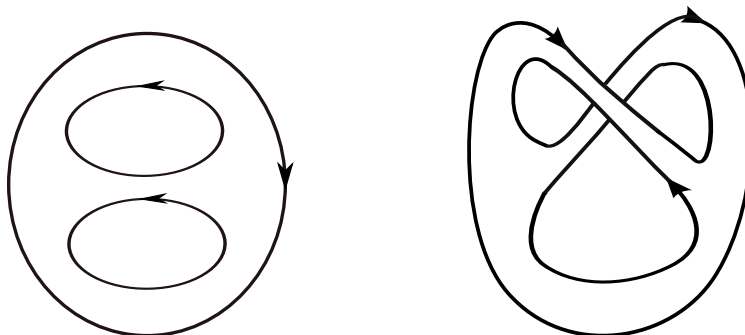
Figure 1.1: Planar (left) and nonplanar (right) vacuum bubbles of gluons in the large N limit of $SU(N)$. The figure on the left can be embedded on a plane or sphere, while the one on the right can be embedded only on a torus. The diagram on the right is therefore suppressed by a factor of N^{-2}, and can therefore be neglected in the large N limit.

Some decades earlier, 't Hooft had proposed the unrelated idea of the large N expansion to study non-Abelian gauge theories [4]. The basic idea being that calculations in an $SU(N)$ gauge theory could be made simpler by making N large, which has the effect of making certain *nonplanar* diagrams subleading and negligible in this limit. In each diagram in figure 1.1, each double line represent the path of a gluon. There are two lines, because a gluon carries two colours simultaneously (one colour and one *anti-colour*) out of the N colour charges of the gauge theory. This occurs because gluons exist in the adjoint representation of the gauge theory, meaning that it transforms as the direct product of

two vectors in the fundamental and anti-fundamental representations of the gauge group. Symbolically this transformation can be written as (summation being implicit)

$$\left(A_\mu^a T^a\right){}^i{}_j \rightarrow A_\mu^a G^i{}_k \left(T^a\right){}^k{}_\ell \left(G^\dagger\right){}_j{}^\ell, \tag{1.2}$$

where A_μ^a is the gauge field, T^a is an $N \times N$ generator of the gauge group, G is an $N \times N$ $SU(N)$ matrix, and $G^\dagger$ is its Hermitian conjugate. Upper matrix-indices are fundamental indices, while lower indices are anti-fundamental, both running from 1 to N. The index μ on the gauge field is a spacetime index, while the index a is a gauge index, running from 1 to $N^2 - 1$, *i.e.*, the dimension of $SU(N)$. The fundamental indices then correspond to colour, while the anti-fundamental indices correspond to anti-colour-charge. This can be seen from the interaction with quarks, namely

$$\bar{q}_i \left(A_\mu^a T^a\right){}^i{}_j q^j, \tag{1.3}$$

where fundamental and anti-fundamental indices are contracted, to make a colour-neutral object. The colour carried by the gauge field therefore cancels the anti-colour carried by the anti-quark, while its anti-colour cancels the colour carried by the quark. There are therefore two free group indices in the gauge field, meaning that the quantized gauge field (*i.e.*, the gluon) has two indices that need to be summed over in an interaction. The closed single lines in figure 1.1 then represent the trace being taken over the colours of the gauge theory, and thus contributes a factor of N to the diagram [5]. At the same time, each vertex in the diagram contributes a factor of $1/g_{YM}^2$, the coupling constant of the gauge particle, while each propagator (double line) contributes a factor of g_{YM}^2. This can be seen from the structure of the Lagrangian of the Yang-Mills theory: ignoring indices, the Lagrangian density is of the form [5]

$$\begin{aligned} \mathcal{L} \;\sim\; & (\partial A)^2 + g_{YM} A^3 + g_{YM}^2 A^4 \\ \sim\; & \frac{1}{g_{YM}^2} \left(\left(\partial \tilde{A}\right)^2 + \tilde{A}^3 + \tilde{A}^4\right), \end{aligned} \tag{1.4}$$

where in the second line we redefined the gauge field by absorbing a factor of g_{YM} into it. Now we see that both three and four-point vertices will contribute a factor of $\frac{1}{g_{YM}^2}$, and the propagator, which is inversely proportional to the coefficient of $\left(\partial \tilde{A}\right)^2$, contributes a factor of g_{YM}^2. When taken together, we obtain an effective gauge theory coupling known as the "'t Hooft coupling" $\lambda = g_{YM}^2 N$. When combined in this way, a Feynman diagram in the large N limit will contribute a factor of $N^{2-2g}\lambda^{P-V}$ to the diagram. Here P is the number of propagators in the diagram and V the number of vertices. The symbol g is the

Euler characteristic of the two-dimensional surface on which the diagram can be embedded. That is, the simplest diagram can be embedded on a plane or sphere, without any lines crossing, for which the Euler characteristic is $g = 0$, while the next simplest surface is that of a torus, with a genus of $g = 1$, meaning that such diagrams are suppressed by a factor of N^{-2}, and can be ignored in the large N limit. This technique was proposed in the hope that physicists might learn about some aspects of QCD –which has a gauge group of $SU(3)$– by studying a version with a large (infinite) number of colours. In his original 1974 paper, 't Hooft made an analogy between quantized strings and these diagrams. However, no direct connection was made with string theory until the late 90's.

The holographic duality, in its current formulation, is due to Maldacena [6]. In his seminal paper, he outlined the duality between several D and M brane constructions, and supergravity solutions (see also [7]). The most famous and influential of these dualities, is the conjectured equivalence between $\mathcal{N} = 4$ super Yang-Mills (SYM) in four spacetime dimensions, and type IIB-superstring theory embedded in $\text{AdS}_5 \times S^5$; that is, the direct product between the maximally symmetric five-dimensional spacetime with constant negative curvature, and a five-sphere of constant radius.

This duality is made manifest in [6] by open and closed strings interacting along a stack of N parallel, flat, concurrent $D3$-branes, where N is taken to be large. Open superstrings interacting at weak effective string coupling $g_s N$ with the branes becomes equivalent to a massless $U(N)$ gauge theory, specifically $\mathcal{N} = 4$ SYM, in the low energy limit [6]. The field theory would be living in four spacetime dimensions, since the $D3$-branes would have a four-dimensional world volume. Furthermore, this quantum field theory is a four-dimensional conformal field theory (CFT), meaning that it is invariant under conformal (angle preserving) transformations of the Minkowski space in which it lives. The string coupling is associated with the Yang-Mills coupling, so that $g_s = g_{YM}^2$. Taking the large N limit while keeping the combination $\lambda = g_{YM}^2 N = g_s N$ small, is the same as taking the large N limit in the perturbative field theory (perturbative in the coupling λ, that is), described above. The expansions in $\frac{1}{N}$ in the YM Feynman diagrams, is equivalent to a genus expansion in the closed string world-sheet theory [5] in the large N limit. Higher-order closed string interactions therefore do not contribute to the gauge theory. Taking the large 't Hooft limit $\lambda \to \infty$, the theory becomes strongly coupled. Hence perturbation theory in the field theory breaks down, and we need some other way to describe it.

In the above discussion we mentioned that the string theory interacting with the D-branes in the low energy limit become equivalent to a gauge theory. We then took the 't Hooft coupling to be large. We could instead take the opposite route, namely by first taking the strong coupling limit in the string theory, and then taking the low energy limit. In the small $g_s N$ limit, closed strings propagate in the ten-dimensional spacetime around

4

the branes, and interact with them. In the large $g_s N$ limit, the closed strings interact strongly with the $D3$-branes, and the D-branes produce a curved soliton in the geometry of the form

$$ds^2 = \left(1 + \frac{L^4}{r^4}\right)^{-1/2} \left(-d\tau^2 + d\vec{y}^2\right) + \left(1 + \frac{L^4}{r^4}\right)^{1/2} \left(dr^2 + r^2 d\Omega_5^2\right), \qquad (1.5)$$

in which the closed strings still propagate, only weakly interacting among each other. This is possible since closed strings interact with coupling g_s, and we can keep g_s small while making $g_s N$ large. In this geometry the D-branes are located at $r = 0$, where the metric seems to be singular, but in fact the geometry is smooth. In the limit where the strings have low energy, they cannot escape the potential around the brane, and get trapped in the throat geometry near the branes, while those strings with enough energy stay in the flat asymptotic geometry in the limit $r \to \infty$. In the limit where the strings are trapped close to the D-branes (*i.e.,* $r \to 0$), the geometry is given by

$$ds^2 = \frac{r^2}{L^2} \left(-d\tau^2 + d\vec{y}^2\right) + \frac{L^2}{r^2} dr^2 + L^2 d\Omega_5^2. \qquad (1.6)$$

Further one can show that the strings in the asymptotically flat spacetime in (1.5) decouple from those in the "throat" geometry (1.6) [6]. Since the open strings' interactions with the closed strings is nonperturbatively equivalent to the soliton's geometry, the degrees of freedom of the field theory must then be encoded in the closed string theory in the throat geometry. The throat geometry in (1.6) turns out to be precisely the geometry of $\text{AdS}_5 \times S^5$. The parameter $L = (4\pi g_s N \alpha'^2)^{1/4}$ [5] is the AdS "radius" and the radius of the five-sphere, when $\frac{1}{2\pi\alpha'}$ is the string tension. The spacetime becomes large compared to the string scale when the in the strong coupling limit where $L/\ell_s \gg 1$, ℓ_s being the string length, and therefore the spacetime consists of propagating strings, interacting at tree level. The scalar curvature of the spacetime is given by $\mathcal{R} \propto -\frac{1}{L^2}$, the large N, strong coupling limit, the subleading corrections are negligible, making the spacetime act like classical Einstein gravity.

The above duality, namely the equivalence between $\mathcal{N} = 4$ SYM in the large N, strong coupling limit and closed type IIB-strings propagating in $\text{AdS}_5 \times S^5$, is the conjectured AdS/CFT correspondence. Some words should be added about the various limits of the coupling strength in the Yang-Mills theory and the limits of the supergravity. The duality as stated above, is that of large N, $\mathcal{N} = 4$ SYM with large 't Hooft coupling λ in its vacuum state, and classical type IIB-string theory in $\text{AdS}_5 \times S^5$. The duality can be made stronger by requiring it to hold when the 't Hooft coupling is not large, which would give the string theory loop corrections [5]. The strongest version of the duality is then the conjecture that

the two theories are equivalent even when the number of colours N is not large, which is stating that the string theory in AdS is fully quantum, and includes all orders of the genus expansion in the closed strings.

A further extension of the AdS/CFT correspondence is allowing the spacetime dual to the field theory to be *asymptotically* AdS, meaning that the bulk spacetime need not be homogeneous and isotropic, but can contain *e.g.,* a black hole or other perturbation. This would then mean that the field theory living on the asymptotic boundary of the spacetime would be $\mathcal{N} = 4$ SYM in some state other than its ground state, possibly with some (if not all) of its supersymmetry broken. In particular, one could introduce new interactions or mass terms in the field theory by switching on fields in the AdS bulk [8,9], as we describe later in this introduction.

It is also believed that the duality is more general than the original construction, meaning that for any d, there exists a CFT in d flat spacetime dimensions, which is dual to a gravity theory in $d + 1$-dimensional AdS spacetime [6] (as will be made clear in the construction in the following subsection).

In this thesis, we will concern ourselves primarily with the original construction[1], but allow for excitations in the bulk geometry, thus considering states of the field theory other than its ground (vacuum) state. That said, the results in chapter 3 are derived for general boundary dimensions d.

1.2   The holographic dictionary

Maldacena's original statement of the correspondence was a huge breakthrough, because it made accessible the physics of strongly coupled relativistic gauge theories. Much subsequent work has been done, studying $\mathcal{N} = 4$ super-Yang-Mills theory as an analogy to QCD and other strongly coupled field theories. While his original paper made the claim that this CFT is dual to classical general relativity (GR) in the appropriate limit, it did not state how to calculate observables in the field theory from the gravity theory. The statement that the field theory is equivalent to a gravity theory, gives the requirement that any observable in the field theory must be calculable from some quantity in the gravity theory. In this section, we will give some examples of observables (*i.e.,* correlation functions, as well as thermal entropy) that can be calculated in the asymptotically AdS bulk spacetime.

---

[1]That is, four-dimensional $\mathcal{N} = 4$ SYM with AdS$_5$. We should mention that we neglect the S^5-component of the dual spacetime. The spherical directions are insensitive to the backreaction of the spacetime during a quench, and so we can simply integrate out these directions, especially since these dimensions aren't present in the field theory spacetime.

1.2.1 Symmetries and scales

We have stated that $\mathcal{N} = 4$ SYM in the large N, large λ limit is dual to supergravity living on $\text{AdS}_5 \times S^5$. Although mapping one theory onto the other lies outside the aim of this thesis, there are some simple constructions which can make this link clear. One such example is matching the symmetries of the two theories.

Anti-de Sitter spacetime can be constructed as the surface of a hyperboloid in Minkowski spacetime in $d + 2$ dimensions, with a $(2, d)$ signature (that is, two time and d spatial dimensions). This surface in Minkowski space can be written as the locus [5]

$$- u^2 - v^2 + \sum_{i=1}^{d} x_i^2 = -L^2. \tag{1.7}$$

We can find a metric on this surface, by defining new coordinates and directional angles, namely

$$
\begin{aligned}
u &= L \cosh R \, \cos \tau \\
v &= L \cosh R \, \sin \tau \\
x_1 &= L \sinh R \, \cos \theta_1 \\
x_2 &= L \sinh R \, \sin \theta_1 \cos \theta_2 \\
x_3 &= L \sinh R \, \sin \theta_1 \sin \theta_2 \cos \theta_3 \\
&\vdots \\
x_{d-1} &= L \sinh R \, \sin \theta_1 \sin \theta_2 \ldots \cos \theta_{d-1} \\
x_d &= L \sinh R \, \sin \theta_1 \sin \theta_2 \ldots \sin \theta_{d-1};
\end{aligned}
\tag{1.8}
\tag{1.9}
$$

R being a radial coordinate with domain $[0, \infty)$ and τ being a time coordinate. The directional angles θ_i are polar coordinates that define the transverse directions to R and τ and form the surface of a $d - 1$-sphere at fixed R and τ. The induced metric on this manifold is then

$$ds^2 = L^2 \left(-\cosh^2 R \, d\tau^2 + dR^2 + \sinh^2 R \, d\Omega_{d-1}^2 \right). \tag{1.10}$$

This metric is clearly Lorentzian, *i.e.,* it has only one time dimension. In order to make the structure of this metric more clear we will recast it in slightly different coordinates. After rescaling the time and radial coordinates by $\tau \to \frac{\tau}{L}$ and $R \to \frac{R}{L}$, we make the change

of coordinates

$$r = L \sinh\left(\frac{R}{L}\right)$$

$$\left(1 + \frac{r^2}{L^2}\right) = \cosh^2\left(\frac{R}{L}\right), \tag{1.11}$$

so that the metric can be rewritten as

$$ds^2 = -\left(1 + \frac{r^2}{L^2}\right)d\tau^2 + \frac{dr^2}{1 + \frac{r^2}{L^2}} + r^2 d\Omega_{d-1}^2. \tag{1.12}$$

This is the metric of "global" AdS_{d+1}, and is asymptotic to the direct product between a $(d-1)$-sphere and the linear time direction on its conformal boundary located at $R = r = \infty$, as indicated by the $d\Omega_{d-1}^2$-part of the metric. The global AdS spacetime is invariant under the symmetry $SO(2,d)$, *i.e.*, the group of Lorentz transformations of the Minkowski space in which AdS_{d+1} is embedded. This group is also the group of conformal transformations in d dimensions. We could instead have chosen coordinates [5, 10]

$$u = \frac{1}{2}\left(r - \frac{L^2}{r} - \frac{r}{L^2}\left(\vec{y}^2 - \tau^2\right)\right)$$

$$v = \frac{r}{L}\tau$$

$$x_i = \frac{r}{L}y_i, \quad 1 \le i \le d-1$$

$$x_d = \frac{1}{2}\left(r + \frac{L^2}{r} + \frac{r}{L^2}\left(\vec{y}^2 - \tau^2\right)\right). \tag{1.13}$$

Note that the since $r \in [0, \infty)$ (the conformal boundary being located at $r = \infty$), we have that $u + x_d > 0$, and the coordinates we defined therefore do not cover the whole of global AdS space as defined in (1.7). This part of AdS is known as the "Poincaré patch". The metric for AdS in Poincaré coordinates is

$$ds^2 = \frac{r^2}{L^2}\left(-d\tau^2 + d\vec{y}^2\right) + \frac{L^2}{r^2}dr^2. \tag{1.14}$$

This is exactly the AdS-part of the metric (1.6). Making the change of coordinates $\rho = \frac{L^2}{r}$, the metric becomes

$$ds^2 = \frac{L^2}{\rho^2}\left(-d\tau^2 + d\rho^2 + d\vec{y}^2\right), \tag{1.15}$$

with the boundary located at $\rho = 0$. The difference in the causal structure of Poincaré AdS and global AdS can be seen in figure 1.2. On the left we show Penrose diagram for the Poincaré patch, and on the right the diagram for global AdS. Poincaré AdS is superimposed onto the global AdS to indicate that Poincaré coordinates do not cover the entire AdS spacetime.
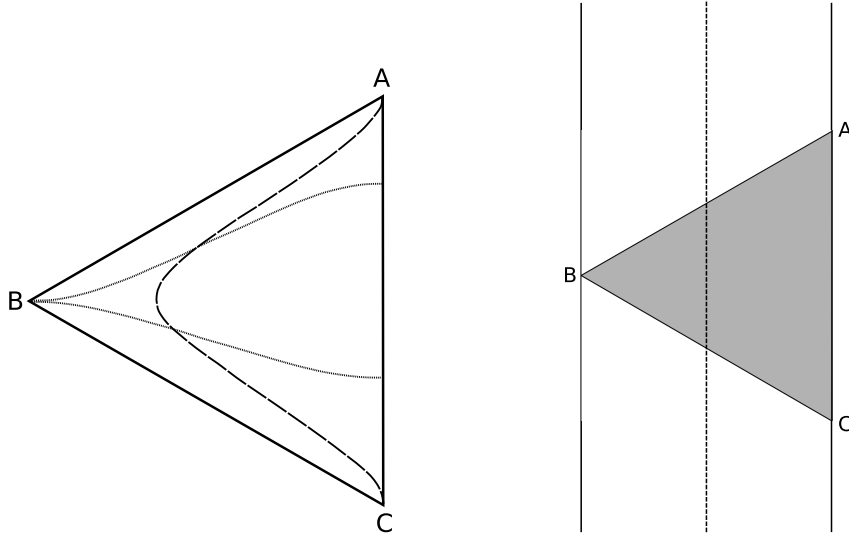
Figure 1.2: The diagrams on the left and right are adapted respectively from figures 22.3 and 22.2(b) in [11]. The diagram on the left is that of Poincaré AdS. The dotted curves are curves of constant τ, and the dashed curve is a curve of constant ρ (τ and ρ being the time and radial coordinates of the metric (1.15)), with the other transverse coordinates suppressed. The line AC represents the boundary of the spacetime at $\rho = 0$, while AB and BC represent $\tau = -\infty$ and $+\infty$ respectively. On the right we show the Penrose diagram of global AdS. The two solid vertical lines are the boundary of global AdS$_{d+1}$, which is $\mathbb{R} \times S^{d-1}$, while the dashed vertical line is the spatial centre of the spacetime. The radial direction in this diagram is horizontal, while the time direction is the infinite vertical direction. The shaded triangle is Poincaré AdS superimposed onto the global AdS.

Note that as opposed to global AdS, the conformal boundary of the Poincaré patch is flat Minkowski space. This is the boundary we will be concerning ourselves with in the studies of holographic quenches. Note however, that the holographic duality is also defined for global AdS. By deforming the background of $\mathcal{N} = 4$ SYM from a flat spacetime to a three-sphere (plus time), one would obtain a global AdS/CFT correspondence. Specializing

9

to $d = 4$ boundary dimensions, the isometry group of the bulk AdS$_5$ is the same group of conformal transformations in the $\mathcal{N} = 4$ SYM theory on its boundary. We have therefore reproduced a large part of the symmetry of $\mathcal{N} = 4$ SYM in the geometry of the dual space.

Recall that the full duality was that of AdS$_5 \times S^5$ with $\mathcal{N} = 4$ SYM. The compact S^5 manifold has a constant radius L and is transverse to the AdS-directions at every point in AdS. S^5 is invariant under the group of rotations $SO(6)$, and it turns out that this group forms an important part of the structure of $\mathcal{N} = 4$ SYM. While we will not write out the action of the SYM theory, we will simply state in words that it contains a set of four fermions in the adjoint representation, which can be transformed amongst each other by an $SU(4)$ symmetry, and six scalars that can be transformed among each other by an $SO(6)$ symmetry [5]. These symmetries can be mapped onto the $SO(6)$ symmetry of the five-sphere in the bulk geometry, particularly because $SU(4)$ is the same group as $SO(6)$. As stated, the group of Lorentz transformations of AdS is the same as the conformal group in one fewer spacetime dimensions. The duality is therefore thought to hold in more than just the rigid construction above, and is frequently studied in more or fewer dimensions, although in many cases the details of the CFT dual of the AdS theory is not known.

1.2.2 Scaling properties

In order to help visualize the duality, it is also useful to see how the AdS and CFT behave under scaling transformations. The metric (1.15) remains unchanged under a scale transformation $\rho \to \kappa\rho$, $\tau \to \kappa\tau$ and $y_i \to \kappa y_i$ [9]. For small κ, we therefore see that distances Δy become smaller by a factor of κ, while the radial coordinate ρ gets mapped closer to the asymptotic boundary of AdS. We therefore see that small distances in the boundary field theory, corresponding to ultraviolet (UV) energies, is dual to the near-boundary region in the AdS spacetime. The converse argument for large κ then implies that large separations in the field theory, which corresponds to infrared (IR) energies, is dual to the deep-bulk region of AdS. In fact, as we will see in chapters 2 and 4, when calculating quantities such as correlation functions in the AdS spacetime, these quantities frequently diverge near the AdS-boundary. It is then necessary to renormalize the quantity, *e.g.*, by subtracting the divergence at some cut-off for small ρ. This cut-off then corresponds to an ultra violet cut-off in the field theory dual.

One other energy scale of the field theory we will encounter, is that of the thermal scale. In chapters 2 and 4, we will work with AdS containing a black hole. The metric of

Poincaré AdS containing a planar black hole, for example, is given by

$$ds^2 = \frac{L^2}{\rho^2} \left[-\left(1 - \frac{\rho^d}{\rho_h^d}\right) d\tau^2 + \frac{d\rho^2}{1 - \frac{\rho^d}{\rho_h^d}} + d\vec{y}^2 \right], \qquad (1.16)$$

where ρ_h is the horizon distance. Clearly, because the black hole horizon is located away from the AdS boundary, the energy scale associated with the black hole is less than that of the UV scale, but also larger than the IR scale (since it is not located at infinity). As is well known, the black hole can be ascribed a temperature T [12]. In fact, in holography we equate the temperature of the black hole in asymptotically AdS, and the temperature of the field theory [13]. This is to be expected, since we have deformed the bulk space away from pure AdS, thus the field theory will no longer be in its vacuum state. If the black hole grows, its horizon moves outward, towards the asymptotic boundary of AdS; *i.e.,* ρ_h would become smaller (due to our choice of coordinates). This means that the thermal energy scale, and therefore the temperature of the black hole, should also grow as ρ_h becomes smaller. In fact, the temperature of the black hole can be calculated to be $T = \frac{1}{\pi \rho_h}$ [13,14], with the expected behaviour. A further consequence of this duality between the thermal state of the field theory and the black hole spacetime, is that the entropy of the black hole horizon will be equated with the thermal entropy of the corresponding plasma in the dual field theory [13].

1.2.3 Correlation functions

An important elucidation of the duality was made by Gubser, Klebanov and Polyakov [8], and Witten [9], respectively. In their respective papers, they took the first important steps in this direction, by showing how correlation functions in the field theory can be calculated from propagators in the gravity theory. In the large N, large 't Hooft coupling limit of the field theory, the dual AdS theory is classical. However, we still have the field theory defined in terms of operators. The key insight in the above-mentioned papers is that the leading coefficient in the asymptotic expansion of the classical fields in the AdS bulk are dual to couplings or sources of the dual operators. In fact, a particular subleading term in the expansion of a bulk field can be shown to be proportional to the expectation value of its dual operator [16], as we will explain later in this section.

To demonstrate the duality, we will focus on the simplest kind of field in AdS, namely a scalar field, and see how it is dual to some quantity in the boundary theory. We will then simply state the duality for the more complicated, but relevant, case of the metric. A

classical scalar field ϕ in AdS is simply the solution to the Klein-Gordon equation in $d+1$ dimensions

$$\left(\Box - m^2\right)\phi = 0, \tag{1.17}$$

$\Box$ being the d'Alembertian on AdS acting on the scalar, which has the form $\Box\phi = \frac{1}{\sqrt{-g}}\partial_\mu g^{\mu\nu}\partial_\nu\phi$. The solution for ϕ has some dependence on the "radial" coordinate ρ of AdS. In fact, it is possible to separate the asymptotic solution of the scalar field into a function with radial dependence and a part depending on the remaining transverse coordinates. This radial coordinate, as defined in the previous section is normal to the coordinates of the asymptotic boundary where the field theory lives. For a quick demonstration of the dual nature of the scalar field, we solve it near the boundary of AdS (that is, for small ρ). In this near-boundary approximation, we will write the field as

$$\phi(x) \xrightarrow{\rho\to 0} \rho^{d-\Delta}\phi_b(\tau, \vec{y}), \tag{1.18}$$

Δ being some undefined constant for now. Taking the limit of small ρ in equation (1.17), the equation becomes

$$
\begin{aligned}
&\left(\frac{1}{\sqrt{-g}}\partial_\mu g^{\mu\nu}\sqrt{-g}\partial_\nu - m^2\right)\rho^{d-\Delta}\phi_b \\
&= \left(\frac{\rho^{d+1}}{L^{d+1}}\left(\partial_\rho \frac{\rho^2}{L^2}\cdot\frac{L^{d+1}}{\rho^{d+1}}\partial_\rho + L^{d-1}\rho^{-d+1}\Box_b\right) - m^2\right)\rho^{d-\Delta}\phi_b \\
&= \frac{\rho^{d-\Delta}}{L^{d-\Delta}}\left(\frac{(d-\Delta)(-\Delta)}{L^2} - m^2 + \frac{\rho^2}{L^2}\Box_b\right)\phi_b \\
&= 0.
\end{aligned}
\tag{1.19}
$$

In the above equation, we split the d'Alembertian acting on a scalar, as expressed in the first line, into its radial ∂_ρ^2 and transverse components $\Box_b$ in the second. Going from the first line to the second, we substitute in the Poincaré metric (1.15). Skipping some steps in the algebra following the radial derivatives of the metric and scalar field, we arrive at the final expression, which is zero by the equations of motion. Note that the term containing the d'Alembertian in the transverse directions has an additional factor of ρ^2, and is therefore subleading for small ρ, and can be neglected for our purposes. We therefore obtain the expression between the mass and leading scaling of the scalar field

$$m^2 L^2 = \Delta\left(\Delta - d\right), \tag{1.20}$$

or we could rather write the constant Δ in terms of the scalar mass-squared as

$$\Delta_\pm = \frac{1}{2}\left(d \pm \sqrt{d^2 + 4m^2 L^2}\right). \tag{1.21}$$

Equation (1.21) shows that there are two independent solutions for the constant Δ. In fact, the solutions are related by

$$\Delta_- = d - \Delta_+. \tag{1.22}$$

This means that the scalar field has two independent asymptotic solutions, one proportional to ρ^{Δ_-}, and one proportional to ρ^{Δ_+}. When combining the two solutions, ρ^{Δ_-} will be the leading asymptotic expansion, while ρ^{Δ_+} will have a subleading contribution. In the rest of this section, we will adopt the notation $\Delta_+ = \Delta$, while $\Delta_- = d - \Delta$.

We have yet to give an interpretation to this constant Δ. To get an interpretation of Δ, it will be useful to first find the mass dimension of the scalar field. In the gravitational action

$$S_{d+1} = \frac{1}{16\pi G_{d+1}} \int d^{d+1}y \sqrt{-g} \left(\mathcal{R} + \frac{d(d-1)}{L^2} - \frac{1}{2}(\partial\phi)^2 - \frac{1}{2}m^2\phi^2 \right), \tag{1.23}$$

the Newton's constant G_{d+1} has mass dimension $d-1$, while the volume element has mass dimension $d+1$. The constant term $\frac{d(d-1)}{L^2} = -2\Lambda$ [15], where Λ is the (negative) cosmological constant. For the action to be dimensionless, therefore, each term in the integral must have mass dimension 2. We see that the two derivatives in the kinetic term of the scalar, and the mass-squared of the scalar already have mass dimension 2. The scalar field must therefore be dimensionless. Note that in conventional field theory, the scalar field would have mass dimension $\frac{d-1}{2}$, however, the prefactor $\frac{1}{16\pi G_{d+1}}$ in the gravitational action absorbs $d-1$ of those mass dimensions, such that the scalar field comes out as being dimensionless. Looking back at the asymptotic form of the scalar field $\rho^{d-\Delta}\phi_b$ we see that since ρ has dimensions of length, for this term to be dimensionless the asymptotic field ϕ_b must have mass dimension $d-\Delta$.

We are now in a position to find the boundary field theory dual of the scalar field in AdS. As we stated in the previous subsection, the Yang-Mills gauge theory lives on the boundary of AdS. The key insight alluded to at the beginning of this section, is the role that ϕ_b plays in the field theory, namely that of a source for the operator in correlation functions. Mathematically, the duality between the field theory and gravity theory can now be stated as [8, 9]

$$\langle e^{\int d^d y \sqrt{-g_b}\phi_b \mathcal{O}} \rangle_{YM} = \mathcal{Z}_{AdS}\left(\phi\right)\big|_{\phi \xrightarrow{\rho \to 0} \rho^{d-\Delta}\phi_b}, \tag{1.24}$$

where the quantity in angular brackets means the path integral over all field configurations in the Yang-Mills theory, with the standard (conformal) action plus $\int d^d y \sqrt{-g_b}\phi_b \mathcal{O}$ in the exponential, with the new term adding an extra interaction to the action, ϕ_b playing the

role of a coupling. Here g_b is the determinant of the metric on the conformal boundary. That is, the left hand side above is the generating functional in the super Yang-Mills theory of correlation functions in $\mathcal{O}$, where $\mathcal{O}$ is some Lorentz scalar operator. On the right hand side, $\mathcal{Z}_{AdS}$ is the partition function of the gravity theory, *i.e.,* the path integral over all field configurations with the boundary condition on the scalar $\phi \xrightarrow{\rho \to 0} \rho^{d-\Delta}\phi_b$. Since we know the mass dimension of ϕ_b is $d-\Delta$, then for the integral on the left hand side of (1.24) to be dimensionless, the operator $\mathcal{O}$ must have mass dimension Δ.

A scalar field in AdS with the asymptotic behaviour given in (1.18), is therefore dual to an operator with mass dimension Δ in the dual field theory. The dimension of Δ has an allowed range, as can be seen from equation (1.21). For $m^2 > 0$, we have $\Delta > d$, and therefore $\mathcal{O}$ is an irrelevant operator, while having $m^2 = 0$ yields $\Delta = d$, and is therefore marginal. We can also achieve a relevant operator with dimension $\Delta < d$, if we allow the scalar field in the bulk to be tachyonic (*i.e., $m^2 < 0$*). It turns out that a tachyonic scalar field on AdS can be stable, as long as the argument of the square-root in equation (1.21) is not negative. This gives the so-called Breitenlohner-Freedman bound [18] of allowed tachyonic mass-squared for the scalar field, namely $m^2 \geq -\frac{d^2}{4L^2}$, with allowed operator dimension[2] $\Delta \geq \frac{d}{2}$. Of course, this operator must be built from fields in the SYM theory, in a combination such that they form a Lorentz scalar with the appropriate mass dimension. There are therefore additional constraints on $\mathcal{O}$ other than its dimension.

To calculate a correlation function, it is useful to take the saddle point approximation of the gravity action, since the classical on-shell solution of the bulk fields will minimize the action, making the exponent of the Euclidean path integral a maximum. The partition function of bulk gravity action can then be written simply as

$$\mathcal{Z}_{AdS}\left(\phi\right)\big|_{\phi\xrightarrow{\rho\to0}\rho^{d-\Delta}\phi_b} \approx e^{-S_{AdS}}\big|_{\phi\xrightarrow{\rho\to0}\rho^{d-\Delta}\phi_b}, \tag{1.25}$$

where the action is now the on-shell action, with the given boundary source for the scalar field. To calculate connected correlation functions in the field theory, we must take the logarithm of the partition function, so that we have

$$-\log\langle e^{\int d^d y \sqrt{-g_b}\phi_b\mathcal{O}}\rangle_{YM} \approx S_{AdS}\big|_{\phi\xrightarrow{\rho\to0}\rho^{d-\Delta}\phi_b}. \tag{1.26}$$

Calculating connected correlation functions then proceeds in the same manner as in the path integral formulation of QFT, namely by taking the functional derivative of both

---

[2]It is, in fact possible to have dual operators with even smaller dimension Δ, if we make the subleading term $\rho^\Delta \phi_\Delta$ in the expansion of the scalar field source the operator in the boundary CFT, as pointed out in [19]. The operator dimension is then bound from below by $\Delta > \frac{d}{2} - 1$, the unitarity bound from the CFT. We will not concern ourselves with such sources in this thesis.

sides of source terms in the generating function (in this case ϕ_b). Therefore, an n-point correlation function in the boundary Yang-Mills theory would be given by

$$\langle \mathcal{O}(y_1) \ldots \mathcal{O}(y_n) \rangle = \frac{\delta^n S_{AdS}}{\sqrt{-g_b(y_1)} \ldots \sqrt{-g_b(y_n)} \delta \phi_b(y_1) \ldots \delta \phi_b(y_n)}. \tag{1.27}$$

In fact, as calculated in [16], the expectation value of the operator $\langle \mathcal{O} \rangle$, is proportional to the coefficient ϕ_Δ of the subleading solution to the scalar field, scaling as ρ^Δ.

The scalar field is of course the simplest field that can live on AdS, and and is dual to a scalar operator. It is, of course possible to calculate the correlation functions of vector and tensor operators on the boundary, by applying the above procedure for appropriate bulk fields. Two quick examples are that of a gauge field A_μ (A_a near the boundary) in AdS being dual to a current operator J_a in the dual field theory (the two must combine in the path integral in a way that is a Lorentz scalar), and that of the metric of AdS being dual to the stress-energy tensor of the Yang-Mills theory. In particular, correlation functions of the Yang-Mills stress tensor can be calculated by the asymptotic boundary metric as

$$\langle T_{a_1 b_1}(y_1) \ldots T_{a_n b_n}(y_n) \rangle = \frac{\delta^n S_{AdS}}{\sqrt{-g_b(y_1)} \ldots \sqrt{-g_b(y_n)} \delta g_b^{a_1 b_1}(y_1) \ldots \delta g_b^{a_n b_n}(y_n)}. \tag{1.28}$$

In chapter 2, we explicitly calculate the one-point functions of the scalar operator and stress tensor, as summarized above. We do this by calculating conformal boundary behaviour of the metric and scalar field in appropriate coordinates, and by cancelling divergences in these quantities using the prescription of Henningson and Skenderis [16], namely by adding covariant counterterms on the small-ρ cut-off surface, which we describe in more detail in chapter 2 and its appendix.

One other approximation that will turn out to be useful in chapter 4, is the geodesic approximation for two-point functions [17]. As ordinary in quantum field theory, the two-point correlator in the boundary field theory is given by the spacetime propagator [8,9,20] $\langle \mathcal{O}(y_1) \mathcal{O}(y_2) \rangle = G(y_1, y_2)$ in the boundary coordinates. It is likewise equal to the AdS boundary-to-boundary propagator (before making the saddle-point approximation in the AdS partition function)

$$\frac{\delta^2}{\sqrt{-g_b(y_1)} \sqrt{-g_b(y_2)} \delta \phi_b(y_1) \delta \phi_b(y_2)} \mathcal{Z}_{AdS}(\phi) = \int \mathcal{D}\rho(y) e^{-m\mathcal{L}(\rho(y))|_{y=y_1}^{y=y_2}}, \tag{1.29}$$

that is, the two-point correlator is given by the integral over all possible paths in AdS with endpoints $x = x_1$ and $x = x_2$ on the asymptotic boundary. In the limit of large operator

dimension, we have from (1.21) that $\Delta \approx m\,L$. When the exponent in the path integral in equation (1.29) becomes large, we can again take the saddle point approximation, that is, we can approximate the integral by its argument with the largest value, which is in fact the exponential with the least negative exponent. This means that the path favoured by the saddle point approximation is the geodesic (which has a positive length for a space-like path). We can therefore approximate the two-point function for a heavy scalar (or operator with large dimension) by

$$\langle \mathcal{O}(y_1)\mathcal{O}(y_2)\rangle = e^{-\frac{\Delta}{L}\mathcal{L}_{min}|_{y=y_1}^{y=y_2}}. \tag{1.30}$$

More details about determining space-like geodesics and their lengths can be found in chapter 4 where we will calculate geodesics with the intent of relating their length to two-point correlators.

We have summarized in this section some of the equivalences between the AdS gravity theory and the boundary Yang-Mills theory. There are of course many more, some of which we will mention in later chapters.

1.3 Quantum quenches

The topic of this thesis is the holographic study of quantum quenches in strongly coupled quantum field theories. To understand the need for such a study, it is necessary to understand the experimental motivation and non-holographic approaches to understanding quenches. In the first subsection we will discuss the definition of a quantum quench in quantum mechanics. We then go on to describe some of the experimental results in heavy ion collisions, followed by results in cold atom physics regarding perturbations that take the system out of equilibrium, and its subsequent thermalization, which has been a main motivation of this work. Finally, we go on to describe some of the theoretical work of quenches in weakly coupled QFT's.

1.3.1 What is a quantum quench?

For a long time, research in quantum mechanics has been concerned with time-independent properties of a system. In quantum field theory, a typical calculation is the the scattering cross-section of two particles. In condensed matter, one might be interested in the temperature corresponding to some phase transition. While such processes occur over a span of time, typically researchers have been interested in the late-time quantities of these systems. In the last decade or so, interest has sparked in time-dependent behaviour of

dynamical systems, in particular far-from-equilibrium systems, motivated by experimental results which have been able to track the evolution of quantum states (see next subsection). Theoretical work has since been done to try and understand the thermalization behaviour of out-of-equilibrium quantum systems. Before describing this research, let us first define what is meant by a quantum quench.

A quantum quench is a process during which a quantum system is strongly perturbed; that is, some parameter of the system is suddenly changed after which the system is allowed to relax, if possible. A simple example based on [21] is the following: A quantum state $|\psi\rangle$ evolves according to the unitary time evolution operator U as

$$|\psi(t)\rangle = U |\psi\rangle, \tag{1.31}$$

where U is given by

$$U(t) = e^{-i H t}. \tag{1.32}$$

H in the above equation is the Hamiltonian of the system. If $|\psi\rangle$ is an eigenstate of the Hamiltonian, it evolves in a very straightforward way, namely as a state with a periodic phase depending on its energy:

$$|\psi(t)\rangle = e^{-i E_\psi t} |\psi\rangle. \tag{1.33}$$

A difficulty sets in when one makes a sudden change to the Hamiltonian, taking $H \to H_*$. Then $|\psi\rangle$ is no longer an eigenstate of the Hamiltonian, but rather some linear combination of the new Hamiltonian's eigenstates, and will rather evolve as

$$|\psi(t)\rangle = \sum_n e^{-i E_{n*} t} |n_*\rangle\langle n_*|\psi\rangle, \tag{1.34}$$

where $|n_*\rangle$ are the new eigenstates of the Hamiltonian. In such a case, if the Hamiltonian has no interaction term between different energy states, the system never equilibrates and the original state may recur sporadically (see for example the Loschmidt echo [22]). It should be mentioned that this example is only valid in the case where the Hamiltonian has discrete eigenstates [21], and in general the original state will not recur in the way we described.

The above example is perhaps the most extreme (and simplest) example of a quench, where a parameter in the Hamiltonian is instantaneously changed. It is possible to alter this picture in a number of ways. One could, for example make a gradual change from the original Hamiltonian to the final one. We thus have two extreme cases, one being the situation described above, the other being the adiabatic limit where it takes an infinitely long

time for the transition between the two systems. In the latter case, the initial eigenstate will evolve into an eigenstate of the final Hamiltonian, with no extra modes being excited (except when there is level crossing between eigenstates). Much work has been done in the intermediate situation in both strongly and weakly interacting QFT's, as we will discuss.

Another modification is if we allow mixing between different energy states in the form of interaction terms between excitations. This will typically allow the system to evolve from some initial equilibrium state to a new equilibrium state, which is expected to look thermal, since the interaction allows for damping of the excitations to occur. This friction would be manifest in the new equilibrium having a higher temperature. There are of course special systems known as integrable which have infinitely many conserved charges, which for that reason never reach an equilibrium state after a quench (see *e.g.,* the first experiment in the following subsection). While such systems are interesting in their own right, in this thesis we will only consider the properties of quenches which do reach equilibrium after some time.

1.3.2   Heavy ion collisions

An important precursor to experiments of quantum qunches were in heavy ion collisions, such as those at RHIC, and now at the LHC [23]. In these experiments, two nuclei of heavy atoms, such as gold, are collided at high energies, and their collision decay products are studied at various detectors. Two such nuclei form a far-from-equilibrium system in the particle accelerator, and evolve from the two nuclei to a quasistable state of matter shortly after they collide (which we will describe in this section), which then decays into hadronic matter. While this system does not truly constitute a quantum quench, it is a far-from-equilibrium system. Holographic approaches of these two-particle collisions, described in more detail in section 1.4.2, have produced important tools for holographically studying quantum quenches. We will therefore give a short overview of the quark-gluon plasma, and why it can be studied through holography.

These experiments were constructed with the aim (amongst others) of producing the *quark-gluon plasma* (QGP), the state of quarks and gluons above a certain critical temperature, at which the quarks becomes deconfined from the protons and neutrons in which they were initially bound in colour-neutral combinations. By colliding heavy nuclei, such as gold, the experimentalists hoped to bring the density of particles high enough, such that the QGP could be observed [24].

The quark-gluon plasma, which forms shortly after the collision [25] (at the relevant timescale) has the fascinating property of being a strongly interacting liquid, rather than a

18

weakly interacting one, as might have been expected if the quarks and gluons were bound into localized bound states in the liquid, and there were only perturbative interactions between such quasiparticles. This interesting property could be seen from the transverse flow of the QGP [24]. When two nuclei collide off-center, the overlapping region is an oval shape, rather than a disk. If a strongly coupled liquid forms, there will be an "elliptical flow" of the liquid in the directions transverse to the collision axis [26]. Elliptical flow is characterized by uneven flow of the elliptical collision product, being more favoured in the direction of the ellipse's shorter axis, and disfavoured in the direction of the longer axis. This occurs due to a pressure gradient in the "shorter" direction. Such a pressure gradient occurs due to a "collective flow" of the constituent particles, but not if the liquid were made up of free particles [25]. Therefore, after the QGP "freezes out" into its final product of hadrons that are detected by an experiment, the hadrons should be distributed in a way reflecting this preferential elliptical flow. This is exactly what was detected at experiments at RHIC [27]!

One consequence of the QGP being strongly interacting, is that it has a very small shear viscosity η. In particular, it was found that $\eta/s \approx 0.1$ (s being the fluid's entropy density), in units where $\hbar$ and k_B are equal to one. This means that the strongly interacting QGP is a near-perfect liquid. This comes close to the famous predicted lower bound $\eta/s \approx 0.08$ for any liquid [28] from holography (although it turns out that this bound can be violated under certain assumptions [29]) for any physical fluid. Since the QGP is strongly interacting, holography has therefore been a good tool for studying the QGP, although it turns out that under the assumption that the QGP is near thermal equilibrium, hydrodynamics work well for predicting its properties. The full far-from-equilibrium dynamics of the nucleus collisions, however, is difficult to study, and holography has turned out to be a useful tool to model the full collision (*i.e.,* the two nuclei before, during and after the collision),as we discuss further in section 1.4.2.

1.3.3   Cold atom experiments

In the last ten years or so, it has become experimentally feasible to study the evolution of quantum states in out-of-equilibrium systems. This has been achieved especially in the field of cold atoms, where gases of atoms can be successfully trapped in optical lattices formed by the interference of two lasers with different frequencies. Unlike the quenches that can only be indirectly observed in the hadron collisions mentioned in the previous subsection, it is possible to track the evolution of the quantum system in real time in these experiments.

Perhaps the best-known example is that of a one-dimensional Bose gas which is modelled well as an integrable system, as studied in [30]. Two coherent packets of Rubidium atoms, trapped in an optical potential, were made to collide many times. The fact that the system is integrable, means that its infinite set of conserved quantities makes it impossible for the momentum distribution of the particles to become Gaussian, *i.e.,* they do not form an equilibrium thermal state. This is exactly what was observed in this experiment, namely that the atoms did not form a diffuse state, but instead the two distinct wavepackets remained distinguishable on a timescale that is much larger than the collision scale.

Another example of experiments probing the time-evolution of quantum states, is the observed decoherence of an interference pattern in a one-dimensional many body system [31]. By observing an interference pattern between two parts of the system, the experimentalists were able to observe how the fringes in the interference pattern became less coherent with time. Again, the timescale of the decoherence was long enough to be observable in real time, so that the out-of-equilibrium quantum state was experimentally accessible to study. Other examples in the literature include studies [32] in which the thermalization of a one-dimensional Bose gas was observed, by looking at how the number density of excited atoms to unexcited atoms equilibrated.

While theoretical techniques developed in the context of condensed matter systems exist, such as tensor network methods (see *e.g.,* [33], which correctly predicted some of the observations in [31]), it is a natural question whether quenches can be studied in the context of higher dimensional and relativistic systems, and in fact whether the traditional approaches of perturbative quantum field theory can handle such time-dependences, as we discuss in the next subsection.

1.3.4 Quenches in weakly-coupled and free QFT's

The need to analytically describe the time-dependent dynamics of a quenched quantum system is a challenging goal of current research in quantum field theory. New theoretical techniques, however, are necessary to describe the evolution of a quantum system after some initial shock or change to a control parameter. Motivated by the above-mentioned experimental results, two seminal contributors to this field have been Calabrese and Cardy, who have written its foundational papers.

In their first important paper [34], they considered the entanglement entropy of a one-dimensional CFT and spin chain. Instantaneously quenching the mass and switching on a magnetic field, respectively, they found that the entanglement entropy (EE) grows linearly until a time when the entropy very quickly equilibrates. They gave the intriguing intuitive

explanation that the EE grows until such a time as a pair of entangled quasi-particles moving at an absolute speed produced within the entangling region have enough time to reach opposite ends of the region, *i.e.,* bring every point in the interior of the region into causal contact with its exterior. They would later propose a similar quasi-particle view for the thermalization of two-point functions in coupled harmonic oscillators and spin chains, namely that the correlators increase linearly until the two ends come into causal contact following the initial quench [35], after which it rapidly flattens out. They were also able to extend their results to higher dimensions. A main result in these systems is that due to the absence of interactions, the system would relax into a state with an effective temperature dependent on each momentum mode excited in the quench. As mentioned in [35], this final state would not be a true thermal state, but a "hidden" pure state. This will be true in general, *i.e.,* not only for integrable systems, since if a quantum system is not in contact with some outside heat bath, the information of the state cannot be lost and the state continues to evolve as described by the unitary time-evolution operator $e^{iH\tau}$. The state only becomes complicated enough that it cannot be distinguished from a true thermal state.

Cardy and Sotiryadis went on to develop techniques to evaluate quenches in interacting QFT's [21]. By making a self-consistent approximation in the large N limit of a scalar ϕ^4-theory, they were able to calculate the final equilibrium value of the scalar field mass following an instantaneous quench of the interaction coupling. This technique was successfully applied to the system with an additional ϕ^6-interaction, where the scalar mass and both interaction couplings were simultaneously quenched [36], to also find the final dependence of the effective scalar mass on the quenched parameters. This technique was also applied to an $\mathcal{N} = 1$ supersymmetric version of the same system [37], where it was found that the quench breaks the supersymmetry.

The state of the art in quantum quenches for perturbative quantum field theory has been successful at evaluating quenches in some special cases, under the self-consistent (WKB) approximation [38]. The situation quickly becomes too complicated to solve with the currently available tools in the case of the full quantum field theory. There is still much to be done to find the time-dependence in general field theoretic systems, and probably will remain one of the more difficult analytic problems in modern physics.

One regime where both analytic and numerical attempts have been particularly fruitful, is in the gauge/gravity duality. The expected robustness of the duality makes many kinds of quantum quenches at strong coupling accessible to study. We discuss some of these attempts in the next section. While these studies provide a valuable insight into quench dynamics, the duality of the field theory is only a general relativistic theory when the field theory is at strong coupling. It is therefore important that more attempts are made in

understanding quantum quenches at weak coupling.

1.4 Holographic thermalization

In order to study the thermalization properties of strongly coupled field theories, researchers have in recent years become interested in pursuing this goal by applying the holographic duality, discussed in the first section of this chapter.

Various holographic models have been proposed for the study of far-from-equilibrium systems, some of which lead up to the main topic of this thesis. First I will briefly discuss some attempts motivated by the analytically more practical model of Vaidya metrics.

1.4.1 Studies based on Vaidya metrics

The Vaidya metric was first discovered in 1943 [39] to model the time-dependent radiation of a star. Following the discovery of the AdS/CFT correspondence, attempts were made to understand black hole formation in AdS. The Vaidya metric that is equivalent to pure AdS at early times and AdS-black brane at late times is an ideal metric to analytically study the problem [40]. Only some years later was it realized to be useful for studying the dynamics of heavy ion collisions and out-of-equilibrium systems.

The AdS-Vaidya metric can be written as [41]

$$ds^2 = -\left(\frac{r^2}{L^2} - \frac{m(v)}{L^2 r^{d-2}}\right) dv^2 + \frac{r^2}{L^2} d\vec{y}^2 + 2\, dv\, dr, \qquad (1.35)$$

where $m(v)$ is some time dependent function, and $d + 1$ is the spacetime dimension. The metric is written here in Eddington-Finkelstein coordinates, where constant v indicates the direction of null rays travelling radially into the bulk from the asymptotically AdS boundary. The metric describes a spacetime with stress-energy tensor [41]

$$T_{vv} = \frac{d-1}{2r^{d-1}} \frac{dm}{dv}, \qquad (1.36)$$

with all other components being zero. The stress-energy tensor for null dust is of the form $T_{\mu\nu} \propto \ell_\mu \ell_\nu$ [42], where ℓ is a null vector. This is indeed the case for equation (1.36), since if ℓ_μ has only a nonzero v-component, $g^{vv}\ell_v\ell_v$ is zero due to g^{vv} being zero. Choosing v to be a function smoothly and monotonically changing from 0 at $v = -\infty$ to some final value at

$v = +\infty$, the metric therefore describes a shell of null-dust (*i.e.,* a shell of massless matter collapsing at the speed of light) collapsing from the infinity in pure AdS to form a black hole. If the function m is a step function, the collapsing shell becomes surface with zero width. An inertial observer inside the shell would see only pure AdS, while an observer outside the shell would see a planar black hole in AdS. As observed by [40], this metric is obtained from the backreaction of a collapsing massless scalar field (*i.e.,* dual to a marginal operator in the field theory) in AdS, in the limit where the source of the scalar field (ϕ_b in section 1.2.3) is switched on and off again in a finite time, and remains small[3].

Other groups were soon able to study the thermalization properties of the dual field theory. Nonlocal probes in the field theory were used to study thermalization of the theory [41,44–47]. The equilibration of the holographic dual of two-point functions, Wilson loops and entanglement entropy were studied in various deformations of the standard Vaidya prescription. These provide nonlocal measures of the thermalization in the dual field theory setup. Specifically, they indicate how the field theory thermalizes at different scales after the initial disturbance. In chapter 4, we will use the evolution of a two-point function and entanglement entropy of a strip to probe the thermalization of the dual field theory.

While it is unclear how closely the Vaidya approach may approximate a true quantum quench of a strongly coupled QFT, what *is* clear is that this cannot provide a fully accurate picture of the dynamics of such a system. A Vaidya quench provides a useful toy model of a quench in the field theory. However, such a quench ignores the interactions between the different scales in the problem, in which the field theory plasma exchanges energy between the different scales in a less instantaneous fashion to that in the Vaidya case. The Vaidya metric is that of an infalling shell, with no dynamical response outside the shell, meaning that the various energy scales in the field theory instantaneously relax in this model, until the black hole forms at some fixed time in the asymptotic boundary, and the thermal energy scale is reached. In a more real-world gravitational collapse, the black hole would be *ringing* away some of its energy in quasi-normal modes [48], which means that there is still some energy exchange between different energy scales in the field theory, that is longer than the scale of the response of the system to the quench (in the Vaidya case, the thermalization time equals the response time of the system). One could therefore say that the Vaidya metric describes a highly constrained quench in the field theory, which could not describe a general situation.

---

[3]In a paper by Das, Nishioka and Takayanagi [43], the Vaidya metric was found be the induced metric on a $D1$ brane rotating about on direction on S^5 in $AdS_5 \times S^5$. When the $D1$ brane is stretching radially from the boundary of AdS infinity in a "straight" line, its holographic dual is energy being injected into the dual $\mathcal{N} = 4$ SYM theory from a a point in space.

1.4.2 Other numerical investigations

The most important advance in the study of holographic quenches was the paper by Chesler and Yaffe [49] that initiated much of the work that has since been pursued. Their initial approach was to add a spatial inhomogeneity to the boundary metric, by making one of the spatial dimensions contract monotonically, while the other two expand. The metric of the boundary field theory can be written as

$$ds^2 = -dt^2 + e^{f(t)}d\vec{y}_{1,2}^2 + e^{-2f(t)}dy_3^2. \tag{1.37}$$

The function f which can be chosen arbitrarily, serves as the non-normalizable mode (source of the quench) of the field theory, on the boundary of its dual asymptotically-AdS spacetime. This sources a backreaction on the bulk geometry, leading to black hole formation and ultimately thermalization sometime after the function f stabilizes. The quench is therefore introduced by deforming the geometry on which the field theory lives, which backreacts onto the bulk spacetime.

Later work (including the work described in the main body of this thesis) saw different ways of sourcing an excitation in the bulk. For example, in a similar spirit as the work above, many papers have been written modelling heavy ion collisions in particle accelerators (motivated primarily by the heavy ion experiments mentioned in the section 1.3.2) by gravitational shock wave collisions in AdS. This amounts to choosing the initial condition of the metric, and then numerically evolving the solution to the Einstein equations in order to see how the system relaxes [50]. It should be noted that it is not always clear what true field theory dual of such a system is, although it is motivated as a toy model for such systems.

Another way is to introduce a quantum quench is to "switch on" an operator in field theory, by making its coupling time-dependent (see for example [48, 51–54]). In this case the holographic dual is a scalar field (as described in section 1.2.3) being excited in the AdS bulk, which in turn backreacts onto the spacetime metric. This approach is especially motivated by cold atom experiments, since in these scenarios the potential of the system can be carefully controlled by the experimenter.

An important difference between the previous subsection and the present examples is that the bulk solutions here is numerical rather than analytical, like the Vaidya solution. In general, it is not possible to analytically solve a gravitational system in terms of the non-normalizable mode. For this, numerics becomes necessary. The benefit of this approach is that more physical scenarios becomes accessible, by using (and extending) some of the techniques developed for numerical relativity. Numerical solutions are less "clean" and

allows for more backreaction between the metric at different bulk radii. This means that the solutions found numerically thermalize in such a way that there is more mixing between the different energy scales of the field theory, possibly revealing more of the physical aspects of the field theory.

It is also important to note that the interpretation of the quench is clear from the holographic duality. Unlike the Vaidya case, it is possible to set up a quench that has a clear interpretation in the dual field theory picture.

1.5 Outline

In the rest of this thesis, I will discuss studies in quenches of a strongly interacting $\mathcal{N} = 4$ SYM, by myself and collaborators.

In chapter 2, we study a quench of a $\mathcal{N} = 4$ SYM plasma, by switching on scalar operators $\mathcal{O}$ of fractional dimension Δ as a smooth function of time, where $2 < \Delta < 4$. This is holographically dual to exciting a scalar field in a dual AdS spacetime in five dimensions, and allowing it to collapse onto the black hole in the spacetime. This is extension of the work done in [48], where scalar and fermionic mass terms (of dimension $\Delta = 2$ and 3, respectively) were switched on in the field theory. By studying the quench for a range of operator dimensions, we were able to find intriguing results, namely universal behaviours in the fast quench limit in the scaling of the final rest energy and pressure (as well as thermal entropy) of the dual field theory as a function of the operator dimension, as well as in the excitation and thermalization time of the one-point correlation function of the operator. We also discuss universal behaviour in the slow quench limit. This chapter is based on the paper

- A. Buchel, L. Lehner, R.C. Myers and A. van Niekerk, "Quantum quenches of holographic plasmas," JHEP **1305**, 067 (2013) [arXiv:1302.2924 [hep-th]],

corresponding to reference [52] in the bibliography. In this paper, I adapted the numerical code used in [48] by my senior collaborators, and carried out the calculations while being advised by my collaborators.

In chapter 3, we analytically derive the scaling behaviour of the energy and other thermodynamic quantities seen in chapter 2, by varying the source in a fixed interval. Since the source is switched on abruptly, there is a lightcone propagating into the bulk geometry from its boundary carrying this information. This means that the scalar field

must be everywhere in the bulk at earlier times than this signal reaches there. In the limit of very fast quenches, we can take into account only the asymptotically-AdS geometry near the boundary. Thus solving the scalar field in the near-boundary limit, we can solve for its normalizable mode using the constraint that its asymptotic series must be zero on the lightcone carrying the information of the quench. We find that the normalizable mode exhibits the desired scaling with the quenching time, to obtain the universal scalings seen in chapter 2. This chapter is based on the paper

- A. Buchel, R. C. Myers and A. van Niekerk, "Universality of Abrupt Holographic Quenches," Phys. Rev. Lett. **111**, 201602 (2013) [arXiv:1307.4740 [hep-th]],

corresponding to reference [54] in the bibliography. In the initial draft I carried out the calculations and was advised by my senior collaborators.

In chapter 4, we again numerically quench the system of [48], specializing to an operator of dimension 3. We again quench the system by switching on a scalar field (in a smooth manner) in AdS_5 containing a planar black hole, and evolve the bulk system numerically, using new numerical code. The new numerical methods allowed us to evolve the profile of the geometry as well as the scalar, enabling us to calculate nonlocal probes in the geometry to observe thermalization at different scales in the system. We calculated both the evolution of the black hole horizon in this perturbed regime, as well as two-point functions of a heavy operator and entanglement entropy of a strip. By calculating the two-point functions and entanglement entropies for regions of different widths, we were able to probe the thermalization time at different length scales of the theory. We observed that for wide enough separations, the correlator and entropy both have thermalization times that scale linearly with separation. We discuss the reason for the observed behaviour. This chapter is based on

- A. Buchel, R. C. Myers and A. van Niekerk, "Nonlocal probes of thermalization in holographic quenches with spectral methods," arXiv:1410.6201 [hep-th].

corresponding to reference [55], in which I applied the numerical code, to evolve the holographic system for quenches of different speeds, and calculated the evolution of the horizon, two-point function and entropy, while being advised by my senior collaborators.

Chapter 2

Quantum quenches of holographic plasmas

2.1 Introduction

Recent advances in cold atom experiments have stimulated a vigorous research program into quantum quenches, processes in which the physical couplings of a quantum system are abruptly changed [56]. The basic motivation is to understand the organizing principles governing the far-from-equilibrium behaviour of such systems. Although such quenches are well understood in the context of quantum mechanics [57], much less is known about such processes in quantum field theories. Theoretical progress has been made for a variety of systems, including two-dimensional conformal field theories, (nearly) free field theories and integrable models – *e.g.,* see [34–37, 58, 59]. However, broadly applicable theoretical techniques, which provide an efficient description of these quenches, remain to be found.

Gauge/gravity duality [5, 6] provides a remarkable new approach to studying certain strongly coupled field theories. Of course, in this framework, questions about the field theory are recast into questions about gravity in one higher dimension. These holographic models seem to be especially well suited for the study of quantum quenches since, with relatively modest efforts, one is able to study strongly coupled quantum field theories, real-time processes and systems at finite temperature, as well as allowing for analysis in general spacetime dimensions. Hence holographic techniques have recently been applied to the study of quantum quenches [43, 60] and the related issue of 'thermalization' [40, 41, 43–47]. However, given the complexities of the bulk description of rapid changes in the

boundary theory, numerical relativity is increasingly being applied to study these far-from-equilibrium processes [49, 51, 62] — see also [63].

In this chapter, we extend the calculations presented in [48], in which the gauge/gravity duality was used to study 'thermal quenches' in a plasma of the strongly coupled $\mathcal{N} = 2^*$ gauge theory. More specifically, [48] studied the response of an initial thermal equilibrium state to variations of the coupling of the boundary theory to either a dimension two or three operator. The analysis was restricted to a high temperature regime where the calculations were carried out to leading order in $m/T \ll 1$. Here m is the relevant mass scale introduced by the new coupling. In the present case, we extend these holographic calculations to consider quenches made by coupling to a relevant operator with an arbitrary conformal dimension in the range $2 \leq \Delta \leq 4$. The behaviour of the strongly coupled boundary theory in the present quenches is very similar to that found in [48]. In fact, for many of the results, we are able to identify a simple function of the conformal dimension which interpolates between the different cases which are explicitly studied both here and in [48]. For example, we find that in fast quenches, the increase in the energy density scales like $(T_i/\delta t)^{2\Delta-4}$, where T_i is the initial temperature and δt is the timescale over which the new coupling is turned on — fast quenches are then those for which $T_i/\delta t \gg 1$.

The remainder of the chapter is organized as follows: In section 2.2, we describe the holographic model which is used to study our quenches and derive the gravitational equations that are to be solved. Next we examine solutions of these equations in section 2.3. In particular, by restricting our attention to the high temperature regime, we show that to leading order we only need to solve the linearized equation for the bulk scalar. We also consider the asymptotic boundary expansion for these solutions in Eddington-Finkelstein coordinates. In section 2.4, we translate the latter expansion to Fefferman-Graham coordinates, which are more suitable to study physical observables in the boundary theory. In section 2.5, after finding the counterterms that renormalize the bulk action, we find expressions for the expectation value of the stress-energy tensor and the quenched operator in terms of gravitational variables. We also show that these observables obey the expected Ward identities. In section 2.6, we identify the appropriate translation between the gravitational variables and quantities in the boundary theory. This dictionary allows us to write expressions for the entropy production and the change in other thermodynamic quantities induced by the quench. Section 2.7 provides a brief description of our numerical procedure. In section 2.8, we provide an independent analysis of the response in the slow quench limit, which later provides a check of our numerical results. We present and discuss various aspects of our numerical solutions in section 2.9. We conclude with a summary of the results and further comments in section 2.10. Finally, there are various appendices describing certain technical details. Appendix 2.11 presents explicit coefficients for the

leading terms in the asymptotic of the expansion in section 2.3. Similarly, appendix 2.12 presents coefficients for the asymptotic expansions appearing in section 2.4. Appendix 2.13 describes the variations of the renormalized bulk action constructed in section 2.5, which yield the expectation value of the stress tensor and the quenched operator. Next, in appendix 2.14, we describe the discretization procedure used in the finite difference method for solving the scalar field profile. Finally in appendix 2.15, we analytically solve for the next-to-leading order behaviour of the scalar field for slow quenches, and compare the result to our numerical results in section 2.8.

2.2   Holographic model

We will apply holographic techniques to study quantum quenches in a strongly coupled four-dimensional QFT. The quantum quench is implemented by adding a relevant operator with time-dependent coupling to the Lagrangian of the QFT, as follows [48]:

$$\mathcal{L}_0 \to \mathcal{L}_0 + \lambda(t)\,\mathcal{O}_\Delta. \tag{2.1}$$

In our calculations, the theory described by $\mathcal{L}_0$ is in fact a conformal field theory. The operator $\mathcal{O}_\Delta$ is relevant, meaning that it has conformal dimension $\Delta < 4$. We will only consider $\Delta > 2$ here, as natural in our holographic framework — see below. In our analysis, we start with the theory in a thermal state with $\lambda = 0$ and quench the system by switching on the coupling to some non-zero value. To further simplify our analysis, we will focus on quenches in the high temperature regime, where the temperature T provides the dominant scale in the problem. That is, we will only study quenches where $\lambda \ll T^{4-\Delta}$ at all stages. Note, however, that we will allow the rate of change of coupling λ to be arbitrarily large. In particular, we allow $\partial_t \lambda(t) \gtrsim T^{5-\Delta}$. Taking this limit makes it questionable whether the perturbative approximation still holds, and whether we can trust our numerical results. However, as we will see in chapter 3, the scaling laws we find in this fast quench limit, are still correct in the nonperturbative regime.

As the unperturbed QFT is a four-dimensional conformal field theory, the gravitational dual of the vacuum state is five-dimensional anti-de Sitter (AdS$_5$) spacetime. Since we are interested instead in a thermal state of the boundary CFT, the appropriate dual spacetime is an asymptotically AdS$_5$ planar black hole [13] — we consider the boundary QFT in $R^{1,3}$, hence the 'planar' geometry for the black hole horizon. Switching on the coupling λ is dual to switching on a massive scalar field in the gravitational theory. More precisely, we are modifying the asymptotic boundary conditions for the bulk scalar field in a way that matches the profile $\lambda(t)$. Using holographic methods, we can easily determine the response

of the QFT by examining the response of the scalar, which yields $\langle \mathcal{O}_\Delta \rangle$, as well as the response of the spacetime metric, which yields the energy density, pressure and entropy density of the boundary field theory. Since we are considering the high temperature regime, our calculations will be perturbative in the amplitude of the bulk scalar. That is, the scalar will only produce 'small' perturbations on the AdS$_5$ black hole background.

The dimension Δ of the operator $\mathcal{O}_\Delta$ is related to the AdS length scale L and the mass m of the bulk scalar field by [8, 9]

$$\Delta = 2 + \sqrt{4 + L^2 m^2}. \tag{2.2}$$

Notice that a relevant operator is dual to a scalar field with $m^2 \leq 0$. Of course, such a tachyonic mass is still consistent in five-dimensional AdS space as long as it respects the Breitenlohner-Freedman bound [18], *i.e.*, $m^2 \geq -4/L^2$. In eq. (2.2), this imposes the constraint $\Delta \geq 2$. The unitarity bound for a scalar operator in the four-dimensional CFT allows for $\Delta \geq 1$, however, to study operators in the range $2 > \Delta \geq 1$, we must use the 'alternative quantization' of the dual bulk scalar set forward in [19]. However, we will not consider this possibility in the following and restrict our attention to $\Delta > 2$.

The dual gravitational theory is Einstein gravity coupled to a cosmological constant and a massive scalar field, *i.e.*,

$$S_{bulk} = \frac{1}{16\pi G_5} \int d^5 x \sqrt{-g} \left(R + 12 - \frac{1}{2} (\partial \phi)^2 - \frac{1}{2} m^2 \phi^2 \right). \tag{2.3}$$

Since Newton's constant appears in an overall factor in front of the action, the scalar field ϕ is dimensionless. Further, we have also implicitly set the AdS curvature scale to one, *i.e.*, $L = 1$, as can be inferred from the cosmological constant term. With this convention, it follows that m^2 will also be a dimensionless number, which is implicitly given in units of $1/L^2$. As explained in [48], the scalar field might have further interactions, *e.g.*, a ϕ^4 potential, but any such higher order terms will not play a role in the following analysis describing the high temperature regime.

As an aside, let us comment that it is natural to think of the unperturbed boundary theory as the $\mathcal{N} = 4$ super-Yang-Mills (SYM) theory, in the limit of large N_c and large 't Hooft coupling. In this case, our conventions are such that the five-dimensional Newton's constant is given by

$$G_5 \equiv \frac{\pi}{2 N_c^2}. \tag{2.4}$$

However, we are slightly liberal in our analysis here in that we allow the conformal dimensions of $\mathcal{O}_\Delta$ to take arbitrary values, rather than restricting ourselves to the spectrum of

$\mathcal{N} = 4$ SYM. In this more general context, we can relate Newton's constant to the central charge of the boundary CFT with

$$C_T \equiv \frac{5}{\pi\, G_5}\,. \tag{2.5}$$

where C_T is the central charge defining the leading singularity in the two-point correlator of the stress tensor — *e.g.*, see [64].

Varying the action (2.3) with respect to the metric g and the scalar field ϕ, one obtains respectively Einstein's equations and the curved-space Klein-Gordon equation

$$0 \;=\; E_{\mu\nu} \equiv R_{\mu\nu} - \frac{1}{2}\,\partial_\mu\phi\,\partial_\nu\phi - g_{\mu\nu}\left(\frac{1}{2}R + 6 - \frac{1}{4}\left(\partial\phi\right)^2 - \frac{1}{4}m^2\phi^2\right), \tag{2.6}$$

$$0 \;=\; \frac{1}{\sqrt{-g}}\,\partial_\mu\!\left(\sqrt{-g}\,g^{\mu\nu}\partial_\nu\phi\right) - m^2\phi\,. \tag{2.7}$$

We express our metric ansatz using infalling Eddington-Finkelstein (EF) coordinates

$$ds_5^2 = -A(v,r)\,dv^2 + \Sigma^2(v,r)\,d\vec{y}^2 + 2\,dvdr\,, \tag{2.8}$$

as was used in [48, 49, 65] in the context of holographic thermal systems. For the scalar in this background, we take $\phi = \phi(v,r)$ (*i.e.*, it is independent of the spatial directions y^i). This choice allows us to describe homogeneous quenches where the coupling λ is spatially constant but varies in time. The above is a convenient gauge (2.8) for numerically evolving the scalar field within a characteristic formulation. The resulting radial vector $\frac{\partial}{\partial r}$ is null and all points on a line with constant v (and y^i) are causally connected. The resulting system of (partial differential) equations provide a nested system of (with both radial and time integrations) that can be evolved the spacetime radially from the boundary at $r = \infty$ inwards and in forward in time. We will return to this discussion when we describe the numerics in section 2.7.

With this metric ansatz (2.8), the Klein-Gordon equation (2.7) and Einstein's equations (2.6) become [48]

$$0 \;=\; 2\Sigma\partial_r(\dot{\phi}) + 3\,(\partial_r\Sigma)\dot{\phi} + 3\dot{\Sigma}\partial_r\phi - m^2\Sigma\phi\,, \tag{2.9}$$

$$0 \;=\; \Sigma\,\partial_r(\dot{\Sigma}) + 2\dot{\Sigma}\,\partial_r\Sigma - 2\Sigma^2 + \frac{1}{12}m^2\phi^2\Sigma^2\,, \tag{2.10}$$

$$0 \;=\; 4 + \partial_r^2 A - \frac{12}{\Sigma^2}\dot{\Sigma}\,\partial_r\Sigma + \dot{\phi}\,\partial_r\phi - \frac{1}{6}m^2\phi^2\,, \tag{2.11}$$

$$0 \;=\; \ddot{\Sigma} - \frac{1}{2}\,\dot{\Sigma}\,\partial_r A + \frac{1}{6}\Sigma\,(\dot{\phi})^2\,, \tag{2.12}$$

$$0 \;=\; \partial_r^2\Sigma + \frac{1}{6}\Sigma\,(\partial_r\phi)^2\,, \tag{2.13}$$

31

where we have defined for any function $h(v, r)$,

$$\dot{h} \equiv \partial_v h + \frac{1}{2} A \, \partial_r h \,. \tag{2.14}$$

More precisely, the above equations are obtained as:

- Eq. (2.9) is equivalent to the Klein-Gordon equation (2.7) multiplied by Σ.

- Eq. (2.10) corresponds to the combination

$$\frac{1}{3} \Sigma^2 E_{vr} + \frac{1}{6} A \Sigma^2 E_{rr} = 0 \,. \tag{2.15}$$

- Eq. (2.11) corresponds to the combination

$$\frac{1}{3\Sigma^2} \left(6 E_{ii} - 8\Sigma^2 E_{vr} - 4A\Sigma^2 E_r \right) = 0 \,. \tag{2.16}$$

  Note that E_{ii} denotes one of the diagonal components of $E_{\mu\nu}$ with $\mu = \nu = i$, *i.e.*, there is no implicit sum over i in this expression.

- Eq. (2.12) corresponds to the combination

$$-\frac{1}{3} \Sigma E_{vv} - \frac{1}{3} A \Sigma E_{vr} - \frac{1}{12} A^2 \Sigma E_{rr} = 0 \,. \tag{2.17}$$

- Eq. (2.13) corresponds to $\Sigma \, E_{rr} = 0$.

Note that eqs. (2.12) and (2.13) are constraint equations, implied by the previous three equations [48].

2.3 Solutions to the equations

2.3.1 Static solutions

As noted above, because we study quenches of the boundary QFT from an initial thermal state, we consider the dual AdS spacetime initially containing a black hole. With $\phi = 0$, the spacetime will have the static solution

$$
\begin{aligned}
A(v, r) &= r^2 - \frac{\mu^4}{r^2}, \\
\Sigma(v, r) &= r,
\end{aligned} \tag{2.18}
$$

32

where the black hole horizon is located at $r = \mu$ and the asymptotic boundary of the spacetime is located at $r = \infty$. This black hole solution gives the gravity description of the original (conformal) boundary theory in thermal equilibrium. The QFT temperature is given by the temperature of the black hole, namely $T = \mu/\pi$.[1]

Now following [48], our analysis will be limited to considering a high temperature regime, where $\lambda(t) \ll T^{4-\Delta}$. As noted above, this means that our calculations in the dual gravitational description are perturbative in the amplitude of the bulk scalar. In other words, we assume that the AdS spacetime contains a 'large' black hole and the scalar only makes 'small' perturbations on this background geometry. If we parameterize the amplitude of scalar field by the small parameter ℓ, if follows from the Einstein equations (2.6) that the scalar only backreacts on the metric at order ℓ^2. At the lowest order in ℓ, the scalar and the metric can therefore be written as [48]

$$
\begin{aligned}
\phi(v,r) &= \ell\,\hat{\phi}(v,r) + o\left(\ell^3\right), \\
A(v,r) &= r^2 - \frac{\mu^4}{r^2} + \mu^2\ell^2 A_{\mathrm{p}}(v,r) + o\left(\ell^4\right), \\
\Sigma(v,r) &= r + \mu\,\ell^2\Sigma_{\mathrm{p}}(v,r) + o\left(\ell^4\right),
\end{aligned}
\tag{2.19}
$$

where factors of μ were introduced above to make both metric functions, $A_{\mathrm{p}}(v,r)$ and $\Sigma_{\mathrm{p}}(v,r)$, dimensionless.

As a matter of convenience, we now change to the dimensionless coordinates $\rho \equiv \mu/r$, $\tau \equiv \mu v$, as well as $\vec{y}' \equiv \mu\vec{y}$. For this choice of radial coordinate, the boundary lies at $\rho = 0$ and the black hole horizon lies at $\rho = 1$. The scalar field and the metric coefficients are then written as

$$
\begin{aligned}
\phi(\tau,\rho) &= \ell\,\hat{\phi}(\tau,\rho) + o\left(\ell^3\right), \\
A(\tau,\rho) &= \mu^2\left(\rho^{-2} - \rho^2 + \ell^2 A_{\mathrm{p}}(\tau,\rho) + o\left(\ell^4\right)\right), \\
\Sigma(\tau,\rho) &= \mu\left(\rho^{-1} + \ell^2\Sigma_{\mathrm{p}}(\tau,\rho) + o\left(\ell^4\right)\right).
\end{aligned}
\tag{2.20}
$$

In these coordinates, the metric then becomes

$$
ds_5^2 = \mu^{-2}\left(-A(\tau,\rho)\,d\tau^2 + \Sigma^2(\tau,\rho)\,d\vec{y}'^2\right) - 2\frac{d\tau d\rho}{\rho^2}.
\tag{2.21}
$$

Note that the factor of μ^{-2} cancels with the μ^2 contained in the metric coefficients A and Σ^2. The metric, and therefore the equations of motion will be independent of the black hole mass parameter μ in these coordinates.

---

[1]Our conventions below will introduce a small correction to this result – see section 2.6.

If we consider the Klein-Gordon equation (2.9) to order ℓ, the field $\hat{\phi}$ decouples from the metric functions A_{p} and Σ_{p} and we are left with the linearized equation [48]

$$-\frac{m^2\hat{\phi}}{\rho} + 3\partial_\tau\hat{\phi} - \left(3+\rho^4\right)\partial_\rho\hat{\phi} - 2\rho\partial_\tau\partial_\rho\hat{\phi} + \left(\rho - \rho^5\right)\partial_\rho^2\hat{\phi} = 0. \qquad (2.22)$$

The metric perturbations can then be determined from eqs. (2.10) and (2.11) at order ℓ^2 [48]:

$$\begin{aligned}
0 &= \left[-2\left(3-\rho^4\right) + \rho^2\left(1-\rho^4\right)\partial_\rho^2 + \rho\left(4\partial_\tau - 4\partial_\rho - 2\rho\partial_\tau\partial_\rho\right)\right]\Sigma_{\mathrm{p}} \\
&\quad + \rho\left[2 - \rho\partial_\rho\right]A_{\mathrm{p}} + \frac{m^2}{6\rho}\hat{\phi}^2\,, \qquad (2.23)
\end{aligned}$$

$$\begin{aligned}
0 &= 24\left[\partial_\tau - \frac{1}{\rho}\left(1-\rho^4\right)\left(1+\rho\partial_\rho\right)\right]\Sigma_{\mathrm{p}} + 2\left[6 - 2\rho\partial_\rho - \rho^2\partial_\rho^2\right]A_{\mathrm{p}} \\
&\quad + \left[2\partial_\tau\hat{\phi} - \left(1-\rho^4\right)\partial_\rho\hat{\phi}\right]\partial_\rho\hat{\phi} + \frac{m^2}{3\rho^2}\hat{\phi}^2\,. \qquad (2.24)
\end{aligned}$$

Again, note that the mass parameter μ does not appear in these equations (2.22)–(2.24).

In the case of a static or equilibrium configuration, eq. (2.22) can be solved for the leading order scalar field

$$\begin{aligned}
\hat{\phi}\left(\rho\right) &= c_1\,\rho^{4-\Delta}\,{}_2\mathrm{F}_1\left(\frac{4-\Delta}{4}, \frac{4-\Delta}{4}, \frac{4-\Delta}{2}, \rho^4\right) \\
&\quad - c_1\frac{\Gamma\left(\frac{4-\Delta}{2}\right)\Gamma\left(\frac{\Delta}{4}\right)^2}{\Gamma\left(\frac{4-\Delta}{4}\right)^2\Gamma\left(\frac{\Delta}{2}\right)}\rho^\Delta\,{}_2\mathrm{F}_1\left(\frac{\Delta}{4}, \frac{\Delta}{4}, \frac{\Delta}{2}, \rho^4\right)\,, \qquad (2.25)
\end{aligned}$$

where ${}_2\mathrm{F}_1$ denotes a hypergeometric function. The constant c_1 is arbitrary but the coefficient of the second term above is chosen to ensure regularity of the scalar at the horizon. Separately, both ${}_2\mathrm{F}_1\left(\frac{4-\Delta}{4}, \frac{4-\Delta}{4}, \frac{4-\Delta}{2}, \rho^4\right)$ and ${}_2\mathrm{F}_1\left(\frac{\Delta}{4}, \frac{\Delta}{4}, \frac{\Delta}{2}, \rho^4\right)$ have a logarithmic divergence near $\rho = 1$ but with the relative factor above, these logarithmic terms cancel in eq. (2.25). This static bulk solution will describe the system (to leading order in ℓ) after it has equilibrated after the quench with a finite coupling λ. Hence it will be useful to extract the relative magnitude of the normalizable and the non-normalizable modes of the bulk scalar in this new equilibrium configuration — see the next section.

2.3.2 Time-dependent solutions

In this subsection, we write down the asymptotic expansion for the leading order scalar $\hat{\phi}\left(\tau, \rho\right)$ and metric functions, $A_{\mathrm{p}}(\tau, \rho)$ and $\Sigma_{\mathrm{p}}(\tau, \rho)$, in a time-dependent solution. Note

that when $\Delta \in \mathbb{Z}$ or $\Delta \in \mathbb{Z}_{n+\frac{1}{2}}$ (e.g., $\Delta = 2$ or 3 as in [48]), logarithmic terms appear in these asymptotic expansions. However, generically these expansions do not contain any logarithmic terms and this is the case that we consider in the following.

The time-dependent solution $\hat{\phi}(\tau, \rho)$ has an asymptotic expansion close to $\rho = 0$ of the form:

$$
\begin{aligned}
\hat{\phi}(\tau, \rho) = \\
\rho^{4-\Delta} \left(p_{(0)}(\tau) + \rho \dot{p}_{(0)} + \frac{(2\Delta - 7)\rho^2}{4(\Delta - 3)} \ddot{p}_{(0)} + \frac{(2\Delta - 9)\rho^3}{12(\Delta - 3)} \dddot{p}_{(0)} + \mathrm{o}\left(\rho^4\right) \right) \\
+ \rho^{\Delta} \left(p_{(2\Delta-4)}(\tau) + \rho \dot{p}_{(2\Delta-4)} + \frac{(2\Delta - 1)\rho^2}{4(\Delta - 1)} \ddot{p}_{(2\Delta-4)} + \frac{(2\Delta + 1)\rho^3}{12(\Delta - 1)} \dddot{p}_{(2\Delta-4)} + \mathrm{o}\left(\rho^4\right) \right) ,
\end{aligned}
\tag{2.26}
$$

where the coefficients $p_{(0)}$ and $p_{(2\Delta-4)}$ are now functions of τ. Here $\dot{h} \equiv \partial_\tau h$, for any τ-dependent function h. In the following, we will choose some function for the coefficient of the non-normalizable mode, $p_{(0)}(\tau)$, and then the normalizable coefficient $p_{(2\Delta-4)}(t)$ is determined by numerically integrating eq. (2.22). However, from the static solution (2.25), we have an analytic solution

$$
\text{equilibrium} : \qquad p_{(2\Delta-4)} = -\frac{\Gamma\left(\frac{4-\Delta}{2}\right)\Gamma\left(\frac{\Delta}{4}\right)^2}{\Gamma\left(\frac{4-\Delta}{4}\right)^2 \Gamma\left(\frac{\Delta}{2}\right)} p_{(0)}
\tag{2.27}
$$

for the late-time configuration describing the boundary theory after it has equilibrated with finite λ.

The solutions for the metric perturbations at order ℓ^2 take the form

$$
A_{\mathrm{p}}(\tau, \rho) = \sum_{n=4} \left[a_{2,n}(\tau)\rho^{n-2} + \alpha_{2,n}(\tau)\rho^{2-2\Delta+n} + \beta_{2,n}(\tau)\rho^{2\Delta-6+n} \right] ,
\tag{2.28}
$$

$$
\Sigma_{\mathrm{p}}(\tau, \rho) = \sum_{n=5} \left[s_{2,n}(\tau)\rho^{n-2} + \sigma_{2,n}(\tau)\rho^{2-2\Delta+n} + \theta_{2,n}(\tau)\rho^{2\Delta-6+n} \right] ,
\tag{2.29}
$$

where (most of) the coefficients can be determined by solving eqs. (2.23) and (2.24) order by order in powers of ρ. However, the coefficient $a_{2,4}$ enters these equations as a free parameter. Now taking the limit $\rho \to 0$, we simplify eq. (2.12) using results for the expansion

35

coefficients from the other equations of motion to produce the following constraint:

$$\dot{a}_{2,4} = \frac{1}{9}\left(\Delta\left(2\Delta - 5\right)p_{(2\Delta - 4)}\dot{p}_{(0)} - \left(4 - \Delta\right)\left(2\Delta - 3\right)p_{(0)}\dot{p}_{(2\Delta - 4)}\right), \quad (2.30)$$

and hence

$$a_{2,4}(\tau) = \mathcal{C} - \frac{1}{9}\left(4 - \Delta\right)\left(2\Delta - 3\right)p_{(0)}(\tau)\,p_{(2\Delta - 4)}(\tau)$$
$$+ \frac{2}{3}\left(\Delta - 2\right)\int_{-\infty}^{\tau}d\tau'\;p_{(2\Delta - 4)}(\tau')\,\dot{p}_{(0)}(\tau')\,, \qquad (2.31)$$

where $\mathcal{C}$ is an integration constant. Following [48], we will choose $\mathcal{C}$ at a later stage so that the entropy production in the quench is proportional to $a_{2,4}(\tau = \infty)$. Note that since initially we have $p_{(0)}(\tau = -\infty) = 0 = p_{(2\Delta - 4)}(\tau = -\infty)$, it follows that $a_{2,4}(-\infty) = \mathcal{C}$. Further if we set $p_{(0)}(\tau = \infty) = 1$, then $a_{2,4}$ asymptotes to

$$a_{2,4}(\infty) = a_{2,4}(-\infty) - \frac{1}{9}\left(4 - \Delta\right)\left(2\Delta - 3\right)p_{(2\Delta - 4)}(\infty)$$
$$+ \frac{2}{3}\left(\Delta - 2\right)\int_{-\infty}^{\infty}d\tau'\;p_{(2\Delta - 4)}(\tau')\,\dot{p}_{(0)}(\tau')\,. \qquad (2.32)$$

All the remaining coefficients appearing in eqs. (2.28) and (2.29) can be determined in terms of $p_{(0)}$, $p_{(2\Delta - 4)}$ and $a_{2,4}$. Explicit expressions of some of the leading coefficients are given in appendix 2.11.

2.4 Fefferman-Graham coordinates

We would like to evaluate the entropy density, the expectation value of the stress-energy tensor and of the operator $\mathcal{O}_\Delta$ in the boundary theory during a quench. Following the standard approach [16, 66], we need to vary the on-shell gravitational action (2.3) with respect to the asymptotic boundary value of the appropriate fields — see section 2.13. While EF coordinates are useful for evaluating the equations of motion, they are not as useful for determining the boundary one-point functions. The reason for the latter is that the "radial" direction ∂_ρ is not orthogonal to the spacetime boundary located at $\rho = 0$, which is clear from the fact that the metric has off-diagonal τ and ρ components. It will therefore be useful to transform to Fefferman-Graham (FG) coordinates [67], in which the radial coordinate is orthogonal to the boundary of the spacetime. The FG coordinates have a spacelike radial coordinate z in contrast to the EF coordinates, with the null radial

coordinate ρ. The FG coordinates are more appropriate for holographic renormalization, since we can choose a planar cut-off surface by simply fixing r to some small parameter ϵ.

In FG coordinates, the (asymptotically) AdS spacetime has the line-element

$$ds_5^2 = \frac{G_{ab}(x,z)\,dx^a\,dx^b}{z^2} + \frac{dz^2}{z^2}, \tag{2.33}$$

a and b running from 0 to 3. By equating this FG line-element (2.33) to the previous EF line-element (2.21) and writing the Eddington-Finkelstein coordinates τ and ρ as functions of the Fefferman-Graham coordinates t and z, we obtain a set of three equations from which we can solve for $\tau(t,z)$ and $\rho(t,z)$, as well as the metric component G_{00}. The set of equations is

$$0 = \mu^{-2}A\rho^2\dot\tau\tau' + (\dot\rho\tau' + \rho'\dot\tau), \tag{2.34}$$

$$-1 = z^2\left(\mu^{-2}A\left(\tau'\right)^2 + \frac{2}{\rho^2}\rho'\tau'\right), \tag{2.35}$$

$$G_{00} = z^2\left(-\mu^{-2}A\dot\tau^2 - \frac{2}{\rho^2}\dot\tau\dot\rho\right), \tag{2.36}$$

where primes denote ∂_z and dots denote ∂_t. We solve eqs. (2.34) and (2.35) by writing τ and ρ as power series in z, with t-dependent coefficients:

$$\frac{\tau(t,z)}{\mu} = t + \sum_{n=1} v_{(n)}(t)z^n +$$
$$\ell^2\left(\sum_{n=5}\vartheta_{(n)}(t)z^n + z^{9-2\Delta}\sum_{n=0}\nu_{(n)}(t)z^n + z^{2\Delta}\sum_{n=1}\omega_{(n)}(t)z^n\right), \tag{2.37}$$

$$\rho(t,z) = \mu z + \sum_{n=1}\rho_{(n)}(t)z^n +$$
$$\ell^2\left(\sum_{n=5}\chi_{(n)}(t)z^n + z^{9-2\Delta}\sum_{n=0}\xi_{(n)}(t)z^n + z^{2\Delta}\sum_{n=1}\zeta_{(n)}(t)z^n\right). \tag{2.38}$$

Upon solving for the above, we can also determine the metric G_{ab} and scalar field $\hat\phi$ in

terms of similar asymptotic expansions in z

$$
\begin{aligned}
G_{ab}(t,z) &= g_{ab}^{(0)} + g_{ab}^{(4)} z^4 \\
&\quad + \ell^2 \left(\sum_{n=4} c_{(n)ab}(t) z^n + z^{8-2\Delta} \sum_{n=0} d_{(n)ab}(t) z^n + z^{2\Delta} \sum_{n=0} e_{(n)ab}(t) z^n \right) \quad (2.39) \\
\hat{\phi}(t,z) &= \left(z^{4-\Delta} \sum_{n=0} f_{(n)}(t)\, z^n + z^{\Delta} \sum_{n=0} g_{(n)}(t)\, z^n \right). \quad (2.40)
\end{aligned}
$$

Explicit expressions of the leading coefficients are given in appendix 2.12. For an asymptotic solution of the nonlinear equations of motion in FG coordinates, see [68].

2.5 Holographic renormalization

Given the metric and scalar field written in FG coordinates, we must evaluate the on-shell gravitational action (2.3). However, a naive evaluation yields a number of divergences associated with integrating out to the asymptotic boundary at $z = 0$. Hence following the standard approach [16,66], we first regulate the calculation by introducing a cut-off surface $z = \epsilon$ and then the divergences are eliminated by adding boundary counterterms. Actually these counterterms are added in addition to the usual Gibbons-Hawking-Brown-York term

$$
S_{GHBY} = -\frac{1}{8\pi G_5} \int d^4x \sqrt{-\gamma} K \Big|_{r=\epsilon}, \quad (2.41)
$$

where $\gamma_{ab}(\epsilon)$ is the induced metric on the cut-off surface and K is the trace of the extrinsic curvature of this surface. Recall that in our study, we choose the boundary geometry to be flat, *i.e.*,

$$
g_{ab}^{(0)} = \lim_{z \to 0} G_{ab}(t,z) = \eta_{ab}, \quad (2.42)
$$

and so the counterterm action turns out to be

$$
S_{count} = \frac{1}{16\pi G_5} \int d^4x \sqrt{-\gamma} \Bigg(-6 - \frac{4-\Delta}{2} \phi^2 \quad (2.43)
$$

$$
+ \frac{1}{4(\Delta-3)} \left(\partial\phi\right)^2 + \frac{1}{24(\Delta-3)} R\left(\gamma\right) \phi^2 \Bigg) \Bigg|_{z=\epsilon},
$$

where $R\left(\gamma\right)$ corresponds to the Ricci scalar constructed with γ_{ab}. The $\left(\partial\phi\right)^2$ and $R\left(\gamma\right)\phi^2$ terms only cancel divergences which occur when $\Delta > 3$ and so they should be discarded

38

when $\Delta \leq 3$. Although the term with $R(\gamma) \phi^2$ vanishes to leading order when evaluated on a planar cut-off surface, it is required to cancel a divergence that arises in varying the metric to determine the stress tensor [69]. In particular, it cancels a divergent contribution to the pressure $\mathcal{P}$ for $\Delta > 3$ at order ℓ^2. Also note that for the special cases $\Delta = 2$, 3 and 4, there are also further logarithmic and finite counterterms, but we do not concern ourselves with these here. The interested reader can find a complete discussion of these cases in [48, 70].

The holographic action $S_{reg} = S_{bulk} + S_{GHBY} + S_{count}$ can now be used to calculate the one-point correlators of the stress tensor and operator $\mathcal{O}_\Delta$. In order to calculate these expectation values, we need to vary S_{reg} with respect to the boundary metric and the scalar field, respectively. The details of these calculations are given in appendix 2.13 and the final results are:

$$8\pi G_5 \, \mathcal{E} \;=\; \frac{3}{2}\mu^4 - \ell^2 \mu^4 \left(\frac{3}{2} a_{2,4} + \frac{1}{6}\, (2\Delta - 3)\,(4 - \Delta)\, p_{(0)} p_{(2\Delta - 4)} \right), \qquad (2.44)$$

$$8\pi G_5 \, \mathcal{P} \;=\; \frac{1}{2}\mu^4 - \ell^2 \mu^4 \left(\frac{1}{2} a_{2,4} - \frac{1}{18}\, (4\Delta - 9)\,(4 - \Delta)\, p_{(0)} p_{(2\Delta - 4)} \right), \qquad (2.45)$$

$$16\pi G_5 \, \langle \mathcal{O}_\Delta \rangle \;=\; 2\mu^\Delta \ell \, \alpha_\lambda \, (\Delta - 2)\, p_{(2\Delta - 4)} . \qquad (2.46)$$

Here $\mathcal{E}$ and $\mathcal{P}$ denote the energy density and pressure in the boundary theory, *i.e.*, $\langle T^{00} \rangle = \mathcal{E}$ and $\langle T^{ij} \rangle = \delta^{ij}\, \mathcal{P}$. Further, α_λ is a proportionality constant relating the leading coefficient in the expansion (2.12.3) of the bulk scalar with the coupling in the boundary theory, *i.e.*, $\ell f_{(0)} = \alpha_\lambda \, \lambda$. We fix the precise value of this constant in section 2.6.1 — see eq. (2.67).

These one-point correlators must respect certain Ward identities [16]. In particular, one has the diffeomorphism Ward identity

$$\partial^i \langle T_{ij} \rangle = \langle \mathcal{O}_\Delta \rangle \, \partial_j \lambda , \qquad (2.47)$$

Of course, when the coupling λ is constant, this expression reduces to the conservation of energy and momentum in the boundary theory. In the present case with a time-dependent coupling, the $j = t$ component of eq. (2.47) yields

$$\partial_t \mathcal{E} = -\langle \mathcal{O}_\Delta \rangle \, \partial_t \lambda . \qquad (2.48)$$

Here the expression on the right-hand side describes the work done by varying the coupling in the boundary theory.[2] Let us verify that eqs. (2.44) and (2.46) satisfy this constraint:

---

[2]Note that a minus sign appears here in accord with our conventions, which differ slightly from those in [48].

First, comparing the expansions of the bulk scalar in eqs. (2.26) and (2.12.3) and recalling the relation $\ell f_{(0)} = \alpha_\lambda \lambda$ from appendix 2.13, we find to leading order

$$p_{(0)} = \mu^{\Delta-4} \, \alpha_\lambda \, \frac{\lambda}{\ell}. \tag{2.49}$$

Then differentiating eq.(2.44), we find

$$
\begin{aligned}
8\pi G_5 \, \partial_t \mathcal{E} &= \ell^2 \mu^4 \left(-\frac{3}{2} \dot{a}_{2,4} - \frac{1}{6} \left(2\Delta - 3\right)\left(4 - \Delta\right) \left(\dot{p}_{(0)} p_{(2\Delta-4)} + p_{(0)} \dot{p}_{(2\Delta-4)} \right) \right) \\
&= -\ell^2 \mu^4 \left(\Delta - 2 \right) p_{(2\Delta-4)} \, \dot{p}_{(0)} ,
\end{aligned}
\tag{2.50}
$$

where we simplified the expression by substituting for $\dot{a}_{2,4}$ from eq. (2.30). Now using eqs. (2.46) and (2.49), we see that this expression precisely matches the expected Ward identity (2.48). Let us comment that this match should be no surprise since the constraint (2.12) (which was used to derive eq. (2.30)) reduces to precisely this Ward identity (2.48) on the asymptotic boundary $z = 0$ [48].

We also have the conformal Ward identify

$$T^a{}_a = (4 - \Delta) \, \langle \mathcal{O}_\Delta \rangle \, \lambda , \tag{2.51}$$

which follows from taking the trace of the stress-energy tensor with eqs. (2.44) and (2.45) and substituting eqs. (2.46) and (2.49). Here we do not find any anomalous terms (at quadratic order in ℓ), since we are assuming that the operator $\mathcal{O}_\Delta$ has a fractional conformal dimension. This result can be contrasted with the discussion in [48] which considered $\Delta = 2$ and 3.

2.6 Temperature and entropy density

In this section we will calculate the temperature of the boundary theory before and after the quench, as well as the entropy produced during the quench. As described above, we are assuming that the quench takes the scalar field from a vanishing initial value with $p_{(0)} = 0$ and $p_{(2\Delta-4)} = 0$ to a final equilibrium solution where $p_{(0)} = 1$ and $p_{(2\Delta-4)} = p_{(2\Delta-4)}(\infty)$. In section 2.6.3, we will consider 'reverse' quenches which instead take the system from $p_{(0)} = 1$ to 0. In our perturbative calculations for high temperature quenches, we find that if the profile for the 'reverse' quench is given by $\tilde{p}_{(0)}(\tau) = 1 - p_{(0)}(\tau)$, where $p_{(0)}(\tau)$ describes some 'forward' quench, then we find that $\tilde{p}_{(2\Delta-4)}(\tau) = p_{(2\Delta-4)}(\infty) - p_{(2\Delta-4)}(\tau)$,

where $p_{(2\Delta-4)}(\tau)$ is the response for the corresponding 'forward' quench. Similarly, we will find that the entropy production is the same in the forward and reverse quenches. Further, in the case of an adiabatic quench, no entropy is created and the process is reversible.

As discussed in section 2.3.1, the initial configuration before the quench is the well-known planar AdS black hole described by eq. (2.18). The calculation of the corresponding temperature is a straightforward exercise with the result $T = \mu/\pi$. However, recall that in eq. (2.31) we established a convention where $a_{2,4}(-\infty) = \mathcal{C}$. That is, our metric perturbation is nonvanishing even at $\tau = -\infty$. The effect of this convention is to shift the black hole mass parameter, *i.e.*, $\mu \to \mu\xi$ where $\xi^4 = 1 - \ell^2 a_{2,4}(-\infty)$. Hence, to quadratic order in the expansion in ℓ, the initial temperature becomes

$$T_i = \frac{\mu\xi}{\pi} = \frac{\mu}{\pi}\left(1 - \frac{\ell^2}{4}\, a_{2,4}(-\infty)\right). \tag{2.52}$$

2.6.1 Final temperature

Next we wish to determine the final equilibrium temperature of the system after the quench has taken place. This calculation is more subtle as with our perturbative calculations, since we will not have the full metric describing the final black hole geometry. Instead then, we turn to the thermodynamics of the boundary theory to determine the final temperature. That is, we will compare the energy density and pressure in QFT variables (already in terms of the final temperature T_f and the coupling λ) to the energy density and pressure calculated holographically in terms of gravitational variables. In doing so, we are able to derive meaningful relations between the field theory coupling and temperature and the bulk parameters μ and ℓ. Of course, by assuming a form for $\mathcal{E}$ and $\mathcal{P}$, our final temperature and entropy production will necessarily depend on the conventions used to define our coupling. This cannot be helped, because we do not know the Lagrangian for the boundary theory when the quench is by an operator of arbitrary dimension Δ. This can be contrasted with the discussion in [48] for the cases of $\Delta = 2, 3$, where the exact equilibrium expressions for $\mathcal{E}$ and $\mathcal{P}$ are known from [71]. Nonetheless, we will find physically meaningful interpretations for our results.

To begin, we make the following ansatz for the energy density and pressure in the final

41

equilibrium of the boundary theory,

$$\mathcal{E}_f = \mathcal{A} T_f^4 \left(1 - \alpha_f \left(\frac{\lambda_f}{T_f^{4-\Delta}} \right)^2 \right), \tag{2.53}$$

$$\mathcal{P}_f = \frac{\mathcal{A}}{3} T_f^4 \left(1 - \left(\frac{\lambda_f}{T_f^{4-\Delta}} \right)^2 \right), \tag{2.54}$$

where $\lambda_f = \lambda(\tau = \infty)$ denotes the final value of the coupling. To leading order our ansatz reduces to the expressions expected for a conformal theory and is in accord with our analysis, the perturbation of these conformal terms is quadratic in the coupling. Further, we have expressed the perturbations in terms of the dimensionless ratio $\lambda_f/T_f^{4-\Delta}$. Setting the pre-factor for this term in the pressure (2.54) really defines our normalization for the coupling. We can compare these expressions with those given in [48, 71]. For example, we find for $\Delta = 3$,

$$\lambda_f^2 = \frac{2\Gamma \left(\frac{3}{4} \right)^4}{\pi^4} m_f^2, \tag{2.55}$$

where m_f was the fermion mass in the boundary theory. Using this expression, we can confirm the results derived below for the equilibrium values

of the observables agree with those given in [48, 71].

Now we need to determine the constant of proportionality α_f in eq. (2.54). To proceed, we only assume that the boundary theory obeys standard thermodynamics, following [72]. First, we write the free energy density as

$$F = \mathcal{E} - T S, \tag{2.56}$$

where S is the entropy density. In the absence of any chemical potentials, $F = -\mathcal{P}$. Therefore combining these expressions with eqs. (2.53) and (2.54), the final entropy density is given by

$$S_f = \frac{\mathcal{A}}{3} T_f^3 \left(4 - (3\alpha_f + 1) \left(\frac{\lambda_f}{T_f^{4-\Delta}} \right)^2 \right). \tag{2.57}$$

We use the first law of thermodynamics (with fixed volume) to write

$$\frac{d\mathcal{E}_f}{dT_f} = T_f \frac{dS}{dT_f}. \tag{2.58}$$

The left-hand side of eq. (2.58) is

$$\frac{d\mathcal{E}_f}{dT_f} = \mathcal{A}\, T_f^3 \left(4 - (2\Delta - 4)\, \alpha_f \left(\frac{\lambda_f}{T_f^{4-\Delta}} \right)^2 \right)$$

whereas the right-hand side is

$$T_f \frac{dS_f}{dT_f} = \mathcal{A}\, T_f^3 \left(4 - \frac{1}{3}\, (3\alpha_f + 1)\, (2\Delta - 5) \left(\frac{\lambda_f}{T_f^{4-\Delta}} \right)^2 \right) .$$

By comparing these two expressions, we solve for α_f as

$$\alpha_f = \frac{2\Delta - 5}{3} . \tag{2.59}$$

Note that it may seem that the quench has no effect on the energy density for $\Delta = \frac{5}{2}$ (when $\alpha_f = 0$), but even in this case, the initial and final temperatures will differ by a term of order λ_f^2. Hence, there will still be a change in $\mathcal{E}$ in this case, contained in the T_f^4 term in eq. (2.53).

Next, we compare these results for the boundary theory with the corresponding expression in the gravitational dual. In particular, we would like to find ℓ in terms of the temperature T_f and the coupling λ_f. However, first we fix the normalization factor $\mathcal{A}$ appearing in eqs. (2.53) and (2.54). This factor would be the unchanged in the initial equilibrium of the conformal boundary theory, $i.e.$, at $t = -\infty$, we would have $\mathcal{E}_i = \mathcal{A}\, T_i^4$. Comparing the latter expression with eq. (2.44) then yields

$$\mathcal{A}\, T_i^4 = \frac{3}{16\pi G_5}\, \mu^4 \left(1 - \ell^2 a_{2,4}(-\infty) \right) . \tag{2.60}$$

Given the expression for the initial temperature in eq. (2.52), we see that

$$\mathcal{A} = \frac{3\pi^4}{16\pi G_5} . \tag{2.61}$$

Next, we take the trace of the stress tensor in both the field theory and the gravitational

dual:

$$(T_{\text{QFT}})^a{}_a \quad = \quad -\frac{2}{3}\,\mathcal{A}\,T_f^4\,(4-\Delta)\left(\frac{\lambda_f}{T_f^{4-\Delta}}\right)^2, \tag{2.62}$$

$$(T_{\text{GR}})^a{}_a \quad = \quad \frac{\mu^4\ell^2}{8\pi G_5}\,(4-\Delta)\,(\Delta-2)\,p_{(0)}p_{(2\Delta-4)}$$

$$\xrightarrow[t\to\infty]{} \quad \frac{\mu^4\ell^2}{8\pi G_5}\,(4-\Delta)\,(\Delta-2)\,p_{(2\Delta-4)}(\infty), \tag{2.63}$$

where $p_{(2\Delta-4)}(\infty)$ is given by eq. (2.27) with $p_{(0)} = 1$, *i.e.*,

$$p_{(2\Delta-4)}(\infty) = -\frac{\Gamma\left(\frac{4-\Delta}{2}\right)\Gamma\left(\frac{\Delta}{4}\right)^2}{\Gamma\left(\frac{4-\Delta}{4}\right)^2\Gamma\left(\frac{\Delta}{2}\right)}. \tag{2.64}$$

Equating the two expressions above and using eq. (2.61), we find

$$\ell^2 \quad = \quad \frac{1}{(\Delta-2)\,|p_{(2\Delta-4)}(\infty)|}\,\left(\frac{\lambda_f}{T_f^{4-\Delta}}\right)^2 + o\left(\lambda_f^4\right), \tag{2.65}$$

to leading order in $\lambda_f/T_f^{4-\Delta}$. Note that here we have also used eq. (2.52) to substitute $\mu^4 = \pi^4 T_f^4 + o(\lambda_f^2)$ since the initial and final temperatures will only differ by $o(\lambda_f^2)$ in our perturbative calculations. Further, the above expression takes account of the fact that $p_{(2\Delta-4)}(\infty)$ is always negative in the range of interest, *i.e.*, $2 < \Delta < 4$ — see eq. (2.64) above. Recalling that we set $p_{(0)}(\infty) = 1$, we note that implicitly the right-hand side of eq. (2.65) is actually $\ell^2 p_{(0)}^2$ and so this equation fixes the normalization between the leading coefficient in the asymptotic expansion of the bulk scalar and the boundary coupling, *i.e.*,

$$\ell p_{(0)} = \frac{1}{\sqrt{(\Delta-2)\,|p_{(2\Delta-4)}(\infty)|}}\,\frac{\lambda}{T^{4-\Delta}} + o\left(\lambda^3\right). \tag{2.66}$$

Alternatively in appendix 2.13, we introduced the proportionality constant α_λ in $\ell f_{(0)} = \alpha_\lambda\,\lambda$. So comparing the expansions of the bulk scalar in eqs. (2.26) and (2.12.3) using eq. (2.175) , we now have

$$\alpha_\lambda = \frac{\pi^{4-\Delta}}{\sqrt{(\Delta-2)\,|p_{(2\Delta-4)}(\infty)|}} + o(\lambda^2), \tag{2.67}$$

where as above, we used $\mu^4 = \pi^4 T^4 + o(\lambda^2)$.

2.6.2   Entropy production during the quench

Here we extend the previous analysis to determine the entropy production during the quench. First using the expression for the free energy density (2.56), as well as $F = -\mathcal{P}$, we find

$$\frac{S_f}{S_i} = \frac{T_i}{T_f} \frac{\mathcal{E}_f + \mathcal{P}_f}{\mathcal{E}_i + \mathcal{P}_i} . \tag{2.68}$$

Initially the boundary theory is conformal and the vanishing trace of the stress tensor requires $\mathcal{E}_i = 3\mathcal{P}_i$. Now the latter can be used to re-express eq. (2.68) as

$$\frac{S_f}{S_i} = \frac{T_i}{T_f} \left(\frac{3}{4} \frac{\mathcal{E}_f}{\mathcal{E}_i} + \frac{1}{4} \frac{\mathcal{P}_f}{\mathcal{P}_i} \right) . \tag{2.69}$$

First, we determine the ratio of the temperatures by equating the final energy densities given in terms of the gravitational variables (2.44) and of the boundary theory (2.53). The initial temperature is introduced here by substituting for μ using eq. (2.52), which then yields

$$\frac{T_i}{T_f} = 1 + \frac{\ell^2}{4} \left(a_{2,4}(\infty) - a_{2,4}(-\infty) + \frac{2}{9} \left(2\Delta^2 - 8\Delta + 9 \right) p_{(2\Delta-4)}(\infty) \right) . \tag{2.70}$$

Now using the expressions for the energy density and pressure in eqs. (2.44) and (2.45) at the initial and final times, we find:

$$\frac{\mathcal{E}_f}{\mathcal{E}_i} = 1 - \ell^2 \left(a_{2,4}(\infty) - a_{2,4}(-\infty) + \frac{1}{9} \left(2\Delta - 3 \right) \left(4 - \Delta \right) p_{(2\Delta-4)}(\infty) \right) , \tag{2.71}$$

$$\frac{\mathcal{P}_f}{\mathcal{P}_i} = 1 - \ell^2 \left(a_{2,4}(\infty) - a_{2,4}(-\infty) - \frac{1}{9} \left(4\Delta - 9 \right) \left(4 - \Delta \right) p_{(2\Delta-4)}(\infty) \right) . \tag{2.72}$$

Combining these results in eq. (2.69) then yields

$$\frac{S_f}{S_i} = 1 - \frac{3\ell^2}{4} \left(a_{2,4}(\infty) - a_{2,4}(-\infty) - \frac{2}{9} \left(\Delta - 3 \right) \left(\Delta - 1 \right) p_{(2\Delta-4)}(\infty) \right) . \tag{2.73}$$

Now recall from eq. (2.31) that $a_{2,4}(-\infty) = \mathcal{C}$, where the latter is an arbitrary integration constant. Hence following [48], we choose this constant to simplify the above ratio of entropies, *i.e.*,

$$a_{2,4}(-\infty) = -\frac{2}{9} \left(\Delta - 3 \right) \left(\Delta - 1 \right) p_{(2\Delta-4)}(\infty) . \tag{2.74}$$

Hence, after substituting for ℓ^2 and $a_{2,4}(-\infty)$ from eqs. (2.65) and (2.74), respectively, the ratio of the final and initial entropies (2.73) becomes

$$\frac{S_f}{S_i} = 1 + \frac{3\,a_{2,4}(\infty)}{4\,(\Delta - 2)\,p_{(2\Delta-4)}(\infty)} \left(\frac{\lambda_f}{T_f^{4-\Delta}}\right)^2. \tag{2.75}$$

Further substituting for ℓ^2 and $a_{2,4}(-\infty)$ in eqs. (2.70)–(2.72), we find the change in temperature, energy density and pressure are given by

$$\frac{\Delta T}{T_i} = \left[\frac{\Delta - 2}{6} + \frac{1}{4}\frac{a_{2,4}(\infty)}{(\Delta - 2)\,p_{(2\Delta-4)}(\infty)}\right] \left(\frac{\lambda_f}{T_f^{4-\Delta}}\right)^2, \tag{2.76}$$

$$\frac{\Delta \mathcal{E}}{\mathcal{E}_i} = \left[\frac{1}{3} + \frac{a_{2,4}(\infty)}{(\Delta - 2)\,p_{(2\Delta-4)}(\infty)}\right] \left(\frac{\lambda_f}{T_f^{4-\Delta}}\right)^2, \tag{2.77}$$

$$\frac{\Delta \mathcal{P}}{\mathcal{P}_i} = \left[\frac{2\Delta - 7}{3} + \frac{a_{2,4}(\infty)}{(\Delta - 2)\,p_{(2\Delta-4)}(\infty)}\right] \left(\frac{\lambda_f}{T_f^{4-\Delta}}\right)^2, \tag{2.78}$$

where our notation is *e.g.*, $\Delta \mathcal{P} = \mathcal{P}_f - \mathcal{P}_i$.

The second law of thermodynamics demands that the ratio S_f/S_i must always be greater than one. Hence requiring $a_{2,4}(\infty) \leq 0$ becomes a test of our numerical solutions and we successfully confirm that this inequality is satisfied in the obtained numerical solutions. Since $p_{(2\Delta-4)}(\infty)$ is always negative in our analysis (and we restrict our attention to $\Delta > 2$), eqs. (2.76) and (2.77) indicate that the changes in the temperature and the energy density are always positive. However, from eq. (2.78), the change in pressure is only guaranteed to be positive for $\Delta \geq 7/2$. Otherwise, the pressure can either increase or decrease depending on the precise value of Δ and the magnitude of $a_{2,4}(\infty)$. A more detailed discussion is given in section 2.9.5, where we consider the effect of the numerically determined values of $a_{2,4}(\infty)$ on the shifts of these quantities.

Another check of the present analysis comes from considering the adiabatic limit. As we discuss in section 2.8 in this case, the system remains in a quasi-static equilibrium with $p_{(2\Delta-4)}(t) = p_{(2\Delta-4)}(\infty)\,p_{(0)}(t)$. Substituting this expression into eq. (2.32), as well as using the integration constant chosen in eq. (2.74), it is straightforward to show that $a_{2,4}(\infty)$ vanishes. Hence as expected for an adiabatic transition, no entropy is produced, as discussed in [48].

As a final consistency check, we consider the speed of sound in the thermal plasma,

which is given by

$$c_s^2 = \frac{d\mathcal{P}}{d\mathcal{E}} = \left(\frac{d\mathcal{P}}{dT_f}\right) \Big/ \left(\frac{d\mathcal{E}}{dT_f}\right)$$

$$= \frac{1}{3} - \frac{1}{9}\left(4 - \Delta\right)\left(\Delta - 2\right)\left(\frac{\lambda_f}{T_f^{4-\Delta}}\right)^2. \tag{2.79}$$

Note the second term is negative for all Δ in the range $2 < \Delta < 4$. Hence we find $c_s^2 < 1/3$, as required by [73] for operators with dimension Δ in this range. While $c_s^2 = 1/3$ for $\Delta = 2$ and 4, our analysis only applies for the conformal dimension strictly limited within the range $2 < \Delta < 4$.

2.6.3 Reverse quenches

Up until now we have assumed that the quenches begin with the boundary theory being conformal, *i.e.*, $\lambda = 0$ and then end with some finite λ. In the gravitational description then, they involve some profile $p_{(0)}(\tau)$ which begins with $p_{(0)} = 0$ at $\tau = -\infty$ and ends with $p_{(0)} = 1$ at $\tau = \infty$. In this section, we consider 'reverse' quenches in which the coupling is initially finite and is brought down to zero. In particular, we can readily repeat the analysis for reverse quenches where the non-normalizable coefficient of the bulks scalar is chosen to be

$$\tilde{p}_{(0)}(\tau) = 1 - p_{(0)}(\tau). \tag{2.80}$$

Because our analysis is limited to the perturbative high temperature regime, the equation of motion (2.22) for the bulk scalar is linear and hence we can add any two solutions to produce a third solution. In particular then, adding the scalar field solutions for the forward and reverse quench must yield the equilibrium solution with $p_{(0)}(\tau) = 1$. Alternatively, the reverse quench produced from eq. (2.80) is simply the equilibrium solution (2.25) (with $c_1 = 1$) minus the time-dependent solution describing the forward quench. In the equilibrium case, the normalizable coefficient in the bulk scalar is $p_{(2\Delta-4)}(\infty)$ and so the corresponding coefficient in the reverse quench must be

$$\tilde{p}_{(2\Delta-4)}(\tau) = p_{(2\Delta-4)}(\infty) - p_{(2\Delta-4)}(\tau), \tag{2.81}$$

where $p_{(2\Delta-4)}(\tau)$ denotes the response produced in the original (forward) quench.

In the reverse quench, the metric coefficient $\tilde{a}_{2,4}$ still satisfies eq. (2.31) and so we have

47

the solution

$$\tilde{a}_{2,4}(\tau) = \tilde{\mathcal{C}} - \frac{1}{9}(4-\Delta)(2\Delta-3)\tilde{p}_{(0)}(\tau)\tilde{p}_{(2\Delta-4)}(\tau)$$
$$+\frac{2}{3}(\Delta-2)\int_{-\infty}^{\tau}d\tau'\tilde{p}_{(2\Delta-4)}(\tau')\dot{\tilde{p}}_{(0)}(\tau'). \tag{2.82}$$

where $\tilde{\mathcal{C}}$ is a new integration constant. Note that in this case, the second term vanishes for $\tau \to \infty$ but as $\tau \to -\infty$, it is proportional to $\tilde{p}_{(2\Delta-4)}(-\infty) = p_{(2\Delta-4)}(\infty)$. Repeating the analysis of the previous section for our reverse quench and demanding that the entropy production is now proportional to $\tilde{a}_{2,4}$, we find that the integration constant must be chosen as

$$\tilde{\mathcal{C}} = \frac{1}{3}(\Delta-2)\tilde{p}_{(2\Delta-4)}(-\infty). \tag{2.83}$$

With this choice then, we have

$$\frac{S_f}{S_i} = 1 + \frac{3\tilde{a}_{2,4}(\infty)}{4(\Delta-2)\tilde{p}_{(2\Delta-4)}(-\infty)}\left(\frac{\lambda_f}{T_f^{4-\Delta}}\right)^2. \tag{2.84}$$

Further, when we compare the expression for $\tilde{a}_{2,4}(\infty)$ with eq. (2.32) for $a_{2,4}(\infty)$, it is straightforward to show that these two constants are equal, *i.e.*,

$$\tilde{a}_{2,4}(\infty) = a_{2,4}(\infty), \tag{2.85}$$

just as was found in [48]. Hence comparing to eqs. (2.75) and (2.84) and noting that $\tilde{p}_{(2\Delta-4)}(-\infty) = p_{(2\Delta-4)}(\infty)$, we see that the entropy production is identical in the forward and reverse quenches.

We can also find the changes in the temperature, the energy density and pressure as before:

$$\frac{\Delta T}{T_i} = \left[-\frac{\Delta-2}{6} + \frac{1}{4}\frac{\tilde{a}_{2,4}(\infty)}{(\Delta-2)\tilde{p}_{(2\Delta-4)}(\infty)}\right]\left(\frac{\lambda_f}{T_f^{4-\Delta}}\right)^2, \tag{2.86}$$

$$\frac{\Delta\mathcal{E}}{\mathcal{E}_i} = \left[-\frac{1}{3} + \frac{\tilde{a}_{2,4}(\infty)}{(\Delta-2)\tilde{p}_{(2\Delta-4)}(\infty)}\right]\left(\frac{\lambda_f}{T_f^{4-\Delta}}\right)^2, \tag{2.87}$$

$$\frac{\Delta\mathcal{P}}{\mathcal{P}_i} = \left[-\frac{2\Delta-7}{3} + \frac{\tilde{a}_{2,4}(\infty)}{(\Delta-2)\tilde{p}_{(2\Delta-4)}(\infty)}\right]\left(\frac{\lambda_f}{T_f^{4-\Delta}}\right)^2, \tag{2.88}$$

48

where again *e.g.,* $\Delta\mathcal{P} = \mathcal{P}_f - \mathcal{P}_i$. Comparing these expressions for the reverse quench with the corresponding results in eqs. (2.76)–(2.78) for the forward case, we see that $a_{2,4}(\infty)$ and $\tilde{a}_{2,4}(\infty)$ have the same coefficients while the constant terms are equal but with opposite sign. Hence for the reverse quenches, whether any of these physical quantities increases or decreases depends on both the magnitude of $\tilde{a}_{2,4}(\infty)$ and the value of Δ — see section 2.9.5 for a further discussion. We also note that in the case of an adiabatic quench (see section 2.8), we find $a_{2,4}(\infty) = 0$ and hence $\tilde{a}_{2,4}(\infty) = 0$. That is, for adiabatic transitions, no entropy is produced. However, we would also find that the changes in the temperature, energy density and pressure are exactly opposite in the forward and reverse cases.

Since the forward and reverse quenches are simply related in our perturbative high temperature analysis, we will continue to focus on the forward quenches in the rest of the chapter.

2.7 Numerical procedure

We now briefly describe the numerical simulations which we used to understand the quenches. Essentially we implemented the same approach as in [48], using numerical techniques developed in [74, 75]. For details on our numerical implementation, please refer to appendix in 2.14. The primary purpose of our simulations was to find the response $p_{(2\Delta-4)}(\tau)$ for a given source $p_{(0)}(\tau)$, as described earlier, it is convenient to work with infalling characteristics and in particular we adopt Eddington-Finkelstein coordinates as in eq. (2.8) or (2.21). These coordinates are regular at the horizon allowing us to excise the black hole from the computational domain (by integrating some distance inwards and stopping the integration as this region is causally disconnected from the outside).

We choose the source term in the asymptotic expansion (2.26) of the bulk scalar to be

$$p_{(0)}(\tau) = \frac{1}{2} + \frac{1}{2}\tanh(\frac{\tau}{\alpha}). \tag{2.89}$$

This describes a family of quenches where, as desired, the source starts at zero in the asymptotic past and ends at one in the asymptotic future. Here α controls the rate at which the quench takes place. In terms of the dimensionful time, we have $\tau = \mu v \simeq \mu t$ and hence the timescale on which the transition from zero to finite coupling is made is

$$\delta t = \frac{\alpha}{\mu} \simeq \frac{\alpha}{\pi T_i}. \tag{2.90}$$

Hence for $\alpha \gg 1$, the quenches are 'slow' which means that the transition occurs on a timescale that is much longer than the thermal relaxation timescale. Alternatively for

$\alpha \ll 1$, the quenches are 'fast', meaning the transition timescale is much shorter than the thermal timescale. The limit $\alpha \to 0$ would correspond to an 'instantaneous' quench, *i.e.*, $p_{(0)}$ becomes a step-function. The limit $\alpha \to \infty$ corresponds to an adiabatic transition — see section 2.8. We note that with eq. (2.89), the source profile has a continuous derivative for all time. More general quenches which are not infinitely differentiable with respect to time will be studied in the following chapter.

Again the goal of our simulations is to find the response $p_{(2\Delta-4)}(\tau)$ for a given source $p_{(0)}(\tau)$. Practically, it is more convenient to solve the linearized scalar equation (2.22) in terms of $\hat{\psi}(\tau, \rho)$, which is defined by

$$
\hat{\phi}\left(t, \rho\right) \;\; = \;\; \rho^{4-\Delta} \left(p_{(0)} + \rho \dot{p}_{(0)} + \frac{(2\Delta - 7)\rho^2}{4(\Delta - 3)} \ddot{p}_{(0)} + \cdots \right) + \rho^\kappa \, \hat{\psi}(\tau, \rho) . \qquad (2.91)
$$

Here the term in brackets contains the leading terms in the asymptotic expansion (2.26) of $\hat{\phi}$. In particular, we include any terms which are leading compared to ρ^Δ. Formally then the leading solution takes the form $= \rho^{\Delta-\kappa} p_{(2\Delta-4)} + \cdots$ and so the leading behaviour in $\hat{\psi}$ contains the desired response function. However, as a practical matter, we obtained noticeably better accuracy for $p_{(2\Delta-4)}$ by fitting $\hat{\psi}$ (at each timestep) with an expansion of the form

$$
\hat{\psi}(\tau, \rho) = \epsilon_0 \rho^{4-\Delta-\kappa} + \epsilon_1 \rho^{5-\Delta-\kappa} + \cdots + \rho^{\Delta-\kappa} p_{(2\Delta-4)} + \delta_n \rho^{4-\Delta-\kappa+n} + o\left(\rho^{\Delta-\kappa+1}\right) , \quad (2.92)
$$

where $\rho^{4-\Delta-\kappa+n}$ is the next leading order after $\rho^{\Delta-\kappa}$. The coefficients ϵ_i are, of course, all very small since the terms at these orders are already included in eq. (2.91). The factor δ_n is typically not small, but including this term nonetheless gives better results when fitting $p_{(2\Delta-4)}$. In the cases that we choose $\kappa > 4 - \Delta$, we only include terms in eq. (2.92) with nonnegative powers of ρ.

We introduce κ for convenience in the fit and choose it so that $\hat{\psi}$ still vanishes at the asymptotic boundary, *i.e.*, $\rho = 0$. We further choose κ so that the relative power of ρ between the two contributions in eq. (2.91) is an integer, *i.e.*, $\Delta + \kappa$ is an integer. This ensures that upon substituting into the equation of motion (2.22), after simplification, only integer powers of ρ appear in the coefficients of $\hat{\psi}$ and its derivatives, as well as in the source terms. Our choices of κ, for each of the conformal dimensions considered in our simulations, are shown in table 2.1.

Once the numerical solution has been obtained at each timestep, we fit $\hat{\psi}$ with a series in ρ with rational exponents, as described above, to determine the coefficient $p_{(2\Delta-4)}$. Repeating this process for each timestep then generates the full profile for $p_{(2\Delta-4)}(\tau)$.

Table 2.1: Choices made for κ while simulating $\hat{\psi}(\tau, \rho)$ for various Δ.

Δ	7/3	8/3	10/3	11/3	4
κ	5/3	4/3	5/3	1/3	2

2.8   Slow quenches and the adiabatic limit

In this section, we consider the case where the transition between the initial and final theories is made arbitrarily slow. In fact, we find an analytic solution of $a_{2,4}$ for such slow quenches below. The results derived from this approach provide an independent check for our numerical solutions — see the discussion in section 2.10.

Let us first consider the adiabatic limit: Given our choice for the integration constant $a_{2,4}(-\infty)$ in eq. (2.74), the expression (2.32) for $a_{2,4}(\infty)$ after equilibration becomes

$$a_{2,4}(\infty) = -\frac{1}{3}\left(\Delta - 2\right) p_{(2\Delta-4)}(\infty) + \frac{2}{3}\left(\Delta - 2\right) \int_{-\infty}^{\infty} d\tau' p_{(2\Delta-4)}(\tau')\, \dot{p}_{(0)}(\tau')\,. \qquad (2.93)$$

As noted in [48], in the adiabatic limit, the system remains in a quasi-static equilibrium throughout the transition. Hence the ratio of the normalizable and non-normalizable coefficients in the bulk scalar are precisely as given in eq. (2.27) at every stage of the transition, *i.e.*,

$$\text{adiabatic}: \qquad p_{(2\Delta-4)}(\tau) = p_{(2\Delta-4)}(\infty)\, p_{(0)}(\tau)\,. \qquad (2.94)$$

In this case, the integral in eq. (2.93) becomes

$$\begin{aligned}\int_{-\infty}^{\infty} d\tau' p_{(2\Delta-4)}(\tau')\, \dot{p}_{(0)}(\tau') &= \frac{1}{2}p_{(2\Delta-4)}(\infty)\, \int_{-\infty}^{\infty} d\tau'\, \partial_{\tau'}\!\left(p_{(0)}(\tau')\right)^2 \\ &= \frac{1}{2}p_{(2\Delta-4)}(\infty)\,. \qquad (2.95)\end{aligned}$$

Given this result, we easily see that $a_{2,4}(\infty)$ (and hence the entropy production) vanishes in the adiabatic limit.

For arbitrarily slow quenches, the response should approach the adiabatic profile (2.94) as a limit. Given the profile in eq. (2.89), this slow limit is achieved by taking α large. Then following [48], we can write the bulk scalar $\hat{\phi}$ in an expansion in inverse powers of α, *i.e.*,

$$\hat{\phi} = p_{(0)}\left(\tau\right) \phi_{\text{e}}(\rho) + \sum_{n=1}^{\infty} \alpha^{-n}\, p_s^{(n)}(\tau)\, R_s^{(n)}(\rho)\,, \qquad (2.96)$$

where $p_{(0)}(\tau)$ is the profile in eq. (2.89) and $\phi_{\mathrm{e}}(\rho)$ is the equilibrium solution given in eq. (2.25) (with $c_1 = 1$). Hence the first term above is the desired solution describing an adiabatic transition, *i.e.*, this term yields the response in eq. (2.94). We have assumed that each of the subsequent terms in the series are separable and this form is easily confirmed, *e.g.*, see below.

Let us solve for the first correction in eq. (2.96), $p_s^{(1)}(\tau) \, R_s^{(1)}(\rho)$, since this term produces the leading contribution to $a_{2,4}$ in the slow quench limit. Substituting our ansatz (2.96) into the decoupled Klein-Gordon equation (2.22), we find at order α^{-1}

$$p_s^{(1)}(\tau) \left[-\rho^2 \left(1 - \rho^4\right) \partial_\rho^2 + \rho \left(\rho^4 + 3\right) \partial_\rho + m^2 \right] R_s^{(1)}(\rho)$$
$$= \alpha \, \dot{p}_{(0)} \, \rho \left(3 - 2\rho \, \partial_\rho\right) \phi_{\mathrm{e}}(\rho) \,. \tag{2.97}$$

Note that $\alpha \, \dot{p}_{(0)}$ is order α^0 in our expansion because the derivative of $p_{(0)}$ brings out a factor of $1/\alpha$. Now solving eq. (2.97), requires that the time-dependent function takes the form $p_s^{(1)}(\tau) = \alpha \, \dot{p}_{(0)}$ while the radial profile satisfies the inhomogeneous equation:

$$\left[-\rho^2 \left(1 - \rho^4\right) \partial_\rho^2 + \rho \left(\rho^4 + 3\right) \partial_\rho + \Delta(\Delta - 4) \right] R_s^{(1)}(\rho) = \rho \left(3 - 2\rho \, \partial_\rho\right) \phi_{\mathrm{e}}(\rho) \,. \tag{2.98}$$

The solution to the above equation can be written in series form as

$$R_s^{(1)}(\rho) = \rho^{4-\Delta} \sum_{n=0}^{\infty} a_{(n)} \rho^n + \rho^{\Delta} \sum_{n=0}^{\infty} b_{(n)} \rho^n \,. \tag{2.99}$$

Here we have two independent integration constants, $a_{(0)}$ and $b_{(0)}$. The first coefficient $a_{(0)}$ is set to zero, since the order $\rho^{4-\Delta}$ contribution to $\hat{\phi}$ defines the source and we do not want any new sources beyond $p_{(0)}$ to appear at higher orders in the $1/\alpha$ expansion in eq. (2.96). To determine $b_{(0)}$, we demand that $R_s^{(1)}(\rho)$ is regular on the event horizon at $\rho = 1$. To analyze the profile close to the horizon, we make the change of coordinates $z = 1 - \rho$ and solve for $R_s^{(1)}(z)$. Near $z = 0$, we may write $R_s^{(1)}(z)$ as the series

$$R_s^{(1)}(z) = \sum_{n=0}^{\infty} c_{(n)} z^n \,, \tag{2.100}$$

which includes only the solution that is well-behaved at $z = 0$. In this series, we now have the undetermined coefficient $c_{(0)}$.

To proceed further, we resorted to solving eq. (2.98) numerically. In particular, we produced independent solutions integrating in from $z = 1$ (or $\rho = 0$) and integrating out

from $z = 0$ (or $\rho = 1$). Then by matching the two solutions for $R_s^{(1)}$ at an intermediate point between the asymptotic boundary and horizon, we solved for both $b_{(0)}$ and $c_{(0)}$ simultaneously. This shooting method was used to solve for the undetermined coefficients in the cases $\Delta = \frac{7}{3}$, $\frac{8}{3}$, $\frac{10}{3}$ and $\frac{11}{3}$. We should emphasize that although this approach is again numerical, it is an independent approach very different in spirit from the numerical approach described previously.[3]

Comparing the present solution with the expansion in eq. (2.26), we see that the corrected response takes the form

$$p_{(2\Delta-4)}(\tau) = p_{(2\Delta-4)}(\infty)\, p_{(0)}(\tau) - b_{(0)}\, \dot{p}_{(0)}(\tau) + o(1/\alpha^2)\,. \tag{2.101}$$

Again the second term above is of order $1/\alpha$ because the derivative acting on $p_{(0)}(\tau)$ brings out this factor. Now upon substituting this expression into eq. (2.93), the adiabatic response yields zero and so we are left with

$$
\begin{aligned}
a_{2,4}(\infty) &= -\frac{2}{3}\,(\Delta - 2)\, b_{(0)} \int_{-\infty}^{\infty} d\tau'\, \dot{p}_{(0)}^2(\tau') + o(1/\alpha^2) \\
&= -\frac{2}{9\alpha}\,(\Delta - 2)\, b_{(0)} + o(1/\alpha^2)\,,
\end{aligned} \tag{2.102}
$$

where the final result is produced by inserting eq. (2.89) for $p_{(0)}$. Hence given the numerical solution for $b_{(0)}$ for each value of Δ listed above, we can determine the leading contribution to $a_{2,4}$ for slow quenches. Our results are as follows:

$$
\begin{aligned}
\Delta = \frac{7}{3}: \quad & a_{2,4}(\infty) = -0.01958\,\frac{1}{\alpha}\,, \\
\Delta = \frac{8}{3}: \quad & a_{2,4}(\infty) = -0.05205\,\frac{1}{\alpha}\,, \\
\Delta = \frac{10}{3}: \quad & a_{2,4}(\infty) = -0.09838\,\frac{1}{\alpha}\,, \\
\Delta = \frac{11}{3}: \quad & a_{2,4}(\infty) = -0.1083\,\frac{1}{\alpha}\,.
\end{aligned} \tag{2.103}
$$

These results compare well to our numerical results, as discussed below in section 2.10. See also appendix 2.15, where we analytically solve equation (2.212) and determine $b_{(0)}$ as a numerical integral, obtaining almost identical results to the shooting method used above.

---

[3]It is straightforward to write a formal Green's function solution for eq. (2.98), as shown in appendix 2.15. Given this form of the solution, the coefficient $b_{(0)}$ can be determined by numerically evaluating a specific integral. The results produced this way agree well with those given in eq. (2.212).

2.9 Results

We now turn to the results of our numerical simulations. We determined the response functions for various values of α and with several different masses of the bulk scalar. Explicitly, the scalar masses for which we studied the quenches are: $m^2 = -\frac{35}{9}$ (with $\Delta = \frac{7}{3}$), $m^2 = -\frac{32}{9}$ (with $\Delta = \frac{8}{3}$), $m^2 = -\frac{20}{9}$ (with $\Delta = \frac{10}{3}$) and $m^2 = -\frac{11}{9}$. The masses were chosen so that the conformal dimension lies in the desired range $2 < \Delta < 4$ and so that $4 - 2\Delta$ is not an integer. The latter ensures that the asymptotic expansion (2.26) for the scalar does not contain any logarithmic terms. We further comment on $\Delta = 4$ case, which together with results of [48] would form a complete picture of perturbative quenches in strongly couple gauge theories induced by the coupling of a relevant operator.

In subsection 2.9.1, we extract the response function $p_{(2\Delta-4)}$ for fast quenches (*i.e.,* $\alpha < 1$) from our numerical data for each Δ. From that we see that $a_{2,4}$ and the maximum displacement of $p_{(2\Delta-4)}$ follows a scaling behaviour for fast quenches. In subsection 2.9.2, we see that the scaling of these quantities follow a universal behaviour, determined by Δ and α only. In subsection 2.9.3, we show the numerical results for slow quenches (*i.e.,* $\alpha > 1$). We show that for very large α, $p_{(2\Delta-4)}$ approaches the adiabatic response (2.94). We also find that $a_{2,4}$ scales as α^{-1}, as expected from the analysis in section 2.8. Finally, in subsection 2.9.4, we study the excitation times of the response, by considering when it first deviates from the adiabatic response by more than 5% (an arbitrary threshold). We find that for fast quenches, the scaled excitation time τ_{ex}/α scales logarithmically with the quenching parameter α. We also see a universal behaviour in the slopes $-\left(\frac{\partial(\tau_{ex}/\alpha)}{\partial \log \alpha}\right)$ in the fast quench limit for fractional Δ. In the same subsection we study the relaxation times for the quenches, defined by the last time that $p_{(2\Delta-4)}$ falls below a 5% deviation from its final equilibrium value.

2.9.1 Response for fast quenches

Here we list the results for intermediate to fast quenches (*i.e.,* $\alpha < 1$). We first find the response $p_{(2\Delta-4)}$ and then determine the coefficient $a_{2,4}(\infty)$ using equation (2.32), as well as the integration constant $a_{2,4}(-\infty)$ in eq. (2.74). By doing multiple simulations of the time-dependent behaviour of $p_{(2\Delta-4)}$ with increasingly finer discretizations, we can extrapolate for the continuum value of $a_{2,4}(\infty)$. Knowing $a_{2,4}(\infty)$, we can determine the response of various physical quantities in the boundary theory to the quench, using eqs. (2.75)–(2.78). Note that these results would also apply to the reverse quenches, as discussed in section 2.6.3. We also study the behaviour of $p_{(2\Delta-4)}$ and $a_{2,4}(\infty)$ as functions of α. In the

next subsection, we compare this α dependence for different values of Δ and identify the universal behaviour for operators of different dimension.

In figure 2.1, we plotted $p_{(2\Delta-4)}$ against time for various values of α. The time is rescaled by a factor of $1/\alpha$ so that the different plots equilibrate in approximately the same distance on the horizontal axis. In each of the plots, we have also rescaled the vertical axis by $\alpha^{2\Delta-4}$. Hence the maximum displacement of $p_{(2\Delta-4)}$ is actually growing with decreasing α. With the rescaled axes, the peaks corresponding to smaller α lie close together, which seems to indicate that there is a universal scaling depending on the operator dimension. Further with these scalings, the response seems to converge to a particular limit with decreasing α. For fast enough quenches, we expect these plots to coincide exactly.

In figure 2.2, we show a different visualization of the same fast quenches. Here, $\alpha^{2\Delta-4}p_{(2\Delta-4)}$ is plotted as a function of the source $p_{(0)}$. It is perhaps easier to see the convergence of the faster quenches to a limiting curve. Note that because of the growth of $p_{(2\Delta-4)}$ for fast quenches, the expression (2.32) for $a_{2,4}(\infty)$ is dominated by the integral. Further the latter can be re-expressed as $\int_0^1 dp_{(0)} p_{(2\Delta-4)}$ and so for these fast quenches, $a_{2,4}(\infty)$ is essentially given by the area under the curves in figure 2.2.

In figure 2.3,[4] we see that $\log(-a_{2,4}(\infty))$ plotted against $\log \alpha$ tends to a straight line for small values of α. This indicates that $a_{2,4}(\infty)$ scales as some power law of the quenching parameter α for very fast quenches. A fit of this linear behaviour suggests the slope matches $4 - 2\Delta$ in each case. The lines shown in the plot are the linear fits through the points corresponding to the three fastest quenches, thus showing the asymptotic behaviour of $a_{2,4}(\infty)$ for fast quenches. Although it is not shown, for small values of α, the logarithm of $\max\{|p_{(2\Delta-4)}|\}$ plotted against $\log \alpha$ also tends to a straight line with the same slope as in the plot of $\log(-a_{2,4}(\infty))$.

As discussed in [48] and the following chapter, the scaling of the response $p_{(2\Delta-4)}$ for fast quenches is more subtle when $\Delta = 2, 3$ and 4. Specifically, it is rather the 'subtracted' response, defined by

$$\hat{p}_{(2\Delta-4)} \equiv p_{2\Delta-4} + \begin{cases} \ln\alpha\; p_{(0)}\,, & \text{for } \Delta = 2\,, \\ \frac{1}{2}\ln\alpha\; \ddot{p}_{(0)}\,, & \text{for } \Delta = 3\,, \\ -\frac{1}{16}\ln\alpha\; \ddddot{p}_{(0)}\,, & \text{for } \Delta = 4\,, \end{cases} \tag{2.104}$$

which scales faithfully in the limit of fast quenches, *i.e.,*

$$\lim_{\alpha \to 0} \alpha^{2\Delta-4}\hat{p}_{(2\Delta-4)} \;=\; \text{constant}\,. \tag{2.105}$$

---

[4]Note that we plot the logarithm of $-a_{2,4}(\infty)$ since $a_{2,4}(\infty)$ is always negative.
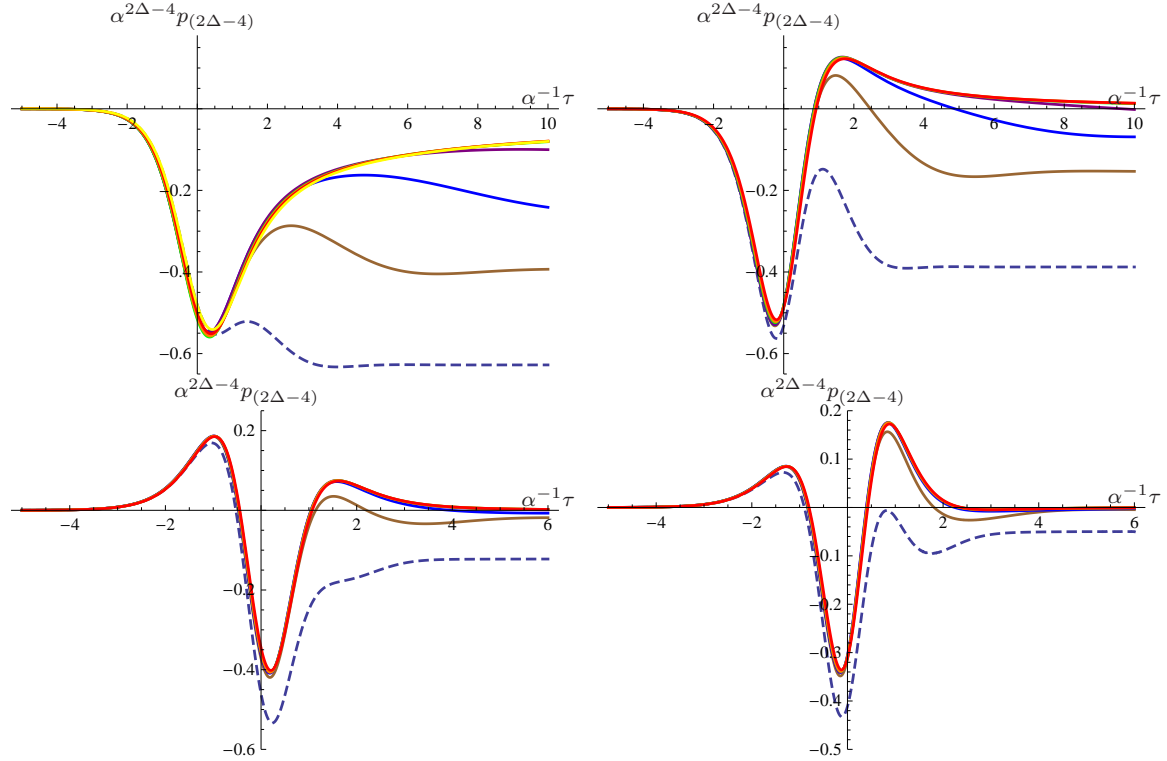
Figure 2.1: Plots of the response coefficient $p_{(2\Delta-4)}$ for quenches of different speeds, in the fast quench regime. Time is rescaled by a factor of $1/\alpha$ and the value of $p_{(2\Delta-4)}$ is rescaled by $\alpha^{2\Delta-4}$. Clockwise from the top left, the plots are for $\Delta = 7/3$, $8/3$, $11/3$ and $10/3$. In each case, the response is presented for $\alpha = 1$ (dashed), $1/2$(brown), $1/4$ (blue), $1/8$ (purple), $1/16$ (green), $1/32$ (orange) and $1/64$ (red) (as well as $\alpha = 1/128$ (yellow) for $\Delta = 7/3$).
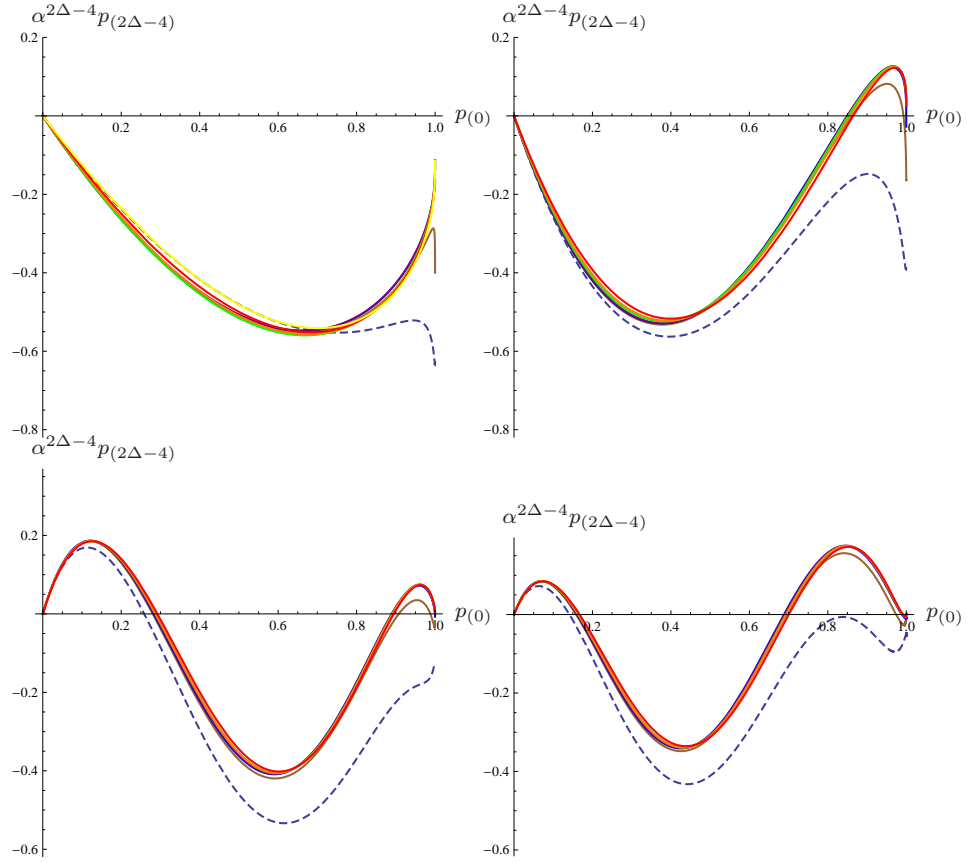
Figure 2.2: Plots of $p_{(2\Delta-4)}$ for quenches of different speeds, in the fast quench regime. $p_{(2\Delta-4)}$ is rescaled by $\alpha^{2\Delta-4}$ and is plotted against the actual value of the source $p_{(0)}$. Clockwise from the top left, the plots are for $\Delta = 7/3$, $8/3$, $11/3$ and $10/3$. In each case, the response is presented for various values of α, which are indicated using the same colour scheme as in figure 2.1.

57
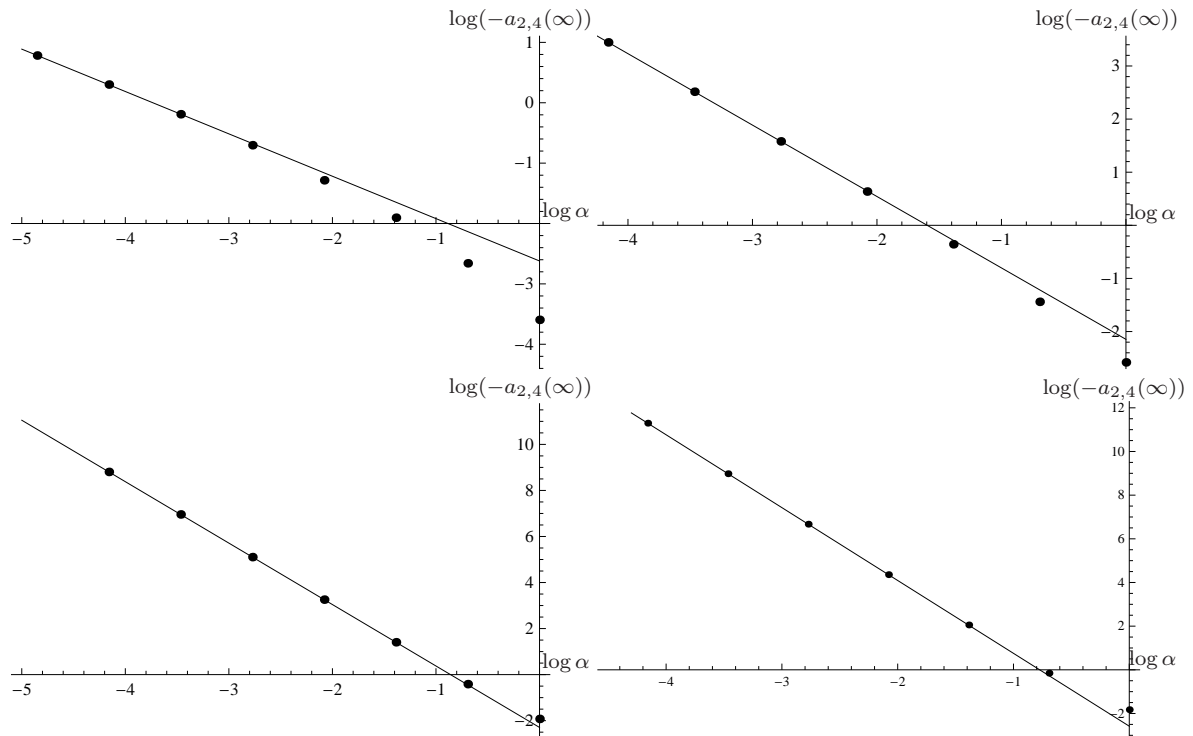
Figure 2.3: log-log plots for $-a_{2,4}(\infty)$ versus α for various Δ, in the fast quench regime. The straight lines shown are least-squares fits through the three leftmost data-points in each case. The fact that the plots tend to straight lines for negative values of $\log \alpha$ means that $a_{2,4}(\infty)$ scales as a power law for small α. Clockwise from the top left, the plots are for $\Delta = 7/3$, $8/3$, $11/3$ and $10/3$.

Notice, however, that the additional $\ln \alpha$ terms in $p_{2\Delta-4}$ above do not contribute to $a_{2,4}(\infty)$ for $\Delta = 3$ or 4. For these cases, we have

$$\Delta = 3 : \qquad \int_{-\infty}^{\infty} d\tau \; \dddot{p}_{(0)}(\tau) \, \dot{p}_{(0)}(\tau) = \left[\frac{1}{2} \dot{p}_{(0)}(\tau)^2 \right]_{-\infty}^{\infty} = 0 \qquad (2.106)$$

$$\Delta = 4 : \qquad \int_{-\infty}^{\infty} d\tau \; p_{(0)}(\tau) \, \dot{p}_{(0)}(\tau) = \left[\dddot{p}_{(0)}(\tau) \, \dot{p}_{(0)}(\tau) - \frac{1}{2} \ddot{p}_{(0)}(\tau)^2 \right]_{-\infty}^{\infty} = 0$$

which, as we have indicated, both vanish for a generic source $p_{(0)}$ as long as the profile becomes constant as $\tau \to \pm\infty$. Hence for $\Delta = 3$ and 4, we still have $a_{2,4}(\infty) \sim 1/\alpha^{2\Delta-4}$ for fast quenches as $\alpha \to 0$. On the other hand, as shown in [48], the logarithmic term in eq. (2.104) gives the dominant contribution in eq. (2.32) for fast quenches with $\Delta = 2$ and we have instead

$$a_{2,4}(\infty) = \frac{1}{6} \, \ln \alpha + o(1), \qquad \text{as } \alpha \to 0 \,. \qquad (2.107)$$

2.9.2 Universal behaviour for fast quenches

For fast quenches, our numerics above suggested that $-a_{2,4}(\infty)$ grows as $\alpha^{-(2\Delta-4)}$ as α becomes arbitrarily small. This behaviour is confirmed in figure 2.4. This plot shows $\frac{-d\log(-a_{2,4}(\infty))}{d\log\alpha}$ versus Δ for $\Delta = 2$, $\Delta = 7/3$, $\Delta = 8/3$, $\Delta = 3$, $\Delta = 10/3$, $\Delta = 11/3$ and $\Delta = 4$. The data-points are the slopes of the straight line fits for the plots shown in figure 2.3. The data-points for $\Delta = 2$ and $\Delta = 3$ are taken from [48] while the data-point for $\Delta = 4$ is taken from [76]. We set the log derivative to zero for $\Delta = 2$ but, as noted above in eq. (2.107), $a_{2,4}(\infty)$ actually scales as a logarithm of α [48].

As well as the individual data-points, we have plotted the line

$$-\frac{d\log[-a_{2,4}(\infty)]}{d\log\alpha} = 2\Delta - 4 \,. \qquad (2.108)$$

In fact, a least-squares fit through the data-points yields

$$-\frac{d\log[-a_{2,4}(\infty)]}{d\log\alpha} = 1.99\Delta - 3.96 \,, \qquad (2.109)$$

which matches the expected trend within our numerical accuracy. Hence figure 2.4 confirms the universal scaling

$$|a_{2,4}(\infty)| \propto \frac{1}{\alpha^{2\Delta-4}} \qquad (2.110)$$

Figure 2.4: Plot of the asymptotic scaling of $-a_{2,4}(\infty)$ as a power of α, in the fast quench limit. The line shown is the predicted theoretical trend $\frac{-d\log(-a_{2,4}(\infty))}{d\log\alpha} = 2\Delta - 4$. Points shown are for $\Delta = 2, 7/3, 8/3, 3, 10/3, 11/3$ and 4. The datapoints for $\Delta = 2, 3$ are taken from [48]. The datapoint for $\Delta = 4$ is taken from [76].

60

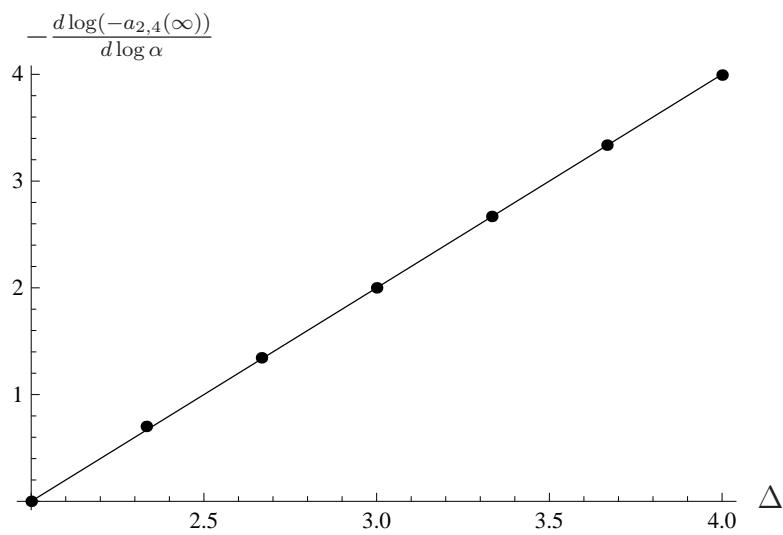for fast quenches by an operator with $2 < \Delta \leq 4$.

As noted above, the maximum displacement of $p_{(2\Delta-4)}$ seems to exhibit the same scaling behaviour as above when Δ is fractional. However, as also commented above for $\Delta = 2$, both $a_{2,4}(\infty)$ and $p_{(2\Delta-4)}$ grow as $-\log \alpha$ for small α [48]. Similarly, for small α with $\Delta = 3$ and 4, $a_{2,4}(\infty)$ has the above scaling but the maximum displacement of $p_{(2\Delta-4)}$ exhibits an additional $\log \alpha$ growth on top of this simple scaling — see further discussion around eq. (2.104) and in [48].

2.9.3 Response for slow quenches

In figure 2.5, we plotted $p_{(2\Delta-4)}$ as a function of τ for the various values of Δ and α. The time is scaled by α^{-1} so that the different plots would equilibrate in approximately the same distance on the horizontal axis. As α grows large, the curves approach an inverted tanh graph, which is the expected adiabatic limit, *i.e.*, $p_{(2\Delta-4)}(\infty) \, p_{(0)}(\tau)$ — see eq. (2.94). Note that in this case there is no need to rescale the vertical axis since $p_{(2\Delta-4)}$ is of the same order in all cases.

As discussed in section 2.8, $a_{2,4}(\infty)$, which controls the entropy production, goes to zero in the adiabatic limit. Further, the analysis there showed that the leading contribution gave $a_{2,4}(\infty) \propto 1/\alpha$ for slow quenches — see eq. (2.102). This behaviour is revealed in our numerical results in figure 2.6. There $\log(-a_{2,4}(\infty))$ is shown as a function of $\log \alpha$ and we see that for large α, the results can be fit with a straight line with a slope of approximately -1 in all the plots shown. Similar to the fast quench case, the straight lines are fit through the last three data-points in each plot.[5] Further the intercepts of the straight lines in figure 2.6 should correspond to (minus the logarithm of) the coefficients given in eq. (2.212). We defer the detailed comparison of the results derived in section 2.8 and with the numerical simulations here until section 2.10.

Again, although not shown, the same behaviour was also found for slow quenches in the case $\Delta = 4$. This behaviour was also found to hold for $\Delta = 2$ and 3 in [48].

For slow quenches, let us define the deviation of the response from the adiabatic limit (2.94) as

$$\hat{p}_{(2\Delta-4)}(\tau) = \alpha \left(p_{(2\Delta-4)}(\tau) - p_{(2\Delta-4)}\left(\infty\right) p_{(0)}(\tau) \right). \tag{2.111}$$

As discussed in section 2.8, this function should be approximately given by $b_{(0)}\dot{p}_{(0)}$, where $b_{(0)}$ was the coefficient of the normalizable mode in the radial profile of the $1/\alpha$ contribution.

---

[5]Note that in the case $\Delta = 7/3$ we fit the line through three intermediate points, since our result for $a_{2,4}(\infty)$ contained a significant numerical error for the largest value of α shown.
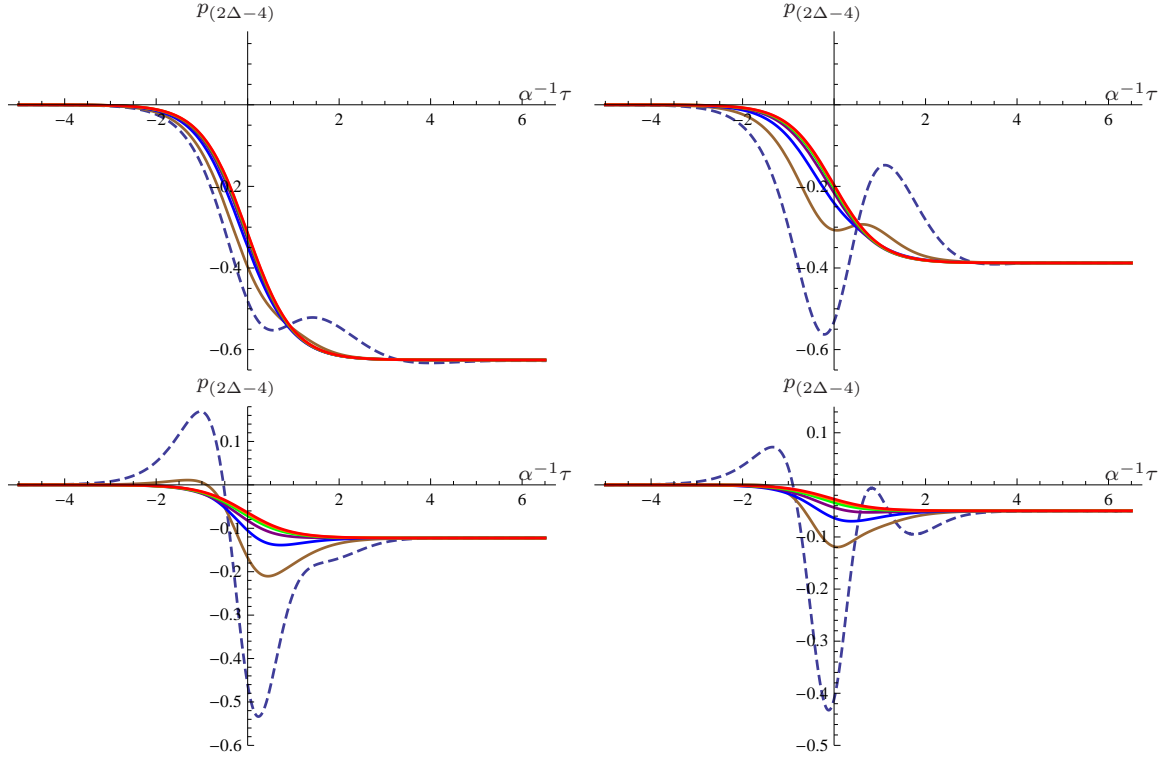
Figure 2.5: Plots of $p_{(2\Delta-4)}$ for quenches of different speeds in the slow quench regime. Time is rescaled by a factor of α^{-1} and the value of $p_{(2\Delta-4)}$ is rescaled by $\alpha^{2\Delta-4}$. Plots for larger α follow an inverted tanh-profile more closely, which is a negative constant times the source. Clockwise from the top left, the plots are for $\Delta = 7/3$, $8/3$, $11/3$ and $10/3$. In each case, the response is presented for $\alpha = 1$ (dashed), 2 (brown), 4 (blue), 8 (purple), 16 (green), 32 (orange) and 64 (red).

62
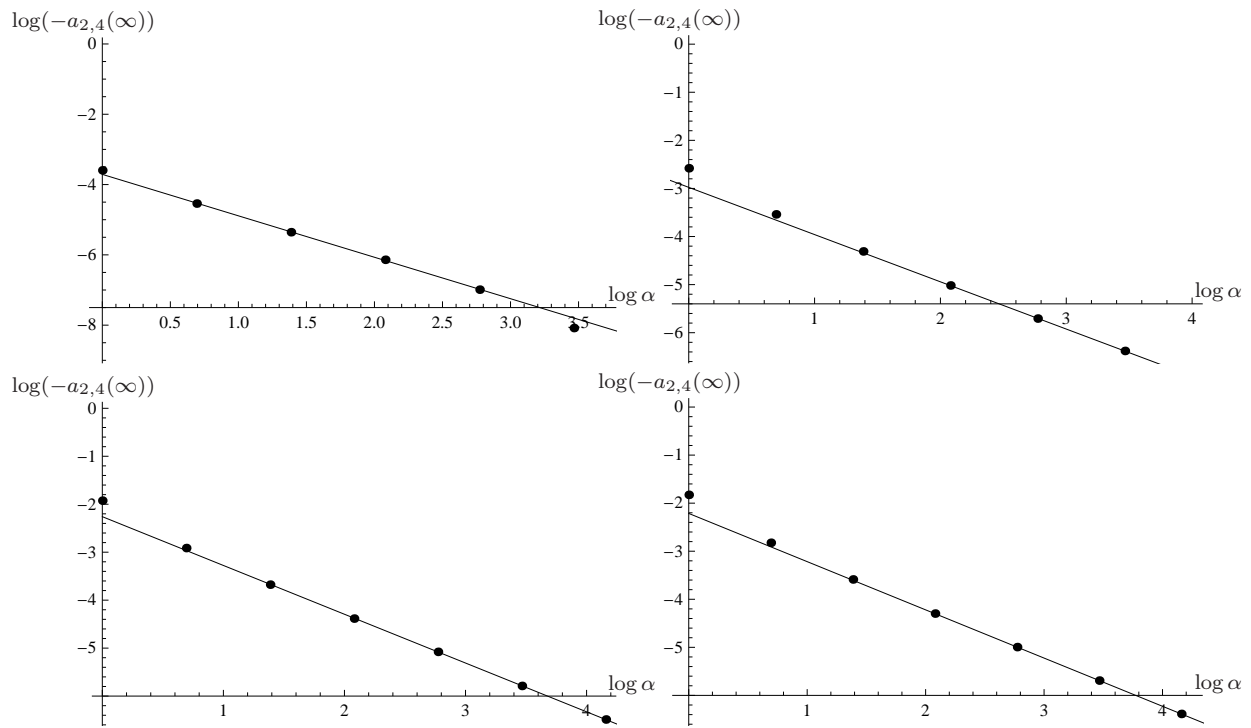
Figure 2.6: log-log plots for $|a_{2,4}|$ versus α for various Δ in the slow quench regime. The fact that the plots tend to straight lines for positive values of $\log \alpha$ means that $a_{2,4}$ scales as a power law for large α. Clockwise from the top left, the plots are for $\Delta = 7/3$, $8/3$, $11/3$ and $10/3$.
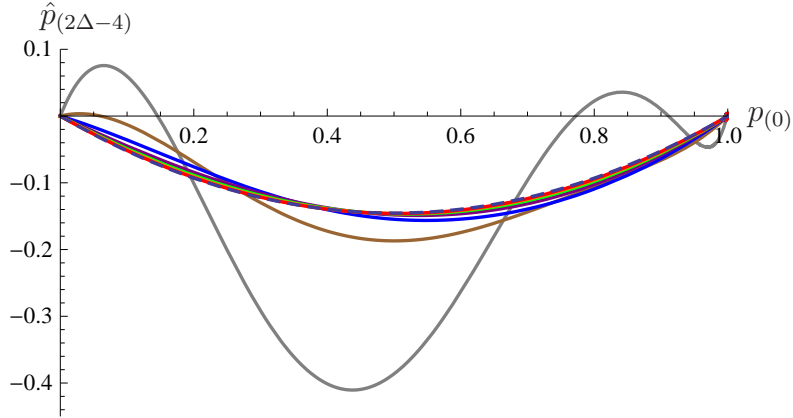
Figure 2.7: Plots of the deviation from the adiabatic response as a function of $p_{(0)}$ for slow quenches with different speeds and $\Delta = 11/3$ — see eq. (2.111) for the definition of $\hat{p}_{(2\Delta-4)}$. The curves correspond to $\alpha = 1$ (grey), 2 (brown), 4 (blue), 8 (purple), 16 (green), 32 (orange) and 64 (red). The dashed curve corresponds to $b_{(0)}\dot{p}_{(0)}$.

Figure 2.7 shows the deviation $\hat{p}_{(2\Delta-4)}$ as a function of $p_{(0)}$ for $\Delta = 11/3$ and different values of α. The dashed curve shows $b_{(0)}\dot{p}_{(0)}$, where $b_{(0)}$ was determined by the shooting method in section 2.8. As we can see in the figure, as α grows large, the deviation determined by our numerical simulations is converging on the expected curve. Those curves corresponding to larger α fit the dashed curve best. The curve for $\alpha = 64$ lies practically on top of the limiting dashed curve.

2.9.4 Excitation and relaxation times

Next, we consider the excitation and relaxation times following the approach presented in [48]. First, we define

$$\delta \equiv \left| \frac{p_{(2\Delta-4)} - p_{(2\Delta-4)}(\infty)p_{(0)}}{p_{(2\Delta-4)}(\infty)} \right|, \tag{2.112}$$

i.e., the absolute value of the relative deviation of the response $p_{(2\Delta-4)}$ from the adiabatic limit $p_{(2\Delta-4)}(\infty)\,p_{(0)}$. Then we define the excitation time τ_{ex} as the first time at which δ reaches $\varepsilon = .05$, where the latter was chosen as an arbitrary threshold. Similarly, the relaxation or equilibration time τ_{eq} is the latest time at which δ drops below the $\varepsilon = .05$ threshold. As an example, δ is shown in figure 2.8 for $\alpha = 1$ and $\Delta = 8/3$. The vertical grid lines indicate the excitation time τ_{ex} and relaxation time τ_{eq}. Note that our definitions
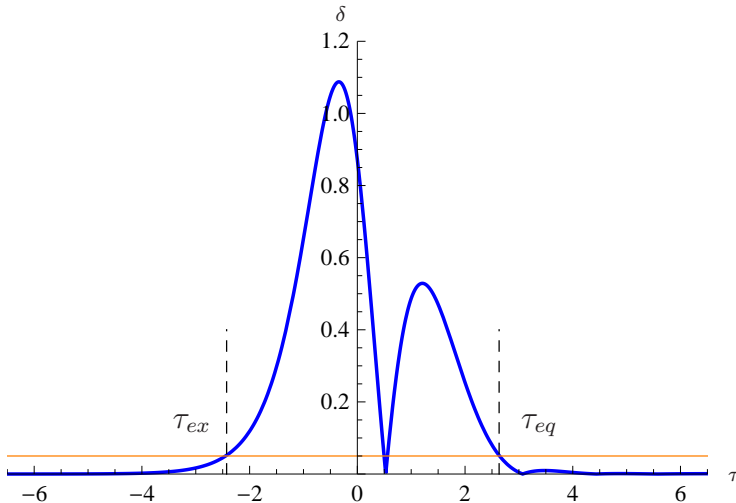
Figure 2.8: Plot of Δ as a function of τ for $\alpha = 1$ and $\Delta = 8/3$. The excitation time τ_{ex} and relaxation time τ_{eq} are shown as the first and final times, respectively, at which δ crosses the threshold of $\varepsilon = .05$ (shown as the orange line).

of τ_{ex} and τ_{eq} is only expected to be meaningful for relatively small α. As α grows large, the response approaches the adiabatic profile (2.94) and so for sufficiently large α, δ will never exceed the chosen threshold.

Figure 2.9 shows the rescaled excitation time $|\tau_{ex}|/\alpha$ as a function of $\log \alpha$ for different values of Δ. For fast quenches (*i.e.*, $\log \alpha \leq 0$), we see that $|\tau_{ex}|/\alpha$ approaches a straight line, indicating that the excitation time scales as $\beta_\Delta \alpha \log \alpha$. Once again the straight lines are fit through the three points with the points corresponding to the fastest quenches, for each Δ. The constants β_Δ can be determined as the slope of the fitted line in these plots. The plots also show that, as expected, the behaviour becomes irregular for $\log \alpha > 0$, in particular for $\Delta = 10/3$ and $11/3$.

Figure 2.10 shows the slopes of the straight-line fits in the previous plots as a function of Δ. This plot also includes data-points for $\Delta = 2$ and 3 using the results in [48].[6] The fact that $\frac{\partial |\tau_{ex}|/\alpha}{\partial \log \alpha} = 0$ for $\Delta = 2$ means that in this case τ_{ex} has no $\log \alpha$-dependence for

---

[6]For these two points, we have used the expressions for $|\tau_{ex}|/\alpha$ after the $\log(-\log \alpha)$ terms have been subtracted.
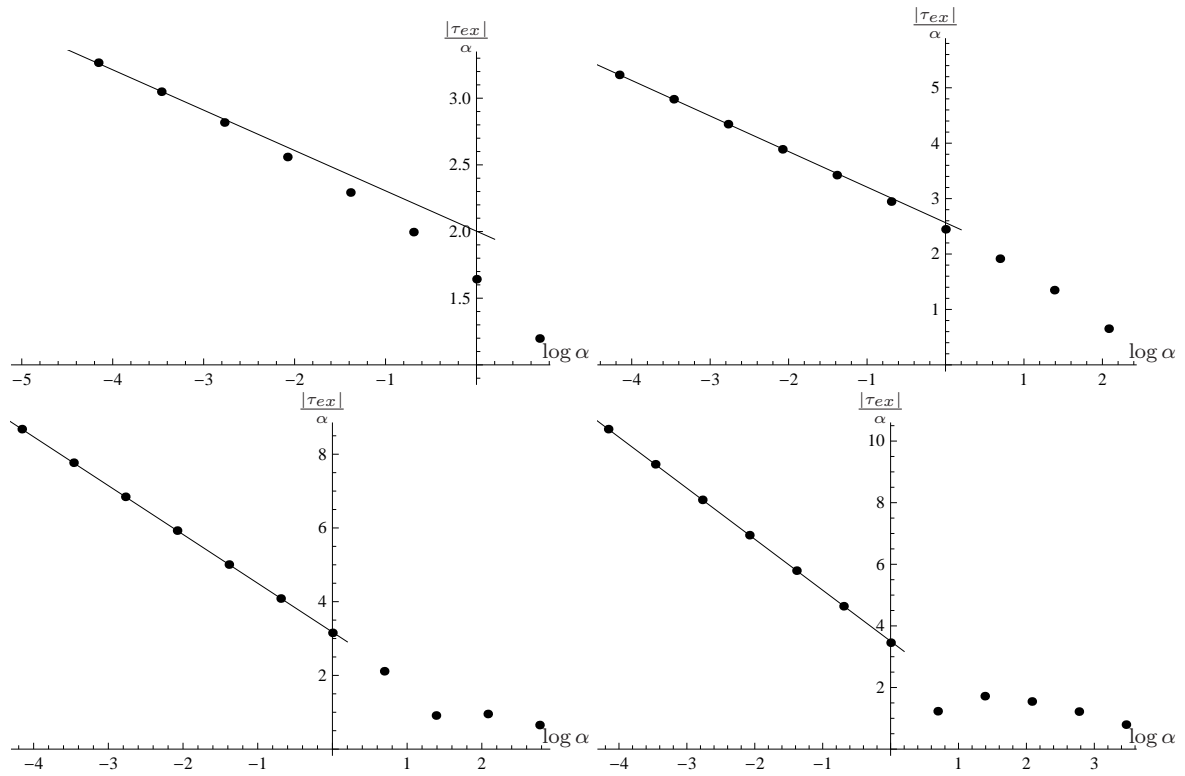
Figure 2.9: Plots of $\frac{|\tau_{ex}|}{\alpha}$ as a function of $\log \alpha$. The straight lines indicate the asymptotic behaviour for fast quenches. Clockwise from the top left, the plots are for $\Delta = 7/3,\ 8/3$, $11/3$ and $10/3$.

66
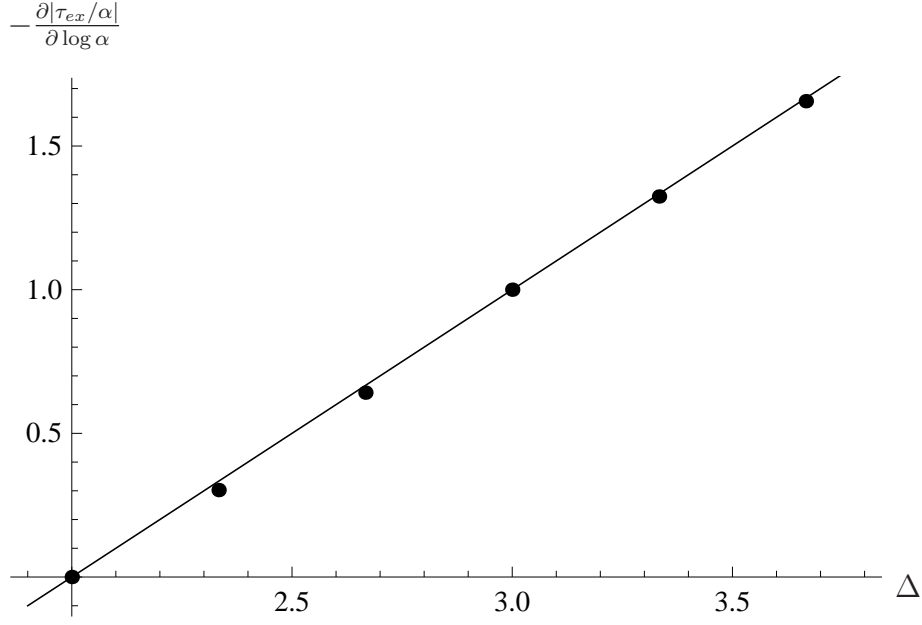
Figure 2.10: A plot of (minus) the slope of the fitted straight lines in figure 2.9. The datapoints lie approximately on the predicted line $-\frac{\partial |\tau_{ex}/\alpha|}{\partial \log \alpha} = \Delta - 2$ shown. Also shown are the data for $\Delta = 2$ and 3 from [48].

this type of quench. We find that the datapoints lie approximately on the line

$$-\frac{\partial |\tau_{ex}|/\alpha}{\partial \log \alpha} = \Delta - 2 \,, \tag{2.113}$$

which is numerically almost identical to the fitted line through all the data-points shown in the figure, namely

$$-\frac{\partial |\tau_{ex}|/\alpha}{\partial \log \alpha} = 1.003\Delta - 2.02 \,. \tag{2.114}$$

Hence for fast quenches, *i.e.*, $\alpha \ll 1$, the excitation time scales as

$$\tau_{ex} \simeq (\Delta - 2)\,\alpha \, \log \alpha \,. \tag{2.115}$$

Using the same approach, we also studied the relaxation time τ_{eq}. In this case for all of the various Δ, we found

$$\tau_{eq} \approx \alpha^0 \,, \tag{2.116}$$

for fast quenches. That is, τ_{eq} is constant for small α, rather than scaling with α in some way, for all (fractional) Δ. This behaviour is consistent with the results for $\Delta = 2$ and 3, found in [48]. In terms of the dimensionful time coordinate t, the relaxation time is $t_{eq} \sim 1/\mu$. In terms of the boundary theory then, the relaxation time is set by the thermal timescale for fast quenches.

2.9.5 Behaviour of the energy and pressure

Recall that our analysis was restricted to considering conformal dimensions in the range $2 < \Delta < 4$. With this restriction, the change in the temperature ΔT and energy density $\Delta \mathcal{E}$ will always be positive in our holographic quenches, as is evident from eqs. (2.76) and (2.77). On the other hand, eqs. (2.86) and (2.87) show that ΔT and $\Delta \mathcal{E}$ may have either sign for the reverse quenches considered in section 2.6.3. In particular, in the adiabatic limit, $\tilde{a}_{2,4}(\infty)$ vanishes and so we have both $\Delta T < 0$ and $\Delta \mathcal{E} < 0$. Then as α becomes smaller, $\tilde{a}_{2,4}(\infty)$ grows and eventually ΔT and $\Delta \mathcal{E}$ become positive. Specifically, eqs. (2.86) and (2.87) indicate:

$$\Delta T > 0 \quad \text{for} \qquad |\tilde{a}_{2,4}(\infty)| > \frac{2}{3}(\Delta - 2)^2 \, |\tilde{p}_{(2\Delta-4)}(-\infty)| , \qquad (2.117)$$

$$\Delta \mathcal{E} > 0 \quad \text{for} \qquad |\tilde{a}_{2,4}(\infty)| > \frac{1}{3}(\Delta - 2) \, |\tilde{p}_{(2\Delta-4)}(-\infty)| . \qquad (2.118)$$

Recall that $\tilde{p}_{(2\Delta-4)}(-\infty) = p_{(2\Delta-4)}(\infty)$ corresponds to the equilibrium response given in eq. (2.64). With our numerical simulations, we determined the value of α at which these thresholds are reached for various values of Δ and the results are shown in table 2.2. We have also included the analogous results for $\Delta = 2$ and 3 from [48]. Note the qualitative trend is that the threshold value of α grows monotonically as Δ increases. Note that eqs. (2.117) and (2.118) imply that the threshold for positive $\Delta \mathcal{E}$ is greater than that for positive ΔT (*i.e.*, larger α) for $\Delta > 2.5$, while the thresholds are reversed for $\Delta < 2.5$. Clearly, this behaviour is reflected in the results shown in table 2.2.

Turning now to the change in the pressure $\Delta \mathcal{P}$, we have eqs. (2.78) and (2.88) for forward and reverse quenches, respectively. In this case, $\Delta \mathcal{P} > 0$ in all forward quenches as long as $\Delta > 7/2$ and in all reverse quenches for $\Delta < 7/2$. Otherwise, the sign of $\Delta \mathcal{P}$ will depend on the rate of the quench. Here we focus on the forward quenches with $\Delta < 7/2$. In this case, $\Delta \mathcal{P} < 0$ for slow quenches and as α decreases, the change in the pressure reverses its sign when

$$\Delta \mathcal{P} > 0 \quad \text{for} \qquad |a_{2,4}(\infty)| > \frac{1}{3}(7 - 2\Delta)(\Delta - 2) \, |p_{(2\Delta-4)}(\infty)| . \qquad (2.119)$$

Table 2.2: Approximate upper bounds on α for which $\Delta T > 0$ and $\Delta \mathcal{E} > 0$ for reverse quenches. The upper bounds on α for $\Delta \mathcal{P} > 0$ is for forward quenches when $\Delta < 3.5$, with different values of Δ. For $\Delta = 2$ the values of $\Delta \mathcal{E}$ and $\Delta \mathcal{P}$ are renormalization scheme dependent, see [48].

Δ	ΔT	$\Delta \mathcal{E}$	$\Delta \mathcal{P}$
2	0.58		
7/3	0.68	0.50	0.23
8/3	0.77	0.92	0.68
3	0.86	1.32	1.32
10/3	1.00	2.00	5.5
11/3	1.41	4.00	–

The value of α at which these thresholds is reached for various values of Δ is shown in table 2.2. Again, we have also included an analogous result for $\Delta = 3$ [48]. The qualitative trend is that the threshold value of α grows monotonically as Δ increases. Further, we may compare the above threshold to those in eqs. (2.117) and (2.118).[7] In particular, the threshold for positive $\Delta \mathcal{P}$ is greater than that for positive $\Delta \mathcal{E}$ for $\Delta > 3$, while the thresholds are reversed for $\Delta < 3$. We also find the threshold for positive $\Delta \mathcal{P}$ is less than that for positive ΔT when $\Delta < 2.75$. Clearly, this behaviour is reflected in the results shown in table 2.2.

2.10 Discussion

In this chapter, we continued the program initiated in [48] of studying quantum quenches in strongly coupled quantum field theories using holography. The process studied here was the quench of a four-dimensional conformal field theory made with a rapid transition in the coupling of a relevant operator $\mathcal{O}_\Delta$ from zero to some finite value λ_f. Reference [48] had considered the special cases where the conformal dimension of the operator was $\Delta = 2$ and 3. Our holographic analysis allowed for operators with general conformal dimensions in the range $2 < \Delta < 4$. Through the gauge/gravity correspondence [5, 6], this quench was translated to a classical problem in five-dimensional Einstein gravity coupled to a

---

[7]Note that here we are comparing a threshold for the forward quenches to thresholds in the reverse quenches.

negative cosmological constant and a (free) massive scalar field. In particular, the quench was implemented by introducing a time-dependent boundary condition on the scalar field in the asymptotically AdS$_5$ spacetime. Our discussion also only considered quenches of a thermal plasma with an initial temperature T_i in the boundary theory and was limited to a high temperature regime[8] where $\lambda_f \ll T_f^{4-\Delta}$. Hence our calculations were perturbative in the ratio $\lambda_f/T_f^{4-\Delta}$, which in the gravitational description meant that they were perturbative in the (dimensionless) amplitude of the bulk scalar. However, there was no restriction on the timescale δt governing the transition rate of the coupling. In particular, with the transition profiles in eq. (2.89), our results were described in terms of the dimensionless parameter: $\alpha = \pi T_i \, \delta t$, *i.e.,* the ratio of the transition timescale to the relaxation timescale of the thermal plasma. In our analysis, we paid special attention to the limit of adiabatic transitions with $\alpha \to \infty$ and of very fast quenches with $\alpha \to 0$. A detailed discussion of the results was given in section 2.9.

In all of these quenches, our computations implicitly gave the response in the one-point correlators of the relevant operator $\langle \mathcal{O}_\Delta \rangle$ and the stress tensor $\langle T_{ij} \rangle$, as described by eqs. (2.44)–(2.46), to leading order in $\lambda_f/T_f^{4-\Delta}$. In section 2.9, our discussion of the results was presented in terms of two gravitational parameters, $p_{2\Delta-4}(\tau)$ and $a_{2,4}(\infty)$. With eq. (2.46), we see the first is directly related to $\langle \mathcal{O}_\Delta \rangle$ during the quench. We can rewrite this expression as

$$\langle \mathcal{O}_\Delta \rangle = \frac{\pi^4 \, C_T}{40} \, (\Delta - 2) \, \frac{\lambda_f}{T_f^{4-2\Delta}} \, \frac{p_{2\Delta-4}(t/\pi T_f)}{|p_{2\Delta-4}(\infty)|} \, , \tag{2.120}$$

using eq. (2.5) and various results from section 2.6. Further $a_{2,4}(\infty)$ controls the entropy production (2.75), as well as the changes in the temperature, energy and pressure as given in eqs. (2.76)–(2.78). One confirmation of our numerical simulations was that we found $a_{2,4}(\infty) \le 0$ for all of our quenches with any values of α and Δ. With eq. (2.75), the latter ensures that the entropy production was always positive, in accord with the second law of thermodynamics.

Another confirmation comes from our analysis of slow quenches in section 2.8. In this case with $\alpha \gg 1$, it was shown that the linearized equation (2.22) for the bulk scalar can be solved using a power series in $1/\alpha$. While $a_{2,4}(\infty)$ vanishes for the leading adiabatic solution, we showed that a $1/\alpha$ contribution appears at the next order in eq. (2.102). Using a shooting method, we explicitly solved for this contribution and the results were given in eq. (2.212). This same leading order contribution to $a_{2,4}(\infty)$ for slow quenches is addressed with the numerical results shown in figure 2.6. In these plots, the same approximate $1/\alpha$

---

[8]In fact, this inequality is satisfied by the coupling and temperature throughout the quench.

scaling was found with an asymptotic straight-line fit in $\log \alpha$ for $\alpha \gg 1$, *i.e.,*

$$\log |a_{2,4}(\infty)| = -c - \log \alpha. \qquad (2.121)$$

The case $\Delta = 7/3$ had the worst fit, with a slope differing from -1 by about 18%. We believe that the slow convergence in our numerical simulations for this case led to this relatively large error. The other three cases in table 2.3 had slopes that differed from the expected slope by 2% or less. As well as obtaining a fair match in the slope above, we can compare the intercept c coming from these numerical results with that calculated from the independently derived results in eq. (2.212). We see in table 2.3 that the intercepts derived from the two approaches agree very well. Recall that in figure 2.7, we also showed that the full time-dependent profile of the numerical response (after subtracting the adiabatic profile) matched well with the form derived in section 2.8 for $\alpha \gg 1$.

Table 2.3: Intercept in eq. (2.121) evaluated by two different methods: c_{shoot} is derived from the results in eq. (2.212), while c_{numer} comes from fitting the data in figure 2.6.

Δ	c_{shoot}	c_{numer}	$\frac{c_{shoot}-c_{numer}}{c_{shoot}}$
7/3	3.93	3.71	5.6%
8/3	2.96	2.98	-0.68%
10/3	2.31	2.26	2.2%
11/3	2.22	2.21	0.45%

In eq. (2.115), we found an interesting scaling behaviour for the excitation time in fast quenches, namely $\tau_{ex} \simeq (\Delta - 2)\,\alpha \log \alpha$. On the one hand, this indicates that the excitation time is longer when the conformal dimension of the operator is larger but it also shows that τ_{ex} becomes shorter for faster quenches. In particular, $\tau_{ex} \to 0$ for $\alpha \to 0$, for which the quench profile (2.89) becomes a step-function at $\tau = 0$. In contrast, as shown in eq. (2.116), the relaxation time remains constant for $\alpha \ll 1$. Hence independent of the precise values of Δ and α, the boundary system relaxes on the thermal timescale $1/T$ for fast quenches.

Perhaps, the most interesting result coming from our analysis was the universal behaviour found in $|p_{2\Delta-4}|$ and $a_{2,4}(\infty)$ for $\alpha \ll 1$. Of course, in terms of the boundary theory, these results translate into universal behaviour in the response of $\langle \mathcal{O}_\Delta \rangle$ and in the thermodynamic quantities for fast quenches. First, the results in figure 2.1 indicate that the maximum value of $|p_{2\Delta-4}|$ scales as $\alpha^{-(2\Delta-4)}$, which with eq. (2.120), translates into a scaling for the expectation value of the quenched operator, *i.e.,*

$$\max \langle \mathcal{O}_\Delta \rangle \propto \frac{1}{\alpha^{2\Delta-4}}. \qquad (2.122)$$

Beyond this scaling, figure 2.2 also indicates that the response and hence $\langle \mathcal{O}_\Delta \rangle$ approach a relatively simple universal form in the limit $\alpha \to 0$. These results are in agreement with those found previously in [48]. However, we might comment that our analysis here assumed that Δ was a fraction, whereas [48] studied the special cases $\Delta = 2$ and 3. In both of these cases, the response also exhibited an additional contribution which scaled faster than shown in eq. (2.122) by an extra logarithmic factor. An extra logarithmic factor is also present for $\Delta = 4$ [76].

The above scaling of $|p_{2\Delta-4}|$ also leads to the scaling of $a_{2,4}(\infty) \propto \alpha^{-(2\Delta-4)}$ for fast quenches, as shown with the numerical data in figure 2.4. This contribution then dominates in eqs. (2.75)–(2.78) and so the changes of the various thermodynamic quantities induced by fast quenches exhibit the same scaling, $e.g.$,

$$\frac{\Delta \mathcal{E}}{\mathcal{E}_i} \propto \frac{1}{\alpha^{2\Delta-4}} \tag{2.123}$$

for $\alpha \ll 1$. Again these results are in agreement with those found in [48]. However, the results there and in [76] indicate that eq. (2.123) is further enhanced by a logarithmic scaling for $\Delta = 2$. While quenches by operators with conformal dimensions in the range $2 \le \Delta \le 4$ are covered by the analysis here and in [48], it would be interesting to understand if this universal behaviour extends to the allowed regime $1 \le \Delta < 2$.

As noted in [48], given the scaling in eqs. (2.122) and (2.123), it appears that 'infinitely fast' quenches seem to be ill-defined because physical quantities are diverging as $\alpha \to 0$. Recall that in this limit, the quench profile (2.89) becomes a step-function at $\tau = 0$. Hence this issue is particularly notable since it is precisely such 'infinitely fast' quenches are studied in the seminal work on this topic [58]. However, we must contrast their description of a quench with the present approach. In [58], the system is evolved from $t = -\infty$ to 0^- to prepare the system in a far-from-equilibrium state of the 'quenched' Hamiltonian, $i.e.,$, the ground state of the initial Hamiltonian. This state is then used as the initial condition at $t = 0^+$ and the subsequent evolution of the system with the 'quenched' Hamiltonian is studied.

Of course, since the present calculations are only perturbative in $\lambda_f/T_f^{4-\Delta}$, one can not take the singularities appearing in eqs. (2.122) and (2.123) for $\alpha \to 0$ too seriously. Hence it would be interesting to study the fast quenches by evolving the full nonlinear equations of the dual gravity theory. At present, our preliminary analysis suggests that in fact these singularities are physical [76]. In any event, the present holographic calculations illustrate that the gauge/gravity correspondence provides a versatile new framework for the study of quantum quenches. Undoubtedly, interesting new lessons will come from

applying holography to study more general physical quantities and the behaviour of more complicated systems under a quench. This will help build our intuition for the behaviour of fast-changing quantum fields that occur when the external parameters are changed in laboratory experiments.

2.11 Appendix: Coefficients in the metric solution

Here we list the expressions of the coefficients in the metric functions (2.28) and (2.29) in terms of the normalizable and non-normalizable modes of the scalar, $p_{(0)}$ and $p_{(2\Delta-4)}$. We only list the coefficients that are needed (and the first subleading coefficient) in calculating the boundary stress tensor and the expectation value of the operator $\mathcal{O}_\Delta$.

Because $\dot{a}_{2,4}$ depends on it, we will give the expression for $a_{2,5}$, even though it is subleading and has only vanishing contributions to physical quantities:

$$a_{2,5} = \frac{1}{18} \left(\Delta(2\Delta - 5)\dot{p}_{(0)}p_{(2\Delta-2)} - (2\Delta - 3)(4 - \Delta)p_{(0)}\dot{p}_{(2\Delta-2)} \right). \tag{2.124}$$

The coefficients of the terms with negative powers of 2Δ in A_{p} are given by

$$\alpha_{2,4} = -\frac{(4 - \Delta)p_{(0)}^2}{6(7 - 2\Delta)}; \tag{2.125}$$

$$\alpha_{2,5} = \frac{(\Delta - 3)p_{(0)}\dot{p}_{(0)}}{3(7 - 2\Delta)}; \tag{2.126}$$

$$\alpha_{2,6} = \frac{(2\Delta^2 - 6\Delta + 15)\dot{p}_{(0)}^2 + (2\Delta^2 - 13\Delta + 24))p_{(0)}\ddot{p}_{(0)}}{12(\Delta - 3)(9 - 2\Delta)}; \tag{2.127}$$

$$\alpha_{2,7} = \frac{(4 - \Delta)\left(-3(\Delta - 2)(9 - 2\Delta)\dot{p}_{(0)}\ddot{p}_{(0)} + (2\Delta^2 - 15\Delta + 36))p_{(0)}\dddot{p}_{(0)}\right)}{36(5 - \Delta)(\Delta - 3)(9 - 2\Delta)}; \tag{2.128}$$

$$\begin{aligned}
\alpha_{2,8} = & -\Big(12(5 - \Delta)(4 - \Delta)^2(\Delta - 3)^2(2\Delta^2 - 11\Delta + 30)p_{(0)}^2 \\
& -3(7 - 2\Delta)^2(5 - \Delta)(2\Delta^3 - 19\Delta^2 + 56\Delta - 54)\ddot{p}_{(0)}^2 \\
& -4(\Delta - 3)(7 - 2\Delta)(2\Delta^2 - 14\Delta + 21)(2\Delta^2 - 17\Delta + 39)\dot{p}_{(0)}p_{(0)}^{(3)} \\
& +(4 - \Delta)(\Delta - 3)(9 - 2\Delta)(2\Delta - 7)(2\Delta^2 - 17\Delta + 51)p_{(0)}p_{(0)}^{(4)}\Big) \\
& \Big/ \Big(288(5 - \Delta)(4 - \Delta)(\Delta - 3)^2(4\Delta^2 - 36\Delta + 77)\Big). \tag{2.129}
\end{aligned}$$

Of the coefficients to the terms with positive of powers 2Δ in $A_{\rm p}$, the coefficient

$$\beta_{2,4} = \frac{\Delta\, p_{(2\Delta-2)}^2}{6(2\Delta-1)} \tag{2.130}$$

will be subleading.

The coefficients in $\Sigma_{\rm p}$ corresponding to integer powers of ρ are given by

$$s_{2,5} \;=\; -\frac{\Delta\,(4-\Delta)\,p_{(0)}p_{(2\Delta-4)}}{36}; \tag{2.131}$$

$$s_{2,6} \;=\; -\frac{1}{60}\left(\Delta\,(5-\Delta)\,\dot{p}_{(0)}p_{(2\Delta-4)} + (4-\Delta)(\Delta+1)\,p_{(0)}\dot{p}_{(2\Delta-4)}\right). \tag{2.132}$$

The coefficients of the terms with negative powers of 2Δ in $\Sigma_{\rm p}$ are given by

$$\sigma_{2,5} \;=\; -\frac{(4-\Delta)p_{(0)}^2}{12(7-2\Delta)}; \tag{2.133}$$

$$\sigma_{2,6} \;=\; -\frac{(5-\Delta)p_{(0)}\dot{p}_{(0)}}{6(9-2\Delta)}; \tag{2.134}$$

$$\sigma_{2,7} \;=\; \frac{2(5-\Delta)^2(\Delta-3)\dot{p}_{(0)}^2 + (6-\Delta)(4-\Delta)(7-2\Delta)p_{(0)}\ddot{p}_{(0)}}{24(5-\Delta)(\Delta-3)(9-2\Delta)}; \tag{2.135}$$

$$\sigma_{2,8} \;=\; \frac{3(6-\Delta)(5-\Delta)(7-2\Delta)\dot{p}_{(0)}\ddot{p}_{(0)}}{72(5-\Delta)(\Delta-3)(11-2\Delta)}$$
$$+\frac{(7-\Delta)(4-\Delta)(9-2\Delta)p_{(0)}p_{(0)}^{(3)}}{72(5-\Delta)(\Delta-3)(11-2\Delta)}; \tag{2.136}$$

$$\sigma_{2,9} \;=\; -\Big(12(8-\Delta)(4-\Delta)^2(\Delta-3)^2 p_{(0)}^2 - 3(7-2\Delta)^2(6-\Delta)^2\ddot{p}_{(0)}^2$$
$$-8(7-\Delta)(5-\Delta)(\Delta-3)(9-2\Delta)\dot{p}_{(0)}p_{(0)}^{(3)}$$
$$-(8-\Delta)(\Delta-3)(11-2\Delta)(9-2\Delta)p_{(0)}p_{(0)}^{(4)}\Big)$$
$$\Big/\Big(576(6-\Delta)(\Delta-3)^2(11-2\Delta)\Big). \tag{2.137}$$

Of the coefficients to the terms with positive of powers 2Δ in $\Sigma_{\rm p}$, the coefficient

$$\theta_{2,5} = \frac{\Delta\, p_{(2\Delta-2)}^2}{12(2\Delta-1)} \tag{2.138}$$

is subleading.

74

2.12 Appendix: Coefficients in the Fefferman-Graham coordinates

2.12.1 The time and radial coordinates

The expansion of the EF time and radial coordinates in terms of the FG time and radial coordinates was given in eqs. (2.37) and (2.38). The expressions of the coefficients can be written in terms of the coefficients $p_{(0)}$, $p_{(2\Delta-4)}$ and $a_{2,4}$. First, the terms containing v_n and ρ_n are given by the series

$$\sum_n v_n z^n = -z - \frac{3z^5\mu^4}{40} - \frac{11z^9\mu^8}{1152} - \frac{23z^{13}\mu^{12}}{13312} + \dots, \tag{2.139}$$

$$\sum_n \rho_n z^n = -\frac{z^5\mu^5}{8} + \frac{3z^9\mu^9}{128} - \frac{5z^{13}\mu^{13}}{1024} + \dots. \tag{2.140}$$

Next, the terms of order ℓ^2 are given by

$$\sum_{n=5} \vartheta_n z^n = \frac{3}{40} z^5\mu^4 a_{2,4} + \frac{1}{240} z^6\mu^4 \left(16\mu a_{2,5} - 11\partial_t a_{2,4}\right) + \dots, \tag{2.141}$$

$$\sum_{n=5} \chi_n z^n = \frac{1}{8} z^5\mu^5 a_{2,4} + \frac{1}{10} z^6\mu^5 \left(\mu a_{2,5} - \partial_t a_{2,4}\right) + \dots, \tag{2.142}$$

where the terms of order z^6 only make subleading contributions in the calculated quantities. The coefficients of the terms with factors of $r^{-2\Delta}$ in τ/μ are given by

$$\nu_0 = \frac{(7-2\Delta)\mu^{2\Delta-8}\alpha_{2,4}}{4(4-\Delta)(9-2\Delta)};$$

$$\nu_1 = \frac{\mu^{8-2\Delta}\left((4\Delta^2 - 30\Delta + 55)\,\partial_t\alpha_{2,4} + 4(4-\Delta)^2\mu\alpha_{2,5}\right)}{8(5-\Delta)(11-\Delta)(9-2\Delta)};$$

$$\nu_2 = \mu^{8-2\Delta}\frac{(4\Delta^2 - 32\Delta + 61)\,\partial_t^2\alpha_{2,4}}{8(5-\Delta)(11-2\Delta)(9-2\Delta)}$$
$$+\mu^{8-2\Delta}\frac{-2\left(4\Delta^2 - 34\Delta + 71\right)\mu\partial_t\alpha_{2,5} + 2(9-2\Delta)^2\mu^2\alpha_{2,6}}{8(5-\Delta)(11-2\Delta)(9-2\Delta)};$$

$$\nu_3 = -\mu^{8-2\Delta}\frac{(4\Delta^2 - 34\Delta + 67)\,\partial_t^3\alpha_{2,4} - 6(2\Delta^2 - 18\Delta + 39)\mu\partial_t^2\alpha_{2,5}}{48(6-\Delta)(5-\Delta)(11-2\Delta)}$$
$$-\mu^{8-2\Delta}\frac{6\left(4\Delta^2 - 38\Delta + 89\right)\mu^2\partial_t\alpha_{2,6} - 24(5-\Delta)^2\mu^3\alpha_{2,7}}{48(6-\Delta)(5-\Delta)(11-2\Delta)}, \tag{2.143}$$

where $\alpha_{2,n}$ are the coefficients defined in eq. (2.28) and given explicitly in eqs. (2.125)–(2.128) — implicitly, functions of the FG time t here. Similarly, the coefficients in ρ with factors of $r^{-2\Delta}$ are given by

$$\xi_0 \;\; = \;\; \frac{\mu^{9-2\Delta}\alpha_{2,4}}{4(4-\Delta)}; \tag{2.144}$$

$$\xi_1 \;\; = \;\; -\frac{\mu^{9-2\Delta}\left(\partial_t\alpha_{2,4} - \mu\alpha_{2,5}\right)}{2(9-2\Delta)}; \tag{2.145}$$

$$\xi_2 \;\; = \;\; \frac{\mu^{9-2\Delta}\left(\partial_t^2\alpha_{2,4} - 2\mu\partial_t\alpha_{2,5} + 2\mu^2\alpha_{2,6}\right)}{8(5-\Delta)}; \tag{2.146}$$

$$\xi_3 \;\; = \;\; -\frac{\mu^{9-2\Delta}\left(\partial_t^3\alpha_{2,4} - 3\mu\partial_t^2\alpha_{2,5} + 6\mu^2\partial_t\alpha_{2,6} - 6\mu^3\alpha_{2,7}\right)}{12(11-2\Delta)}; \tag{2.147}$$

$$\xi_4 \;\; = \;\; -\frac{\mu^{9-2\Delta}\left((2\Delta^2 - 13\Delta + 30)\,\mu^4\alpha_{2,4} - (4-\Delta)\partial_t^5\alpha_{2,4}\right)}{32(6-\Delta)(4-\Delta)}$$
$$\;\; - \frac{\mu^{9-2\Delta}\left(4\mu\partial_t^3\alpha_{2,5} - 12\mu^2\partial_t^2\alpha_{2,6} + 24\mu^3\partial_t\alpha_{2,7} - 24\mu^4\alpha_{2,8}\right)}{96(6-\Delta)}. \tag{2.148}$$

The coefficients of the terms with factors of $z^{2\Delta}$ in v are given by

$$\omega_1 \;\; = \;\; \frac{(2\Delta - 1)\mu^{2\Delta}\beta_{2,4}}{4\Delta(2\Delta + 1)}; \tag{2.149}$$

$$\omega_2 \;\; = \;\; -\frac{\mu^{2\Delta}\left((4\Delta^2 - 2\Delta - 1)\,\partial_t\beta_{2,4} - 4\Delta^2\mu\beta_{2,5}\right)}{8\Delta(\Delta + 1)(2\Delta + 1)}; \tag{2.150}$$

$$\omega_3 \;\; = \;\; \mu^{2\Delta}\frac{\left(4\Delta^2 - 3\right)\partial_t^2\beta_{2,4}}{8\left(4\Delta^3 + 12\Delta^2 + 11\Delta + 3\right)}$$
$$\;\; - \mu^{2\Delta}\frac{2\left(4\Delta^2 + 2\Delta - 1\right)\mu\partial_t\beta_{2,5} - 2(2\Delta + 1)^2\mu^2\beta_{2,6}}{8\left(4\Delta^3 + 12\Delta^2 + 11\Delta + 3\right)}; \tag{2.151}$$

$$\omega_4 \;\; = \;\; -\mu^{2\Delta}\frac{(4\Delta^2 + 2\Delta - 5)\partial_t^3\beta_{2,4} - 6(2\Delta^2 + 2\Delta - 1)\mu\partial_t^2\beta_{2,5}}{48(\Delta + 1)(\Delta + 2)(2\Delta + 3)}$$
$$\;\; - \mu^{2\Delta}\frac{(4\Delta^2 + 6\Delta + 1)\,\mu^2\partial_t\beta_{2,6} - 4(\Delta + 1)^2\mu^3\beta_{2,7}}{12(\Delta + 1)(\Delta + 2)(2\Delta + 3)}, \tag{2.152}$$

where $\beta_{2,n}$ are the coefficients defined in eq. (2.28) — implicitly, functions of the FG time t here. Similarly, the coefficients in ρ with factors of $z^{2\Delta}$ are given by

$$\zeta_1 = \frac{\mu^{2\Delta+1}\beta_{2,4}}{4\Delta}; \tag{2.153}$$

$$\zeta_2 = -\frac{\mu^{2\Delta+1}(\partial_t\beta_{2,4} - \mu\beta_{2,5})}{2(2\Delta+1)}; \tag{2.154}$$

$$\zeta_3 = \frac{\mu^{2\Delta+1}(\partial_t^2\beta_{2,4} - 2\mu\partial_t\beta_{2,5} + 2\mu^2\beta_{2,6})}{8(\Delta+1)}; \tag{2.155}$$

$$\zeta_4 = -\frac{\mu^{2\Delta+1}(\partial_t^3\beta_{2,4} - 3\mu\partial_t^2\beta_{2,5} + 6\mu^2\partial_t\beta_{2,6} - 6\mu^3\beta_{2,7})}{12(2\Delta+3)}; \tag{2.156}$$

$$\zeta_5 = -\mu^{2\Delta+1}\frac{3(2\Delta^2 - 3\Delta + 10)\mu^4\beta_{2,4} - \Delta\partial_t^4\beta_{2,4}}{96\Delta(\Delta+2)}$$
$$-\mu^{2\Delta+1}\frac{\Delta(4\mu\partial_t^3\beta_{2,5} - 12\mu^2\partial_t^2\beta_{2,6} + 24\mu^3\partial_t\beta_{2,7} - 24\mu^4\beta_{2,8})}{96\Delta(\Delta+2)}. \tag{2.157}$$

2.12.2 The metric

The expansion of the metric in the FG coordinates was given in eq. (2.39). The nonzero components for our purposes are the parts G_{00}, which correspond to the EF metric function $-A$, and the diagonal components of G_{ij}, which correspond to Σ^2. The order ℓ^0 terms in the metric are given by

$$g_{00}^{(0)} + z^4 g_{00}^{(4)} = -1 + \frac{3z^4\mu^4}{4} + o\left(z^8\right), \tag{2.158}$$

$$g_{ii}^{(0)} + z^4 g_{ii}^{(4)} = 1 + \frac{\mu^4 z^4}{4} + o\left(z^8\right), \tag{2.159}$$

where in the second line, we are indicating the three individual diagonal components, *i.e.*, there is no implicit sum over i. Next we list the terms of order ℓ^2:

$$c_{(4)00} = -\frac{3}{4}\mu^4 a_{2,4}, \tag{2.160}$$

$$c_{(4)ii} = -\frac{\mu^4}{4}\left(a_{2,4} + \frac{2}{9}\Delta(4-\Delta)\,p_{(0)}p_{(2\Delta-4)}\right). \tag{2.161}$$

The coefficients of the terms with factors of $z^{-2\Delta}$ in G_{00} are given by

$$
d_{(0)00} = -\frac{(7-2\Delta)\mu^{8-2\Delta}\alpha_{2,4}}{2(4-\Delta)};
$$
(2.162)

$$
d_{(1)00} = -2\mu^{8-2\Delta}\frac{(\Delta-3)\partial_t\alpha_{2,4}+(4-\Delta)\mu\alpha_{2,5}}{9-2\Delta};
$$
(2.163)

$$
d_{(2)00} = \mu^{8-2\Delta}\frac{(\Delta-3)(7-2\Delta)\partial_t^2\alpha_{2,4}}{4(5-\Delta)(4-\Delta)}
$$
$$
+\mu^{8-2\Delta}\frac{2(7-2\Delta)\mu\partial_t\alpha_{2,5}-2(9-2\Delta)\mu^2\alpha_{2,6}}{4(5-\Delta)};
$$
(2.164)

$$
d_{(3)00} = -\mu^{8-2\Delta}\frac{(\Delta-3)(7-2\Delta)\partial_t^3\alpha_{2,4}+3(4-\Delta)(7-2\Delta)\mu\partial_t^2\alpha_{2,5}}{3(4\Delta^2-40\Delta+99)}
$$
$$
+\mu^{8-2\Delta}\frac{(4-\Delta)\partial_t\alpha_{2,6}-2(9-2\Delta)\mu^2\left((5-\Delta)\mu\alpha_{2,7}\right)}{4\Delta^2-40\Delta+99};
$$
(2.165)

$$
d_{(4)00} = -\mu^{8-2\Delta}\frac{\left(2\Delta^3-25\Delta^2+107\Delta-162\right)\mu^4\alpha_{2,4}}{8(6-\Delta)(5-\Delta)}
$$
$$
+\mu^{8-2\Delta}\frac{4(4-\Delta)(7-2\Delta)\mu\partial_t^3\alpha_{2,5}-12(9-2\Delta)(4-\Delta)\mu^2\partial_t^2\alpha_{2,6}}{48(6-\Delta)(5-\Delta)}
$$
$$
+\mu^{8-2\Delta}\frac{24(9-2\Delta)\mu^3\partial_t\alpha_{2,7}-24(11-2\Delta)\mu^4\alpha_{2,8}}{48(6-\Delta)}
$$
$$
+\mu^{8-2\Delta}\frac{(\Delta-3)(7-2\Delta)\partial_t^4\alpha_{2,4}}{48(6-\Delta)(5-\Delta)},
$$
(2.166)

78

where $\alpha_{2,n}$ are the coefficients defined in eq. (2.28) — implicitly, functions of the FG time t here. Similarly, the coefficients in G_{ii} with factors of $z^{-2\Delta}$ are given by

$$d_{(0)ii} \;=\; -\mu^{8-2\Delta}\frac{\alpha_{2,4} - 4(4-\Delta)\sigma_{2,5}}{2(4-\Delta)}; \tag{2.167}$$

$$d_{(1)ii} \;=\; \mu^{8-2\Delta}\frac{\partial_t\alpha_{2,4} - 2(9-2\Delta)\partial_t\sigma_{2,5} - \mu\alpha_{2,5} + 2(9-2\Delta)\mu\sigma_{2,6}}{9-2\Delta}; \tag{2.168}$$

$$d_{(2)ii} \;=\; -\mu^{8-2\Delta}\frac{\partial_t^2\alpha_{2,4} - 4(5-\Delta)\partial_t^2\sigma_{2,5}}{4(5-\Delta)}$$
$$+\mu^{8-2\Delta}\frac{\mu\partial_t\alpha_{2,5} - 4(5-\Delta)\mu\partial_t\sigma_{2,6} - \mu^2\alpha_{2,6} + 4(5-\Delta)\mu^2\sigma_{2,7}}{2(5-\Delta)}; \tag{2.169}$$

$$d_{(3)ii} \;=\; \frac{\mu^{8-2\Delta}}{6(11-2\Delta)}\Big(\partial_t^3\alpha_{2,4} - 2(11-2\Delta)\partial_t^3\sigma_{2,5} - 3\mu\partial_t^2\alpha_{2,5} + 6(11-2\Delta)\mu\partial_t^2\sigma_{2,6}$$
$$+\partial_t\alpha_{2,6} - 2(11-2\Delta)\partial_t\sigma_{2,7} - 6\mu^2\left(\mu\alpha_{2,7} + 2(11-2\Delta)\mu\sigma_{2,8}\right)\Big), \tag{2.170}$$

where $\sigma_{2,n}$ are the coefficients defined in (2.29) — implicitly, functions of the FG time t here.

The coefficients of the terms with factors of $z^{2\Delta}$ in G_{00} are given by

$$e_{(0)00} \;=\; -\frac{(2\Delta-1)\,\mu^{2\Delta}\beta_{2,4}}{2\Delta}; \tag{2.171}$$

$$e_{(1)00} \;=\; 2\mu^{2\Delta}\frac{(\Delta-1)\partial_t\beta_{2,4} - \Delta\mu\beta_{2,5}}{2\Delta+1}, \tag{2.172}$$

where $\beta_{2,n}$ is defined in eq. (2.28). Similarly, in G_{ii} the coefficients of the $z^{2\Delta}$ are given by

$$e_{(0)ii} \;=\; -\mu^{2\Delta}\frac{\beta_{2,4} - 4\Delta\theta_{2,5}}{2\Delta}; \tag{2.173}$$

$$e_{(1)ii} \;=\; \mu^{2\Delta}\frac{\partial_t\beta_{2,4} - 2(2\Delta+1)\partial_t\theta_{2,5} - \mu\beta_{2,5} + 2(2\Delta+1)\mu\tau_{2,6}}{2\Delta+1}, \tag{2.174}$$

where $\tau_{2,n}$ was defined in eq. (2.29).

2.12.3   The scalar field

The coefficients of the scalar field $f_{(n)}$ and $g_{(n)}$ in the FG coordinates can be written in terms of the coefficients $p_{(0)}$ and $p_{(2\Delta-4)}$ in eq. (2.26). The coefficients of $z^{4-\Delta}$ in $\hat{\phi}$ are

given by

$$
\begin{aligned}
\sum_{n=0} f_{(n)}(t) z^n &= \mu^{4-\Delta} \Bigg(p_{(0)} + z \partial_t p_{(0)} - \frac{z^2 (7 - 2\Delta) \partial_t^2 p_{(0)}}{4(\Delta - 3)} - \frac{z^3 (9 - 2\Delta) \partial_t^3 p_{(0)}}{12(\Delta - 3)} \\
&\quad + z^4 \left(\frac{1}{8} (4 - \Delta) \mu^4 p_{(0)} - \frac{(4\Delta^2 - 40\Delta + 99) \partial_t^4 p_{(0)}}{96(4 - \Delta)(\Delta - 3)} \right) + o\left(z^5\right) \Bigg),
\end{aligned}
$$

(2.175)

while the only coefficient of z^Δ that may play a role is

$$
g_{(0)} = \mu^\Delta \, p_{(2\Delta - 4)}.
$$

(2.176)

2.13 Appendix: Boundary stress-energy tensor and $\langle \mathcal{O}_\Delta \rangle$

In section 2.5, we constructed the holographic action $S_{reg} = S_{bulk} + S_{GHBY} + S_{count}$ which is now finite, *i.e.,* no divergences appear in the limit $\epsilon \to 0$. Hence, so are all quantities that can be calculated from this action. Of course, the latter includes the one-point functions of the stress tensor and operator $\mathcal{O}_\Delta$. In order to calculate these expectation values, we need to vary S_{reg} with respect to the boundary metric and the coupling to boundary operator, respectively. Recall that the boundary metric $g_{ab}^{(0)}$ appears as the leading coefficient in the expansion (2.39) of the bulk metric. Similarly, the coupling λ is proportional to the leading coefficient $f_{(0)}$ in the expansion (2.12.3) of the bulk scalar. We will establish our conventions for the precise normalization of the coupling in section 2.6.1 and so at this point, we simply introduce a dimensionless proportionality constant[9] with $\ell f_{(0)} = \alpha_\lambda \lambda$. Then the desired one-point functions are given by [69]

$$
\begin{aligned}
8\pi G_5 \langle T^{ab} \rangle &= \lim_{\epsilon \to 0} \frac{16\pi G_5}{\sqrt{-g^{(0)}}} \frac{\delta S_{reg}}{\delta g_{ab}^{(0)}} \\
&= \lim_{\epsilon \to 0} \frac{16\pi G_5}{\sqrt{-\gamma} \epsilon^4} \left(\frac{\delta S_{reg}}{\delta \gamma_{cd}} \frac{\delta \gamma_{cd}}{\delta g_{ab}^{(0)}} + \frac{\delta S_{reg}}{\delta \phi} \frac{\delta \phi}{\delta g_{ab}^{(0)}} \right)
\end{aligned}
$$

(2.177)

---

[9] The constant α_λ is fixed in eq. (2.67).

and

$$
\begin{aligned}
16\pi G_5 \langle \mathcal{O}_\Delta \rangle &= \lim_{\epsilon \to 0} \frac{16\pi G_5}{\sqrt{-g^{(0)}}} \frac{\delta S_{reg}}{\delta \lambda} = \lim_{\epsilon \to 0} \frac{16\pi G_5\, \alpha_\lambda}{\sqrt{-g^{(0)}}\, \ell} \frac{\delta S_{reg}}{\delta f_{(0)}} \\
&= \lim_{\epsilon \to 0} \frac{16\pi G_5\, \alpha_\lambda}{\sqrt{-\gamma}\, \ell\, \epsilon^4} \left(\frac{\delta S_{reg}}{\delta \gamma_{ab}} \frac{\delta \gamma_{ab}}{\delta f_{(0)}} + \frac{\delta S_{reg}}{\delta \phi} \frac{\delta \phi}{\delta f_{(0)}} \right) .
\end{aligned} \tag{2.178}
$$

We proceed by first evaluating the variations of the action with respect to γ and ϕ, then the variations of γ and ϕ with respect to $g_{ab}^{(0)}$ and $f_{(0)}$. The variation of the action on the cut-off surface $z = \epsilon$ is:

$$
\begin{aligned}
\frac{16\pi G_5}{\sqrt{-\gamma}} \frac{\delta \left(S_{\text{bulk}} + S_{\text{GHBY}} \right)}{\delta \gamma_{ab}} &= \frac{z}{2} \left(\gamma^{ac} \gamma^{bd} \partial_z \gamma_{cd} - \gamma^{ab} \gamma^{cd} \partial_z \gamma_{cd} \right) \Big|_{z=\epsilon} , \\
\frac{16\pi G_5}{\sqrt{-\gamma}} \frac{\delta \left(S_{\text{bulk}} + S_{\text{GHBY}} \right)}{\delta \phi} &= z \partial_z \phi \Big|_{z=\epsilon} , \\
\frac{16\pi G_5}{\sqrt{-\gamma}} \frac{\delta S_{\text{count}}}{\delta \gamma_{ab}} &= -\frac{1}{2} \gamma^{ab} \left(6 + \frac{4-\Delta}{2} \phi^2 - \frac{1}{4(\Delta-3)} (\partial\phi)^2 \right) \Big|_{z=\epsilon} \\
&\quad + \frac{1}{24(\Delta-3)} \left(\left(\nabla^a \nabla^b - \gamma^{ab} \Box \right) \phi^2 - 6\gamma^{ac} \gamma^{bd} \partial_c \phi\, \partial_d \phi \right) \Big|_{z=\epsilon} , \\
\frac{16\pi G_5}{\sqrt{-\gamma}} \frac{\delta S_{\text{count}}}{\delta \phi} &= -(4-\Delta)\phi - \frac{1}{2(\Delta-3)} \Box\phi \Big|_{z=\epsilon} .
\end{aligned} \tag{2.179}
$$

In the above we only showed the terms that would contribute at the orders of ℓ we are considering. Using the results of appendix 2.12, we find the variation of the bulk fields with respect to their boundary values (at leading order) are

$$
\begin{aligned}
\frac{\delta \gamma_{cd}}{\delta g_{ab}^{(0)}} &= \delta^a_{(c} \delta^b_{d)}\, z^{-2} \Big|_{z=\epsilon} , & \frac{\delta \phi}{\delta g_{ab}^{(0)}} &= o\left(z^{5-\Delta} \right) , \\
\frac{\delta \gamma_{ab}}{\delta f_{(0)}} &= -\frac{1}{6} \eta_{ab}\, \ell^2\, f_{(0)} z^{6-2\Delta} \Big|_{z=\epsilon} , & \frac{\delta \phi}{\delta f_{(0)}} &= \ell\, z^{4-\Delta} \Big|_{z=\epsilon} .
\end{aligned} \tag{2.180}
$$

The second equation in eq. (2.180) leads to a vanishing contribution to the stress tensor in eq. (2.177). The third equation above only contributes to eq. (2.178) when $\Delta = 4$ and hence can be ignored for our purposes. Inserting the variations from eqs. (2.179) and (2.180) into eqs. (2.177) and (2.178), we get the results presented in the main text in eqs. (2.44)–(2.46). Note that for these final results, we have replaced $f_{(0)}$ and $g_{(0)}$ by their expressions in terms of $p_{(0)}$ and $p_{(2\Delta-4)}$ given in appendix 2.12.3.

81

2.14 Appendix: The finite difference procedure in solving the scalar field equation

In order to solve for $\hat{\psi}(\tau, \rho)$ defined in section 2.7, we follow the same discretization procedure of [48]. Substituting $\hat{\phi}(\tau, \rho)$ as written in equation (2.91) into the linearized scalar equation of motion (2.22), we obtain an equation of motion for $\hat{\psi}$. In order to solve for the time dependent radial profile of $\hat{\psi}$, we disretize the bulk spacetime. We write down the form of our differential equation for $\hat{\psi}$ in order to show the derivative terms we need to discretize:

$$0 = d_1\hat{\psi} + d_2\partial_\tau\hat{\psi} + d_3\partial_\rho\hat{\psi} + d_4\partial_\tau\partial_\rho\hat{\psi} + d_5\partial_\rho^2\hat{\psi} + e, \qquad (2.181)$$

where the coefficients d_n are (known) functions of ρ, and e is a source term which depends both on ρ and τ, since it consists of the terms in the series expansion of $\hat{\phi}$ containing the source and its time-derivatives.

The discretization is as follows: we consider a radial interval $\rho \in [0, L_\rho]$, where L_ρ lies inside the black hole horizon. We discretize this interval into N points ρ_i, with $\rho_1 = 0$ and $\rho_N = L_\rho$. We also discretize the time direction into M slices τ_j, where τ_1 is chosen such that $p_0(\tau_1) \approx 0$ and τ_M such that $p_0(\tau_M) \approx 1$. Furthermore we must choose M large enough such that the timesteps in the discretization

$$\delta\tau \equiv \tau_{j+1} - \tau_j \lesssim \delta\rho \equiv \rho_{i+1} - \rho_i, \qquad (2.182)$$

such that, during our time evolution the round-off error stays small. Setting $\hat{\psi} = 0$ on the initial surface τ_1, we evolve it forward in time. We must solve for $\hat{\psi}$ at each radial point in the discretization on the timeslices τ_2 and onward. We set $\hat{\psi}(\tau_j, \rho_1) = 0$. This is automatically true, since $\hat{\psi}$ represents terms in the expansion of $\hat{\phi}$ of order ρ^Δ and higher and must vanish on the boundary of the spacetime. With the above initial and boundary conditions on our field, we use the values of the field at each previous timeslice to solve it on the next time slice. The solution of the field at a radial position ρ_j will depend on its value at the previous radial position ρ_{j-1}, in addition to values on the previous timeslice, as we will make clearer. Thus we solve for $\hat{\psi}$ stepwise into the bulk. We do this until we reach some depth into the horizon. In order to calculate the values of $\hat{\psi}$ at the point (τ_{i+1}, ρ_{j+1}) we calculate the derivatives and function values at the point $(\tau_i + \frac{1}{2}\delta\tau, \rho_j - \frac{1}{2}\delta\rho)$. Writing $\hat{\psi}(\tau_i + \frac{1}{2}\delta\tau, \rho_j - \frac{1}{2}\delta\rho)$ as $\hat{\psi}_{(i+1/2, j-1/2)}$, the function and its derivatives at this point

are given by

$$\hat{\psi}_{(i+1/2,j-1/2)} = \frac{\hat{\psi}_{(i+1,j-1)} + \hat{\psi}_{(i,j)}}{2} \tag{2.183}$$

$$\partial_\rho\hat{\psi}_{(i+1/2,j-1/2)} = \frac{\left(\hat{\psi}_{(i+1,j)} - \hat{\psi}_{(i+1,j-1)}\right) + \left(\hat{\psi}_{(i,j)} - \hat{\psi}_{(i,j-1)}\right)}{2\delta\rho} \tag{2.184}$$

$$\partial_\tau\hat{\psi}_{(i+1/2,j-1/2)} = \frac{\left(\hat{\psi}_{(i+1,j)} + \hat{\psi}_{(i+1,j-1)}\right) - \left(\hat{\psi}_{(i,j)} + \hat{\psi}_{(i,j-1)}\right)}{2\delta\tau} \tag{2.185}$$

$$\partial_\tau\partial_\rho\hat{\psi}_{(i+1/2,j-1/2)} = \frac{\left(\hat{\psi}_{(i+1,j)} - \hat{\psi}_{(i+1,j-1)}\right) - \left(\hat{\psi}_{(i,j)} - \hat{\psi}_{(i,j-1)}\right)}{2\delta\tau\delta\rho} \tag{2.186}$$

$$\partial_\rho^2\hat{\psi}_{(i+1/2,j-1/2)} = \frac{\left[\left(\hat{\psi}_{(i+1,j)} - \hat{\psi}_{(i+1,j-1)}\right) - \left(\hat{\psi}_{(i+1,j-1)} - \hat{\psi}_{(i+1,j-2)}\right)\right]}{2\delta\rho^2}$$
$$+\frac{\left[\left(\hat{\psi}_{(i,j+1)} - \hat{\psi}_{(i,j)}\right) - \left(\hat{\psi}_{(i,j)} - \hat{\psi}_{(i,j-1)}\right)\right]}{2\delta\rho^2}; \tag{2.187}$$

where the error in each derivative is of order $\delta\rho^2$ or $\delta\tau^2$. Since the coefficient d_n and the source term e_n in equation (2.181) are smooth functions of ρ and τ, we can calculate them exactly at the point $(\tau_i + \frac{1}{2}\delta\tau, \rho_j - \frac{1}{2}\delta\rho)$. Then, since equation (2.181) is linear, we can solve for the term $\hat{\psi}_{(i+1,j)}$ be separating it out of the discretized derivatives. Having solve for $\hat{\psi}$ at the point $(\tau_i + \delta\tau, \rho_j)$, we can solve for it at the next point, $(\tau_i + \delta\tau, \rho_j + \delta\rho)$, using the same procedure, until we solve for it at the point $(\tau_i + \delta\tau, \rho_N)$. We then proceed to solve for $\hat{\psi}$ on the timeslice τ_{i+2}, and keep repeating the process until we complete the final timeslice τ_M.

The reader may have noticed that the discretization of $\partial_\rho^2\hat{\psi}_{(i+1/2,j-1/2)}$ does not work as written in equation (2.187) for $j = 2$ and $j = N$, since the points ρ_{j-2} is not defined in the former case, and ρ_{N+1} in the latter case. To solve for $\hat{\psi}$ at these two locations, we

define the second-order radial derivative as

$$\partial_\rho^2 \hat{\psi}_{(i+1/2,2-1/2)} = \frac{\left(\hat{\psi}_{(i,3)} - \hat{\psi}_{(i,2)}\right) + \left(\hat{\psi}_{(i,2)} - \hat{\psi}_{(i,1)}\right)}{2\delta\rho} \tag{2.188}$$

$$\partial_\rho^2 \hat{\psi}_{(i+1/2,N-1/2)} = \frac{\left[\left(\hat{\psi}_{(i+1,N)} - \hat{\psi}_{(i+1,N-1)}\right) - \left(\hat{\psi}_{(i+1,N-1)} - \hat{\psi}_{(i+1,N-2)}\right)\right]}{2\delta\rho^2}$$

$$+ \frac{\left[\left(\hat{\psi}_{(i,N)} - \hat{\psi}_{(i,N-1)}\right) - \left(\hat{\psi}_{(i,N-1)} - \hat{\psi}_{(i,N-2)}\right)\right]}{2\delta\rho^2}. \tag{2.189}$$

Note that in both of the equations above, there is an error in the derivative of order $\delta\rho$, rather than $\delta\rho^2$ as in the other discretized derivatives above. As stated before, we choose the maximum depth in the bulk L_ρ to be well within the event horizon of black hole, such that the errors in calculating $\hat{\psi}$ do not propagate back outside the black hole where we care about the value of the scalar field.

2.15 Appendix: Analytic slow quenches

2.15.1 Analytic solution for slow quenches

The equation for the order α^{-1}–correction to the response for slow quenches is given in equation (2.98)

$$\left[\partial_\rho^2 - \frac{(\rho^4+3)}{\rho\left(1-\rho^4\right)}\partial_\rho - \frac{\Delta(\Delta-4)}{\rho^2\left(1-\rho^4\right)}\right] R_s^{(1)}(\rho) = -\frac{(3-2\rho\,\partial_\rho)}{\rho\left(1-\rho^4\right)}\phi_e(\rho)\,, \tag{2.190}$$

where $\phi_e(\rho)$ is the equilibrium solution of the scalar field (2.25), explicitly given in terms of hypergeometric functions as

$$\phi_e(\rho) = \rho^{4-\Delta}\,{}_2F_1\left(\frac{4-\Delta}{4},\frac{4-\Delta}{4},\frac{4-\Delta}{2},\rho^4\right)$$

$$-\frac{\Gamma\left(\frac{4-\Delta}{2}\right)\Gamma\left(\frac{\Delta}{4}\right)^2}{\Gamma\left(\frac{4-\Delta}{4}\right)^2\Gamma\left(\frac{\Delta}{2}\right)}\rho^\Delta\,{}_2F_1\left(\frac{\Delta}{4},\frac{\Delta}{4},\frac{\Delta}{2},\rho^4\right)\,, \tag{2.191}$$

where the proportionality constant is chosen such that the solution remains regular at the black hole horizon located at $\rho = 1$.

To solve the equation, we will first solve the homogeneous version of equation (2.190), and then construct a particular solution of the nonhomogeneous equation out of the two basis solutions we will find. The homogeneous equation (2.190) is in fact the same equation satisfied by the static solution of the scalar field and therefore our two basis solutions are

$$Y(\rho) = \rho^{4-\Delta} \, {}_2F_1\left(\frac{4-\Delta}{4}, \frac{4-\Delta}{4}, \frac{4-\Delta}{2}, \rho^4\right),$$ (2.192)

$$Z(\rho) = \rho^{\Delta} \, {}_2F_1\left(\frac{\Delta}{4}, \frac{\Delta}{4}, \frac{\Delta}{2}, \rho^4\right).$$ (2.193)

Out of these two homogeneous solutions, we now construct a particular solution

$$R_{\mathrm{p}}(\rho) = u_1(\rho) \, A(\rho) + u_2(\rho) \, Z(\rho).$$ (2.194)

and then a general solution to the inhomogeneous equation

$$R_s^{(1)}(\rho) = c_1 \, Y(\rho) + c_2 \, Z(\rho) + R_{\mathrm{p}}(\rho).$$ (2.195)

The constants c_1 and c_2 will be determined from boundary conditions.

The functions u_1 and u_2 are given by the two definite integrals

$$u_1(\rho) = -\int_0^{\rho} dy \frac{J(y) \, Z(y)}{W(Y(y), Z(y))}$$ (2.196)

$$u_2(\rho) = -\int_{\rho}^1 dy \frac{J(y) \, Y(y)}{W(Y(y), Z(y))}.$$ (2.197)

We are free to choose the limits of integration, and since we will be expanding around $\rho = 0$ and $\rho = 1$, these limits will turn out to be the most useful. The signs in front of the integrals are chosen such that u_1 acquires a minus sign to leading order in ρ when its derivative is taken, while u_2 acquires a plus sign. This is necessary in order to get the source out when substituting our particular solution into equation (2.190). In the above equations, J is the source term in the equation (2.190), *i.e.,*

$$J(\rho) = -\frac{(3 - 2\rho \, \partial_{\rho})}{\rho (1 - \rho^4)} \phi_{\mathrm{e}}(\rho),$$ (2.198)

while W is the Wronskian of the two homogeneous solutions

$$W(Y, Z) = Y \, Z' - Y' \, Z.$$ (2.199)

85

As it turns out, it can be shown that the Wronskian satisfies the differential equation

$$W' - \frac{(\rho^4 + 3)}{\rho(1 - \rho^4)}W = 0, \tag{2.200}$$

$-(\rho^4 + 3)/\rho(1 - \rho^4)$ being the coefficient of $\partial_\rho R_s^{(1)}$ in equation (2.190). W has the solution

$$
\begin{aligned}
W(\rho) &= a\exp\left[\int d\rho \frac{(\rho^4 + 3)}{\rho(1 - \rho^4)}\right] \\
&= a\exp\left[3\log\rho - \log(1 - \rho^4)\right] \\
&= a\frac{\rho^3}{1 - \rho^4}.
\end{aligned} \tag{2.201}
$$

Series expanding the definition of the Wronskian (2.15.1) about $\rho = 0$, we find that for equation (2.190) to be satisfied near the asymptotic boundary, the appropriate choice of a is $2\Delta - 4$, such that

$$W(\rho) = (2\Delta - 4)\frac{\rho^3}{1 - \rho^4}. \tag{2.202}$$

We therefore have our particular solution R_{p}, and need to solve the boundary conditions for the coefficients c_1 and c_2 in the general solution $R_s^{(1)}$.

2.15.2 Solving for the coefficients c_1 and c_2

$R_s^{(1)}$ has the expansion near $\rho = 0$

$$R_s^{(1)}(\rho) = \rho^{4-\Delta}\sum_{n=0}^{\infty} a_{(n)}\rho^n + \rho^{\Delta}\sum_{n=0}^{\infty} b_{(n)}\rho^n. \tag{2.203}$$

It is necessary to solve for $b_{(0)}$ in order to find the $1/\alpha$ correction to the static normalizable mode, and therefore to $a_{2,4}$, which controls the change in the thermodynamic quantities mentioned in section 2.6. Substituting this perturbative solution into equation (2.190), we see that $a_{(0)} = 0$, while $b_{(0)}$ remains undetermined. Expanding the integrands contained in the particular solution R_{p} about $\rho = 0$, we see that that R_{p} contains no terms of the order $\rho^{4-\Delta}$. This means that the only term of order $\rho^{4-\Delta}$ in the solution equation (2.195) is contained in $Y(\rho)$. Since

$$Y(\rho) = \rho^{4-2\Delta} + \dots, \tag{2.204}$$

86

we have that $c_1 = a_{(0)} = 0$. In order to solve for c_2 (and therefore $b_{(0)}$), we expand $R_s^{(1)}$ near $\rho = 1$ and choose c_2 to cancel the $\log(1 - \rho)$-divergence.

Expanding R_{p} near $\rho = 1$, we see that u_2, due to its limits of integration, must be vanishing as ρ approaches 1, and therefore the total $u_2(\rho)Z(\rho)$ term must vanish near $\rho = 1$. On the other hand, in order to evaluate u_1 near $\rho = 1$, it is useful to change the limits of integration via

$$u_1(\rho) = -\int_0^\rho \frac{ZJ}{W} = \left(-\int_0^1 + \int_\rho^1\right)\frac{ZJ}{W}. \tag{2.205}$$

The second integral vanishes as ρ approaches 1, and therefore will also lead to a vanishing contribution in the combination $u_1 Y$ in the solution (2.194). However, the first term can be numerically integrated on the interval from 0 to 1, giving a finite result in (2.205). When expanding around $\rho = 1$, this integral multiplies with the coefficient of the log–divergence in Y, giving the only other divergence at the horizon. We therefore find the constant coefficient of B in equation (2.195) to be

$$c_2 = \frac{\delta_Y}{\delta_Z}\int_0^1 \frac{Z(y)J(y)}{W(y)}dy, \tag{2.206}$$

where $\delta_{Y,Z}$ is the coefficient of $\log(1 - \rho)$ in the expansion of Y, Z near $\rho = 1$, respectively.

2.15.3 Solving for $b_{(0)}$

Next we would like to find the solution to the coefficient $b_{(0)}$ of ρ^Δ in the expansion of $R_s^{(1)}$ near $\rho = 0$. Expanding u_1 near the boundary, we see that it contains no terms in its expansion that can be multiplied with the terms in the expansion of Y to give a term of order ρ^Δ. Given that it is also regular at the boundary, this term will play no further role in determining $b_{(0)}$. On the other hand, we see that the integrand of u_2 contains a single divergence of order $\rho^{4-2\Delta}$ at the boundary. This divergence will remain upon integration when $\Delta > 5/2$. This is a further motivation for choosing the integration limits given in equation (2.197).

In order to expand u_2 close to the boundary, we break the integrand up into its regular and divergent part, as

$$\frac{Y(y)J(y)}{W(y)} = f(y) + \frac{5 - 2\Delta}{2\Delta - 4}y^{4-2\Delta}. \tag{2.207}$$

Once this is done, we can evaluate u_2 close to the boundary as

$$
\begin{aligned}
u_2(\rho) &= -\int_\rho^1 \left(f(y) + \frac{5 - 2\Delta}{2\Delta - 4} y^{4 - 2\Delta} \right) dy \\
&= -\int_0^1 f(y) dy + \int_0^\rho f(y) dy - \frac{1}{2\Delta - 4} \left(1 - \rho^{5 - 2\Delta} \right).
\end{aligned}
\tag{2.208}
$$

Therefore close to $\rho = 0$, u_2 contains two pure numbers, a contribution that vanishes close to the boundary (the integral from 0 to ρ) and a divergent term (for $\Delta > 5/2$). Note, however, that since u_2 multiplies Z, the lowest order term in Z, ρ^Δ, makes the divergence vanish near the boundary of the spacetime. Since there are no other constant terms in u_2, we can completely determine $b_{(0)}$ now.

The leading term in the expansion of $B(\rho)$ close to to the boundary is ρ^Δ, with coefficient 1. Therefore the total coefficient $b_{(0)}$ is given by

$$
b_{(0)} = c_2 - \int_0^1 f(y) dy - \frac{1}{2\Delta - 4}.
\tag{2.209}
$$

In practice, we evaluate $\int_0^1 f(y) dy$ numerically by

$$
\int_\varepsilon^1 \left(\frac{A(y) J(y)}{W(y)} - \frac{5 - 2\Delta}{2\Delta - 4} y^{4 - 2\Delta} \right) dy,
\tag{2.210}
$$

where ε is small cutoff (of the order of 10^{-4}). The numerical integrals were performed using Mathematica's built-in numerical integrator.

2.15.4 Values for $a_{2,4}$ at order α^{-1}.

We find that the values of $b_{(0)}$ calculated here compare very well with the values calculated using a shooting method. In particular, using this pseudo-analytical solution for $b_{(0)}$ for various values of Δ, we can calculate the asymptotic value of the metric response $a_{2,4}$ at order α^{-1} using equation (2.102):

$$
\begin{aligned}
\Delta = \frac{7}{3} : \quad & a_{2,4}(\infty) = -0.0196 \, \frac{1}{\alpha}, \\
\Delta = \frac{8}{3} : \quad & a_{2,4}(\infty) = -0.0521 \, \frac{1}{\alpha}, \\
\Delta = \frac{10}{3} : \quad & a_{2,4}(\infty) = -0.0984 \, \frac{1}{\alpha}, \\
\Delta = \frac{11}{3} : \quad & a_{2,4}(\infty) = -0.108 \, \frac{1}{\alpha}.
\end{aligned}
\tag{2.211}
$$

Comparing this to the results found using a shooting method, we see excellent agreement:

$$
\begin{aligned}
\Delta = \frac{7}{3} : \quad & a_{2,4}(\infty) = -0.0196 \, \frac{1}{\alpha} \,, \\
\Delta = \frac{8}{3} : \quad & a_{2,4}(\infty) = -0.0521 \, \frac{1}{\alpha} \,, \\
\Delta = \frac{10}{3} : \quad & a_{2,4}(\infty) = -0.0981 \, \frac{1}{\alpha} \,, \\
\Delta = \frac{11}{3} : \quad & a_{2,4}(\infty) = -0.108 \, \frac{1}{\alpha} \,.
\end{aligned}
\tag{2.212}
$$

Only for $\Delta = 10/3$ can the results be distinguished at the order shown, and the difference amounts to less than 1%.

Chapter 3

Universality of Abrupt Holographic Quenches

3.1 Introduction

Quantum quenches have recently become accessible in laboratory experiments [30–32,56], which has initiated much activity by theoretical physicists to understand such systems. Up until now, most analytic work on the topic of relativistic quantum quenches have assumed that the field theory is at weak coupling [58,59].

The study of quantum quenches at strong coupling is accessible through the gauge/gravity duality [5,6]. Much related work studying thermalization in the boundary theory was done by studying the gravity dual under the assumption that the non-equilibrium evolution can be approximated by a uniformly evolving spacetime, *e.g.,* [40,41,45,47,61,77]. Other approaches study the evolution of a probe on the static spacetime [43]. The approach of numerically evolving the dual gravity theory was initiated in [49]. Further numerical studies of quenches in a variety of holographic systems were presented in [48,52,62].

In [48,52], holography was applied to study quenches of the coupling to a relevant scalar operator in the boundary theory. A numerical approach was taken to study the evolution of the dual scalar field in the bulk spacetime. For fast quenches, evidence was found for a universal scaling of the expectation value of the boundary operator. Similar scaling was observed for the change in energy density, pressure and entropy density. However, no analytic understanding of this behaviour was available.

In this chapter, we investigate these holographic quenches analytically, focusing on the

work done by the quench. Unlike [48, 52] in which the coupling was an analytic function of time, we abruptly (but with some degree of smoothness) switch on this source at $t = 0$. The coupling is then varied over a finite interval δt (the dimensionful version of α as defined in equation (2.90)) and is held constant afterwards. We find that for fast quenches, the essential physics can be extracted by solving the linearized scalar field equation in the asymptotic AdS geometry. Note that our analysis is naturally driven to this regime by the limit $\delta t \rightarrow 0$[1]. In contrast to [48, 52], we are *not* a priori limiting our study to a perturbative expansion in the amplitude of the bulk scalar. Our analytic results also cover any spacetime dimension d for the boundary theory, whereas [48, 52] were limited to $d = 4$.

Let us describe the quenches in more detail: The coupling in the boundary theory is determined by the leading non-normalizable mode of the bulk scalar [5]. We set this mode to zero before $t = 0$, vary it in the interval $0 < t < \delta t$ and hold it fixed afterwards. Because the energy density can only change while the coupling is changing, we are only interested in the response of the scalar field during the timespan $0 < t < \delta t$. Further, since the response propagates in from the boundary of the spacetime, the field will only be nonzero within the lightcone $t = \rho$. Hence to determine the work done, we need only solve for the bulk evolution in the triangular region bounded by this lightcone, the surface $t = \delta t$ and the AdS boundary, as shown in figure 3.1. As is also illustrated, as $\delta t \rightarrow 0$, this triangle shrinks to a small region in the asymptotic spacetime. The normalizable component of the scalar field, which determines the expectation value of the boundary operator, can be solved analytically in this situation, and its scaling with δt can readily be seen from this solution. From this, we also obtain the scaling of the energy density in the boundary.

3.2 The physical setup

Consider a generic deformation of a conformal field theory (CFT) in d spacetime dimensions by the time-dependent coupling $\lambda = \lambda(t)$ of a relevant operator $\mathcal{O}_\Delta$ of dimension Δ: $\mathcal{L}_0 \rightarrow \mathcal{L} = \mathcal{L}_0 + \lambda \mathcal{O}_\Delta$. The quenches are then characterized by two distinct scales: the mass scale set by the change $\delta\lambda$ and that associated with the rate of change, *i.e.,* $1/\delta t$. As described above, we will be particularly interested in rapid quenches where the second scale is much larger than the first, that is, quenches where $\delta\lambda(\delta t)^{d-\Delta} \ll 1$. The gravity

---

[1]We assume that the timescale δt is still larger than the Planck scale, so that quantum gravity effects can be ignored.
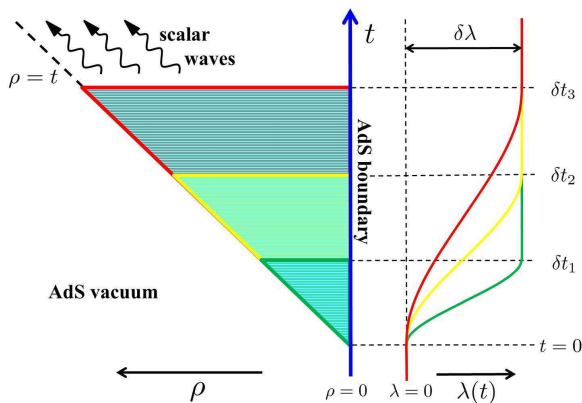
Figure 3.1: The shaded triangle is the region close to the boundary of the AdS spacetime where we must solve for the scalar field. We show several cases with $\delta t_1 < \delta t_2 < \delta t_3$. The profile $\lambda(t/\delta t)$ is held fixed in each case. In particular, the amplitude $\delta \lambda$ of the quench remains constant as δt becomes smaller. As the quench becomes more rapid, the bulk region shrinks closer to the asymptotic boundary.

dual describing this system is given by the action

$$
\begin{aligned}
S_{d+1} = {} & \frac{1}{16\pi G_{d+1}} \int d^{d+1}x \sqrt{-g} \\
& \times \left(R + d(d-1) - \frac{1}{2}(\partial \phi)^2 - \frac{1}{2}m^2\phi^2 - u(\phi) \right),
\end{aligned}
\tag{3.1}
$$

where we have chosen an AdS radius of 1. The bulk scalar ϕ is dual to $\mathcal{O}_\Delta$ with $m^2 = \Delta(\Delta - d)$. The potential $u(\phi)$ contains terms of order ϕ^3 or higher. To simplify our discussion, we will consider quenches where the conformal dimension of the operator is non-integer (for even d and not half-integer for odd d — see comments below). Further, we initially consider dimensions in the range $\frac{d}{2} \leq \Delta < d$.

Since we are interested in quenches that are homogeneous and isotropic in the spatial boundary directions, we assume that both the background metric and the scalar field depends only on a radial coordinate ρ and a time t. We will work in a spacetime asymptotic to the AdS Poincaré patch as $\rho \to 0$. Hence the bulk metric is

$$
ds^2 = -A(t,\rho)dt^2 + \Sigma(t,\rho)^2 d\vec{x}^2 + \rho^{-4}A(t,\rho)^{-1}d\rho^2.
\tag{3.2}
$$

The (nonlinear) Einstein equations and the scalar field equation then take the form:

$$
0 = -\frac{2(d-3)}{(d-1)A}u(\phi) + \frac{2d(d-3)}{A} + \rho^4 (\phi')^2 - \frac{d-3}{(d-1)A}m^2\phi^2 - \left(\frac{\dot\phi}{A}\right)^2 + \frac{2\rho^2 (\rho^2 A')'}{A}
$$

$$
+2(d-2)(d-1)\left[\left(\frac{\dot\Sigma}{A\Sigma}\right)^2 - \left(\frac{\rho^2\Sigma'}{\Sigma}\right)^2\right] - 4\left(\frac{\dot A}{A^2}\right)^2 + 2\frac{\ddot A}{A^3} , \tag{3.3}
$$

$$
0 = d - \frac{u(\phi)}{(d-1)} - \frac{m^2\phi^2}{2(d-1)} + \frac{\rho^4 A}{2(d-1)}(\phi')^2 + \frac{\dot\phi^2}{A} - \rho^4\frac{A'\Sigma'}{\Sigma} - (d-2)\rho^4 A\frac{(\Sigma')^2}{\Sigma^2}
$$

$$
+\frac{2\ddot\Sigma}{A\Sigma} - \frac{\dot A\dot\Sigma}{A^2\Sigma} + (d-2)\frac{\dot\Sigma^2}{A\Sigma^2} , \tag{3.4}
$$

$$
0 = \frac{(\phi')^2}{2(d-1)} + \frac{1}{2(d-1)}\left(\frac{\dot\phi}{\rho^2 A}\right)^2 + \frac{\Sigma''}{\Sigma} + \frac{2\Sigma'}{\rho\Sigma} + \frac{\ddot\Sigma}{\rho^4 A^2\Sigma} , \tag{3.5}
$$

$$
0 = \frac{\phi'\dot\phi}{d-1} + \frac{\dot A\Sigma'}{A\Sigma} - \frac{A'\dot\Sigma}{A\Sigma} + 2\frac{\dot\Sigma'}{\Sigma} , \tag{3.6}
$$

$$
0 = -\frac{\delta u(\phi)}{\delta\phi} - m^2\phi + \rho^4 A\phi'' + 2\rho^3 A\phi' + \rho^4 A'\phi' + \frac{(d-1)\rho^4 A\Sigma'\phi'}{\Sigma} + \frac{\dot A\dot\phi}{A^2}
$$

$$
-\frac{(d-1)\dot\Sigma\dot\phi}{A\Sigma} - \frac{\ddot\phi}{A} . \tag{3.7}
$$

where dots and primes denote derivatives with respect to t and ρ, respectively. The scalar field will have an asymptotic expansion of the form

$$
\phi(t,\rho) \sim \rho^{d-\Delta}\left(p_0(t) + o(\rho^2)\right) + \rho^\Delta\left(p_{2\Delta-d}(t) + o(\rho^2)\right) , \tag{3.8}
$$

where the non-normalizable coefficient p_0 is proportional to λ, while the normalizable coefficient $p_{2\Delta-d}$ is proportional to $\langle\mathcal{O}_\Delta\rangle$. Similarly,

$$
A \sim \rho^{-2}\left(1 + a_{d-2}(t)\rho^d + o(\rho^{d+4-2\Delta})\right) . \tag{3.9}
$$

Here, the coefficient a_{d-2} controls the energy density (and pressure) of the dual field theory, as shown in [48]. Equation (3.6) is a constraint, which in the limit $\rho \to 0$, determines $\partial_t a_{d-2}$. Integrating over t, we then find

$$
a_{d-2}(t) = \mathcal{C} - \frac{(2\Delta-d+1)(d-\Delta)}{(d-1)^2}p_0(t)p_{2\Delta-d}(t)
$$

$$
+\frac{2\Delta-d}{d-1}\int_0^t d\tilde t\, p_{2\Delta-d}(\tilde t)\frac{d}{d\tilde t}p_0(\tilde t) . \tag{3.10}
$$

Here $\mathcal{C} = a_{d-2}(-\infty)$ is an integration constant. With $d = 4$, this expression matches that found in [52], using Eddington-Finkelstein coordinates.

3.3 Rescaling procedure

In our quenches, the coupling to $\mathcal{O}_\Delta$ is made time-dependent with a characteristic time δt as

$$\lambda = \lambda\left(t/\delta t\right). \tag{3.11}$$

For general δt, the response $p_{2\Delta-d}$ in equation (3.8) cannot be solved analytically. However, as described in [48, 52], for large δt (adiabatic quenches), we can find a series solution for ϕ in inverse powers of δt and in principle, we can solve for $p_{2\Delta-d}$ analytically.

We now present a new analytic approach for the opposite limit of fast quenches. That is, for quenches where δt is much smaller than any other scale. As described above, to answer the question of how much work is done by the quench, we need only consider the interval $0 \leq t \leq \delta t$. Intuitively, we may expect that when δt is very short, there is no time for nonlinearities in the bulk equations to become important, *i.e.,* for the metric to backreact on the scalar.

To make this intuition manifest, we rescale the coordinates and fields by the parameter δt considering their (leading) dimension in units of the AdS radius: $\rho = \delta t\,\hat{\rho}$, $t = \delta t\,\hat{t}$, $A = \hat{A}/\delta t^2$, $\Sigma = \hat{\Sigma}/\delta t$ and $\phi = \delta t^{d-\Delta}\hat{\phi}$. With this rescaling, the limit $\delta t \to 0$ then removes the scalar from the Einstein equations (3.3–3.6), while leaving the form of the Klein-Gordon equation (3.7) unchanged.

The coefficient a_{d-2} controls the next-to-leading order term in A at small ρ. As we will show, this coefficient scales as $\delta t^{d-2\Delta}$. Further in equation (3.9), this coefficient is accompanied by a factor of ρ^d and hence this term has an overall scaling of $\delta t^{2(d-\Delta)}$. Hence as long as we are considering a relevant operator, this term vanishes in the limit $\delta t \to 0$. The same is true of the subleading contributions in the expression of Σ. Hence for fast quenches with small δt, we can approximate the metric coefficients as simply

$$\hat{\Sigma} = \hat{\rho}^{-1}, \qquad \hat{A} = \hat{\rho}^{-2}. \tag{3.12}$$

The equation for $\hat{\phi}$ becomes the Klein-Gordon equation in the AdS vacuum spacetime, *i.e.,*

$$\hat{\rho}^2\partial_{\hat{\rho}}^2\hat{\phi} - (d-1)\hat{\rho}\partial_{\hat{\rho}}\hat{\phi} - \hat{\rho}^2\partial_{\hat{t}}^2\hat{\phi} + \Delta\left(d - \Delta\right)\hat{\phi} = 0. \tag{3.13}$$

That is, in the limit of small δt, the work done in the full nonlinear quench can be determined by simply solving the linear scalar field equation (3.13) in empty AdS space!

94

3.4 Solving for the response

In the rescaled coordinates, the scalar field has an asymptotic series solution (in the rescaled coordinates) to (3.13) of the form

$$\phi(\hat{t}, \hat{\rho}) = \delta t^{d-\Delta} \hat{\rho}^{d-\Delta} \sum_{n=0} f_{2n} \hat{\rho}^{2n} p_0^{(2n)}(\hat{t}) + \delta t^{\Delta} \hat{\rho}^{\Delta} \sum_{n=0} g_{2n} \hat{\rho}^{2n} p_{2\Delta-d}^{(2n)}(\hat{t}), \qquad (3.14)$$

where f_{2n} and g_{2n} are known constants depending on d and Δ. Now we consider sources that vanish for $t \leq 0$ and are constant for $t \geq \delta t$. In $0 < t < \delta t$, we vary the source as

$$p_0(t) = \delta p \ (t/\delta t)^{\kappa} \qquad (3.15)$$

where κ is a positive exponent. Note that here $p_0(t \geq \delta t) = \delta p$. Since $\phi = 0$ before we switch on the source at $t = 0$, it remains zero throughout the bulk up to the null ray $t = \rho$. Therefore we impose

$$\phi(t = \rho, \rho) = 0. \qquad (3.16)$$

Evaluating the scalar field solution (3.14) given the source coefficient (3.16), we see that the boundary condition subject to the boundary condition (3.15) can only be satisfied if the normalizable coefficient is of the form

$$p_{2\Delta-d}(t) = b_{\kappa} \ \delta t^{d-2\Delta} \ \delta p \ (t/\delta t)^{d-2\Delta+\kappa}, \qquad (3.17)$$

b_{κ} being a constant depending on κ, d and Δ. Substituting in for the f_{2n} and g_{2n} in the asymptotic series for ϕ, and setting $t = \rho$, the boundary condition (3.16) becomes

$$0 = \sum_{n=0}^{\infty} \frac{(-1)^n \prod_{k=0}^{2n-1}(\kappa-k)}{4^n n! \prod_{k=1}^{n}(\Delta-k-d/2)} + b_{\kappa} \sum_{n=0}^{\infty} \frac{\prod_{k=0}^{2n-1}(d-2\Delta+\kappa-k)}{4^n n! \prod_{k=1}^{n}(\Delta+k-d/2)}, \qquad (3.18)$$

where we have cancelled a factor of $\rho^{d-\Delta+\kappa}$ as well as a factor of $\delta t^{-\kappa}$ from each term. With some rearrangement of the products in the above equation, equation (3.18) can be rewritten as

$$\begin{aligned}
0 &= \sum_{n=0}^{\infty} \frac{\left(\frac{1-\kappa}{2}\right)_n \left(\frac{-\kappa}{2}\right)_n}{n! \left(\frac{d+2}{2}-\Delta\right)_n} + b_{\kappa} \sum_{n=0}^{\infty} \frac{\left(\frac{1-d+2\Delta-\kappa}{2}\right)_n \left(\frac{-d+2\Delta-\kappa}{2}\right)_n}{n! \left(\Delta-\frac{d-2}{2}\right)_n} \\
&= {}_2F_1\left(\frac{1-\kappa}{2}, \frac{-\kappa}{2}; \frac{d+2}{2}-\Delta; 1\right) \\
&\quad + b_{\kappa} \, {}_2F_1\left(\frac{1-d+2\Delta-\kappa}{2}, \frac{-d+2\Delta-\kappa}{2}; \Delta-\frac{d-2}{2}; 1\right), \qquad (3.19)
\end{aligned}$$

where in the first line the symbol $(k)_n \equiv k(k+1)\ldots(k+n)$, and in the second line the functions $_2F_1$ are hypergeometric functions which we substituted in from the definition of their Taylor series. Using the identities

$$_2F_1\left(a, b; c; 1\right) = \frac{\Gamma(c)\Gamma(c - a - b)}{\Gamma(c - a)\Gamma(c - b)}; \quad c > a + b, \tag{3.20}$$

and

$$\Gamma\left(x\right)\Gamma\left(x + \frac{1}{2}\right) = 2^{1-2z}\sqrt{\pi}\Gamma\left(2x\right), \tag{3.21}$$

we can finally solve for b_κ in equation (3.19):

$$b_\kappa = -\frac{2^{d-2\Delta}\,\Gamma(\kappa + 1)\,\Gamma(\frac{d+2}{2} - \Delta)}{\Gamma(d + 1 + \kappa - 2\Delta)\,\Gamma(\Delta - \frac{d-2}{2})}\,. \tag{3.22}$$

Of course, if we construct more complicated sources with a series expansion of monomials as in equation (3.15) (for a non-monomial example of a source, see appendix 3.6), then since equation (3.13) is linear, the response is simply given by the sum of corresponding terms as in equation (3.17). As an example, consider the source

$$p_0(\hat{t}) = 16\,\delta p\left(\hat{t}^2 - 2\hat{t}^3 + \hat{t}^4\right) \tag{3.23}$$

as shown in figure 3.2. In this case, the source vanishes in both the initial and final state and it reaches the maximum δp at $t = \delta t/2$. Figure 3.3 shows the corresponding response for various values of Δ in $d = 4$.

The response coefficient (3.17) exhibits two noteworthy features: First, we see that the overall scaling of the response is $\delta t^{d-2\Delta}$. This is precisely the behaviour found in the numerical studies of [52] in the case $d = 4$. Second of all, $p_{2\Delta-d}$ varies in time as $t^{d+\kappa-2\Delta}$. Therefore if $\kappa < 2\Delta - d$, the response (*i.e.*, the operator expectation value $\langle\mathcal{O}_\Delta\rangle$ in the boundary theory) diverges at $t = 0$! For a source constructed as a series, both of these features in the response are controlled by the smallest exponent, as illustrated in figure 3.3 equation (3.23).

For homogeneous quenches, the diffeomorphism Ward identity reduces to $\partial_t \mathcal{E} = -\langle\mathcal{O}_\Delta\rangle\,\partial_t\lambda$ [48, 52]. Hence we can evaluate change in the energy density as

$$\Delta\mathcal{E} = -\mathcal{A}_\mathcal{E}\int_{-\infty}^{+\infty} p_{2\Delta-d}\,\partial_t p_0\,dt\,, \tag{3.24}$$

Figure 3.2: Normalized source $p_0/\delta p$ for equation (3.23) as a function of the rescaled time $\hat{t} = t/\delta t$.
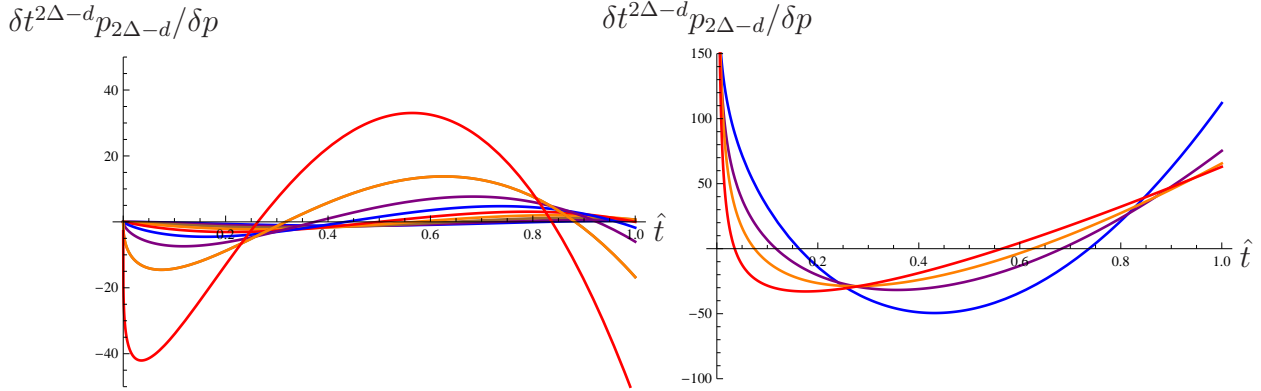

Figure 3.3: The response to the source (3.23) in $d = 4$ for $\Delta = 2.1$ through 2.9 on the left, and for $\Delta = 3.1$ through 3.4 on the right in steps of 0.1. On the left the plots with larger amplitudes correspond to larger Δ, while on the right the colours blue, purple, orange, and red correspond to the response for $\Delta = 3.1$ through 3.4 respectively.

with[2]

$$\mathcal{A}_{\mathcal{E}} = \frac{2\Delta - d}{16\pi G_{d+1}} = \frac{(2\Delta - d)(d-1)\pi^{\frac{d}{2}}\Gamma\left(\frac{d}{2}\right)}{2(d+1)\Gamma(d+1)}\, C_T\,. \tag{3.25}$$

Since $\partial_t p_0$ vanishes for $t < 0$ and $t > \delta t$, the above integral reduces to an integral from 0 to δt. It is for this reason that we do not need to determine the response $p_{2\Delta - d}$ after[3] $t = \delta t$. Further, for fast quenches, the change in energy density will scale as $\delta t^{d-2\Delta}$. Note that $\partial_t p_0$ scales as δt^{-1}, but the range of the integral $0 < t < \delta t$ adds an additional scaling of δt^{+1}. Hence the net scaling of $\Delta \mathcal{E}$ is precisely the scaling of $p_{2\Delta - d}$. Again this precisely matches the scaling found numerically in [52] for $d = 4$. In fact, this behaviour can be fixed as follows: Since equation (3.13) is linear, we must have $p_{2\Delta - d} \propto \delta p$ and hence $\Delta \mathcal{E} \propto \delta p^2$ from equation (3.24). Finally, dimensional analysis demands $\Delta \mathcal{E} \simeq \delta p^2 / \delta t^{2\Delta - d}$, up to numerical factors.

However, recall the singular behaviour in the response at $t = 0$ for $\kappa < 2\Delta - d$. Despite this divergence, one can easily see that in fact, the corresponding integral (3.24) remains finite as long as $\kappa > \Delta - \frac{d}{2}$. That is, for fixed Δ and d, we are constrained as to how quickly the source may be turned on. In fact, a more careful examination of the bulk solutions indicates that our analysis is valid for $\kappa > \Delta - \frac{d}{2} + \frac{1}{2}$. This condition comes from the fact that the identity (3.20) is only valid when the third argument of the hypergeometric function must be larger than the sum of the first two. When $a + b$, then $_2F_1(a, b; c; 1)$ diverges. In the solution for b_κ in terms of the two hypergeometric functions, this implies the bound $\kappa > \Delta - \frac{d}{2} + \frac{1}{2}$. For quenches not satisfying this inequality, we can no longer ignore the backreaction of the scalar on the spacetime geometry.

3.5 Discussion

To summarize, we have shown that in the limit of fast, abrupt quenches, the response and the energy density of a strongly coupled system which admits a dual gravitational description scales as $\delta t^{d-2\Delta}$. Here $\frac{d}{2} \leq \Delta < d$ is the conformal dimension of the quenched operator in the vicinity of the ultraviolet fixed point. Although we considered a quench

---

[2]C_T is a 'central charge' characterizing the leading singularity in the two-point function of the stress tensors — see [64] for details.

[3]To fully understand the dynamical evolution of the system for $t \geq \delta t$ would require a full numerical GR simulation. To leading order in the amplitude of the source this was discussed in [48] and [52]. Note, however, that for the fast quenches with $\Delta \geq \frac{d}{2}$, an arbitrarily large energy density is injected into the bulk as $\delta t \to 0$ and hence one can be confident that the gravitational dynamics results in the formation of a black hole.

from a vacuum state at $t = 0$, our results are universal. That is, they are independent of the initial state of the system, *e.g.,* we may start with a thermal state, as in [48,52]. This is again a reflection of the fact that abrupt holographic quenches are completely determined by the UV dynamics of the theory — see figure 3.1. Also, if different operators are quenched simultaneously, the response is dominated by the one with the largest conformal dimension.

We emphasize that while our calculations only considered the linearized scalar equation (3.13), our results apply for the full nonlinear quench. In the limit $\delta t \to 0$, the relevant physics occurs in the far asymptotic geometry (see figure 3.1) where the bulk scalar and perturbations of the AdS metric are all small. This contrasts with [48, 52], which only worked within a perturbative expansion in the amplitude of the scalar. Of course, the scalings determined there match those found here, but it was uncertain if they would persist in a full nonlinear analysis.

Of course, the present analysis does not predict the dynamical evolution of the system for $t > \delta t$. However, for the fast quenches above, an arbitrarily large energy density is injected into the bulk in the limit $\delta t \to 0$ and hence we can expect quite generally that a black hole forms. Further, we can deduce the properties of the final state black hole or, alternatively, of the equilibrium thermal state on the boundary as $t \to \infty$. Indeed, since the coupling and energy density are constant for $t > \delta t$, $\lambda(+\infty) = \lambda(\delta t)$ while equation (3.24) determines the final energy density of the system, to leading order in δt. Together, these parameters completely specify the final thermal equilibrium state.

Note that our analysis strictly applies to relevant operators, for which $d - \Delta > 0$. With a marginal operator (*i.e.,* $\Delta = d$), we can expect $\Delta \mathcal{E} \propto \delta t^{-d}$ on purely dimensional grounds [49]. While this matches the scaling found above, our numerical coefficients would no longer be valid. Marginal operators were also considered in [40,77] with a four-dimensional bulk. This case is analytically accessible because the scalar propagates on the light-cone. Extending this analysis to an odd-dimensional bulk is more challenging [40] because the scalar propagator is nonvanishing throughout the interior of the light-cone, similar to that for the relevant operators studied here.

Our discussion was also limited to $\frac{d}{2} \leq \Delta < d$, while unitarity bounds also allow for $\frac{d}{2} - 1 \leq \Delta < \frac{d}{2}$. In the latter range, we must consider the so-called 'alternate quantization' of the bulk scalar [19]. In fact, the asymptotic expansion of the scalar takes precisely the same form as in equation (3.8). However, in this regime, p_0 ($p_{2\Delta-d}$) is the coefficient of the (non-)normalizable mode. Our analysis applies equally well for this range of Δ and so one still finds $p_{2\Delta-d} \simeq \delta p \, \delta t^{d-2\Delta}$. That is, the response becomes vanishingly small as $\delta t \to 0$ with δp kept fixed. Hence to produce a finite $\langle \mathcal{O}_\Delta \rangle$ or finite $\Delta \mathcal{E}$, we would need to scale δp with an inverse power of δt.

When Δ is an integer for even d or half-integer for odd d, the scaling of the response $\langle \mathcal{O}_\Delta \rangle$ receives additional $\log(\delta t)$ corrections [48]. These logarithmic corrections arise from $\log \rho$ modifications in the asymptotic expansion (3.8) of the bulk scalar and are easily computed analytically following the present approach.

Another exceptional case arises with $\kappa = 2\Delta - d - n$ where n is a positive integer. In this case, equation (3.22) indicates $b_\kappa = 0$. Hence if the source is given by a series of monomials (3.15), the scaling of the response will be controlled by the first subleading contribution. With a single monomial, the (subleading) scaling of the response is controlled by nonlinearities in the bulk equations, $i.e.$, $p_{2\Delta-d} \simeq \delta t^{-\Delta}(\delta p\, \delta t^{d-\Delta})^n$ where $n = 2$ if the potential contains a ϕ^3 term and $n = 3$ otherwise.

It is interesting to consider the limit of abrupt quenches with $\delta t = 0$, as this usually sets the starting point in analyses at weak coupling $e.g.$, [34,58]. Our holographic result, $\Delta\mathcal{E} \simeq \delta p^2/\delta t^{2\Delta-d}$, indicates that the energy density diverges for an abrupt quench with $\Delta > \frac{d}{2}$ (a logarithmic divergence appears for $\Delta = \frac{d}{2}$ [48]). Hence it would be interesting to carefully compare these holographic results with those for previous weak coupling calculations [79]. Let us note here that many of these studies $e.g.$, [21,58] consider the regime $\Delta < d/2$ where $\Delta\mathcal{E}$ does not diverge in our holographic framework. However, singular behaviour was observed for abrupt quenches where our holographic model also produces divergences [37]. Of course, the preceding considerations assume a standard protocol where δp is held fixed in the limit $\delta t \to 0$. Instead, if we scale the source to zero as $\delta p \propto \delta t^{\Delta - \frac{d}{2}}$, $\Delta\mathcal{E}$ will remain finite. However, such a limit still produces a divergent response since $p_{2\Delta-d} \sim \delta t^{d-2\Delta}\, \delta p \propto \delta t^{\frac{d}{2}-\Delta}$. An alternate choice would be to scale $\delta p \propto \delta t^{2\Delta-d}$, which would leave $\langle \mathcal{O}_\Delta \rangle$ finite while $\Delta\mathcal{E} \to 0$.

An important question to ask is to what extent our results are relevant for everyday physical systems. Gauge theories with a dual gravitation description are necessarily strongly coupled and have an ultraviolet fixed point with large central charge. The framework of the gauge-string duality allows for the study of both the finite 't Hooft coupling corrections (the higher-derivative corrections in the gravitational dual) and non-planar (quantum string-loop) corrections. We expect that our gravitational analysis are robust with respect to the former, as the relevant near-boundary space-time region is weakly curved. Whether finite central charge corrections are important or not is an open question.

The universal behaviour uncovered is of relevance to fast quenches of relevant couplings in the vicinity of an ultraviolet fixed point — as such, it is challenging to observe it in experimental settings. We expect that fixed points in condensed matter systems described by relativistic CFT's may exhibit the same universal behaviour.

3.6 Appendix: Two special cases

Specializing to $d = 4$, and choosing the source coefficient which interpolates smoothly from 0 at $t = 0$, and δp at $t = \delta t$

$$p_0(t) = \frac{\delta p}{2} \left(1 - \cos\left(\frac{\pi t}{\delta t} \right) \right), \tag{3.26}$$

we can find an exact solution to the equation (3.13) in the form of a Fourier transform and is (compare with [5])

$$\phi(r, \rho) = \int_0^\infty d\omega \left(\mathcal{F}_c^\omega(\omega\rho) \, \cos(\omega t) + \mathcal{F}_s^\omega(\omega\rho) \, \sin(\omega t) \right), \tag{3.27}$$

where

$$\mathcal{F}_{c,s}^\omega(x) = a_{c,s}(\omega) x^2 J_{\Delta-2}(x) + b_{c,s}(\omega) x^2 Y_{\Delta-2}(x). \tag{3.28}$$

J and Y are Bessel functions of the first and second kind, respectively. The expansion of $\mathcal{F}_{c,s}^\omega(x)$ is

$$
\begin{aligned}
\mathcal{F}_{c,s}^\omega(x) &= x^{4-\Delta} \left(\chi_1(\Delta) b_{c,s}(\omega) - \frac{\chi_1(\Delta) b_{c,s}(\omega)}{4(\Delta - 3)} x^2 + \dots \right) \\
&\quad + x^\Delta \left(\chi_2(\Delta) a_{c,s}(\omega) + \chi_3(\Delta) b_{c,s}(\omega) + \dots \right),
\end{aligned} \tag{3.29}
$$

where

$$
\begin{aligned}
\chi_1(\Delta) &= \frac{2^{\Delta-2} \Gamma(\Delta - 2)}{\pi} \\
\chi_2(\Delta) &= \frac{2^{2-\Delta}}{\Gamma(\Delta - 1)} \\
\chi_3(\Delta) &= -\frac{2^{2-\Delta} \cos(\pi(\Delta - 2)) \Gamma(\Delta - 2)}{\pi}.
\end{aligned} \tag{3.30}
$$

Comparing the asymptotic solution (3.29) to the scalar field expansion (3.13), we see that the Fourier coefficients $b_{c,s}(\omega)$ entirely determine the non-normalizable coefficient p_0, and can be chosen arbitrarily. This means that in an asymptotic expansion close to the boundary, the terms of order $\rho^{4-\Delta}$ which determine the source are contained in the Bessel functions $Y_{\Delta-2}$.

To find the Fourier coefficients $a_{c,s}(\omega)$, we can impose the boundary condition (3.16), and try to find a suitable choice for $a_{c,s}(\omega)$ to satisfy the boundary condition. This constraint on the Fourier integral translates to

$$
\begin{aligned}
&- \int_0^\infty d\omega \, (\omega\rho)^2 \, Y(\omega\rho) \, (b_c^\omega \cos(\omega\rho) + b_s^\omega \sin(\omega\rho)) \\
&= \int_0^\infty d\omega \, (\omega\rho)^2 \, J(\omega\rho) \, (a_c^\omega \cos(\omega\rho) + a_s^\omega \sin(\omega\rho)) \, .
\end{aligned}
\tag{3.31}
$$

Because the integral is over ω, and the Fourier coefficients $a_{c,s}(\omega)$ and $b_{c,s}(\omega)$ depend only on ω, the asymptotic expansion of the integrals in ρ is the same as that of the integrands. Expanding both the left and right hand sides of the equation in small ρ, we see that only $Y_{\Delta-2}$ contains terms of the form $\rho^{n-\Delta}$, where n is an integer. Meanwhile the expansion of $J_{\Delta-2}$ only contains terms of the form $\rho^{n+\Delta}$. There is therefore no obvious way to cancel the two sides for general Δ. The Fourier integral in (3.31) may still converge correctly to cancel the two sides, as numerics suggest, however the correct choice of $a_{c,s}(\omega)$ is not obvious in general, and the scaling with δt is not manifest.

Two notable exceptions to the above difficulty are $\Delta = \frac{5}{2}$ and $\Delta = \frac{7}{2}$, since $\rho^{n-\Delta}$ is also of the form $\rho^{n+\Delta}$.

In these two special cases, it turns out that the boundary condition *can* be made to work. Since the solution of the response is almost identical to in both cases, we will focus our attention on $\Delta = 5/2$ for a specific source, and simply state the solution for $\Delta = 7/2$.

Applying the boundary condition $\phi(\rho, \rho) = 0$ we can compare the terms in the asymptotic expansions of (3.31). We see that the expansions in small x that

$$
x^2 Y_{1/2}(x) \cos(x) = x^2 J_{1/2}(x) \sin(x) - \sqrt{\frac{2}{\pi}} x^{3/2},
\tag{3.32}
$$

$$
x^2 Y_{1/2}(x) \sin(x) = -x^2 J_{1/2}(x) \cos(x).
\tag{3.33}
$$

In order for (3.31) to be valid, it would therefore be appropriate to choose

$$
a_c(\omega) = b_s(\omega), \qquad a_s(\omega) = -b_c(\omega) - \sqrt{\frac{\pi}{2}} \frac{1}{2\omega^{3/2}} \delta(\omega) \, .
\tag{3.34}
$$

Let's consider the specific source (3.26). Expansion (3.29) requires that

$$
b_c(\omega) = \frac{\pi \omega^{\Delta-4}}{2^{\Delta-1} \Gamma(\Delta-2)} \left(\delta(\omega) - \delta\left(\omega - \frac{\pi}{\delta t}\right) \right),
\tag{3.35}
$$

$$
b_s(\omega) = 0,
\tag{3.36}
$$

for general Δ. In the case $\Delta = \frac{5}{2}$ these expressions become

$$b_c(\omega) = -\sqrt{\frac{\pi}{2}} \frac{1}{2\omega^{3/2}} \left(\delta(\omega) - \delta\left(\omega - \frac{\pi}{\delta t}\right)\right), \tag{3.37}$$

$$b_s(\omega) = 0. \tag{3.38}$$

The corresponding choices for the $a(\omega)$ coefficients are then

$$a_s^\omega = -\sqrt{\frac{\pi}{2}} \frac{1}{2\omega^{3/2}} \delta\left(\omega - \frac{\pi}{\delta t}\right), \tag{3.39}$$

$$a_c^\omega = 0. \tag{3.40}$$

This gives a solution to the response of

$$p_2(t) = -\frac{\pi}{2\delta t} \sin\left(\frac{\pi t}{\delta t}\right). \tag{3.41}$$

This shows that p_2 grows as δt gets smaller. Specifically p_2 therefore grows as δt^{-1}, consistent with the prediction in [52] that the response grows as $\delta t^{4-2\Delta}$. This solution agrees precisely with the response of the form (3.17).

For reference, in the case $\Delta = 7/2$, with the same source as above, the correct choice for the coefficients b^ω is

$$b_c(\omega) = -\sqrt{\frac{\pi}{2}} \frac{1}{2\omega^{1/2}} \left(\delta(\omega) - \delta\left(\omega - \frac{\pi}{\delta t}\right)\right), \tag{3.42}$$

$$b_s(\omega) = 0. \tag{3.43}$$

The corresponding choice for the a^ω coefficients is

$$a_s(\omega) = -\sqrt{\frac{\pi}{2}} \frac{1}{2\omega^{1/2}} \delta\left(\omega - \frac{\pi}{\delta t}\right), \tag{3.44}$$

$$a_c(\omega) = 0. \tag{3.45}$$

This gives us a response coefficient

$$p_2(t) = -\frac{1}{6} \left(\frac{\pi}{\delta t}\right)^3 \sin\left(\frac{\pi t}{\delta t}\right), \tag{3.46}$$

again agreeing with the behaviour in [52]. The response again grows as δt^{-3}, as the universal behaviour $\delta t^{4-2\Delta}$ predicts.

103

Chapter 4

Nonlocal probes of thermalization in holographic quenches with spectral methods

4.1 Introduction

Quantum quenches are processes where an isolated system is driven to a far-from-equilibrium state by rapidly varying some control parameters. It has been possible to produce and study such processes in laboratory experiments in recent years, in particular, with ultracold atomic gases [30–32, 56, 80]. This experimental progress has provided a great impetus to improve our theoretical description of quenched systems. Certainly theoretical progress made with investigations within a variety of different frameworks, *e.g.,* two-dimensional conformal field theories [35, 58, 81], (nearly) free field theories [34, 58, 82] and integrable models [34, 59, 83], as well as some results applying to weakly interacting relativistic quantum field theories in higher dimensions [21, 36–38]. It remains a challenge to find broadly applicable and efficient techniques, as well as extracting insights into general organizing principles for the behaviour of far-from-equilibrium systems.

A new theoretical tool allows for the investigation of quenches for (certain) strongly coupled field theories is gauge/gravity duality [5, 6]. Assuming the robustness of this holographic duality in non-equilibrium situations, as studied in *e.g.,* [40, 61], it is possible to study the behaviour of the boundary field theory, either when it is perturbed, or far from equilibrium. Initial work by [43, 49] has lead to a large body of work in the field of quantum quenches of field theories at strong coupling, including [48, 51–54, 60, 62, 84–86].

In the gravity dual of the quantum field theory, the quench usually has a simple geometric interpretation and is introduced, *e.g.,* in the form of a gravitational shock wave collapsing into a black hole and a collapsing shell of matter described by the Vaidya metric, collapsing into a black hole [40, 41, 45–47, 87]. Applications of holographic quenches include quenches across phase transition points in the field theory [60], and to model hadron collisions in particle accelerators such as RHIC [50].

In an ongoing research program including [48], [52] and [54], we study the response of a strongly coupled $\mathcal{N} = 4$ supersymmetric Yang-Mills thermal plasma, quenched by a relevant operator, using the holographic duality. Having previously studied such quenches, we now apply more powerful numerical techniques to find the full time-dependent profiles of the perturbations of the metric and scalar field in the dual AdS spacetime. This allows us to utilize nonlocal probes such as two-point functions and entanglement entropy to better understand thermalization at various distance scales.

The quench that we study here for the Yang-Mills plasma in four spacetime dimensions, is that of switching on a fermionic operator in a smooth manner, by giving it a time-dependent mass. This is dual to a radially collapsing scalar field in an AdS black brane geometry in five dimensions. Since the mass is turned on in a homogeneous manner in the boundary theory, we are studying a global quench. Further, as implied in our description of the gravitational dual, we are studying a thermal quench where the theory begins in a thermal state, rather than in the vacuum — the latter simplifies the analysis, as we will describe below.

It is straightforward to find the solution for a static scalar field on an AdS background containing a planar black hole — see [72] for the solution in $\mathcal{N} = 2^*$ theory, and [88] for general operators satisfying the constraint $2 \le \Delta < 4$. However, once the scalar field is given a time-dependent source, the nonlinear Einstein and Klein-Gordon equations become highly nontrivial to solve. Treating the scalar field as a perturbation backreacting on the metric only at second order, the problem becomes more tractable, since the scalar field and metric components decouple at leading order in the Klein-Gordon equation. The solution to the metric then becomes that of the static background, plus a time-dependent contribution which is second order in the amplitude of the scalar. Despite this simplification, in the asymptotic series for the scalar field, one (time-dependent) coefficient remains undetermined, and can only be solved by evolving the scalar field forward in time from a known initial configuration. In [48] and [52], a finite difference method was employed, which is computationally quite costly. These studies were limited to first order in the amplitude of the scalar, meaning that the normalizable coefficient in the asymptotic expansion of the scalar field was calculated, as well as some terms in the metric's asymptotic expansion which could be directly calculated from this normalizable coefficient. However, the full sec-

ond order profile of the metric could not be determined in this way, making the calculation of nonlocal probes in the geometry impossible.

Chebyshev spectral methods are powerful methods for solving systems of differential equations [89]. Representing the solution to the equations by a series of Chebyshev polynomials, we can approximate the full radial profile of the solutions to a high degree of accuracy. In the present chapter we will apply these methods to the problem of solving for a massive scalar field in a five-dimensional AdS spacetime, as well as the time-dependent profiles of the metric perturbations.

The organization of the rest of our chapter is as follows: we first introduce the physical setup of the scalar field on the AdS-black brane spacetime in sections 2 and 3, as well as the coordinate system used. We then go on in section 4 to show the calculation of the thermalization of the system, by studying different nonlocal quantities that can be calculated in this spacetime. First we examine the evolution of the apparent and event horizons. We then go on to calculate the two-point correlation functions. Finally we calculate the entanglement entropy of a strip on the boundary. These calculations require knowing the full time-dependent geometry, *i.e.,* the full profile of the second order metric components, and therefore rely on our numerical simulations of the evolution. We find in particular that the apparent and event horizons thermalize much sooner than the local one-point functions of the quenching operator, and that wider separations in the two-point correlator and entanglement entropy thermalize later than for narrower regions. Furthermore, two-point functions and entanglement entropies that are wide enough will thermalize later than the one-point function as well.

In section 5 we investigate the thermalization behaviour of the previous section in closer detail. The entanglement entropy and two-point functions are dual to minimal surfaces and geodesics extending into the geometry of the spacetime, respectively. Since the radial direction in the AdS geometry is related to the energy scales in the field theory, we can see the thermalization as happening due to the interaction of a range of energy scales, rather than a scalar quantity equilibrating over time. We end this section by discussing how the different scales of the problem contribute to the thermalization.

In appendix 4.7 we discuss a method for solving the perturbative problem using interpolating Chebyshev polynomials, which is far less costly computationally than the finite difference methods used in [48,52]. This method leads to equivalent results compared to the finite difference method used in the above-mentioned papers. We also discuss convergence properties of this method.

In the present chapter we will focus on a bulk spacetime of dimension $d + 1 = 5$, with

a scalar field of mass[1] $m^2 = \Delta\,(\Delta - d) = -3$. We emphasize that we specialize to these cases by way of example, and the methods and algorithms described in this chapter can easily be adapted for different d and Δ (with the restriction $\frac{d}{2} \leq \Delta < d$).

This will serve as a prelude to the new solution of the full non-perturbative backreaction of the scalar field on the AdS-black brane geometry.

4.2   The physical setup

The physical system we would like to study is that of a scalar field ϕ on an AdS-black brane spacetime. The evolution equations of the metric and scalar can be found by varying the five-dimensional Einstein-Hilbert action

$$S_5 = \frac{1}{16\pi G_5} \int d^5\xi \sqrt{-g} \left(R + 12 - \frac{1}{2}(\partial\phi)^2 - \frac{1}{2}m^2\phi^2 + \mathcal{O}(\phi^4) \right). \tag{4.1}$$

Of particular interest to us is the case $m^2 = -3$, since the scalar field is then dual to a fermionic mass operator with $\Delta = 3$ in a thermal $\mathcal{N} = 2^*$ gauge theory living in four flat spacetime dimensions [90–92]. We use the background ansatz of an infalling Eddington-Finkelstein metric and a scalar field which depend only on the radial and time directions in the spacetime, while being isotropic in the four transverse directions:

$$ds_5^2 = -A(v,r)\,dv^2 + \Sigma(v,r)^2\,(d\vec{y})^2 + 2dr dv, \qquad \phi = \phi(v,r). \tag{4.2}$$

In (4.2) r is the light-like radial coordinate of the spacetime, v is the time coordinate and $\vec{y}$ are the coordinates corresponding to the spatial directions on the conformal boundary. We would like to send in a scalar field $\phi\,(v,r)$ from the boundary of this spacetime at $r = \infty$. Varying the metric and scalar field in (4.1) leads to the equations of motion [48]

$$
\begin{aligned}
0 =\, & \Sigma\,\partial_r(\dot{\Sigma}) + 2\dot{\Sigma}\,\partial_r\Sigma - 2\Sigma^2 + \frac{1}{12}m^2\phi^2\Sigma^2, \\
0 =\, & \partial_r^2 A - \frac{12}{\Sigma^2}\dot{\Sigma}\,\partial_r\Sigma + 4 + \dot{\phi}\,\partial_r\phi - \frac{1}{6}m^2\phi^2, \\
0 =\, & \frac{2}{A}\,\partial_r(\dot{\phi}) + \frac{3\,\partial_r\Sigma}{\Sigma A}\,\dot{\phi} + \frac{3\,\partial_r\phi}{\Sigma A}\,\dot{\Sigma} - \frac{m^2}{A}\,\phi, \\
0 =\, & \ddot{\Sigma} - \frac{1}{2}\partial_r A\,\dot{\Sigma} + \frac{1}{6}\Sigma\,(\dot{\phi})^2, \\
0 =\, & \partial_r^2\,\Sigma + \frac{1}{6}\Sigma\,(\partial_r\phi)^2,
\end{aligned}
\tag{4.3}
$$

---

[1]We set the AdS radius to 1.

where

$$\dot{h} \equiv \partial_v h + \frac{1}{2} A \, \partial_r h, \tag{4.4}$$

for any h.

Setting the scalar field to zero, there is no longer a source for dynamics in the spacetime. We are then left with a static, planar black hole metric which can be described by the line-element [48, 52]

$$ds^2 = -(r^2 - \frac{\mu^4}{r^2}) \, dv^2 + r^2 (d\vec{y})^2 + 2dr dv, \tag{4.5}$$

where $r = \mu$ is the position of the event horizon. Of course, this parameter also sets the temperature of the corresponding plasma in the boundary theory, $i.e.,$ $T = \mu/\pi$. Since the scalar field is initially zero when we turn on the quench in the asymptotic past, the above static spacetime is the initial equilibrium configuration of our system and μ sets the initial temperature in our thermal quenches. As the mass coupling of the fermionic operator is switched on, the changing boundary conditions excite the scalar field in the AdS-black brane background, collapsing into the black hole. The scalar field excitations evolve and backreact on the metric, and the bulk fields reach a different equilibrium configuration in the asymptotic future. In this final static configuration, the metric will be modified from its initial form in (4.5). In particular, the black hole would have grown due to the energy it absorbed from the infalling scalar field excitations. The scalar field will also have a nonzero static profile because of the new boundary conditions imposed at asymptotic infinity.

Beginning with an initial state allows us to simplify the analysis of the quenches. In particular, the initial state is provides an energy scale, $i.e.,$ the initial temperature T_i, and we will only study quenches where the final mass m_f of the fermionic operator is small compare to that scale. That is, we only consider quenches where $m_f/T_i \ll 1$, following [48, 52]. In the dual gravitational description, this choice corresponds to treating the scalar as a perturbation on the background geometry. In other words, we assume that the black hole is very large so that it is possible to perform an expansion in the amplitude of the scalar field in equations (4.3), as in [48, 52]. To leading order in its amplitude the scalar field equation becomes the equation of a scalar field on the static background metric (4.5). In references [72, 88], the analytic profile of the static perturbative scalar field was found for both particular and general values of m, respectively. In the special case where $m^2 = -3$ that we will be considering, the scalar field was found to have the profile [48]

$$\phi(r) = \ell \pi^{-1/2} \Gamma \left(\frac{3}{4} \right)^2 \left(\frac{\mu}{r} \right)^3 {}_2F_1 \left(\frac{3}{4}, \frac{3}{4}, 1, 1 - \frac{\mu^4}{r^4} \right), \tag{4.6}$$

where ℓ parameterizes the amplitude of the bulk scalar and also the value of the mass coupling in the boundary theory. Regardless of the dynamics during the evolution of

the quench, the scalar will relax to profile of the above form in the final equilibrium configuration. In [48,52], it was still necessary to know the full evolution of the bulk scalar in order to calculate late-time quantities such as the change in the stress-energy tensor of the dual field theory and the change in temperature, which were determined in terms of integrals of the normalizable mode over time.

4.3   Dimensionless coordinates

We introduce the dimensionless coordinates by scaling out a factor of the black hole horizon position μ (which has units of energy)

$$\rho = \frac{\mu}{r}, \qquad \tau = \mu v. \tag{4.7}$$

After scaling out the appropriate factor of μ, the warp factors become

$$A = \mu^2 a, \qquad \Sigma = \mu s. \tag{4.8}$$

Despite having dimensions of length, a more careful analysis shows that the scalar field should not be rescaled by a factor of μ^{-1}. The new radial coordinate ρ is particularly useful, since now the conformal boundary of the spacetime is located at $\rho = 0$. As noted above the dimensionful constant μ can be interpreted as the initial position of the black brane horizon. Therefore, the initial horizon is now situated at $\rho = 1$. With these redefinitions, the field equations (4.3) become the dimensionless equations

$$0 = \partial_\tau \partial_\rho \phi - \frac{1}{2}\rho^2 a \partial_\rho^2 \phi + \left(-\frac{1}{2}\rho^2 \partial_\rho a - \rho a - \frac{3}{2}a\rho^2 \partial_\rho \ln s + \frac{3}{2}\partial_\tau \ln s\right)\partial_\rho \phi + \frac{3}{2}\partial_\rho \ln s \partial_\tau \phi$$

$$+ \frac{m^2 \phi}{2\rho^2}, \tag{4.9}$$

$$0 = \partial_\tau \partial_\rho s - \frac{1}{2}\rho^2 a \partial_\rho^2 s - \frac{\rho^2 a}{s}(\partial_\rho s)^2 + \frac{2}{s}\partial_\tau s \partial_\rho s + \left(-\frac{1}{2}\rho^2 \partial_\rho a - \rho a\right)\partial_\rho s$$

$$+ \frac{1}{12}\frac{s(24 - m^2 \phi^2)}{\rho^2}, \tag{4.10}$$

$$0 = \partial_\rho^2 a + \frac{2}{\rho}\partial_\rho a + \left(-6(\partial_\rho \ln s)^2 + \frac{1}{2}(\partial_\rho \phi)^2\right)a + \frac{12}{\rho^2}\partial_\rho \ln s \partial_\tau \ln s + \frac{4}{\rho^4} - \frac{1}{\rho^2}\partial_\rho \phi \partial_\tau \phi$$

$$- \frac{m^2 \phi^2}{6\rho^4}. \tag{4.11}$$

These are the evolution equations for the scalar field and the two warp factors in the metric. Along with these, the Einstein equations provide two constraints, namely

$$0 = \frac{1}{6}(\partial_\rho \phi)^2 s + \partial_\rho^2 s + \frac{2}{\rho}\partial_\rho s, \tag{4.12}$$

$$0 = \partial_\tau^2 s - \frac{1}{2}\rho^2 \partial_\tau a \partial_\rho s - a\rho^2 \partial_\tau \partial_\rho s + \frac{1}{4}a^2 \rho^4 \partial_\rho^2 s + \frac{1}{2}a^2 \rho^3 \partial_\rho s + \frac{1}{2}\rho^2 \partial_\rho a \partial_\tau s + \frac{1}{6}s(\partial_\tau \phi)^2$$
$$- \frac{1}{6}sa\rho^2 \partial_\tau \phi \partial_\rho \phi + \frac{sa^2}{24\rho^4}(\partial_\rho \phi)^2. \tag{4.13}$$

Used in combination, (4.12) and (4.13) determine the response of the warp factor a up to an arbitrary integration constant [48].

4.3.1 $m^2 = -3$

Specializing equations (4.9) – (4.13) to a scalar with mass $m^2 = -3$, we find an asymptotic solution to the scalar and warp factors as $\rho \to 0$ of [48]

$$\phi = p_0\, \rho + p_0'\, \rho^2 + \rho^3 \left(p_2 + \ln\rho \left(\frac{1}{2}p_0'' + \frac{1}{6}p_0^3 \right) \right) + \mathcal{O}(\rho^4 \ln\rho),$$

$$a = \frac{1}{\rho^2} - \frac{1}{6}p_0^2 + \rho^2 \left(a_2 + \ln\rho \left(\frac{1}{6}(p_0')^2 - \frac{1}{6}p_0 p_0'' - \frac{1}{36}p_0^4 \right) \right) + \mathcal{O}(\rho^3 \ln\rho), \tag{4.14}$$

$$s = \frac{1}{\rho} - \frac{1}{12}\rho p_0^2 - \frac{1}{9}\rho^2 p_0 p_0' + \mathcal{O}(\rho^3 \ln\rho),$$

where p_0, p_2 and a_2 are functions of τ, a prime here denotes a derivative with respect to τ. The coefficient p_0 is the so-called 'non-normalizable mode' or the source coefficient [5, 93]. Here we will choose this coefficient to have a time-dependent profile, implying that the scalar field is sourced at the conformal boundary of the AdS spacetime and excitations are sent into the bulk geometry in a time-dependent manner. The coefficient p_2 is the so-called 'normalizable mode', or the response coefficient. This is the coefficient which is to be determined given a source p_0. While analytic solutions of p_2 are known when p_0 varies very slowly from time $\tau = -\infty$ to $\tau = +\infty$ [48, 52], as well as for p_0 made time-dependent abruptly and over a very short period of time [54], no analytic solutions for the normalizable mode are currently known for a source with general time-dependence.

The solutions presented in (4.14) are for the full nonlinear equations. There is an additional constraint on a_2 coming from eqs. (4.12) and (4.13) [48]:

$$0 = -\frac{1}{6}p_0' p_2 + \frac{1}{36}p_0' p_0'' - \frac{5}{108}p_0^3 p_0' + \frac{1}{2}a_2' - \frac{1}{9}p_0 p_0''' + \frac{1}{6}p_0 p_2'. \tag{4.15}$$

The full warp factors can in principle therefore be determined completely given p_0 and p_2.

The nonlinearities in the equation determining the scalar field make it challenging to extract the response coefficient p_2. For this reason, in [48, 52], the scalar field was treated as a perturbation on the spacetime, linearizing the Klein-Gordon equation (4.9). It then becomes a simple procedure to numerically determine the response. In the following, we also carry this amplitude expansion to second order in the metric coefficients in order to determine the leading-order backreaction of the scalar field on the background.

In the following subsection we will describe the asymptotic solution of the scalar field and warp factors in this perturbative regime. In the appendix we show how to solve the system using Chebyshev interpolation methods, which allow us to find the full profile of these metric perturbations, rather than single terms in the asymptotic expansion.

4.3.2 Leading-order backreaction

Since in our analysis, the scalar field backreacts only perturbatively on the spacetime, we are implicitly probing the limit of a very large black brane in the AdS spacetime. This is the gravitational dual of switching on an operator in a thermal plasma at a very high temperature. In the boundary theory, the dual of the expansion in the amplitude of the scalar field is the expansion in $\frac{m_f}{T_i} \ll 1$, where m_f indicates the mass of the fermionic operator and T_i is the temperature of the initial thermal state, as described above. As discussed in detail in [48, 54], the long-time evolution of the warp factors found in the perturbative regime is questionable in the very short quench limit. In this limit we find that the change in radius of the black brane becomes significant. Nonetheless, we were able to find fully general results for certain questions, namely the scaling of the response (at early times) and the energy injected into the system, as described in [54]. This justifies the perturbative approach at all quenching rates in [48, 52].

Expanding the scalar field in a small parameter ℓ, it backreacts only at order ℓ^2 on the metric, because the stress tensor of the gravity theory is quadratic (and higher) in ϕ. Hence the metric has a static part and a dynamical part as

$$
\begin{aligned}
\phi(\tau, \rho) &= \ell \, \hat{\phi}(\tau, \rho) + \mathcal{O}(\ell^3), \\
a(\tau, \rho) &= \frac{1}{\rho^2} - \rho^2 + \ell^2 \, \hat{a}(\tau, \rho) + \mathcal{O}(\ell^4), \\
s(\tau, \rho) &= \frac{1}{\rho} e^{\ell^2 b(\tau, \rho)} + \mathcal{O}(\ell^4).
\end{aligned}
\tag{4.16}
$$

Given equation (4.14), the leading perturbative part of the scalar field and metric are then

$$\hat{\phi}(\tau, \rho) = \rho \left(p_0 + \rho \, p_0' + \rho^2 \left(p_2 + \frac{1}{2} p_0'' \ln \rho \right) + \ldots \right), \tag{4.17}$$

$$\hat{a}(\tau, \rho) = -\frac{1}{6} p_0^2 + \rho^2 \left(a_{2,2} + \ln \rho \left(\frac{1}{6} (p_0')^2 - \frac{1}{6} p_0 p_0'' \right) \right) + \ldots, \tag{4.18}$$

$$b(\tau, \rho) = -\frac{1}{12} \rho^2 p_0^2 - \frac{1}{9} \rho^3 p_0 p_0' + \ldots, \tag{4.19}$$

and the equations of motion (4.9)-(4.11) take form:

$$0 = \partial_\tau \partial_\rho \hat{\phi} - \frac{1 - \rho^4}{2} \partial_\rho^2 \hat{\phi} + \frac{3 + \rho^4}{2\rho} \partial_\rho \hat{\phi} - \frac{3}{2\rho} \partial_\tau \hat{\phi} - \frac{3}{2\rho^2} \hat{\phi}, \tag{4.20}$$

$$0 = \partial_\rho^2 \hat{a} + \frac{2}{\rho} \partial_\rho \hat{a} - \frac{6}{\rho^2} \hat{a} + \frac{12(1 - \rho^4)}{\rho^3} \partial_\rho b - \frac{12}{\rho^3} \partial_\tau b + \frac{1 - \rho^4}{2\rho^2} (\partial_\rho \hat{\phi})^2 - \frac{1}{\rho^2} \partial_\rho \hat{\phi} \partial_\tau \hat{\phi} + \frac{1}{2\rho^4} \hat{\phi}^2, \tag{4.21}$$

$$0 = \partial_\tau \partial_\rho b - \frac{1 - \rho^4}{2} \partial_\rho^2 b + \frac{3 - \rho^4}{\rho} \partial_\rho b - \frac{3}{\rho} \partial_\tau b + \frac{\rho}{2} \partial_\rho \hat{a} - \hat{a} + \frac{1}{4\rho^2} \hat{\phi}^2, \tag{4.22}$$

while the constraints (4.12)-(4.13) take form:

$$0 = \partial_\rho^2 b + \frac{1}{6} (\partial_\rho \hat{\phi})^2, \tag{4.23}$$

$$0 = \partial_\tau^2 b + \left(\rho^7 - 4\rho^3 + \frac{3}{\rho} \right) \partial_\rho b + \frac{\rho^4 - 3}{\rho} \partial_\tau b + (1 - \rho^4) \left(\frac{1}{2} \rho \partial_\rho \hat{a} - \hat{a} \right) + \frac{1}{2} \rho \partial_\tau \hat{a}$$
$$+ \frac{1}{6} (\partial_\tau \hat{\phi})^2 - \frac{1 - \rho^4}{6} \partial_\rho \hat{\phi} \partial_\tau \hat{\phi} + \frac{(1 - \rho^4)^2}{12} (\partial_\rho \hat{\phi})^2 + \frac{1 - \rho^4}{4\rho^2} \hat{\phi}^2. \tag{4.24}$$

4.3.3 Rescaling the parameters

In this chapter we give the scalar field source p_0 the time-dependent profile

$$p_0(\tau) = \frac{1}{2} \left(1 + \tanh \left(\frac{\tau}{\alpha} \right) \right), \tag{4.25}$$

where α is the characteristic timescale on which the quench takes place. It will be useful to rescale our coordinates and fields such that we can compare different quenches on the

112

same time and length scale, which make it easier to see how quantities behave in the fast quench limit.

As discussed in [48], the required rescaling is $\rho \to \alpha\rho$, $\tau \to \alpha\tau$ and $\vec{y} \to \alpha\vec{y}$. The fields rescale as[2] $a \to a/\alpha^2$, $s \to s/\alpha$ and $\phi \to \alpha\phi$. In these rescaled coordinates the horizon of the black hole will be located at $\rho = 1/\alpha$, and the source of the scalar field would be

$$p_0(\tau) = \frac{1}{2}\left(1 + \tanh\left(\tau\right)\right).$$ (4.26)

The expression for the metric remains unchanged:

$$ds_5^2 = -a \; d\tau^2 + s^2 \; (d\vec{y})^2 - 2\frac{d\rho d\tau}{\rho^2}.$$ (4.27)

4.4   Probes of thermalization

Knowing the profiles of the metric coefficients and the response coefficient in the asymptotic expansion of the scalar field, we would like to obtain a meaningful measure of the thermalization time of the field theory following the quench. Since the geometry fluctuates, but then returns to a static configuration after some time, we can conclude that the gauge theory plasma does (effectively) thermalize. An interesting question to ask then is whether the broken conformality of the theory introduces different scales for which thermalization occurs at different rates. Indeed, in [46, 47, 87] it was observed for Vaidya-type metrics that the theory thermalizes at the UV (short distance) range before thermalizing in the IR (large distance) range.

The Vaidya approach [46, 47, 87] considers a thin planar collapsing shell of null dust in AdS spacetime (an expanding shell in its original construction [39]), which produces a metric outside the shell equal to that of an AdS-black brane, and leaves the inside of the shell to be that of empty AdS spacetime. While this may seem an exotic form of bulk matter to consider, these constructions can be related to a collapsing thin shell of a massless scalar field in AdS [40]. In any event, the gravitational picture suggests that the dual field theory thermalizes instantaneously at the higher energy scales, while working its way down from the UV to the IR scales. This type of setup certainly describes exceptional quenches of the dual field theory, and it is not clear to what extent the lessons learned from these studies extend to general quenches. Hence in the present case, as in [48, 52], we

---

[2]More correct is to say that this is a leading order fast-quench rescaling. The rescaling to second order is $a \to \frac{1}{\alpha^2}\left(\frac{1}{\rho^2} - \alpha^4\rho^2\right) + \ell^2\hat{a}$. In other words $\hat{a}$ is not rescaled

are considering rapid but smooth quenches, where in the gravitational dual the bulk scalar field evolves smoothly in space and time throughout the background geometry.

In [48, 52], the thermalization time was approximated by observing when the response coefficient of the scalar field was within 5% of its final equilibrium value.[3] Of course, one limitation of this method is that it is essentially measuring the thermalization time using the one-point correlator of the quenching operator $\langle \mathcal{O}_\Delta \rangle$. While in principle, the response of the one-point function depends on the whole range of energies from the IR to the UV, it cannot be used to distinguish between the different contributions from the different scales. It is therefore be interesting to employ nonlocal probes, as in [46, 47], to study the thermalization process more carefully.

An important step in this direction was made by [53], in which the authors probed the thermalization of a periodically driven quench using holographic two-point functions and entanglement entropy. We will now extend their results for a non-periodic quench. An important difference between the current chapter and [53] is that the source we use is not periodic, and can be tuned to be a step function in the case of an instantaneous quench. Periodic quenches are not truly realizable in the perturbative regime we are considering, since after a finite time the full nonlinear backreaction of the scalar field on the background must be considered.

In this section we first describe the analytic and numerical methods used to calculate the perturbation of the apparent and event horizons of the black brane. We then go on to discuss the calculation of two-point function and entanglement entropy in the field theory using holographic methods. We then show that our results agree with the results in the literature [46, 47], namely that wider probes have longer thermalization times than narrower ones.

4.4.1   Evolution of the apparent and event horizons

As the scalar excitations are sent into the bulk geometry, and fall onto the black hole, the black hole will necessarily grow. While one would need a fully nonlinear evolution of the spacetime to see the full reaction of the geometry, it is still possible to probe the growth of the black hole horizon in the perturbative regime, as per [53].

When one speaks of the black hole horizon, it can mean either the apparent or the event horizon. In the case of a static black hole, the two horizons necessarily coincide. In the

---

[3]In this chapter, we will use a stricter 2% criterion — see below.

dynamical case, they can evolve at different rates, with the condition that they coincide again once equilibrium is reached.

The apparent horizon is located at the radius where an outward pointing null geodesic stays at constant radius at that moment in time, *i.e.,* it is the trapped surface of null geodesics. The event horizon is the surface outside which a light ray must be in order to escape to infinity. Intuitively a light ray may be able to move toward the outside of the black hole, but if it is inside the event horizon, then the apparent horizon, which is also growing outward, will eventually catch up with the light ray and cause it to fall into the black hole.

Locating the apparent and event horizons is useful, because it gives a nonlocal measure for the thermalization of the quenched system. It further is a good consistency check of our numerics, since these properties of a spacetime is well understood. If our numerical methods correctly evolve the metric, we would expect the apparent horizon to always be located inside the event horizon. We would also always expect the area of the event horizon to grow monotonically as we pump energy into the black hole.

The apparent horizon is located at the radius where the expansion θ of a congruence of outward pointing null vectors vanishes (*i.e.,* it stops expanding outwards). Working in the coordinates of equation (4.2), we we characterize such a congruence with the null vector $k = \partial_v + \frac{A}{2}\partial_r$. The null vector k points toward the boundary of the spacetime outside of the initial stationary black hole, and points inward inside the initial horizon.

Following [42], the expansion of a congruence of affine parameterized null vectors n is given by

$$\theta = \nabla_\alpha n^\alpha. \tag{4.28}$$

However, it turns out that $k^\beta \nabla_\beta k^\alpha = \frac{1}{2} A' k^\alpha$, *i.e.,* k is not affine (the prime meaning the derivative with respect to r). To remedy this, we rescale k by $\exp\{-\int \left(\frac{1}{2}A'\right) d\lambda\}$, where λ is the parameter along which the congruence k evolves. This ensures that the rescaled null vector satisfies the geodesic equation with λ as an affine parameter.

Reference [42] then gives the expansion of k to be

$$\theta = \exp\left[-\int \left(\frac{1}{2}\dot{a}\right) d\lambda\right]\left(\nabla_\alpha k^\alpha - \frac{1}{2}a'\right). \tag{4.29}$$

Substituting in for $\nabla_\alpha k^\alpha$, we see that $\theta = 0$, when

$$A\Sigma' + 2\dot{\Sigma} = 0, \tag{4.30}$$

where the prime represents a derivative with respect to r, and the dot represents a derivative with respect to v.

In order to solve the equation, we change coordinates to the rescaled coordinates ρ and τ, in which the unperturbed event horizon is located at $\rho = \frac{1}{\alpha}$, α being the quenching rate. Equation (4.30) then gets modified to be

$$\alpha^2 \rho^2 a\, s' - 2\dot{s} = 0, \tag{4.31}$$

where the equation is now in terms of the new radial and time coordinates ρ and τ. Expanding a and s in terms of the perturbation parameter ℓ, and using the ansatz that the time-dependent position of the apparent horizon is $\frac{1}{\alpha} + \ell^2 \rho_a(\tau)$, we see that to zeroth order in ℓ, (4.31) is trivially satisfied. However, at order ℓ^2, (4.31) gives an expression for ρ_a, namely

$$\rho_a = \left[\frac{1}{4\alpha} \hat{a} + \frac{\dot{b}}{2\alpha^2} \right]_{\rho = \frac{1}{\alpha}}. \tag{4.32}$$

The entropy of a black hole at equilibrium is related to its horizon surface area by the Bekenstein-Hawking entropy formula [1]

$$S = \frac{A_{hor}}{4\, G_5}, \tag{4.33}$$

G_5 being Newton's constant. Of course, for the planar black hole under consideration, the area of the event horizon is infinite and hence we consider instead the *area density* of the horizon. That is, we can calculate the measure which would be integrated over the (spatial) gauge theory directions to evaluate the total area of the horizon. In a static configuration, *i.e.*, at equilibrium, this area density can be related as above in (4.33) to an entropy density

$$\mathcal{S} = \frac{V_{hor}}{4\, G_5}, \tag{4.34}$$

which is dual to the thermal entropy density of the corresponding plasma in the dual field theory. It was proposed, *e.g.*, in [94], that this entropy density of the apparent horizon should have the same interpretation as the dual entropy density in the boundary theory even in dynamical situations.

As above, we use V to denote the area density or volume element of the black hole horizon. The full (dynamical) area density is then given by

$$\begin{aligned} V_a &= s(\tau, \frac{1}{\alpha} + \ell^2 \rho_a)^3 \equiv 1 + \ell^2\, \delta V_a \\ &= 1 + \ell^2\, \left[-3\alpha \rho_a + 3b \right]_{\rho = \frac{1}{\alpha}}. \end{aligned} \tag{4.35}$$

116

Therefore the perturbation of the area density of the apparent horizon is given by

$$\delta V_a = \left[3b - \frac{3}{4}\hat{a} - \frac{3}{2\alpha}\dot{b} \right]_{\rho=\frac{1}{\alpha}}. \tag{4.36}$$

Note that at late times, after the system has equilibrated, $\dot{b} = 0$, and therefore

$$\delta V_a = \left[3b - \frac{3}{4}\hat{a} \right]_{\rho=\frac{1}{\alpha}} \tag{4.37}$$

at equilibrium. We expect that the area density of the black hole should increase due to the energy it absorbs, and therefore that the above perturbation should be positive. However, this positivity is by not immediately obvious, *e.g.*, we do not have an analytic proof that $\delta V_a > 0$. It is therefore a useful test of our numerics that this quantity comes out to be positive at equilibrium.

We would also like to calculate the location and area of the event horizon of the black hole. This is a more involved calculation, since it is a global property of the spacetime, and therefore cannot be read off from the fields at any one moment in time.

The equation satisfied by the event horizon can be obtained from the line-element. The position of the event horizon is the outermost radius at a point in time from which a null ray cannot escape to infinity. Since the event horizon is an expanding null surface, an outward-pointing null ray lying on the event horizon will move outward with the event horizon and will stay at the same radius as the event horizon throughout the evolution, until it becomes stationary again when equilibrium is reached. In other words, the event horizon follows a null trajectory.

Working in the rescaled coordinate system, and working at fixed position in the transverse directions, we can therefore set the proper-time along a radial geodesic situated at the event horizon to zero:

$$0 = -ad\tau^2 - 2\frac{d\rho\,d\tau}{\rho^2}. \tag{4.38}$$

Substituting for $a = \frac{1}{\alpha^2\rho^2} - \alpha^2\rho^2 + \ell^2\hat{a}$, and $\rho = \frac{1}{\alpha} + \ell^2\rho_e$, and dividing by $d\tau^2$, equation (4.38) simplifies to [53]

$$\frac{d\rho_e}{d\tau} = 2\alpha\rho_e - \frac{1}{2}\hat{a}. \tag{4.39}$$

Notice that at late times when $\frac{d\rho_e}{d\tau} = 0$, the equation has the solution $\rho_e = \frac{1}{4\alpha}\hat{a}$, therefore coinciding with the radius of the apparent horizon (4.32) at late times. The differential

117

equation (4.39) has a general solution

$$\rho_e(\tau) = e^{2\alpha\tau} \left(\rho_i e^{-2\alpha\tau_i} - \frac{1}{2} \int_{\tau_i}^{\tau} e^{-2\alpha t} \hat{a} \left(t, \frac{1}{\alpha} \right) dt \right), \tag{4.40}$$

where ρ_i is the radius of the event horizon at initial time τ_i. Taking the limit for late times $\tau \to \infty$ in equation (4.40), we see that the prefactor $\exp(2\alpha\tau)$ diverges. In order that the null ray (lying on the event horizon) does not shoot off to plus or minus infinity, and for the solution to make physical sense, we need

$$\left[\rho_i e^{-2\alpha\tau_i} - \frac{1}{2} \int_{\tau_i}^{\infty} e^{-2\alpha t} \hat{a} \left(t, \frac{1}{\alpha} \right) dt \right] \to 0 \quad \text{as} \quad \tau \to \infty. \tag{4.41}$$

This gives the position of the event horizon at time τ_i as

$$\rho_e(\tau_i) = \frac{1}{2} e^{2\alpha\tau_i} \int_{\tau_i}^{\infty} e^{-2\alpha t} \hat{a} \left(t, \frac{1}{\alpha} \right) dt. \tag{4.42}$$

To calculate this quantity numerically, it is somewhat easier to integrate the interval $-\infty < \tau \le \tau_i$ than $\tau_i \le \tau < \infty$, since one only needs to know the past evolution of the system (as well as the overall evolution). The position of the event horizon can then be expressed as

$$\rho_e(\tau_i) = \frac{1}{2} e^{2\alpha\tau_i} \left(\int_{-\infty}^{\infty} - \int_{-\infty}^{\tau_i} \right) e^{-2\alpha t} \hat{a} \left(t, \frac{1}{\alpha} \right) dt. \tag{4.43}$$

To implement the evolution of the event horizon, we calculate the function

$$\rho_{temp}(\tau) = \int_{-\infty}^{\tau} e^{-2\alpha t} \hat{a} \left(t, \frac{1}{\alpha} \right) dt, \tag{4.44}$$

at each timestep. At the end of the numerical evolution of the spacetime, we can calculate ρ_e as

$$\rho_e(\tau) = \frac{1}{2} e^{2\alpha\tau} \left(\rho_{temp}(\infty) - \rho_{temp}(\tau) \right). \tag{4.45}$$

The value of $\rho_{temp}(\infty)$ is determined by numerically taking the limit $\lim_{\tau \to \infty} \rho_{temp}(\tau)$. The result is accurate, because we calculate the function up until late times, after the evolution has reached equilibrium.

Similar to the case above, the area density of the event horizon is given by

$$V_e \equiv 1 + \ell^2 \, \delta V_e = 1 + \ell^2 \left[-3\alpha\rho_e + 3b \right]_{\rho = \frac{1}{\alpha}}. \tag{4.46}$$

118

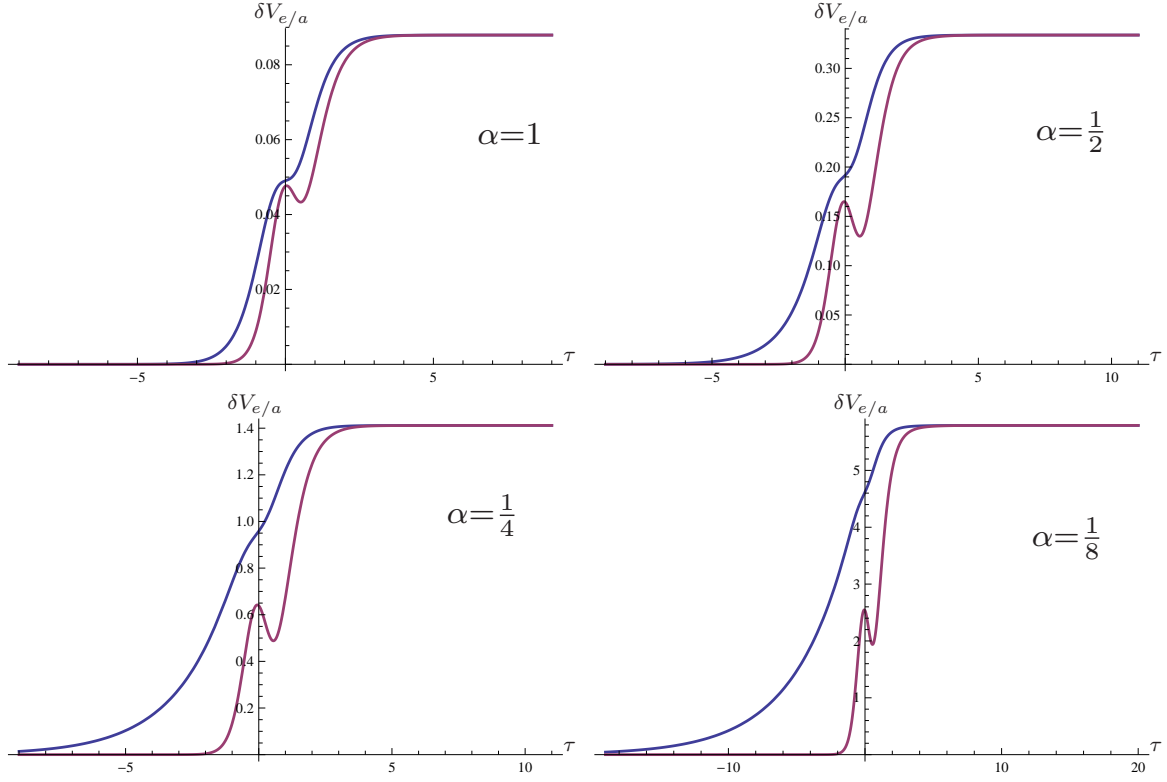Figure 4.1: Plots of the evolution of the perturbation of the area of the event horizon (blue) and the apparent horizon (purple) for various quenching times α. The plots are (from left to right, top to bottom) for $\alpha = 1, \frac{1}{2}, \frac{1}{4}$ and $\frac{1}{8}$, respectively. Note that the area of the apparent horizon can decrease, but the event horizon necessarily increases monotonically with time.
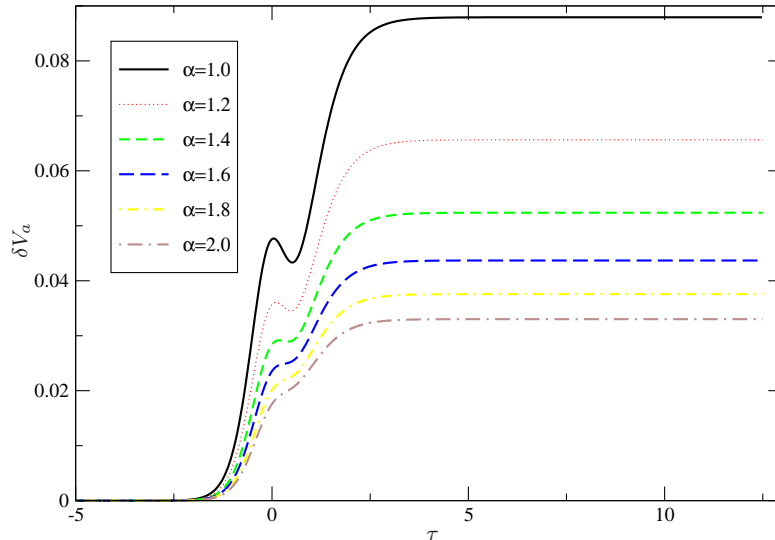
Figure 4.2: Evolution of the perturbation of the area of the apparent horizon for various quenching times α. Transition between monotonic and and non-monotonic evolution of the apparent horizon occurs in the range $\alpha = (1.4 - 1.6)$ (in units of the thermal time).

We are now ready to calculate and compare the evolution of the area density of the apparent and event horizons. See figure 4.1 for the compared evolution of the apparent and event horizons for various quenching times $\alpha = \{1, \frac{1}{2}, \frac{1}{4}, \frac{1}{8}\}$. As we argue in appendix 4.7.4, $\alpha = \frac{1}{8}$ essentially corresponds to abrupt quenches. Notice that the area of the apparent horizon can decrease, but the event horizon necessarily increases monotonically with time. In fact, the apparent horizon evolution is already non-monotonic for quenches occurring at a thermal time-scale (see figure 4.2 for more details). Also note that the perturbation of the event horizon always has a larger area density than the apparent horizon, as expected. As α decreases, *i.e.,* the quenches become faster, we know that more energy gets pumped into the geometry [54] and the final area density of the perturbed horizon also grows. Finally, both apparent and event horizons equilibrate to the same area density (*i.e.,* the same radius) towards the end of the evolution. This, in addition to the convergence tests of the code (see appendix 4.7.3) gives us confidence that our numerical evolution captures the correct evolution of the radial profile of the metric perturbation's evolution.

Intuitively, the evolution of the perturbed horizons of the black hole should provide us with a measure of the time required for the system to return to thermal equilibrium after the quantum quench. However, to produce quantitative results, we need to provide a
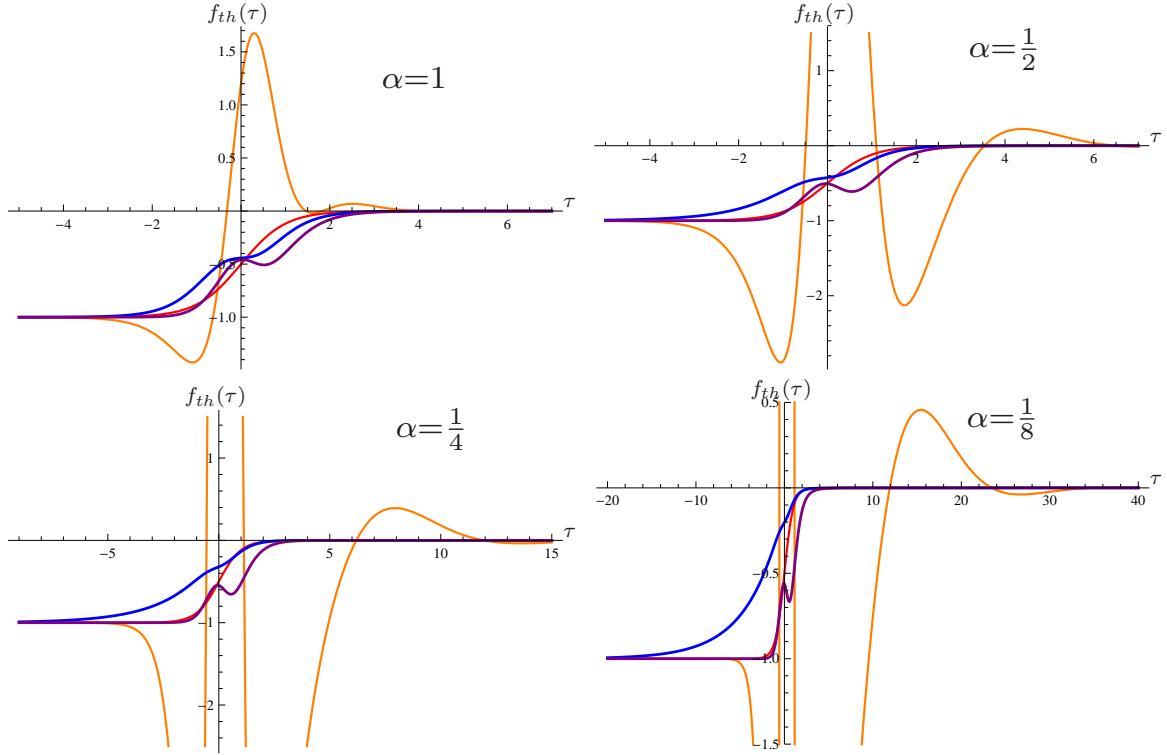
Figure 4.3: Here we compare the thermalization measure (4.47) for the apparent and event horizons (δV_a in purple and δV_e in blue) with the thermalization measure for the normalizable mode p_2 of the scalar field (orange), as well as its non-normalizable mode p_0 in red. The plots are (from left to right, top to bottom) for $\alpha = 1, \frac{1}{2}, \frac{1}{4}$ and $\frac{1}{8}$, respectively. In all cases, the horizon thermalizes before the one-point function, and this becomes more noticeable for smaller α.

precise measure with which we can extract the thermalization time. Hence we define our thermalization measure for a general dynamical quantity $f(\tau)$ as,[4]

$$f_{th}(\tau) = \frac{f(\tau) - f(\infty)}{f(\infty) - f(-\infty)}, \tag{4.47}$$

which we will apply throughout the following, *i.e.,* both here in examining the horizon behaviour and also in considering various nonlocal probes in the following sections. From the above definition of the thermalization measure above, we see that $f_{th}(-\infty) = -1$, and $f_{th}(\infty) = 0$. Throughout the following, our criterion for saying that a quantity has thermalized will be that the corresponding measure comes within 2% of its final value, *i.e.,* the thermalization time τ_{th} will be defined with $|f_{th}(\tau)| \leq 0.02$ for $\tau \geq \tau_{th}$.

Figure 4.3 shows the thermalization measure (4.47) for δV_e and δV_a, *i.e.,* the entropy densities on the event and apparent horizons, as a function of time. For comparison, we also plot the thermalization measure for the expectation value of the fermionic mass operator $\langle \mathcal{O}_3 \rangle$, *i.e.,* for the coefficient p_2 in the bulk scalar field. The corresponding thermalization or equilibration times determined with our 2% criterion are given in table 4.1. In figure 4.3, we also shown the result of applying equation (4.47) to the source coefficient p_0. In the figure, we see that $p_{2(th)}$ makes excursions far beyond $(-1, 0)$ while δV_e and δV_a remain within this range at all times. However, we note that although p_2 fluctuates much more than the horizon position, it reaches small values compared to its extrema before the horizons equilibrate. Nonetheless we see in table 4.1 that the thermalization time is slower for the expectation value than for the equilibration of the horizons. This relative difference becomes more pronounced as we make α smaller. Note that figure 4.3 is plotted in terms of the (dimensionless) rescaled time, as in equation (4.26), and so the thermalization times in table 4.1 are measured in terms of the same rescaled time. The physical thermalization times[5] would carry an extra factor of α, *i.e.,* $\tau_{physical} = \alpha \, \tau_{rescaled}$. In the table, we see that the equilibration times of the horizon become approximately constant for small α, in terms of the rescaled time τ. Hence, in the physical time, the equilibration of the horizon perturbation therefore scales approximately as α. In contrast, as shown in the table, the

---

[4] Note that for example by equations (4.35) and (4.46), $\delta V_{e/a}$ represents only a perturbative correction to the leading area density. Hence if we were to use the naive measure $\frac{V(\tau) - V(\infty)}{V(\infty)}$, the result would only be $\mathcal{O}(\ell^2)$. This reflects the fact that the system is actually only goes barely out of equilibrium, given our perturbative approach. Hence the equation (4.47) gives a more reasonable measure of the thermalization for our present study. Of course, similar comments also apply for the observables considered in the following.

[5]Note that the physical time and the quench parameter α are both dimensionful and are implicitly measured in units of $1/(\pi T)$, which is set to one in our conventions.

equilibration time of p_2 becomes approximately constant when measured in the physical time, as previously noted in [52, 54].

Table 4.1: The equilibration times of the area densities of the event and apparent horizons and the thermalization time for the one-point correlator, which thermalizes as p_2, (as defined by the 2% threshold of equation (4.47)), for different values of the quenching parameter α. We also give $\alpha \, \tau_{th}[\langle \mathcal{O}_3 \rangle]$ which corresponds to the physical time, as discussed in the main text.

α	1	$\frac{1}{2}$	$\frac{1}{4}$	$\frac{1}{8}$
$\tau_{eq}[\delta V_e]$	2.37	2.22	2.12	1.97
$\tau_{eq}[\delta V_a]$	2.73	2.77	2.95	3.25
$\tau_{th}[\langle \mathcal{O}_3 \rangle]$	3.41	6.16	15.25	30.46
$\alpha \, \tau_{th}[\langle \mathcal{O}_3 \rangle]$	3.41	3.08	3.81	3.81

4.4.2 Two-point correlators

Analytic expression for the correlator

We now consider two-point correlators as probes of thermalization in the field theory. More specifically, we mainly consider perturbations to the equal-time two-point correlator due to the quench. This is because the mass coupling of the quenching operator in the field theory is small compared to the thermal scale, and therefore only perturbations of the correlator will be time-dependent and contain information about thermalization (as noted in footnote 4).

For ease of computation on the AdS side, we will consider the correlator of an operator with large conformal dimension (*i.e.,* not the quenching operator). The correlator of such an operator can be calculated in the geometric optics limit by the length of a boundary-to-boundary spacelike geodesic [17].

Because it will turn out that the perturbations of the length of the geodesic remain finite, we needn't concern ourselves with the regularization of the static geodesic length. As a reminder to the reader, the line element of the spacetime in dimensionless, rescaled coordinates is given by

$$ds^2 = -a d\tau^2 + s^2 d\bar{y}^2 - \frac{2 d\rho d\tau}{\rho^2}, \tag{4.48}$$

where we have defined $\vec{y} = \mu\vec{x}/\alpha$ as the dimensionless boundary spatial directions.

To calculate the two-point correlator, we will calculate the length of a spacelike geodesic with endpoints at $(\tau = \tau_*, y_1 = -y_m, y_2 = 0 = y_3)$ and $(\tau = \tau_*, y_1 = y_m, y_2 = 0 = y_3)$ (*i.e.*, with endpoints at equal times, and symmetric in the y_1 axis.) If we allow the geodesic to extend into the bulk, it will have both ρ and τ profiles that depend on y_1. The length of the geodesic is given by

$$\mathcal{L} = \int_{-y_m}^{y_m} dy_1 \sqrt{s^2(\tau(y_1), \rho(y_1)) - a(\tau(y_1), \rho(y_1))\tau'(y_1)^2 - \frac{2\rho'(y_1)\tau'(y_1)}{\rho(y_1)^2}}, \qquad (4.49)$$

where a prime denotes a derivative with respect to y_1. The geodesic can then be viewed as the solution of the Euler-Lagrange equation obtained from (4.49) when treating $\mathcal{L}$ as an action.

Expanding the metric coefficients in the perturbative parameter in ℓ^2 as given in equations (4.18) and (4.19), and the time and radial profiles of the geodesic as

$$\begin{aligned} \tau &= \tau_0 + \ell^2 \tau_2, \\ \rho &= \rho_0 + \ell^2 \rho_2, \end{aligned} \qquad (4.50)$$

the geodesic length can be written as $\mathcal{L} = \mathcal{L}_0 + \ell^2 \mathcal{L}_2$. Rescaling the coordinates as in section 4.3.3 coordinates the length of the geodesic in the unperturbed geometry is expressed as[6] [53]

$$\mathcal{L}_0 = \int_{-y_m/\alpha}^{y_m/\alpha} dy_1 \frac{\sqrt{D(\tau_0, \rho_0)}}{\rho_0}, \qquad (4.51)$$

and a perturbation of that length given by

$$\begin{aligned} \mathcal{L}_2 &= \int_{-y_m/\alpha}^{y_m/\alpha} dy_1 \frac{b - \alpha^2 \rho_0^2 \hat{a}(\tau_0')^2/2}{\rho_0 \sqrt{D(\tau_0, \rho_0)}} \\ &+ \int_{-y_m/\alpha}^{y_m/\alpha} dy_1 \left(-\frac{\sqrt{D(\tau_0, \rho_0)}}{\rho_0^2} \rho_2 - \frac{\tau_0' - 2\alpha^3 \rho_0^3 \tau_0'^2}{\rho_0 \sqrt{D(\tau_0, \rho_0)}} \rho_2' - \frac{(1 - \alpha^4 \rho_0^4)\tau_0' - \rho_0'}{\rho_0 \sqrt{D(\tau_0, \rho_0)}} \tau_2' \right), \end{aligned} \qquad (4.52)$$

where

$$D(\tau_0, \rho_0) = 1 - (1 - \alpha^4 \rho_0^4)\tau_0'^2 - 2\rho_0' \tau_0'. \qquad (4.53)$$

---

[6]The various coordinates and fields are the rescaled version of these fields, as explained in section 4.3.3. We leave will leave physical constants such as the geodesic half-width y_m un-rescaled. That is to say, the physical width of the surface in the rescaled coordinates is $\Delta y_1 = 2\frac{y_m}{\alpha}$, and the physical height of the geodesic will be $\rho_0 = \frac{\rho_m}{\alpha}$, with the black hole horizon located at $\rho = \frac{1}{\alpha}$.

If we perform integration by parts, we can change the term involving ρ_2' to a term involving ρ_2 plus a total derivative term. In the case of a geodesic, this total derivative term vanishes when integrated. We are then left with terms involving ρ_2 and τ_2'. It turns out that since we are perturbing around an extremal trajectory, these two terms vanish by the equations of motion of ρ_0 and τ_0, and we therefore needn't consider perturbations of the radial and time profiles of the geodesic in order to calculate the perturbations of its length [53]. Since the perturbations on the shape of the geodesic τ_2 and ρ_2 play no role in the calculation, we will for simplicity refer to τ_0 and ρ_0 as τ and ρ, respectively. Because $\mathcal{L}_2$ depends on the unperturbed profile of the geodesic, we must first solve for ρ and τ. Since y_1 is an arbitrary transverse direction, we will simply refer to it as y.

As it turns out, it is useful to solve the problem by choosing ρ as our independent parameter, and τ and y as our dependent parameters[7]. We can find a closed form solution of $\tau(\rho)$. The independence of the integral in (4.51) on constant shifts in τ and the condition that the geodesic be smooth at $y = 0$ lead to the equation [53]

$$(1 - \alpha^4 \rho^4)\tau' + \rho' = 0. \tag{4.54}$$

Dividing equation (4.54) by ρ', and using the chain rule, the equation becomes

$$\tau'(\rho) = -\frac{1}{1 - \alpha^4 \rho^4}, \tag{4.55}$$

with a general solution of

$$\tau(\rho) = \tau_* - \frac{\tan^{-1}(\alpha\rho) + \tanh^{-1}(\alpha\rho)}{2\alpha}. \tag{4.56}$$

In the above solution, τ_* is the arbitrary boundary time of the geodesic, *i.e.,* the time of the equal-time correlator, which follows from the time translation invariance of the equation for the geodesic. While this solution for the time-profile may look strange, it is in fact related to the change in coordinates between Poincaré coordinates and Eddington-Finkelstein coordinates. The line-element of the Poincaré patch is of the form (ignoring the transverse coordinates)

$$ds^2 = \frac{1}{z^2}\left(-f(z)dt^2 + \frac{dz^2}{f(z)}\right). \tag{4.57}$$

---

[7]Because of the fact that the perturbations of the geodesic shape do not contribute to the two-point correlator at order ℓ^2, we only consider the static geodesic in our calculations. As such, we can parameterize the geodesic with either y or ρ, using the fixed endpoints $\pm\frac{y_m}{\alpha}$ and $\frac{\rho_m}{\alpha}$, respectively. If τ_2 or ρ_2 do contribute, as it does in the case of the entanglement entropy, that integral must be evaluated in y-coordinates, since ρ_m would change at order ℓ^2, while we would have to make the choice of keeping y_m fixed.

It turns out that the change of coordinates relates $\rho = z$, and

$$\tau(t, z) = t - \frac{\tan^{-1}(\alpha z) + \tanh^{-1}(\alpha z)}{2\alpha}, \tag{4.58}$$

where the Poincaré time will agree with the EF boundary time τ_*. Replacing t with τ_* and z with ρ, the above expression is identical to the geodesic contour in time given in equation (4.56). The $\tau(\rho)$ of the geodesic therefore corresponds to a constant time slice in Poincaré coordinates on the static background. Inverting equation (4.58), expressing t as a function of τ and z, we see that constant τ corresponds to an infalling null ray in the static Poincaré geometry, and constant τ in EF coordinates is actually the path of a lightray falling into the black hole from the spacetime boundary.

Since the integrand in (4.52) has no explicit dependence on y, we know that the "Hamiltonian"

$$\rho' \partial_{\rho'} \mathcal{L}_0 + \tau' \partial_{\tau'} \mathcal{L}_0 - \mathcal{L}_0 \tag{4.59}$$

will be constant in y. The equation simplifies to [53]

$$\alpha^2 D(\tau, \rho)\rho^2 = \rho_m^2, \tag{4.60}$$

$\rho(y = 0) = \frac{\rho_m}{\alpha}$, i.e., the maximum value of ρ on the geodesic. Substituting in for $\tau'(y)$ in $D(\tau, \rho)$ from (4.54), (4.60) can be simplified to [53]

$$\rho'(y) = -\frac{\sqrt{(\rho_m^2 - \alpha^2\rho^2)(1 - \alpha^4\rho^4)}}{\alpha\,\rho}. \tag{4.61}$$

Changing the integration variable from y to ρ in (4.51) and (4.52), and substituting in from equation (4.60), the new expressions are

$$\begin{aligned}
\mathcal{L}_0 &= 2\int_0^{\rho_m/\alpha} d\rho \frac{\rho_m}{\rho\sqrt{(\rho_m^2 - \alpha^2\rho^2)(1 - \alpha^4\rho^4)}}, \\
\mathcal{L}_2 &= -2\alpha \int_0^{\rho_m/\alpha} d\rho \frac{b - \alpha^2\rho^2(\tau')^2\hat{a}/2}{\rho'\rho_m}.
\end{aligned} \tag{4.62}$$

The expression for τ' is given by (4.54), i.e., an expression depending on ρ and ρ'. The ρ' terms in the integral can be substituted by an expression depending on ρ and ρ_m from (4.61). The expression for the integral therefore has no explicit y dependence, and other than knowing the solution for τ in terms of ρ, we need not know the profile of y in terms of ρ at all! The additional factor of 2 in (4.62) comes from the fact that the integration limits

126

correspond only to half the y-interval, $[0, y_m/\alpha]$. Making the above substitutions give us the perturbation of the two-point function as being

$$\mathcal{L}_2 = \alpha^2 \int_0^{\rho_m/\alpha} d\rho \frac{\rho \left(2 \left(1 - \alpha^4 \rho^4\right) b - \alpha \left(\rho_m^2 - \alpha^2 \rho^2\right) \hat{a}\right)}{\rho_m \sqrt{\left(\rho_m^2 - \alpha^2 \rho^2\right) \left(1 - \alpha^4 \rho^4\right)^3}}. \tag{4.63}$$

Numerical calculation of the perturbed two-point function

There is still some difficulty with integral (4.63), namely that the integrand diverges near $\rho = \rho_m$. Although it is a one-over-square-root divergence, and the integral itself will still be finite, this does pose a problem numerically. In order to avoid integrating a divergent quantity, we introduce a second change of variables:

$$\rho = \frac{\rho_m}{\alpha} \left(1 - q^2\right). \tag{4.64}$$

Therefore the interval in ρ, $[0, \rho_m]$ corresponds to the reverse of the interval $[0, 1]$ in q. This transforms the integral into its final form

$$\mathcal{L}_2 = \int_0^1 dq \frac{2 \left(1 - q^2\right)}{\sqrt{2 - q^2} \left(1 - \left(1 - q^2\right)^4 \rho_m^4\right)^{3/2}} \times \left(2 \left(1 - \rho_m^4 \left(1 - q^2\right)^4\right) b(\tau(q), \rho(q))\right.$$
$$\left. - \rho_m^2 q^2 \left(2 - q^2\right) \hat{a}(\tau(q), \rho(q))\right). \tag{4.65}$$

This new integrand in terms of q contains no divergences, and can easily be integrated numerically.

With the numerical evolution of the scalar field-metric system, we found the profiles of the metric components $\hat{a}$ and b, as described in appendix 4.7. This was done by solving at each timestep τ_i for the coefficients to the Chebyshev polynomials, and interpolating the values of the functions at the collocation points (see appendix 4.7.2):

$$\hat{a}(\tau_i, \rho) = -\frac{1}{6}(p_0'(\tau_i))^2 + a_{log}(\tau_i, \rho) + a_c(\tau_i, \rho), \qquad b(\tau_i, \rho) = b_{log}(\tau_i, \rho) + b_c(\tau_i, \rho),$$

$$a_c(\tau_i, \rho) = \left(\frac{L_\rho}{2}\right)^2 \sum_{j=1}^{N-2} \mathcal{F}_{g_c}^j(\tau_i) \left[\sum_{s=1}^{j+2} \mathcal{C}_{j,s} T_{s-1} \left(\frac{2\rho}{L_\rho} - 1\right)\right],$$

$$b_c(\tau_i, \rho) = \sum_{j=1}^N \mathcal{F}_{b_c}^j(\tau_i) T_{j-1} \left(\frac{2\rho}{L_\rho} - 1\right),$$

<div style="text-align: center">(4.66)</div>

127

where L_ρ is a numerical domain of the radial coordinate defined in (4.143), and the fixed coefficients $\mathcal{C}_{j,s}$ are given by (4.182). N is the number of collocation points at which we choose to solve the functions, and also the number of Chebyshev polynomials we choose to use to model the functions at each timestep. By recording the coefficients $\mathcal{F}^j_{g_c}$ and $\mathcal{F}^j_{b_c}$ of the polynomials, we can calculate $\hat{a}$ and b for any values of τ, by simply interpolating between the values of the coefficients for intermediate times. In equation (4.66) we can therefore replace $\tau_i \to \tau$.

In order to calculate the value of (4.65), we discretize the q-interval, and simply integrate the interpolating function calculated by Mathematica. Doing this for multiple values of τ_*, we can see the full time evolution of the perturbed two-point function. Doing this for multiple values of ρ_m and the quenching parameter α, we can see how the system thermalizes at different length scales at different quenching rates.

In figures 4.4 and 4.5, we plotted the thermalization measure $\mathcal{L}_{2(th)}$ of the two-point function (as defined in (4.47)) for various values $\rho_m = \rho_h \times \{0.1, 0.5, 0.9, 0.99, 0.999\}$ ($\rho_h = 1/\alpha$ being the horizon position in the current coordinates) of the depth that the geodesic extends into the geometry. It is straightforward to convert ρ_m into the corresponding separation of the end-points in the two-point function, *i.e.*, $2y_m$, by making the replacement $\rho = \frac{z\rho_m}{\alpha}$ in equation (4.61) and then integrating:

$$
2y_m = 2\rho_m \int_0^1 \frac{z\,dz}{(1-z^2)^{1/2}(1-z^4\rho_m^4)^{1/2}} \,,
\tag{4.67}
$$
$$
\{(\rho_m, 2y_m)\} \approx \{(0.1,\ 0.2),\ (0.5,\ 2.0),\ (0.9,\ 2.35),\ (0.99,\ 4.00),\ (0.999,\ 5.56)\},
$$

Of course, as we vary the rate of the quenches, α provides a natural scale with which to compare these separations. In particular, we examined $\alpha = \{1, \frac{1}{2} = 0.5, \frac{1}{4} = 0.25, \frac{1}{8} = 0.125\}$. Alternatively, we can associate an energy with the two-point correlators using $E_{2pt} = 1/y_m$, which is roughly the minimum energy scale to which these nonlocal probes are sensitive. For the different quenches, we might then compare E_{2pt} with the quenching rate $1/\alpha$. In each plot, the thermalization measure is plotted for a range of quenching times α. Since the two-point functions we calculate are for points on the boundary of the spacetime $\rho = 0$, we plot the thermalization measure against the boundary time τ_*. We see in figure 4.4 that compared to the time-scale α set by the quench, the faster the quench is, the longer the two-point function takes to equilibrate. We notice in figure 4.5 that faster quenches still equilibrate faster in the unrescaled "physical" time $\alpha\tau_*$. That is to say, as we increase the rapidity of the quench, α decreases faster than the thermalization time τ_{therm} for a correlator with fixed width $2\frac{y_m}{\alpha}$. This behaviour is more accurately reflected in figure 4.7, where we plot the thermalization times (both rescaled and unrescaled) for
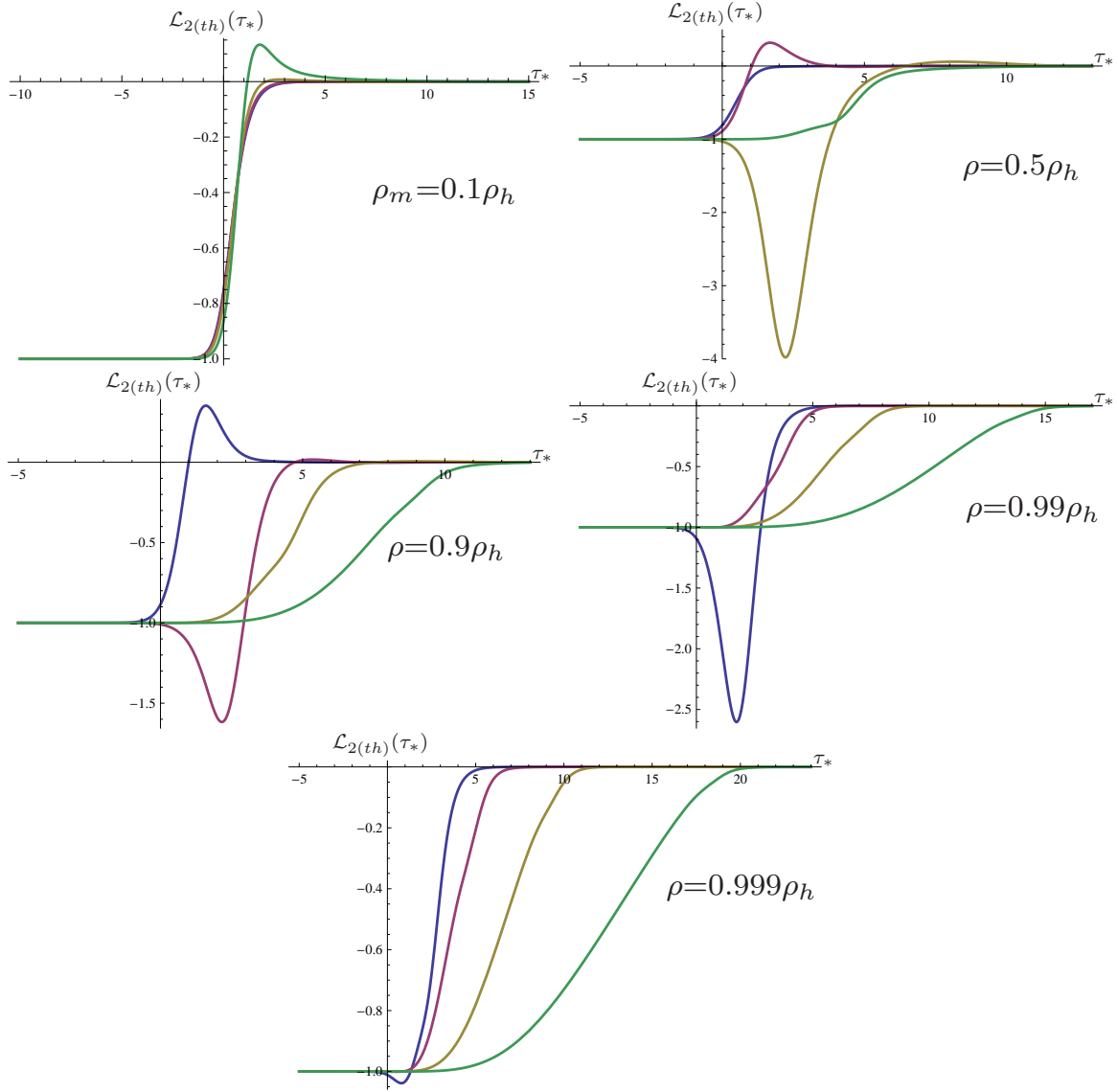
Figure 4.4: The thermalization measure as defined in (4.47) of the perturbation of the two-point functions for different-sized geodesics. The evolution is a function of the rescaled boundary time τ_*. The plots are, from left to right, top to bottom, for $\rho_m = 0.1\rho_h$, $0.5\rho_h$, $0.9\rho_h$ $0.99\rho_h$ and $0.999\rho_h$. In each plot the thermalization measure is shown for quenching parameters $\alpha = 1$ (blue), $\alpha = \frac{1}{2}$ (purple), $\alpha = \frac{1}{4}$ (brown) and $\alpha = \frac{1}{8}$ (green). Note that the smaller α is, the longer equilibration takes, in this rescaled boundary time.
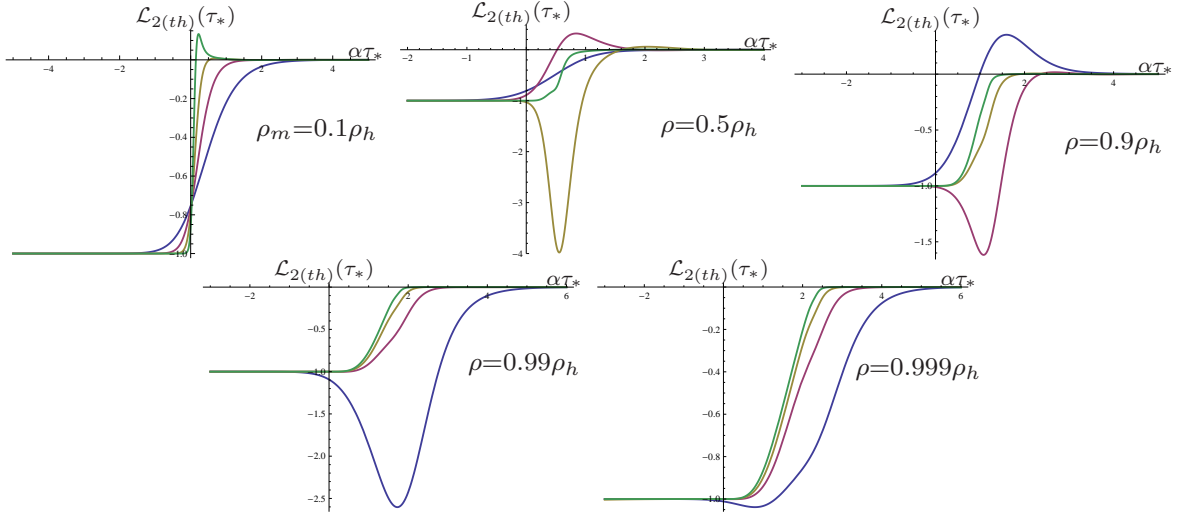
Figure 4.5: An alternative view of figure 4.4. The same plots are shown, but with the thermalization measures being functions of the unrescaled boundary time $\alpha\tau_*$. In this case one can see that the smaller α is, the shorter equilibration tends to take, from an absolute point of view.
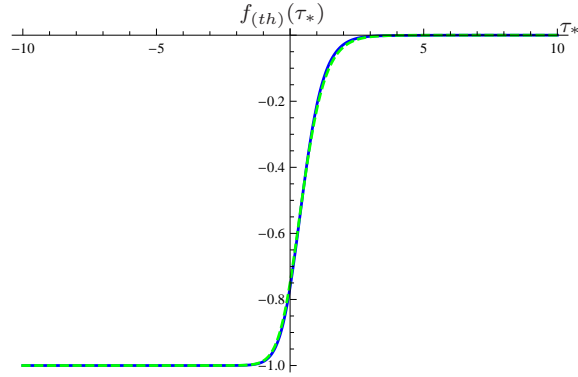

Figure 4.6: Here we show the thermalization measures as defined in (4.47) of $\mathcal{L}_2$ in blue when $\rho_m = 0.1$ and $\alpha = \frac{1}{2}$, and of p_0^2 in the dashed green curve. They closely coincide, since for such a small surface, the behaviour of the two-point function is dominated by the near-boundary metric.
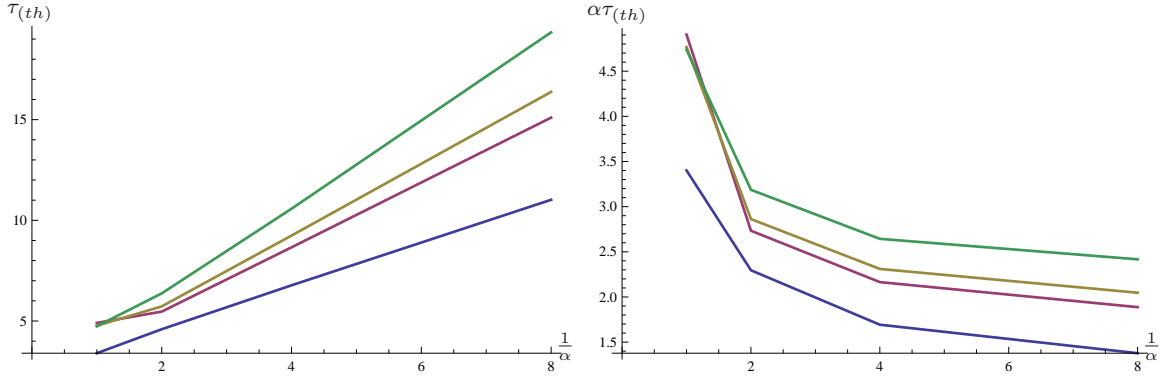
Figure 4.7: We show the equilibrium times of $\mathcal{L}_2$ for various values of ρ_m as a function of the inverse of the quenching parameter α, for $\alpha = 1$, $\frac{1}{2}$, $\frac{1}{4}$ and $\frac{1}{8}$. On the left we show the rescaled equilibrium time $\tau_{(th)}$ as defined in (4.47), while on the right we show the same plot, but for the unrescaled equilibrium time $\alpha\tau_{(th)}$. The blue, purple, yellow and green curves correspond to $\rho_m = 0.9\rho_h$, $0.99\rho_h$, $0.995\rho_h$ and $0.999\rho_h$ respectively. Notice how the trends change sign from the left to the right plots.

different ρ_m, as a function of α. We see that as α decreases ($\frac{1}{\alpha}$ increases) the slopes of the monotonic curves change sign.

In figure 4.6 we plot the thermalization measures of the perturbation of the two-point function for $\alpha = \frac{1}{2}$ and $\rho_m = 0.1$, as well as the thermalization measure of the non-normalizable mode-squared. They very closely match each other, as one might expect for small separations. For such small separations, the geodesic does not dip very far into the bulk geometry, and only "sees" the near-boundary metric, and its perturbations. Since in the near boundary limit, the metric perturbations $\hat{a}$ and b are proportional to p_0^2, so will $\mathcal{L}_2$ be, as can be seen from equation (4.62). In the dual field theory picture, one would say that for small separations the two-point function probes the UV.

In figure 4.8, we compare the thermalization times for two-point functions with different separations, but the same quenching parameter α. We notice that the larger the separation of the two points, the longer the two-point function takes to equilibrate. Although not shown in the above plots, it is possible with wide enough separations for the two-point function to have longer equilibration times, than for $\langle\mathcal{O}_3\rangle$, as we discuss in section 4.5.4.
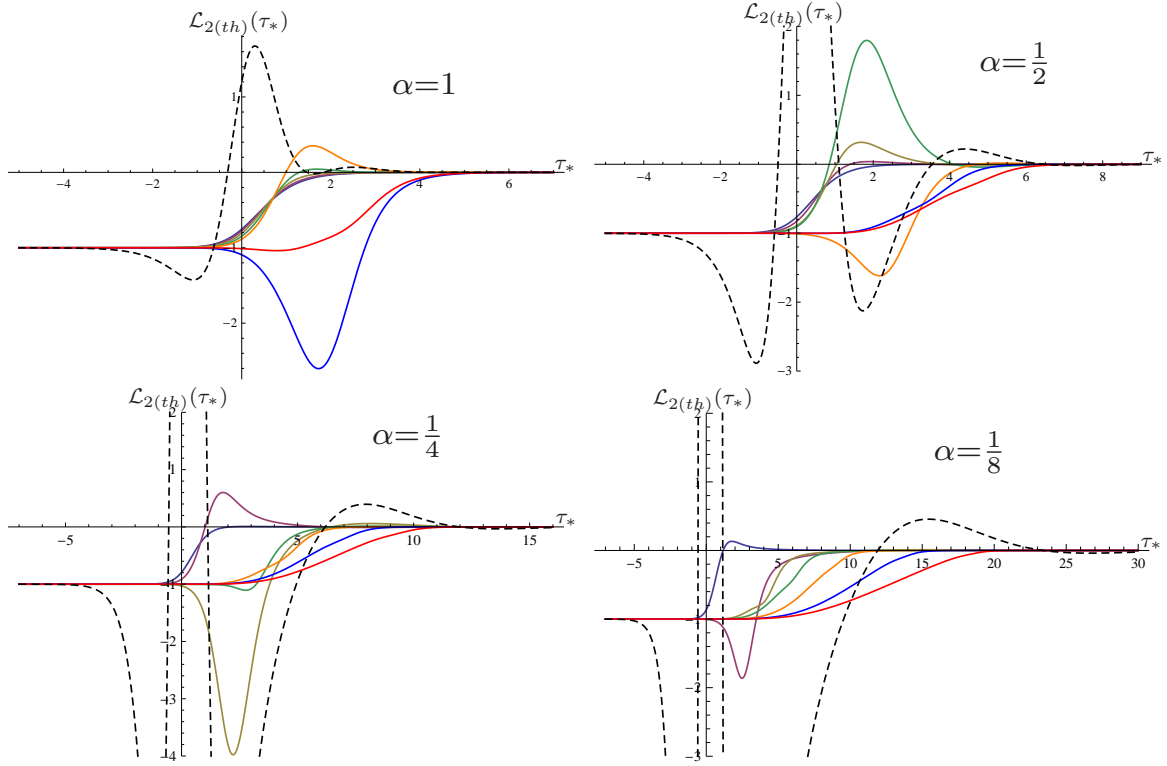
Figure 4.8: The evolution of $\mathcal{L}_{2(th)}$ as a function of the boundary time of the two-point correlator. The plots are (from left to right, top to bottom) for $\alpha = 1, \frac{1}{2}, \frac{1}{4}$ and $\frac{1}{8}$, respectively. Each figure contains the plot for an equal time two-point function $\rho_m = 0.1\rho_h$, $0.3\rho_h$, $0.5\rho_h$, $0.7\rho_h$, $0.9\rho_h$ $0.99\rho_h$ and $0.999\rho_h$, respectively. The plots for $0.9\rho_h$ $0.99\rho_h$ and $0.999\rho_h$ are orange, bright blue, and red, respectively. We also plotted $p_{2(th)}$ in dashed lines, to compare with the equilibration of the two-point functions. We can see that the larger the separation of the two points (i.e., the depth ρ_m), the longer the thermalization time is in each case.

4.4.3 Entanglement entropy

Analytic expression for the entanglement entropy

Another useful scale-dependent probe of thermalization is entanglement entropy (EE). An elegant method was proposed by Ryu and Takayanagi [95, 96] to calculate EE for holographic theories. In particular, The Ryu-Takayanagi prescription involves evaluating the Bekenstein-Hawking formula (4.33) on all bulk surfaces γ which are homologous to the entangling region on the boundary of the bulk spacetime. The holographic EE is then given by extremizing over all such bulk surfaces:

$$S_{EE} = \text{ext} \, \frac{A_\gamma}{4 \, G_5}. \tag{4.68}$$

Note that this prescription was originally proposed for static situations but has extended to consider dynamical bulk geometries in [97]. We will simplify our calculations by evaluating the entanglement entropy for regions on constant time slices in the boundary. Further in equation (4.68), G_5 would be the Newton's constant in the bulk theory but for our purposes, we have set $4 \, G_5 = 1$. The EE depends on the size of the entangling region at the asymptotic AdS boundary. Observing how fast the EE of the region stabilizes can therefore serve as an indicator of thermalization at different length scales, in analogy to the two-point function.

For simplicity, we consider a boundary entangling region Σ with a strip-geometry. That is, the region is three dimensional, and is infinite in the directions y_2 and y_3 (regulated by K), but has a finite width in the y_1-direction. The metric for the bulk spacetime can be expressed as

$$ds^2 = -a \, d\tau^2 + s^2 d\bar{y}^2 - \frac{2d\rho d\tau}{\rho^2}. \tag{4.69}$$

A surface γ in the bulk spacetime connecting to the boundary of Σ, has a surface area given by

$$\begin{aligned} S_\Sigma &= \int_{-\infty}^{\infty} dy_2 \, dy_3 \int_{-y_m}^{y_m} dy_1 \, s^2 \sqrt{-a \, (\tau')^2 + s^2 - 2\tau' \rho' / \rho^2} \\ &= 2 \, K^2 \int_0^{y_m} dy \, s^2 \sqrt{-a \, (\tau')^2 + s^2 - 2\tau' \rho' / \rho^2}. \end{aligned} \tag{4.70}$$

In (4.70) the factor of 2 comes from us only integrating over half the interval of y_1 (renamed to y) in the second line, since γ is symmetric about $y = 0$. Following the Ryu-Takayanagi prescription [95, 96] described above, the appropriate surface γ for calculating the EE is

then the one that minimizes S_Σ. Once again, the quench is treated as a perturbation on the spacetime, and as in the case of the correlator, this splits the entropy into the static part plus a perturbation:[8]

$$S_\Sigma = S_{\Sigma(0)} + \ell^2 S_{\Sigma(2)}. \tag{4.71}$$

In the rescaled coordinates, the entropy has a time-independent zeroth-order contribution

$$S_{\Sigma(0)} = 2K^2 \int_0^{y_m/\alpha} dy \frac{\sqrt{D(\tau_0, \rho_0)}}{\rho_0^3}, \tag{4.72}$$

(where D was defined in (4.53)) while the time-dependent perturbation of the EE, $\ell^2 S_{\Sigma(2)}$, is given by

$$S_{\Sigma(2)} = 2K^2 \int_0^{y_m/\alpha} dy \frac{1}{2\rho_0^3 \sqrt{D}} \left(b \left(2 + 4\,D\right) - \alpha^2 \rho_0^2 \left(\tau_0'\right)^2 \hat{a} \right). \tag{4.73}$$

Once again we will drop the subscripts on the coordinates. The perturbations on the shape of the surface τ_2 and ρ_2 *do* enter at order ℓ^2 of the EE (although only ρ_2 actually contributes to the entropy), but we will be explicit when referring to them.

Notice that as in the case of the two-point function, the expressions for the zeroth and second order entanglement entropy have no explicit y-dependence. This is due to the simple choice of geometry of the entangling surface. Treating (4.72) as an action, we can find the conserved charge from time translation invariance, as well as the Hamiltonian like we did in the case of the two-point function.

From time translation invariance, we find the conserved quantity [53]

$$(1 - \alpha^4 \rho^4)\tau' + \rho' = C. \tag{4.74}$$

The condition that the surface is closed and smooth at $y = 0$, makes the choice $C = 0$. By dividing by ρ', the chain rule again leads to the solution for the time-profile of the minimal surface of

$$\tau(\rho) = \tau_* - \frac{\tan^{-1}(\alpha\rho) + \tanh^{-1}(\alpha\rho)}{2\alpha}. \tag{4.75}$$

The Hamiltonian to our action (4.72) will be constant because it has no y-dependence, and leads to the identity

$$D(\tau, \rho)\,\alpha^6 \rho^6 = \rho_m^6. \tag{4.76}$$

---

[8]Strictly speaking, equation (4.71) is valid only when considering the static extremal surface γ. In fact, the perturbations on γ due to the backreaction of the metric causes a separate contribution at order ℓ^2 from the first term which is different from the order ℓ^2 contribution coming from the metric perturbations in equation (4.73). We come back to the contribution from the surface perturbations in section 4.4.3.

Using expression (4.53) for D, and substituting in for τ' from (4.74), we have find the equation for the radial profile

$$\rho' = -\frac{\sqrt{\left(1 - \alpha^4\rho^4\right)\left(\rho_m^6 - \alpha^6\rho^6\right)}}{\alpha^3\rho^3}. \tag{4.77}$$

From the chain rule, we have that $\frac{d\rho}{dy} = \left(\frac{dy}{d\rho}\right)^{-1}$. This gives us the additional equation

$$\frac{dy}{d\rho} = -\frac{\alpha^3\rho^3}{\sqrt{\left(1 - \alpha^4\rho^4\right)\left(\rho_m^6 - \alpha^6\rho^6\right)}}. \tag{4.78}$$

Using equations (4.74), (4.76), (4.77), and (4.78), we can express (4.72) and (4.73) as integrals over ρ only. This makes the calculation much simpler since we do not need to solve for the y-profile of the surface γ (*e.g.*, we would need to solve for the y-profile in the case of a spherical entangling surface). The expression for the EE at zeroth and second order in perturbation theory then becomes

$$S_{\Sigma(0)} = 2K^2 \int_\epsilon^{\rho_m/\alpha} d\rho\, \frac{\rho_m^3}{\rho^3\sqrt{\left(1 - \alpha^4\rho^4\right)\left(\rho_m^6 - \alpha^6\rho^6\right)}}, \tag{4.79}$$

and

$$S_{\Sigma(2)} = 2K^2 \int_\epsilon^{\rho_m/\alpha} d\rho\, \frac{-\alpha^2\hat{a}\,\rho^2\left(\rho_m^6 - \alpha^6\rho^6\right) + 2\,b\,\left(1 - \alpha^4\rho^4\right)\left(2\rho_m^6 + \alpha^6\rho^6\right)}{2\rho^3\rho_m^3\left(1 - \alpha^4\rho^4\right)\sqrt{\left(1 - \alpha^4\rho^4\right)\left(\rho_m^6 - \alpha^6\rho^6\right)}}, \tag{4.80}$$

respectively. In (4.79) and (4.80), ϵ is the near-boundary cut-off, which we introduced since both the leading order and perturbative EE have UV divergences.

Both $S_{\Sigma(0)}$ and $S_{\Sigma(2)}$ have divergences close to the boundary of the spacetime [53]. We can identify these divergences by using the perturbation series of $\hat{a}$ and b near the boundary of the spacetime (*i.e.*, in small ρ):

$$\hat{a} = -\frac{1}{6}p_0^2 + \mathcal{O}\left(\rho^2\right), \tag{4.81}$$

$$b = -\frac{\alpha^2}{12}p_0^2\rho^2 + \mathcal{O}\left(\rho^3\right). \tag{4.82}$$

We then substitute these series into the expressions for the integrands in (4.79) and (4.80), and expand the integrand close to $\rho = 0$ to find its divergent parts. Upon integrating, the divergence of the EE in terms of the cut-off is

$$\mathcal{S}_{\text{div}} = K^2\left(\frac{1}{\epsilon^2} + \ell^2\frac{\alpha^2 p_0^2\left(\tau_*\right)}{6}\log\epsilon\right). \tag{4.83}$$

135

It is worth noting that the logarithmic term is universal, as pointed out in [68, 98]. This divergence can be recast in the form

$$\chi \, A_\Sigma m_f^2 \log(\epsilon), \tag{4.84}$$

where χ is a universal numerical constant, A_Σ is the area of the entangling surface Σ on the boundary, and m_f is the mass of the fermionic operator $\mathcal{O}_3$ (our quenching operator) in the boundary CFT. Comparing our divergence to the desired form, we see that $2\alpha^2 K^2$ is the surface area (density) of Σ (the factor of 2 coming form the fact that there is a surface of area density K^2 on either side of the strip), $\ell \, p_0$ is the nonnormalizable mode of our scalar field, and by the holographic duality (and our conventions) is equal to m_f. This means that the remaining numerical constant in the divergence $\frac{1}{12}$ times some proportionality factor will be equal to the universal constant χ. In fact, this proportionality factor agrees with the above two references, and therefore the factor $\frac{1}{12}$ is our universal coefficient and must agree for the logarithmic term for any entangling surface Σ. As a further test that we have the correct constant, we calculate the logarithmic term for a spherical entangling surface Σ. Showing the final result, we obtain a logarithmic divergence in ρ of

$$4\pi R^2 \frac{\ell^2 p_0^2}{12} \log(\epsilon), \tag{4.85}$$

R being the radius of the sphere on the boundary. We see that since $4\pi R^2$ is the surface area of the spherical entangling surface, we indeed obtain the same universal coefficient of $\frac{1}{12}$.

We should note that in our calculations of *e.g.,* the thermalization time associated with the entanglement entropy, we will simply discard the divergent contributions in equation (4.83) and work only with the finite part of the entanglement entropy — see equation (4.110) below. In fact, given the definition of the entanglement measure in equation (4.47), the area law divergence in equation (4.83) will drop out, since these agree for the EE at all times. However, the logarithmic divergence shown there will not cancel, since it is proportional to $p_0^2(\tau)$, and are therefore different at early and late times. Hence one might worry that the precise results will be sensitive to cutoff redefinitions. However, we do not expect this issue will effect the qualitative features determined in the following. This matter could be avoided altogether by using a renormalized version of the entanglement entropy, *e.g.,* $y_m \, \partial_{y_m} S_\Sigma$ [99, 100]. We hope to return to this approach in future work.

Contribution from surface perturbation

As mentioned, the perturbation of the static surface γ, namely ρ_2 and τ_2 does not contribute to the entropy at order ℓ^2, with the exception of the boundary term of the EE. Expanding

136

$S_{\Sigma(0)}$ in (4.72) in terms of ρ_2 and τ_2 as

$$S_{\Sigma(0)} = S_{\Sigma(0,0)} + \ell^2 \delta S(\rho_2, \tau_2), \tag{4.86}$$

$S_{\Sigma(0,0)}$ depending only on the unperturbed profile ρ_0 and τ_0, we obtain the integral

$$\delta S = 2\, K^2 \ell^2 \int_0^{y_m/\alpha} dy \left(\frac{2\tau'^2 \rho^4 - 3D}{\alpha^4 \rho^4 \sqrt{D}} \rho_2 - \frac{\tau'}{\alpha^3 \rho^3 \sqrt{D}} \rho_2' - \frac{(1 - \alpha^4 \rho^4)\, \tau' - \rho'}{\alpha^3 \rho^3 \sqrt{D}} \tau_2' \right). \tag{4.87}$$

Notice that the numerator of the factor multiplying τ_2' is the left hand side of equation (4.74), and is therefore zero on-shell. We therefore only care about the terms involving ρ_2 and its derivative. Performing integration by parts on the second term, we obtain a term multiplying ρ_2 plus a total derivative term. The term involving ρ_2 combines with the first term in (4.87) to give the equation of motion for ρ, and is therefore zero on-shell. All that remains is the total derivative term, which we can integrate to evaluate at the limits of integration:

$$\delta S = 2\, K^2 \ell^2 \left(\frac{\tau'}{\alpha^3 \rho^3 \sqrt{D}} \rho_2 \right) \Big|_0^{y_m/\alpha}. \tag{4.88}$$

Solving perturbatively for $\rho(y)$ in (4.77) in small y, we see that factor of ρ_2 in the above equation vanishes when $y = 0$. We can solve (4.77) using the new coordinate

$$x = (y_m/\alpha - y). \tag{4.89}$$

In that case we can evaluate the coefficient of ρ_2 near $x = 0$ ($y = y_m/\alpha$). We see that the coefficient diverges as

$$- 2\, K^2 \ell^2 \frac{1}{2\sqrt{2} \rho_m^{9/4} \alpha^2 \delta^{3/4}}, \tag{4.90}$$

where δ is the cut-off in the x-direction. Since this factor contains a divergence, it is necessary to find the small-x expansion for ρ_2 in order to find potential divergent and finite contributions to the EE from the boundary term.

In order to solve for the perturbation ρ_2 of the surface γ, we derive its Euler-Lagrange equation from S_Σ in equation (4.70) for both ρ_2 and τ_2. The equations

$$0 = \delta_{\rho_2} S_\Sigma - \frac{d}{dx} \left(\delta_{\rho_2'} S_\Sigma \right), \tag{4.91}$$

$$0 = \delta_{\tau_2} S_\Sigma - \frac{d}{dx} \left(\delta_{\tau_2'} S_\Sigma \right) \tag{4.92}$$

yield the equations of motion for ρ_0 and τ_0 at order ℓ^2, and the coupled linear equations of motion for τ_2 and ρ_2 at order ℓ^4. These equations involve $\hat{a}$, b, τ_2 and ρ_2 and their

137

derivatives up to second order. These full equations also contain nonlinearities in τ_0 and ρ_0 and are too formidable to be explicitly included in this chapter. Nonetheless, we can find the leading order expansions for ρ_2 and τ_2. We do this by substituting in for the perturbation series of $\hat{a}$ and b in small ρ_0 and the asymptotic series for τ_0 and ρ_0 in small x.

We find the leading order *degenerate* solutions in terms of the boundary time τ_* to be

$$\tau_2(x) = m(\tau_*)x^{3/4} + \ldots, \tag{4.93}$$
$$\rho_2(x) = n(\tau_*)x^{3/4} + \ldots, \tag{4.94}$$

where

$$m(\tau_*) + n(\tau_*) = -\frac{\sqrt{2}}{9}\alpha^2 \rho_m^{9/4} p_0^2(\tau_*). \tag{4.95}$$

This means that to leading order ρ_2 has the right behaviour in x to cancel the divergence in (4.90) and have the boundary term make a finite contribution to the entanglement entropy. Although the equation above does not tell us the exact value of n, we can reasonably expect it to be of the form

$$n(\tau_*) \propto \alpha^2 \rho_m^{9/4} p_0^2(\tau_*), \tag{4.96}$$

with a purely numerical factor missing.

In order to solve for the numerical factor in (4.96), we solve for ρ_2 and τ_2 again in a static background. That is, we solve the system at large times, after it has fully equilibrated, and $p_0(\tau_*) = 1$. In that case, we can find a simpler equation of motion for τ_2, since the metric perturbations have no explicit time-dependence. The Euler-Lagrange equation for τ_2 becomes

$$\frac{d}{dx}\left(\delta_{\tau_2'} S_\Sigma\right) = 0. \tag{4.97}$$

Furthermore, this equation implies that

$$\delta_{\tau_2'} S_\Sigma = \kappa, \tag{4.98}$$

where κ is a constant. By similar arguments as for the unperturbed time-profile of γ in the previous subsection, we can set $K = 0$. The resulting equation is much simpler than we obtained in the time-dependent case, and contains only terms either independent of τ_2, or terms that are linear in τ_2'. It is therefore possible to solve for τ_2' as

$$\tau_2'(x) = F(\rho_2, \hat{a}, b; \rho_0, \tau_0). \tag{4.99}$$

In the above equation, F is linear in ρ_2, $\hat{a}$, b and their derivatives, but is nonlinear in the unperturbed profile ρ_0 and τ_0 of the minimal surface.

Substituting in for τ_2' (and τ_2'') in the static Euler-Lagrange equation for ρ_2, we have an equation where the only unknown function is ρ_2. Solving again for ρ_2 perturbatively in x, we can find an exact solution for its leading coefficient. In the static case

$$\rho_2(x) \xrightarrow[\tau_* \to \infty]{} -\frac{5}{18\sqrt{2}}\alpha^2 \rho_m^{9/4} x^{3/4} + \dots. \tag{4.100}$$

Knowing it's time-dependence on the source, we can write the leading solution for ρ_2 as

$$\rho_2(x) = -\frac{5}{18\sqrt{2}}\alpha^2 \rho_m^{9/4} p_0^2(\tau_*) x^{3/4} + \dots. \tag{4.101}$$

Substituting back for the leading-order solution of ρ_2 evaluated at the cut-off δ, we see that the boundary term has a finite contribution to the EE of

$$\delta S = \alpha^2 \ell^2 K^2 \left(\frac{5}{36} p_0^2(\tau_*)\right). \tag{4.102}$$

We note that it is necessary to work with $\rho_2(y)$ rather than $y_2(\rho)$ in the treatment above. To leading order in ℓ the profile of γ remains static, and we can parameterize it with either ρ or y. The expressions (4.72) and (4.79), as well as (4.73) and (4.80) are therefore related by a change in coordinates. However, when dealing with the perturbations of the minimal surface, depending on whether one lets it fluctuate in the y-direction or ρ-direction, either y_m or ρ_m will be corrected for by the perturbations. We must therefore make a choice of which of these parameters to keep fixed. Since y_m is the field theory observable, $i.e.,$ it determines the width of the strip in the boundary, we choose the perturbations of ρ and τ to be functions of y, allowing for ρ_m to be adjusted at order ℓ^2, though not affecting the results calculated on the static surface γ.

We further note that this is a very unexpected result, since in the case of unperturbed holographic EE, the boundary term is typically ignored as it is assumed to vanish from the equations of motion — see for example [53, 68, 84, 98], in which the boundary term is implicitly set to zero in the presence of a relevant perturbation. We point out that in the case of a spherical entangling surface on the AdS boundary, the boundary term above contributes both a log-divergence as well as a finite contribution. While the divergence in that case is readily obtainable by the same perturbative treatment as we did for the strip, the boundary term also has a finite contribution depending on a normalizable mode, which would require knowing the full profile of ρ_2 in y in order to be extracted. That is outside the scope of this chapter.

139

Regularization of the entanglement entropy

In equations (4.79) and (4.80), the integrands have inverse square-root divergences near $\rho = \frac{\rho_m}{\alpha}$. This is not a problem mathematically, but since we have to numerically integrate these expressions, our results would be more accurate if the integrands didn't diverge at all.

In order to separate the EE into a finite and divergent part, we use the perturbation series of the metric perturbations

$$\hat{a} = -\frac{1}{6}p_0^2 + \rho\,\hat{a}_2, \tag{4.103}$$

$$b = -\frac{\alpha^2}{12}p_0^2\rho^2 + \rho^3 b_2, \tag{4.104}$$

since only the leading-order terms in these series contribute to the divergence of the EE. We therefore have a finite part of the EE,

$$S_{\Sigma(2)(fin)} = K^2 \int_0^{\rho_m/\alpha} d\rho \frac{-\alpha^2\hat{a}_2\,(\rho_m^6 - \alpha^6\rho^6) + 2\,b_2\,(1 - \alpha^4\rho^4)\,(2\rho_m^6 + \alpha^6\rho^6)}{\rho_m^3\,(1 - \alpha^4\rho^4)\,\sqrt{(1 - \alpha^4\rho^4)\,(\rho_m^6 - \alpha^6\rho^6)}}, \tag{4.105}$$

as well as the divergent part

$$S_{\Sigma(2)(div)} = K^2 \int_\epsilon^{\rho_m/\alpha} d\rho\, p_0^2(\tau(\rho)) \frac{-\,(\rho_m^6 - \alpha^6\rho^6) + (1 - \alpha^4\rho^4)\,(2\,\rho_m^6 + \alpha^6\rho^6)}{6\,\rho\,\rho_m^3\,(1 - \alpha^4\rho^4)\,\sqrt{(1 - \alpha^4\rho^4)\,(\rho_m^6 - \alpha^6\rho^6)}}. \tag{4.106}$$

In order to regularize $S_{\Sigma(2)(div)}$, we add the counterterm

$$S_{counter} = \alpha^2 K^2 \int_\epsilon^{\rho_m/\alpha} d\rho \frac{p_0^2(\tau_*)}{6\,\rho}. \tag{4.107}$$

There is some ambiguity in the counterterm (4.107), namely that it need only have the right asymptotic behaviour to cancel the divergence of the integrand in (4.106). That means we could *e.g.,* use $p_0^2(\tau(\rho))$ instead of $p_0^2(\tau_*)$ in (4.107), and it would still cancel the divergence of the EE, but yield a different finite result for the regularized EE. In order to circumvent this ambiguity, we need to add back the finite contribution that gets subtracted in the counterterm, that is, the non-divergent limit of the integral. Therefore, we need to add back the finite contribution

$$S_{cor} = -\frac{1}{6}\alpha^2 K^2 \log\left(\frac{\rho_m}{\alpha}\right) p_0^2(\tau_*), \tag{4.108}$$

to obtain a finite EE that is invariant under this particular regularization scheme.

In order for these equations to be accurately integrable numerically, we make the same change of coordinates (4.64) as we did for the two-point function, namely

$$\rho = \frac{\rho_m}{\alpha} \left(1 - q^2\right). \tag{4.109}$$

This change of equations yields the new full expression for the regularized EE at order ℓ^2 of

$$
\begin{aligned}
S_{\Sigma(2)} &= S_{\Sigma(2)(fin)} + S_{\Sigma(2)(div)} + S_{counter} + S_{cor} + \delta S \\
&= K^2 \int_0^1 dq\, 2 \frac{\rho_m q}{\alpha} \frac{2\, b_2 \cdot (2 + (1-q^2)^6)\,(1 - \rho_m^4(1-q^2)^4) - \alpha^2 \hat{a}_2 \cdot (1 - (1-q^2)^6)}{\sqrt{1 - (1-q^2)^6}\,(1 - \rho_m^4(1-q^2)^4)^{3/2}} \\
&\quad - \alpha^2 K^2 \int_0^1 dq\, \frac{2q p_0^2(\tau(\rho))[(1-q^2)^6 - 1 + (2 + (1-q^2)^6)\,(1 - (1-q^2)^4 \rho_m^4)]}{6\sqrt{(1 - (1-q^2)^6)\,(1 - (1-q^2)^4 \rho_m^4)}\,(1 - q^2 - (1-q^2)^5 \rho_m^4)} \\
&\quad + \alpha^2 K^2 p_0^2(\tau_*) \left(\left[\int_0^1 \frac{2\,q}{6(1-q^2)} \right] - \frac{1}{6} \log\left(\frac{\rho_m}{\alpha}\right) + \frac{5}{36} \right), \tag{4.110}
\end{aligned}
$$

δS being the boundary term defined in equation (4.87), and its final expression before change of coordinates shown in (4.102).

Numerical calculation of the entanglement entropy

Using equation (4.110), we can calculate the evolution of the entanglement entropy for different quenching rates α and for entangling surfaces with different widths y_m (corresponding to different surface heights ρ_m). The procedure is very similar to the one described for the two-point function, and we give only a brief overview here.

We calculate the EE by discretizing the integrand in the first term of (4.110) in q, and then integrating the interpolating function instead. This shows a speedup in the numerical calculation, without noticeable loss of precision. The other terms in (4.110) do not require such a discretization procedure, since they do not involve the numerical metric components $\hat{a}_2$ and b_2.

The metric components are calculated from their numerically calculated Chebyshev coefficients, as described in the appendix.

The evolution of the perturbation of the EE is seen by calculating it in a range of boundary times τ_*.
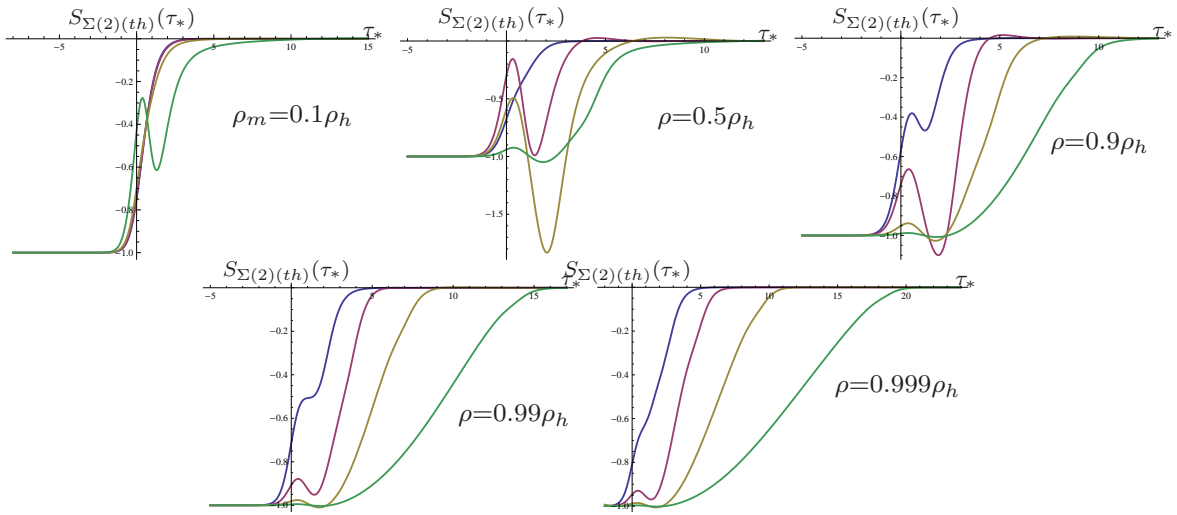
Figure 4.9: The thermalization measure of the perturbation of the entanglement entropy (as defined in (4.47)) for different-sized entangling regions. The evolution is a function of the rescaled boundary time τ_*. The plots are, from left to right, top to bottom, for $\rho_m = 0.1\rho_h$, $0.5\rho_h$, $0.9\rho_h$, $0.99\rho_h$ and $0.999\rho_h$. In each plot the thermalization measure is shown for quenching parameters $\alpha = 1$ (blue), $\alpha = \frac{1}{2}$ (purple), $\alpha = \frac{1}{4}$ (brown) and $\alpha = \frac{1}{8}$ (green). Note that the smaller α is, the longer thermalization takes, in this rescaled boundary time.
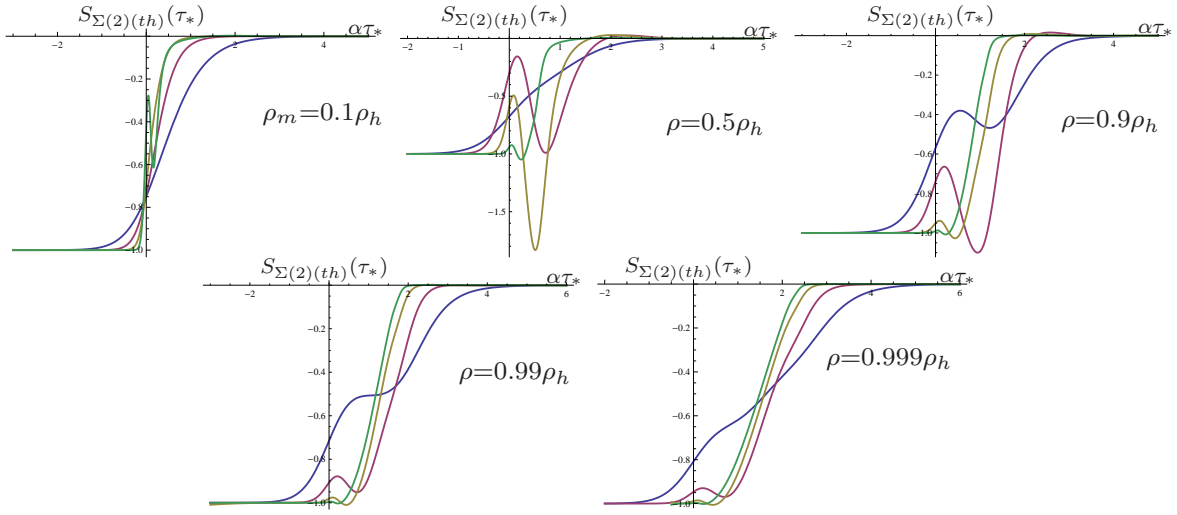
142

Figure 4.10: An alternative view of figure 4.9. The same plots are shown, but with the thermalization measures being functions of the unrescaled boundary time $\alpha\tau_*$. In this case one can see that the smaller α is, the shorter thermalization of the entropy tends to take, from an absolute point of view.
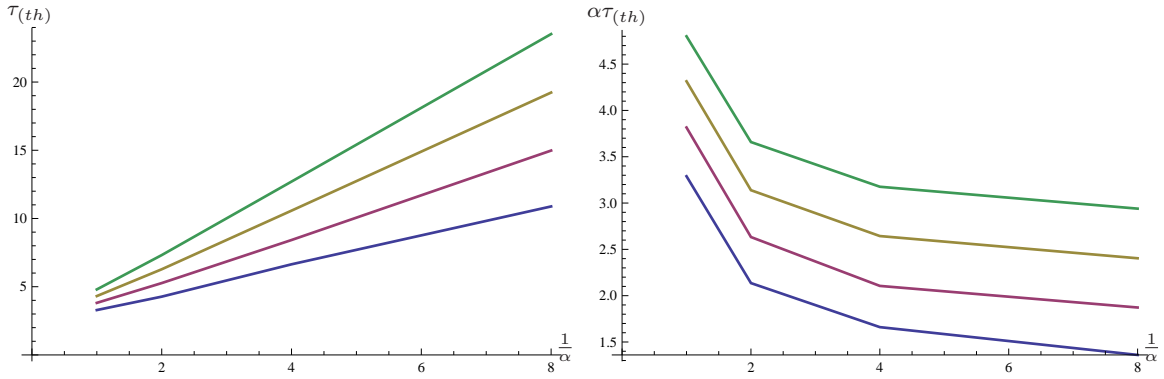

Figure 4.11: We show the thermalization times of $\mathcal{S}_{\Sigma(2)}$ for various values of ρ_m as a function of the inverse of the quenching parameter α, for $\alpha = 1$, $\frac{1}{2}$, $\frac{1}{4}$ and $\frac{1}{8}$. On the left we show the rescaled thermalization time $\tau_{(th)}$, while on the right we show the same plot, but for the unrescaled thermalization time $\alpha\tau_{(th)}$. The blue, purple, yellow and green curves correspond to $\rho_m = 0.9\rho_h$, $0.99\rho_h$, $0.999\rho_h$ and $0.9999\rho_h$ respectively. Notice how the trends change sign from the left to the right plots.

143
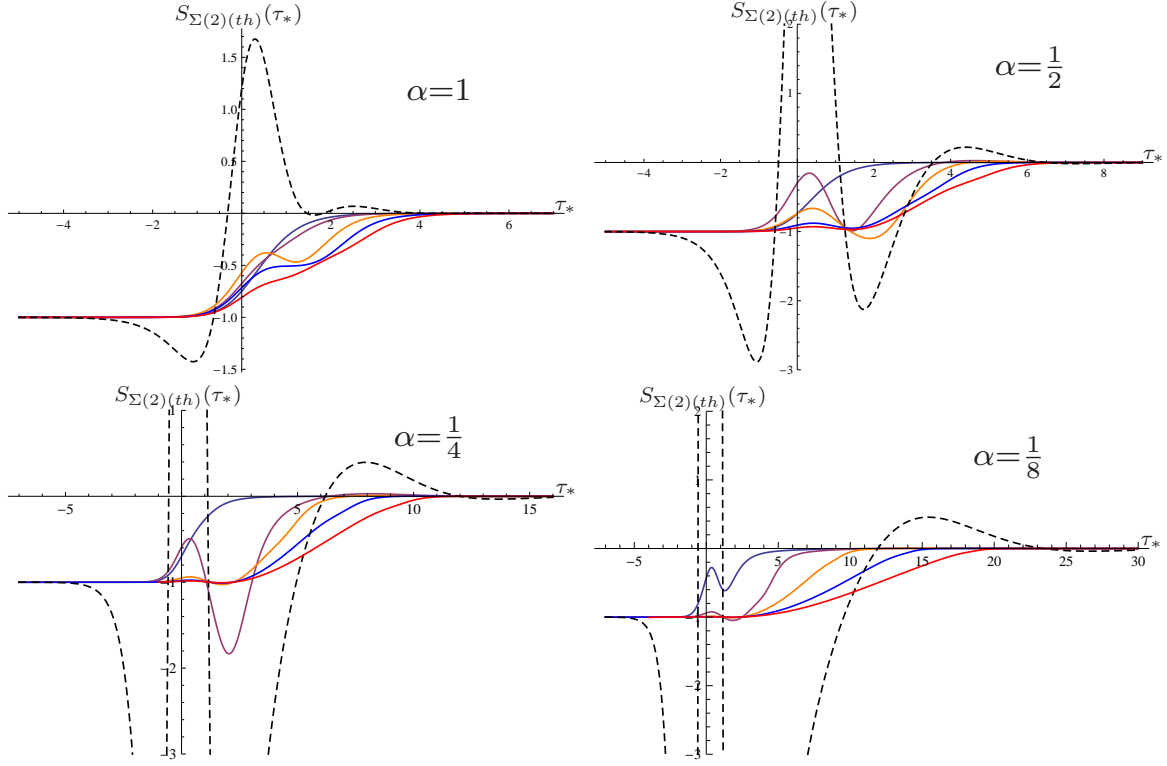
Figure 4.12: The evolution of $S_{\Sigma(2)(th)}$ as a function of the boundary time. The plots are (from left to right, top to bottom) for $\alpha = 1, \frac{1}{2}, \frac{1}{4}$ and $\frac{1}{8}$, respectively. Each figure contains the plot for a minimal surface of height $\rho_m = 0.1\rho_h$, $0.5\rho_h$, $0.9\rho_h$, $0.99\rho_h$ and $0.999\rho_h$, respectively. The plots for $0.9\rho_h$ $0.99\rho_h$ and $0.999\rho_h$ are orange, bright blue, and red, respectively. We also plotted $p_{2(th)}$ in dashed lines for comparison. We can see that the larger the entangling surface Σ (i.e., the depth ρ_m), the longer the thermalization time of the entanglement entropy is in each case.

144

We plotted the thermalization measure of the regularized EE at different quenching parameters α for the different sizes of the entangling surface Σ in figures 4.9 and 4.10,[9] as we did for the two-point functions in section 4.4.2. We see a similar behaviour as we saw for the two-point functions, namely that the faster quenches have longer equilibration times as measured by the rescaled boundary time τ_* than the slower quenches for each surface size. We also see that, as in the case of two-point functions, the faster quenches have faster equilibration times when we measure the thermalization in unrescaled boundary time $\alpha\tau_*$. We also plot these opposite trends in figure 4.11 as we did in the two-point function case.

We also plotted $S_{\Sigma(2)(th)}$ for each quenching parameter α separately in figure 4.12, but for the different sizes of the entangling surface (measured by the depth that the minimal surface γ extends into the bulk). We again obtain similar results as for the two-point functions, namely that the EE of the larger entangling regions equilibrates slower, but that the thermalization time for fixed ρ_m decreases at a slower rate than α. Since it is possible to have longer thermalization times for the EE than for the one-point function for larger α, we believe that it may be possible to obtain larger thermalization times for arbitrarily small α if we let the entangling surface Σ be large enough.

4.4.4 Scaling of the thermalized correlator and entropy

After reaching equilibrium, we expect our Yang-Mills plasma to satisfy equilibrium thermodynamics. At the level of the thermal entropy, we know that [52]

$$
S_f \sim T_f^3 + T_f^3 \left(\frac{\lambda}{T_f} \right)^2 ,
\tag{4.111}
$$

meaning that up to constant prefactors, the above relation gives the equilibrium behaviour for the system. Here T_f is the final temperature of the system, and λ is the field theory coupling of the quenching operator. It should also be noted that $\lambda/T_f \propto \ell$ relates the small parameter in the AdS picture to the coupling λ in the field theory picture.

For wide entangling regions, as the ones we considered in the previous subsection,the minimal surface γ will become wide, with the largest contribution coming from the part deep in the bulk. As the surface becomes wide in the transverse y-direction, more of it will lie close to, and parallel with the horizon of the AdS black brane. Most of its area will come from a surface that almost coincides with a part of the horizon of roughly the

---

[9]Recall that the thermalization measure is only calculated for the finite part of the entanglement entropy in (4.110).
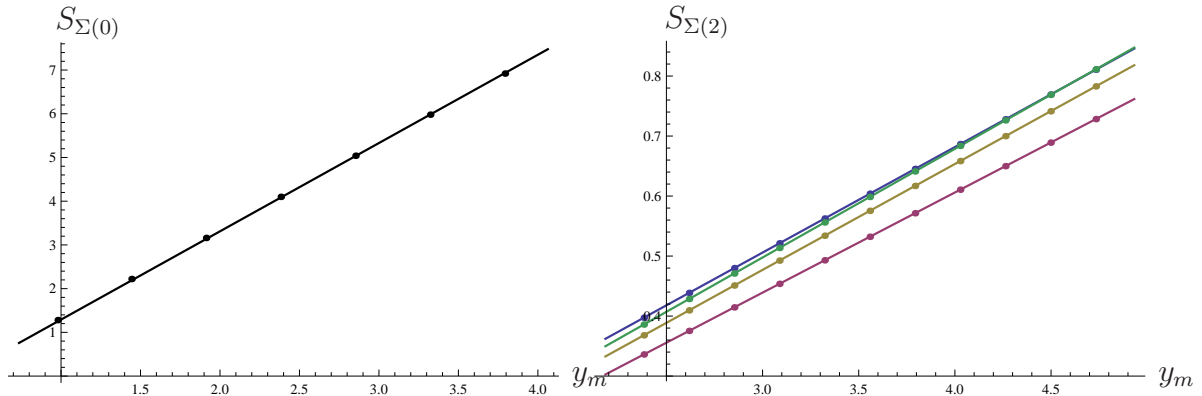
Figure 4.13:   Here we show the entanglement entropy as a function of the width of the entangling surface. On the left, we show the unperturbed EE for various values of the width y_m. We also show the best-fit line $2.02 y_m - 0.73$ through the data. On the right, we plot the perturbation of the EE for different quenching rates, namely $\alpha = 1, \frac{1}{2}, \frac{1}{4}$ and $\frac{1}{8}$ corresponding to the coloured plots blue, purple, yellow and green, respectively. We show the perturbations of the entropy for different values of y_m, as well as the best-fit straight lines through the data. The data in each case is clearly well approximated by straight lines.

same width. In the dual picture, since the entanglement entropy is proportional to the area of γ, an entangling region will have the largest contribution of its EE be proportional to the thermal entropy. In the limit of infinitely wide surfaces, the EE is simply equal to the thermal entropy [101].

Equation (4.111) now implies that both the zeroth order and and second order EE (expressed as $\mathcal{O}(\ell^2)$) should be proportional to T_f^3. In this chapter we have thus far kept the dependence on the temperature hidden, by setting the black hole radius μ (in unrescaled r-coordinates) to 1. It happens that the temperature is proportional to μ, so we should reintroduce μ, as well as the AdS radius L, to see what behaviour to expect from our EE.

It is easy to see that by reintroducing L into our equations, that $S_\Sigma \propto L^3$, which already has the correct units for the area of γ. Therefore we should introduce a factor of μ for each other factor with units of length. Since the profile of ρ in y becomes proportional to y_m for wide surfaces (γ becomes a slab shape), we expect $S_{\Sigma(0)}$ to scale as $L^2 y_m$ (as we verified). Therefore we need a factor of μ^3 to give the entropy the correct units.

The second order EE, $S_{\Sigma(2)}$ also has a factor of L^2. We should expect it to also scale linearly with y_m in order to balance the factor of μ^3, as required by the arguments above.
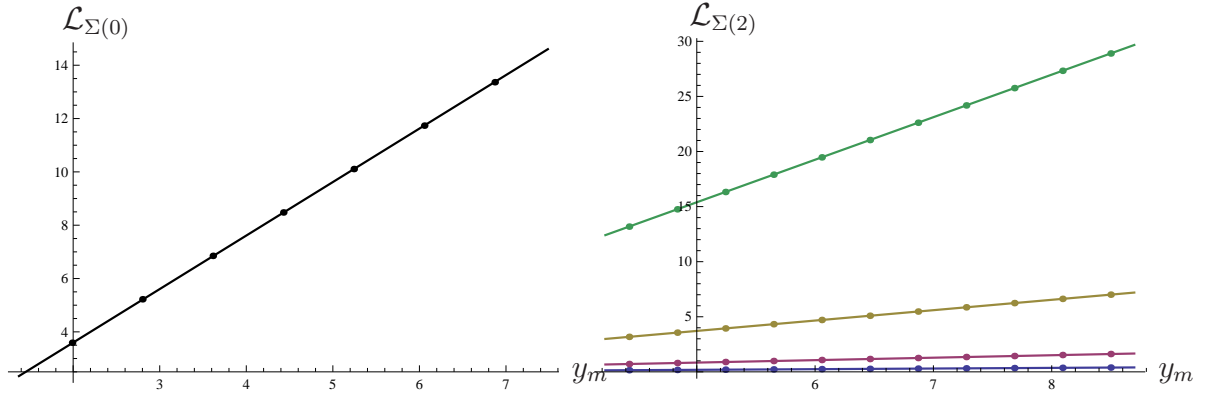
146

Figure 4.14:   Similar to figure 4.13, we show the two-point correlator as a function of the separation of the points. We see that the unperturbed correlator scales linearly with the separation and with the correct slope of ~ 2. The best fit line here is $2.01y_m - 0.41$. The perturbations of the correlator are also shown for various quenching rates α (same colour scheme as figure 4.13), and the data are clearly well approximated by straight lines.

In figure 4.13 we show that both $S_{\Sigma(0)}$, and $S_{\Sigma(2)}$ scale linearly with y_m, as we would expect it to. Moreover, $S_{\Sigma(0)}$ has the correct slope of 2 which we would expect because of y_2 being exactly half of the width, and therefore being proportional to $\frac{1}{2}$ of the area of the minimal surface.

We therefore see that the EE scales as $\mu^3 \propto T_f^3$, as predicted from equation (4.111). Note that the additional scaling of T_f^{-2} in the EE at perturbative order is contained in the perturbation parameter ℓ^2.

By similar horizon arguments we can predict that the two-point correlator should also scale linearly with y_m for wide separations. In figure 4.14 we see that both $\mathcal{L}_0$ and $\mathcal{L}_2$ scale linearly with y_m for wide separations, and moreover that $\mathcal{L}_0$ scales with the correct slope of 2.

4.5   Thermalization

We have so far discussed the different probes of the thermalization of the system. In this section we explore the mechanisms behind the thermalization behaviour seen in the two-point correlator and entanglement entropy.

We first discuss the thermalization times for the different probes introduced, before going on to examine how the different scales of the problem contribute to the observed thermalization. The correlator and entropy are integrals over the radius of the AdS space-time, and different parts of the profile make different contributions. We compare these contributions with the thermalization times of the integrands at fixed radii. We then go on to see how the profile of the scalar field and different components of its stress-energy tensor equilibrate. We end this section by bringing all these observations together, and speculate about the cause of thermalization at the different scales.

4.5.1 Thermalization times of the entanglement entropy and two-point correlator

We can ask how long the two-point function and the entanglement entropy take to thermalize for different separations of the points, or widths of the strip, respectively. Here we show the plots of the thermalization times of the EE and correlator as a function of the width of the surface and separation of the points, respectively. The thermalization time is determined by applying equation (4.47) to the EE and correlators, and choosing a thermalization threshold of 2% of its final equilibrium value.

We plotted the thermalization times of both the correlator and EE for various values of α in figure 4.15. As one can see for narrow surfaces, the increase in the thermalization time is not monotonic. This occurs due to the fluctuations that occur in the quasinormal modes, which are large compared to the size of the EE and correlator for small widths. For wider surfaces we see a linear growth of thermalization time with the width of the surface. Although these thermalization times observed here are smaller than that for the normalizable mode *i.e.,* the one-point function which are also shown in figure 4.15 (at least for faster quenches), its monotonic nature, and its linear nature, indicates that for wide enough separations and widths, the two-point correlator and EE should have longer thermalization times than the normalizable mode.

4.5.2 Equilibration of the correlator and entropy profiles

We would like to know how the two-point correlator and the entanglement entropy thermalize. The thermalization time of the previous subsection is informative, insofar as it tells us that wider surfaces have longer equilibration times than narrow surfaces or separations, as well as the limiting behaviour for wide surfaces. The regions with wider separations
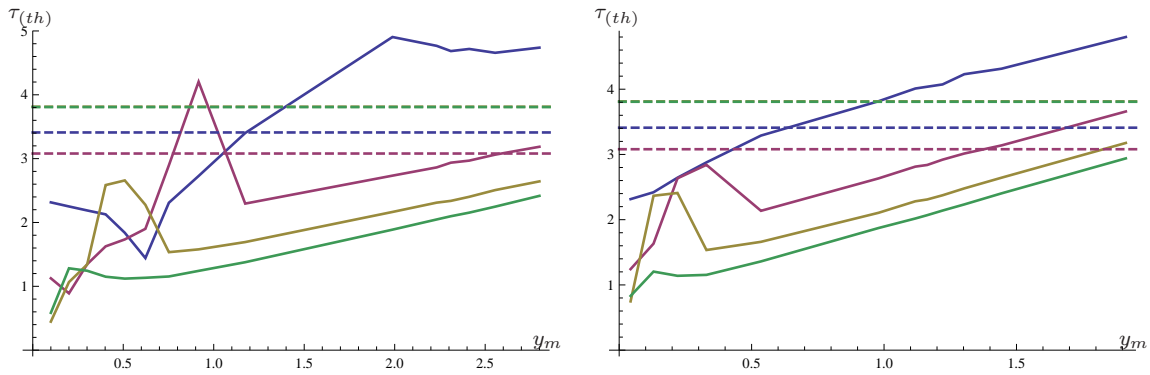
Figure 4.15: The thermalization times for the two-point correlator on the left and entanglement entropy on the right, respectively, as a function of the half-width of the correlator and entanglement regions, respectively. The blue, purple, yellow and green curves are for $\alpha = 1$, $\frac{1}{2}$, $\frac{1}{4}$, and $\frac{1}{8}$, respectively. The thermalization times in unrescaled boundary time τ_* are functions of the unrescaled separations and widths, respectively. We also show the thermalization times of the one-point correlator $\langle \mathcal{O}_3 \rangle$ for the various values of α as the horizontal dashed lines with the same colour scheme. Note that the thermalization time for the one-point function is nearly the same for $\alpha = \frac{1}{4}$ and $\alpha = \frac{1}{8}$.

have minimal surfaces or geodesics that probe deeper into the bulk geometry. This provides us with a clue as to what may be causing the observed difference in thermalization time, namely that the part of the surface deeper in the geometry equilibrates later than parts near the boundary.

In this subsection we will show how the thermalization of the EE and two-point correlators depend on different parts of the dual minimal surfaces or geodesics at different depths in the AdS-geometry. First, it turns out that the parts of the integrands of the correlator or EE integrals corresponding to larger ρ in the regularized (*i.e.,* finite) version of integral (4.80) make larger contributions to the full integral. This makes sense for wide surfaces, since most of the area is near ρ_m, close to the black brane horizon. Secondly we show that it is at larger ρ that the integrand thermalizes last.

In figure 4.16, we show the fractional contribution to the regularized entanglement entropy (4.80)

$$S_{frac} = \frac{\int_0^{\tilde{\rho}} [\text{regularized integrand}] \, d\rho}{S_{\Sigma(2)(finite)}}, \tag{4.112}$$

when integrating up to a particular fraction of the full range of the integral. Notice how especially for the wider surfaces, most of the contribution comes from the deepest part of the integration interval. As an example, in the figure we show the line at which point the integral reaches 20% of its final value. As ρ_m increases, so does $\frac{\tilde{\rho}}{\rho_m}$ at which the $S_{frac} = 20\%$ fraction is achieved. The roughly interpolated values of $\frac{\tilde{\rho}}{\rho_m}$ when this occurs are:

$$\{(\frac{\rho_m}{\rho_h}, \frac{\tilde{\rho}}{\rho_m})\} \approx \{(0.9, \ 0.47), \ (0.99, \ 0.62), \ (0.999, \ 0.77), \ (0.9999, \ 0.85)\}. \tag{4.113}$$

That means that for $\rho_m = 0.9999\rho_h$, approximately the last 15% of the integration interval contributes 80% of the total regularized entropy.

Next, in figure 4.17, we plot the excitation (*i.e.,* when the equilibration measure (4.47) of the integrand at a particular radius is more than 2% of its final value away from its initial equilibrium value) and equilibration boundary time τ_* of the EE integrand (for various α and for a wide surface) as a function of its radial position, for the minimal surface where $\rho_m = 0.999\rho_h$. Note that the we say the profile "equilibrates", rather than thermalizes, since the integrand of the correlator or EE at a particular radius is not a physical quantity in the boundary theory that can thermalize. Rather, it comes to rest in some equilibrium, after which it is equilibrated.

We can conclude from these plots that the parts of the surface that lie deeper into the geometry are also generally the ones that thermalize the latest (note that is fig. 4.17,
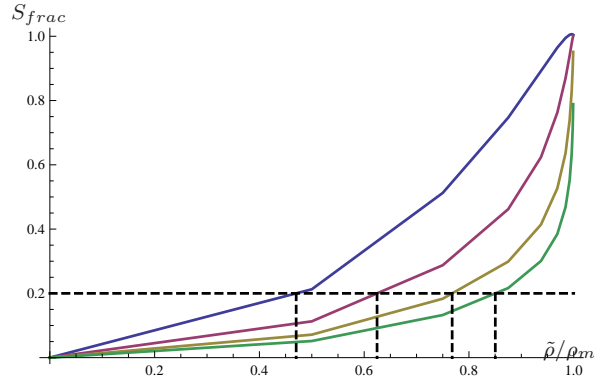
Figure 4.16: The fractional contribution to the total renormalized entanglement entropy (after thermalization) that the integral in (4.80) has, when only integrated up to a particular fraction of the full integration region. These particular curves are for $\alpha = \frac{1}{8}$, and $\rho_m = 0.9\rho_h$, $0.99\rho_h$, $0.999\rho_h$ and $0.9999\rho_h$, when the curve is blue, purple, yellow and green, respectively. The analogous curves for the correlator are very similar, and therefore omitted here. For wider surfaces, the deepest part of the integrand in the geometry contributes significantly more to the full value of the EE, than the near-boundary part. For comparison we show the horizontal dashed line $S_{frac} = 0.2$, and the vertical dashed lines where this line (roughly) intersects each curve. Note that when $\rho_m = 0.9999\rho_h$, integrating up to $\frac{\tilde{\rho}}{\rho_m} = 0.85$ only contributes 20% of the full regularized entropy.
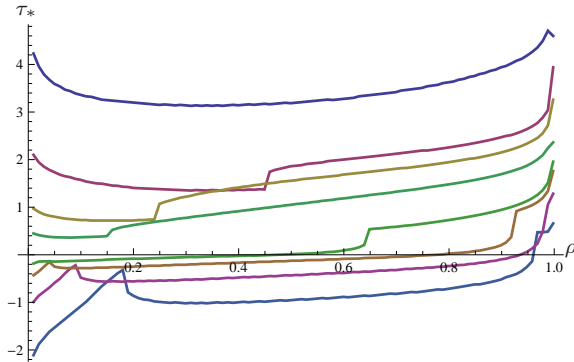

Figure 4.17: Here we show the excitation and equilibration times of the integrand in (4.80) as a function of radius (both in unrescaled coordinates). The blue, purple, yellow and green curves show the excitation (bottom) and equilibration boundary (top) times for $\alpha = 1$, $\frac{1}{2}$, $\frac{1}{4}$ and $\frac{1}{8}$, respectively.

the equilibration curve for $\alpha = 1$ is not significantly later deep in the bulk than near the boundary, while the effect becomes more pronounced for the smaller values of α). It is precisely this part of the surface that contributes the most to the EE. Although not shown, we see a similar behaviour in the case of the correlator.

In the next subsection, we show why it may be that these deeper parts of the geodesics and minimal surfaces thermalize later than the near-boundary part.

4.5.3 Equilibration profile of the scalar field and its stress-energy

The scalar field encodes both the source and response of the field theory to the quench. For this reason, we will consider the scalar field and its stress-energy as an indicator of how the energy of the quench enters the interior of the AdS bulk. It should be remembered that $\frac{1}{\rho}$ is proportional to the energy scale of the field theory. Therefore the propagation of energy into the bulk is in a sense dual to the energy of the quench being distributed through the different energy scales of the field theory – from the UV down to the thermal scale.

We show the contour plot with excitation and equilibration curves of the scalar $\frac{\phi}{\rho}$ in figure 4.18. We show $\frac{\phi}{\rho}$ rather than ϕ, because $\frac{\phi}{\rho}$ is the natural quantity that was calculated in our numerical simulations. Also note that in this figure, as well as in figures 4.19 and 4.20 we show a contour plot of the fields' profiles, where its values are the contours shown in the plot, while the solid coloured regions between the contours have intermediate values. We remind the reader that lines of constant τ in these plots are null rays infalling into the black brane, rather than constant time slices, as also explained in section 4.4.2 after equation (4.58).

We will also plot two of the components of the stress-energy of the scalar field, T^{ϕ}_{00} and $T^{\phi}_{\rho\rho}$, because it is the "matter" stress-energy which sources the backreaction of the metric in the Einstein equations. The stress-energy is given by

$$
\begin{aligned}
T^{\phi}_{\mu\nu} &= -2\frac{\delta\, S_{\phi}}{\sqrt{-g}\delta g^{\mu\nu}} \\
&= \partial_{\mu}\phi\,\partial_{\nu}\phi - \frac{1}{2}\left((\partial\phi)^2 + m^2\phi^2\right)g_{\mu\nu}.
\end{aligned}
\tag{4.114}
$$

In the first line above, S_{ϕ} is the part of the bulk action (4.1) containing only scalar field terms, *i.e.,* the matter action. We show the contour plots for the these two components of the stress-energy in figures 4.19 and 4.20, respectively.
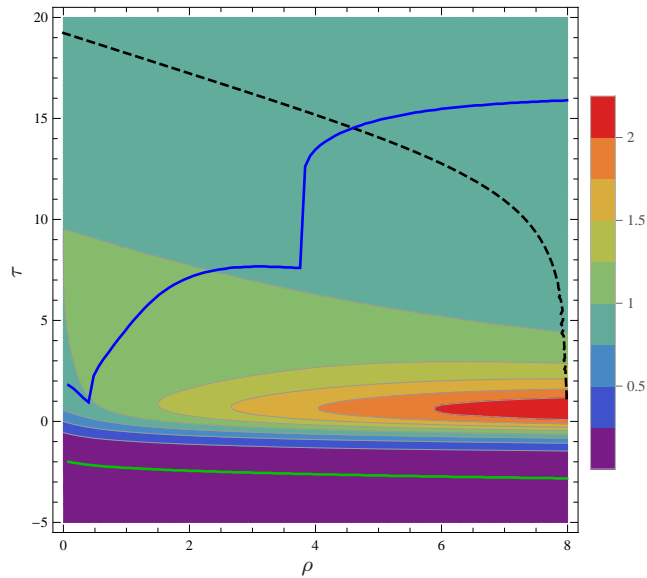
Figure 4.18: A contour plot of $\frac{\phi}{\rho}$ with $\alpha = \frac{1}{8}$ as a function of ρ and τ_* (the boundary located at $\rho = 0$, the horizon at $\rho = 8$). We add in the excitation and equilibration curves in blue for the scalar field. The bottom green curve represents the time τ at a particular radius ρ_p where $\left(\frac{\phi(\tau,\rho_p)}{\rho_p}\right)_{(therm)}$ is outside of the 2% threshold for excitation. The top blue curve represents the scalar field likewise being within the 2% threshold for equilibration at that radius. The dashed curve shows the time contour for the minimal surface with height $\rho_m = 0.999\,\rho_h$, at which it time the EE thermalizes.

Figure 4.19: A contour plot of T_{00}^{ϕ} with $\alpha = \frac{1}{8}$ as a function of ρ and τ_*. We add in the excitation and equilibration curves for the tensor component in green, as we did for the scalar field in figure 4.18. We also show the same contour for the thermalized entanglement entropy.
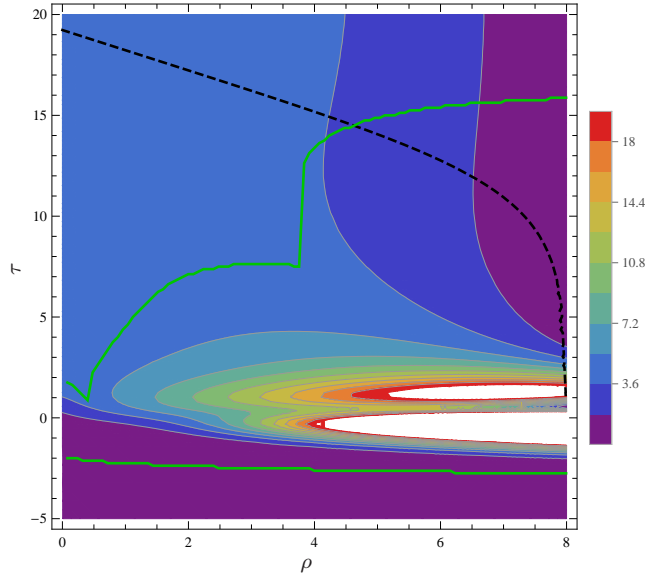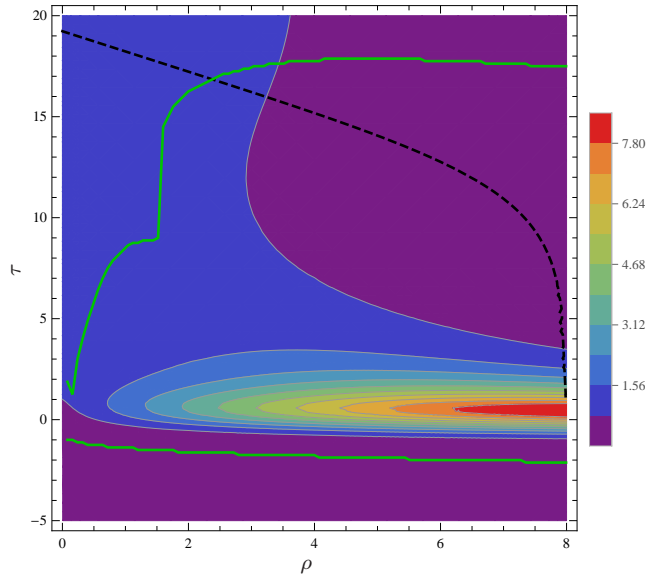
Figure 4.20: A contour plot of $T_{\rho\rho}^{\phi}$ with $\alpha = \frac{1}{8}$ as a function of ρ and τ_*. We add in the excitation and equilibration curves for the tensor component in green, as we did for the scalar field in figure 4.18. We also show the same equilibration curve for the entanglement entropy.

We see several discontinuities in the equilibration curves of these quantities. This however is not showing some novel physics, but is rather a remnant from the strict 2% cut-off, as seen in figure 4.21. That is to say that points on either side of such a discontinuity does not have very different behaviour in time, but rather one would have a slightly higher amplitude, which allows it to cross the 2% threshold at a much later time than one with a slightly smaller amplitude, giving the discrete jump in equilibration time. What is interesting in each of the plots 4.18 – 4.20, is that the equilibration time deep into the bulk is much later than near the boundary. We have also included the τ profile of a minimal surface γ, corresponding to a wide entangling region at the thermalization time of the corresponding entanglement entropy. As can be seen in the three figures, the profile is mostly outside of the spacetime regions where the scalar field and the stress tensor fluctuate most. We can therefore think of these contour profiles as indicating the level of disturbance the EE (and correlator) experience at a certain boundary time τ_*, from how much of the τ-profile extends into these regions. The minimal surface or geodesic can be seen as being dragged through this contour plot of $\frac{\phi}{\rho}$ and $T^{(\phi)}$, exciting the entropy and two-point correlator, until most of this profile has passed through the disturbed region and is deemed thermalized. Because the time-profile of the minimal surfaces/geodesic can stretch infinitely far into the past as $\rho_m \to \rho_h$, we can expect that the thermalization time of the entanglement entropy or two-point correlator could be made arbitrarily long.

4.5.4 Heuristics of thermalization

As we have seen, the nonlocal probes that thermalized most like the source were those that had relatively small separations, and reflect the physics closer to the AdS boundary. Those that thermalized most slowly were those with larger separations. The time scales here approached (and potentially exceed for wide-enough surfaces) the thermalization time of the one-point function.

For the local quantities in sections 4.5.2 and 4.5.3, we saw a wide range of equilibration times. For the quantities close to the boundary, we saw that they equilibrated on a time scale similar to the non-normalizable mode. This makes sense, since near the boundary, the dominant term in the respective asymptotic series is in fact the one containing the source term p_0, or p_0^2. However, deeper into the geometry the higher-order terms in the expansion containing the response coefficient p_2 will have an increasing contribution, so that we can expect longer thermalization times. This is exactly what was observed.

The only scales that we introduced in this system are the quenching parameter α (corresponding to the non-normalizable mode p_0), the emergent response p_2, and the temperature
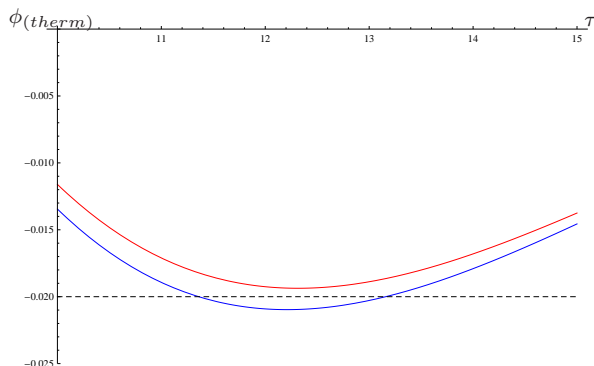
Figure 4.21: A zoomed-in version of the thermalization curves (as defined by the 2% criterion from equation (4.47)) for the scalar field for particular radial values on either side of the discontinuity seen at $\rho \approx 3.8$ in fig 4.18. The red curve is for ρ slightly smaller than 3.8, and the blue curve for ρ slightly larger. The blue one crosses the dashed line representing the equilibration threshold, and will therefore have a much later equilibration time than the red curve, although the behaviour of the function is very similar at the two radii.

of the system. The other scale that comes into play for the geodesic or entanglement entropy is the width of the probes. We should expect wider separations in the entangling surface and the points of the correlator to introduce an extra scale, since their boundaries are causally disconnected in the boundary spacetime. In figure 4.15 we see that the thermalization time of the two-point correlator and entanglement entropy grow (at least, roughly) linearly as a function of the separation in the function. The thermal wavelength of the dual field theory is $\lambda_T \equiv \frac{1}{T} = \pi$, given our conventions [52]. One might expect that if the thermalization process occurs quasilocally in the field theory, correlation functions or entanglement entropies on scales larger than the thermal wavelength (*i.e.,* involving points or boundaries separated by more than λ_T) should thermalize with approximately the same time. Nevertheless, we see monotonic, linear growth in these probes' thermalization times for separations $2\,y_m > \lambda_T$. In fact, in figure 4.15, the widest separation for our two-point function is approximately twice the thermal wavelength. This behaviour suggests that arbitrarily large regions will see arbitrarily long thermalization times set by the time for these points to come into causal contact. This is the behaviour observed by Calabrese and Cardy [34] in considering the entanglement entropy of an interval in a two-dimensional free field theory, and which lends itself to a simple quasiparticle interpretation. They saw a linear increase in the entropy after the quench, until such a time as the two ends of the region

would come into causal contact (as though the information was carried by quasiparticles), after which the EE would quickly thermalize. As in our case, they did not see an upper bound on the thermalization time. For holographic calculations of two-point functions and EE in a two and higher dimensional boundary theories, similar behaviour was found[10] in studies using a Vaidya metric in the bulk [46, 47] and the precise evolution by which the entanglement entropy is saturated was extensively studied in [87]. Hence our results are in agreement with these other holographic studies and hence it seems that the trend of longer thermalization times at larger length scales holds true in both strongly and weakly coupled field theories.

This discussion pertains only directly to perturbative quenches. However, we may expect to see similar behaviour for fully nonlinear quenches, since the response p_2 would be appropriately modified in the nonlinear regime.

4.6   Discussion

The standard toolkit of numerical relativity [42, 102] faces challenges when confronted with typical problems in asymptotically anti-de Sitter spacetimes, motivated by the gauge theory/string theory correspondence [6]. The main challenge is that gravitational simulations in asymptotically Minkowski spacetimes mostly have a compact physical dependence domain; on the contrary, in AdS, control over the whole space-time, and especially near the boundary is crucial. The latter is emphasized in problems related to holographic quenches, where the temporal history of a quantum gauge theory coupling is encoded as a nonnormalizable component of the gravitationally dual bulk scalar field near the boundary. In this chapter we described the application of pseudo-spectral methods based on Chebyshev polynomial expansion to problems of holographic quantum quenches. We paid special attention to convergence and accuracy issues of the proposed spectral framework.

Our main physical application was the extension of the earlier work on holographic quenches in strongly coupled $\mathcal{N} = 4$ supersymmetric gauge theory plasma induced by a time-varying coupling of certain dimension $\Delta = 3$ operator [48]. Here, having access to the full bulk metric (albeit only to the leading order in the gravitational scalar backreaction), enabled us to compare *local* and *nonlocal* probes of the ensuing thermalization process. Specifically, we compared the relaxation of event and apparent horizons, the equal time

---

[10]In some Vaidya studies [46], the thermalization time at a particular length scale is estimated as the time when the entire probe is completely contained inside the collapsing shell. With this geometric definition, it is clear that the thermalization time can become arbitrarily long since in terms of the boundary time, the shell takes infinitely long to cross the location of the black hole horizon.

two-point correlation function of operators of large conformal dimension, the entanglement entropy of strip-shaped regions with the relaxation of the one-point correlation function of the quenching operator. The nonlocal probes of thermalization were discussed earlier in the literature [46, 47]. In fact, our discussion of non-local probes parallel that of [53]. The important difference is that the authors of the latter work considered periodically-driven holographic quenches, in which the boundary gauge theory never reaches an equilibrium, thus making the comparison of various thermalization criteria impossible.

As a criterion for thermalization of a probe f we considered the quantity (4.47)

$$f_{th}(\tau) \equiv \frac{f(\tau) - f(\infty)}{f(\infty) - f(-\infty)}. \tag{4.115}$$

If f is a non-local probe, there is an additional dependence in f_{th} on a characteristic energy scale of f: the separation between the points in two-point equal-time correlation functions; the size of the entanglement region. Note that if f vanishes in the initial state (as it did for our probes), $f_{th}(-\infty) = -1$ and $f_{th}(\infty) = 0$. If $f = \langle \mathcal{O}_\Delta \rangle$ is the expectation value of the quenching operator of dimension Δ, $\max[\frac{f(\tau)}{f(\infty)}] \propto \alpha^{4-2\Delta}$ ($\propto \alpha^{-2}$ for $\Delta = 3$) in the limit of fast quenches, *i.e.,* as $\alpha \ll 1$ [54]. Probably our most dramatic finding is that for all nonlocal probes discussed (and for wide range of probing energy scales, if applicable), $f_{th}^{non-local}$ remains finite in the limit of fast quenches. As a result the thermalization of non-local probes, within criteria (4.115), appears to be faster than that of $\langle \mathcal{O}_\Delta \rangle$. This effect becomes more pronounced as the quenching rate $\frac{1}{\alpha}$ increases. While we focused in this chapter on $d = 4$ boundary space-time dimensions and for $\Delta = 3$ of the quenching operator, we believe that this observation would extend to general d and Δ insofar as $\frac{d}{2} < \Delta < d$.

For moderate quenches, $\alpha = \{1, \frac{1}{2}\}$, we observe the expected characteristic energy dependence in f_{th}, in comparison with $\langle \mathcal{O}_3 \rangle$, see top panels of figure 4.8. A short distance two-point correlator probes the dual bulk geometry close to the boundary; thus, its evolution would mimic that of the square of the quenching coupling — it would thermalize earlier than $\langle \mathcal{O}_3 \rangle$ (see the dark blue curve, or figure 4.6). As the point separation in the two-point correlator increases, the dual geodesic dips deeper into the bulk, probing the more infrared features — as a result it thermalizes later than $\langle \mathcal{O}_3 \rangle$ (see the red curve). The entanglement entropy behaves in a similar manner: entanglement of narrow strips evolves as the quenching coupling-squared; the entanglement of wider regions takes a longer time to thermalize.

We now finish with open problems. First, it is important to lift the restriction of 'leading order backreaction' — for this, one needs to extend the proposed numerical framework

158

to the full nonlinear evolution. We believe that this does not pose conceptual or technical difficulties: all the numerical steps can be easily generalized, even our spectral uplift procedure from $g_c(\tau, \rho)$ to $a_c(\tau, \rho)$ (see appendix 4.7.2). Likewise, using realistic dual scalar potentials, as in [90], does not pose a problem either. Another benefit of the spectral approach is that it relatively easy allows for a generalization to spatially non-homogeneous and non-isotropic quenches. We hope to report on the latter problem in a future work.

4.7 Appendix: Numerical solution of the dynamical metric and scalar field

4.7.1 Definition and solution of fields in perturbative regime

Let us introduce the functions that are involved in the numerical recipe, namely $\hat{\phi}_c$, g_c and b_c. These fields are related to the dimensionless warp factors and scalar field $\hat{a}$, b and $\hat{\phi}$ defined in eqs. (4.17)-(4.19) in various ways. The solution of the usual dimensionless functions can be expressed in the rescaled coordinates in terms of the new functions as:

$$
\begin{aligned}
\hat{\phi}(\tau, \rho) &= \phi_{log}(\tau, \rho) + \phi_c(\tau, \rho), \\
b(\tau, \rho) &= b_{log}(\tau, \rho) + b_c(\tau, \rho), \\
\hat{a}(\tau, \rho) &= -\frac{1}{6}(p_0')^2 \, \rho^2 + a_{log}(\tau, \rho) + a_c(\tau, \rho).
\end{aligned}
\tag{4.116}
$$

The ϕ_{log}, a_{log} and b_{log} terms remove (subtract) logarithms[11] close to the boundary ($\rho \to 0$) in the asymptotic expansion of $\hat{\phi}$ and the warp factors a and b, while staying bounded close to the horizon ($\rho \to \frac{1}{\alpha}$). Of course, there is a choice in selecting ϕ_{log}, a_{log} and b_{log}. For $\phi_{log}(\tau, \rho) = \phi_{log}(p_0(\tau), \rho)$ we choose

$$
\phi_{log} = \log \rho \sum_{i=2}^{8} \frac{\rho^i}{(1+\rho)^{1+i}} \mathcal{F}_i(p_0(\tau)),
\tag{4.117}
$$

where the coefficients $\mathcal{F}_i(p_0(\tau))$ are (uniquely) adjusted in such a way that the resulting $\hat{\phi}_c$ are free from $\ln \rho$ up to terms $\mathcal{O}(\rho^9 \log \rho)$. Explicitly, the first few coefficients $\mathcal{F}_i(p_0(\tau))$ are

$$
\mathcal{F}_2 = \frac{1}{2}p_0'', \qquad \mathcal{F}_3 = \frac{1}{2}p_0''' + \frac{3}{2}p_0'', \qquad \mathcal{F}_4 = \frac{5}{16}p_0^{(4)} + 2p_0''' + 3p_0''.
\tag{4.118}
$$

---

[11]We found that the presence of the logarithmic terms in the AAdS boundary asymptotics of various fields renders spectral (or finite difference) numerical method unstable.

Note that the subtraction ϕ_{log} remains bounded all the way to the horizon for fast quenches $\alpha \leq 1$. Similarly, we take

$$b_{log} = (\alpha\rho)^2 \left[\log \rho \sum_{i=2}^{5} \frac{\rho^i}{(1+\rho)^{1+i}} \mathcal{B}_{1,i}(p_0(\tau), p_2(\tau)) + \log^2 \rho \sum_{i=4}^{5} \frac{\rho^i}{(1+\rho)^{1+i}} \mathcal{B}_{2,i}(p_0(\tau)) \right],$$

$$a_{log} = \log \rho \sum_{i=2}^{5} \frac{\rho^i}{(1+\rho)^{1+i}} \mathcal{A}_{1,i}(p_0(\tau), p_2(\tau)) + \log^2 \rho \sum_{i=4}^{5} \frac{\rho^i}{(1+\rho)^{1+i}} \mathcal{A}_{2,i}(p_0(\tau)). \tag{4.119}$$

Ideally, we would like to subtract as many log-terms near the boundary as possible; this would make spectral expansion of the functions more precise. It is possible to expand (4.117) to arbitrary order: for any i, $\mathcal{F}_i$ depends on a source p_0 and its higher time derivatives, and thus is known analytically for our quenches, where

$$p_0 = \frac{1}{2} \left(1 + \tanh \tau \right). \tag{4.120}$$

The asymptotic expansions for $\hat{a}$ and b contain log-terms with prefactors that, in addition to the functional source dependence, depend on response function $p_2(\tau)$ and its derivatives. Specifically, both $\mathcal{B}_{1,i}$ and $\mathcal{A}_{1,i}$ for $i \geq 6$ depend on the derivatives of the response $p_2(\tau)$ up to order $(i-5)$. We can extract reliably $p_2(\tau)$ from the evolution of the ϕ_c:

$$p_2(\tau) = \frac{1}{2} \partial_\rho^2 \phi_c(\tau, 0), \tag{4.121}$$

however, we find that the errors in extracting derivatives of $p_2(\tau)$ does not justify truncating the (4.119) beyond the terms employed. Explicit expressions of the first few logarithm prefactors in (4.119) are given by

$$\mathcal{B}_{1,2} = -\frac{1}{24} p_0 p_0'', \qquad \mathcal{B}_{1,3} = -\frac{1}{30} p_0 p_0''' - \frac{1}{20} p_0' p_0'' - \frac{1}{8} p_0 p_0'',$$

$$\mathcal{A}_{1,2} = \frac{1}{6} ((p_0')^2 - p_0 p_0''), \qquad \mathcal{A}_{1,3} = -\frac{1}{12} (p_0 p_0''' - p_0' p_0'') - \frac{1}{2} (p_0 p_0'' - (p_0')^2), \tag{4.122}$$

$$\mathcal{B}_{2,4} = -\frac{1}{80} (p_0')^2, \qquad \mathcal{A}_{2,4} = -\frac{1}{40} (p_0'')^2.$$

We further define the functions that occur naturally in equations (4.20) – (4.22), namely π, β and g_c:

$$\pi(\tau, \rho) = \partial_t \hat{\phi}(\tau, \rho) + \frac{\alpha^4 \rho^4 - 1}{2} \partial_\rho \hat{\phi}(\tau, \rho),$$

$$\beta(\tau, \rho) = \partial_t b(\tau, \rho) + \frac{\alpha^4 \rho^4 - 1}{2} \partial_\rho b(\tau, \rho). \tag{4.123}$$

160

As in (4.117), we subtract the logarithmic terms of $\pi(\tau, \rho)$ near the boundary

$$\pi(\tau, \rho) = \pi_c(\tau, \rho) + \pi_{log}(\tau, \rho),$$

$$\pi_{log} = \ln \rho \sum_{i=1}^{7} \frac{\rho^i}{(1+\rho)^i} \mathcal{P}_i(p_0(\tau)),$$

$$\mathcal{P}_1 = -\frac{1}{2} p_0'', \qquad \mathcal{P}_2 = -\frac{1}{4} p_0''' - p_0'', \qquad \mathcal{P}_3 = -\frac{1}{8} p_0^{(4)} - \frac{3}{4} p_0''' - \frac{3}{2} p_0''.$$

(4.124)

We now present the equations which we separate into the *evolution* (containing time derivatives of the functions) and the *constraint* (without time derivatives of the functions) ones,

- evolution equations:

$$\partial_t \phi_c(\tau, \rho) = \pi_c(\tau, \rho) + \frac{1 - \alpha^4 \rho^4}{2} \partial_\rho \phi_c(\tau, \rho) + k_{log}(\tau, \rho),$$

(4.125)

with

$$k_{log}(\tau, \rho) = \pi_{log}(\tau, \rho) + \frac{1 - \alpha^4 \rho^4}{2} \partial_\rho \phi_{log}(\tau, \rho) - \partial_\tau \phi_{log}(\tau, \rho).$$

(4.126)

- constraint equations:

$$\partial_\rho \pi_c - \frac{1}{2\rho} \pi_c = -\left(J_\pi + \partial_\rho \pi_{log} - \frac{1}{2\rho} \pi_{log} \right),$$

(4.127)

$$\partial_\rho^2 b_c = -\left(J_b + \partial_\rho^2 b_{log} \right),$$

(4.128)

with

$$J_\pi = \frac{1}{4\rho} \partial_\rho \hat{\phi} - \frac{1}{4} \alpha^4 \rho^3 \partial_\rho \hat{\phi} + \frac{1}{2} \alpha^4 \rho^2 \hat{\phi},$$

(4.129)

$$J_b = \frac{1}{6} \alpha^2 \left(\hat{\phi} + \rho \partial_\rho \hat{\phi} \right)^2.$$

(4.130)

One additional constraint equations is obtained combining (4.21) and (4.22). First, using the second equation in (4.123) we rewrite the latter equation as

$$\partial_\rho^2 \hat{a} + \frac{2}{\rho} \partial_\rho \hat{a} - \frac{6}{\rho^2} \hat{a} - \frac{12}{\alpha^2 \rho^3} \beta = -J_{\hat{a}},$$

$$\partial_\rho \beta - \frac{3}{\rho} \beta + \alpha^2 \left(\frac{\rho}{2} \partial_\rho \hat{a} - \hat{a} \right) = -J_\beta,$$

(4.131)

161

with

$$J_{\hat{a}} = \left(\frac{6}{\alpha^2\rho^3} - 6\alpha^2\rho\right)\partial_\rho b - \partial_\tau\hat{\phi}\left(\partial_\rho\hat{\phi} + \frac{1}{\rho}\hat{\phi}\right) + \frac{1}{2}(1 - \alpha^4\rho^4)\left(\partial_\rho\hat{\phi} + \frac{1}{\rho}\hat{\phi}\right)^2 + \frac{1}{2\rho^2}\hat{\phi}^2,$$

$$J_\beta = \left(\frac{3}{2\rho} - \frac{3\alpha^4\rho^3}{2}\right)\partial_\rho b + \frac{1}{4}\alpha^2\hat{\phi}^2.$$

(4.132)

Algebraically solving for $\beta(\tau, < r)$ from the first equation in (4.131), we can represent the remaining equation in (4.131) as

$$\partial_\rho g = -J_g, \qquad g \equiv \partial_\rho^2\hat{a} + \frac{2}{\rho}\partial_\rho\hat{a}, \tag{4.133}$$

or

$$\partial_\rho g_c = -J_{g_c}, \qquad g_c \equiv \partial_\rho^2 a_c + \frac{2}{\rho}\partial_\rho a_c,$$

$$J_{g_c} = J_g + \partial_\rho\left[\partial_\rho^2 a_{log} + \frac{2}{\rho}\partial_\rho a_{log}\right],$$

(4.134)

with

$$J_g = \left(\frac{1}{2\rho^2}\hat{\phi} - \partial_\rho^2\hat{\phi} - \frac{3}{2\rho}\partial_\rho\hat{\phi}\right)\pi + \left(\frac{1}{2\rho}\hat{\phi} - \frac{1}{2}\alpha^4\rho^3\hat{\phi}\right)\partial_\rho^2\hat{\phi} - \left(\frac{1}{4}\alpha^4\rho^2\hat{\phi} + \frac{1}{4\rho^2}\hat{\phi}\right)\partial_\rho\hat{\phi}$$

$$+ \left(\frac{1}{4}\alpha^4\rho^3 - \frac{1}{4\rho}\right)(\partial_\rho\hat{\phi})^2 + \frac{1}{2}\alpha^2\left(\alpha^2\rho\hat{\phi}^2 - 48\partial_\rho b\right).$$

(4.135)

Note that given $g_c(\tau, \rho)$, and using the definition of $\hat{a}$ in (4.116), we can always reconstruct $a_c(\tau, \rho)$ as

$$a_c(\tau, \rho) = \int_0^\rho \frac{dx}{x^2}\left[\int_0^x dy \ y^2 g_c(\tau, y)\right]. \tag{4.136}$$

So far, we have not used (4.24) — this equation contains two τ derivatives, and so appears to be an evolution equation. It turns out that this is a *momentum constraint*, and should be imposed at a single spatial point, say $\rho = 0$; the equations (4.20)-(4.23) guarantee that (4.24) would then be true at any other point. The latter constraint determines $a_{2,2}(\tau)$ (see (4.18)) in terms of the source $p_0(\tau)$ and the response $p_2(\tau)$:

$$0 = a'_{2,2} + \frac{1}{3}(p_0 p'_2 - p'_0 p_2) + \frac{1}{18}p'_0 p''_0 - \frac{2}{9}p_0 p'''_0. \tag{4.137}$$

162

In practice, we find it convenient to introduce

$$\hat{a}_2 \equiv a_{2,2} + \frac{5}{36}\left(p_0'\right)^2 - \frac{2}{9}p_0p_0'' + \frac{1}{3}p_0p_2, \tag{4.138}$$

which allows to rewrite (4.137) as

$$0 = \hat{a}_2' - \frac{2}{3}p_0'p_2. \tag{4.139}$$

Evolution equations (4.125) and (4.139) are solved subject to appropriate initial conditions. In our simulations we assume thermally equilibrium $\mathcal{N} = 4$ state in the limit $\tau \to -\infty$:

$$\phi_c(-\infty, \rho) = 0, \qquad \hat{a}_2(-\infty) = 0. \tag{4.140}$$

The constraint equations (4.127), (4.128) and (4.134) are solved subject to the boundary condition at $\rho = 0$, which are found using the asymptotic expansions (4.17)-(4.19) and following the chain of redefinitions (4.116), (4.124) and (4.134):

$$
\begin{aligned}
\pi_c(\tau, 0) &= \frac{1}{2}p_0', \\
b_c(\tau, 0) &= 0, \qquad \partial_\rho b_c(\tau, 0) = 0, \\
g_c(\tau, 0) &= 6a_{2,2} + \frac{5}{6}((p_0')^2 - p_0p_0'').
\end{aligned}
\tag{4.141}
$$

As explained in [48], there is no need to impose the boundary condition at the horizon provided we extend the radial integration past its location:

$$\rho \in [0, L_\rho], \qquad L_\rho = \frac{1.2}{\alpha}, \qquad \rho_{horizon} = \frac{1}{\alpha}\left(1 + \mathcal{O}(\ell^2)\right). \tag{4.142}$$

4.7.2 Numerical implementation

We use pseudo-spectral methods [89] to solve numerically equations (4.125), (4.139) and (4.127), (4.128), (4.134), subject to the initial and boundary conditions (4.140) and (4.141) on a domain:

$$\rho \in [0, L_\rho], \qquad \tau \in [\tau_{initial}, \tau_{final}]. \tag{4.143}$$

163

In practice we choose $\tau_{initial} = -7.5$, corresponding to the source value $p_0(\tau_{initial}) \approx 3 \times 10^{-7} \ll 1$ (see (4.120)); and $\tau_{final} = 12.5$ (or later for smaller α). In a nutshell, any function $f(\tau, \rho)$ we represent as truncated sum over Chebyshev polynomials $T_j(x)$,

$$f(\tau, \rho) \sim \sum_{j=1}^{N} \mathcal{F}_f^j(\tau) T_{j-1}\left(-1 + \frac{2\rho}{L_\rho}\right),$$

(4.144)

$$T_0(x) = 1, \qquad T_1(x) = x, \qquad T_{j+1}(x) = 2xT_j(x) - T_{j-1}(x), \qquad j \geq 1.$$

All constraints equations are then reduced to linear-algebraic equations evaluated at N-collocation points [89]. We use fourth-order Runge-Kutta method (RK4) to evolve functions in time.

We now describe the implementation steps of our numerical package in detail:
- The range of ρ:

$$\rho \in [0, L_\rho],$$

(4.145)

where we include the boundary points;
- we introduce the collocation grid points:

$$x_i = \cos\frac{(i-1)\pi}{N-1}, \qquad i = 1, \cdots N; \qquad \rho_i = \frac{L_\rho}{2}(1 + x_i).$$

(4.146)

Note: $\rho_1 = L_\rho$ and $\rho_N = 0$, and

$$\frac{dx}{d\rho} = \frac{2}{L_\rho}.$$

(4.147)

- We use a recursive relation to compute Chebyshev polynomials $T(i, j) \equiv T_{j-1}(x_i)$, and their derivatives at the collocation points, *i.e.*, $d_n T(i, j) \equiv P_{i-1}^{(n)}(x_i)$, for $n = 1, 2$:

$$T(i, 1) = 1, \qquad T(i, 2) = x_i, \qquad T(i, j+2) = 2x_i\, T(i, j+1) - T(i, j),$$
$$d_n T(i, j+2) = 2x_i\, d_n T(i, j+1) + 2nx_i\, d_{n-1} T(i, j+1) - d_n T(i, j).$$

(4.148)

- We store data at spatial collocation point at time $\tau = \tau^o$ in arrays with superscript ^{o}, and data at time $\tau = \tau^n \equiv \tau^o + n\,\Delta\tau$ in arrays with superscript ^{n}. For convergence, we choose

$$\Delta\tau = \frac{1}{N^2} \times \min\{1, \alpha\}.$$

(4.149)

- RK4 is used to evolve from ϕ_c and $\hat{a}_2$:

164

- **RK step 1**: Given,
$$\phi_i^o \equiv \phi_c(\tau^o, \rho_i), \qquad a_{2,2}^o \equiv a_{2,2}(\tau^o), \tag{4.150}$$

we compute Chebyshev coefficients $\mathcal{F}_{\phi_c}^j$ solving

$$\phi_i^o = \sum_{j=1}^N \mathcal{F}_{\phi_c}^j \, T(i,j), \qquad i = 1, \cdots N. \tag{4.151}$$

Next, we evaluate

$$d_1 \phi_i^o \equiv \partial_\rho \phi_c(\tau^o, \rho_i) = \sum_{j=1}^N \mathcal{F}_{\phi_c}^j \, d_1 T(i,j) \, \frac{dx}{d\rho},$$

$$p_2^o = \frac{1}{2} \sum_{j=1}^N \mathcal{F}_{\phi_c}^j \, d_2 T(i,j) \, \left(\frac{dx}{d\rho}\right)^2, \tag{4.152}$$

$$\hat{a}_2^o = a_{2,2}^o + \frac{5}{36} \left(p_0'(\tau^o)\right)^2 - \frac{2}{9} p_0(\tau^o) p_0''(\tau^o) + \frac{1}{3} p_0(\tau^o) p_2^o, \tag{4.153}$$

$$(\phi_{log})_i \equiv \phi_{log}\phi_{log}(\tau^o, \rho_i), \qquad d_1(\phi_{log})_i \equiv \partial_\rho \phi_{log}(\tau^o, \rho_i),$$

$$(\pi_{log})_i \equiv \pi_{log}(\tau^o, \rho_i), \qquad d_1(\pi_{log})_i \equiv \partial_\rho \pi_{log}(\tau^o, \rho_i), \tag{4.154}$$

$$(k_{log})_i \equiv k_{log}(\tau^o, \rho_i).$$

We now have all the data needed to compute (see (4.129))

$$J_{\pi,i} \equiv J_\pi(\tau^o, \rho_i; \partial_\rho \hat{\phi} = d_1 \phi_i^o + d_1(\phi_{log})_i, \hat{\phi} = \phi_i^o + (\phi_{log})_i). \tag{4.155}$$

Next, we use (4.127) and the boundary condition in (4.141) to compute Chebyshev coefficients $\mathcal{F}_{\pi_c}^j$:

$$i = 1, \cdots N - 1 \ :$$

$$\sum_{j=1}^N \left(d_1 T(i,j)\frac{dx}{d\rho} - \frac{1}{2\rho_i}T(i,j)\right) \mathcal{F}_{\pi_c}^j = -\left(J_{\pi,i} + d_1(\pi_{log})_i - \frac{1}{2\rho_i}(\pi_{log})_i\right),$$

$$\sum_{j=1}^N T(N,j) \, \mathcal{F}_{\pi_c}^j = \frac{1}{2} p_0'(\tau^o). \tag{4.156}$$

We can now determine

$$\pi_i \equiv \pi_c(\tau^o, \rho_i) = \sum_{j=1}^N \mathcal{F}_{\pi_c}^j \, T(i,j), \qquad i = 1, \cdots N. \tag{4.157}$$

Finally, we complete the first RK step ($i = 1, \cdots N$):

$$k_{1,\phi_c,i} = \Delta\tau \left(\pi_i + \frac{1}{2}(1 - \alpha^4\rho_i^4) \, d_1\phi_i^o + (k_{log})_i \right),$$
$$k_{1,\hat{a}_2} = \Delta\tau \, \frac{2}{3}p_0'(\tau^o) \, p_2^o. \tag{4.158}$$

- **RK step 2**: With the shift

$$\tau^o \to \tau^o + \frac{1}{2}\Delta\tau, \qquad \phi_i^o \to \phi_i^o + \frac{1}{2}k_{1,\phi_c,i}, \tag{4.159}$$

  we repeat RK step 1, producing $k_{2,\phi_c,i}$, $k_{2,\hat{a}_2}$.

- **RK step 3**: With the shift

$$\tau^o \to \tau^o + \frac{1}{2}\Delta\tau, \qquad \phi_i^o \to \phi_i^o + \frac{1}{2}k_{2,\phi_c,i}, \tag{4.160}$$

  we repeat RK step 1, producing $k_{3,\phi_c,i}$, $k_{3,\hat{a}_2}$.

- **RK step 4**: With the shift

$$\tau^o \to \tau^o + \Delta\tau, \qquad \phi_i^o \to \phi_i^o + k_{3,\phi_c,i}, \tag{4.161}$$

  we repeat RK step 1, producing $k_{4,\phi_c,i}$, $k_{4,\hat{a}_2}$.

- We now update to a time-step τ^n:

$$\phi_i^n = \phi_i^o + \frac{1}{6}k_{1,\phi_c,i} + \frac{1}{3}k_{2,\phi_c,i} + \frac{1}{3}k_{3,\phi_c,i} + \frac{1}{6}k_{4,\phi_c,i}, \qquad i = 1, \cdots N,$$
$$\hat{a}_2^n = \hat{a}_2^o + \frac{1}{6}k_{1,\hat{a}_2} + \frac{1}{3}k_{2,\hat{a}_2} + \frac{1}{3}k_{3,\hat{a}_2} + \frac{1}{6}k_{4,\hat{a}_2}. \tag{4.162}$$

- At this stage we introduce dissipation [103]. We compute Chebyshev coefficients $\mathcal{F}_{\phi_c}^j$ solving

$$\phi_i^n = \sum_{j=1}^{N} \mathcal{F}_{\phi_c}^j \, T(i,j), \qquad i = 1, \cdots N. \tag{4.163}$$

166

and re-evaluate ϕ_i^n suppressing the higher harmonics:

$$\phi_i^n = \sum_{j=1}^{N-N_{diss}} \mathcal{F}_{\phi_c}^j \, T(i,j), \qquad i = 1, \cdots N,$$

$$p_2^n = \frac{1}{2} \sum_{j=1}^{N-N_{diss}} \mathcal{F}_\phi^j \, d_2 T(i,j) \, \left(\frac{dx}{d\rho}\right)^2.$$

(4.164)

where, in practice, we choose

$$N_{diss} = [0.2N].$$

(4.165)

We use (4.138) to compute $a_{2,2}^n$:

$$a_{2,2}^n = \hat{a}_2^n - \frac{5}{36} \left(p_0'(\tau^n)\right)^2 + \frac{2}{9} p_0(\tau^n) p_0''(\tau^n) - \frac{1}{3} p_0(\tau^n) p_2^n.$$

(4.166)

- In preparation to computation of

$$b_i^n \equiv b_c(\tau^n, \rho_i), \qquad g_i^n \equiv g_c(\tau^n, \rho_i),$$

(4.167)

we evaluate $d_1\phi_i^n \equiv \partial_\rho\phi_c(\tau^n, \rho_i)$, $d_2\phi_i^n \equiv \partial_\rho^2\phi_c(\tau^n, \rho_i)$ and $\pi_i^n \equiv \pi_i(\phi_i^n; a_{2,2}^n)$, following corresponding computations in RK step 1, and further identify

$$\begin{aligned}
&(\phi_{log})_i \equiv \phi_{log}(\tau^n, \rho_i), \qquad d_1(\phi_{log})_i \equiv \partial_\rho\phi_{log}(\tau^n, \rho_i), \\
&d_2(\phi_{log})_i \equiv \partial_\rho^2\phi_{log}(\tau^n, \rho_i), \\
&(b_{log})_i \equiv b_{log}(\tau^n, \rho_i; p_2^n), \qquad d_1(b_{log})_i \equiv \partial_\rho b_{log}(\tau^n, \rho_i; p_2^n), \\
&d_2(b_{log})_i \equiv \partial_\rho^2 b_{log}(\tau^n, \rho_i; p_2^n), \\
&d_1(a_{log})_i \equiv \partial_\rho a_{log}(\tau^n, \rho_i; p_2^n), \qquad d_2(a_{log})_i \equiv \partial_\rho^2 a_{log}(\tau^n, \rho_i; p_2^n), \\
&d_3(a_{log})_i \equiv \partial_{\rho\rho\rho}^3 a_{log}(\tau^n, \rho_i; p_2^n), \\
&d_1(g_{log})_i \equiv d_3(a_{log})_i + \frac{2}{\rho_i} d_2(a_{log})_i - \frac{2}{\rho_i^2} d_1(a_{log})_i.
\end{aligned}$$

(4.168)

- Note that at this stage we have all the data necessary to evaluate $J_{b,i}$ (see (4.130)),

$$J_{b,i} \equiv J_b(\tau^n, \rho_i; \partial_\rho\hat{\phi} = d_1\phi_i^n + d_1(\phi_{log})_i, \hat{\phi} = \phi_i^n + (\phi_{log})_i).$$

(4.169)

We compute Chebyshev coefficients $\mathcal{F}_{b_c}^j$ solving (4.128)

$$\sum_{j=1}^N \mathcal{F}_{b_c}^j \, d_2 T(i,j) \, \left(\frac{dx}{d\rho}\right)^2 = -(J_{b,i} + d_2(b_{log})_i), \qquad i = 1, \cdots N-2.$$

(4.170)

167

along with the boundary conditions (4.141):

$$\sum_{j=1}^{N} \mathcal{F}_{b_c}^j \, T(N, j) = 0, \qquad \sum_{j=1}^{N} \mathcal{F}_{b_c}^j \, d_1 T(N, j) \left(\frac{dx}{d\rho} \right) = 0. \qquad (4.171)$$

Given $\mathcal{F}_{b_c}^j$ we evaluate

$$b_i^n = \sum_{j=1}^{N} \mathcal{F}_{b_c}^j \, T(i, j), \qquad d_1 b_i^n = \sum_{j=1}^{N} \mathcal{F}_{b_c}^j \, d_1 T(i, j) \left(\frac{dx}{d\rho} \right), \qquad i = 1, \cdots N. \quad (4.172)$$

- We can now compute (see (4.135))

$$J_{g,i} \equiv J_g(\tau^n, \rho_i), \qquad (4.173)$$

with obvious substitutions:

$$\partial_\rho^2 \hat{\phi} = d_2 \phi_i^n + d_2 (\phi_{log})_i, \qquad \partial_\rho \hat{\phi} = d_1 \phi_i^n + d_1 (\phi_{log})_i, \qquad \hat{\phi} = \phi_i^n + (\phi_{log})_i,$$
$$\pi = \pi_i^n + (\pi_{log})_i, \qquad \partial_\rho b = d_1 b_i^n + d_1 (b_{log})_i. \qquad (4.174)$$

Next, we solve for Chebyshev coefficients following (4.134), (4.168)

$$\sum_{j=1}^{N} \mathcal{F}_{g_c}^j \, d_1 T(i, j) \left(\frac{dx}{d\rho} \right) = -(J_{g,i} + d_1 (g_{log})_i), \qquad i = 1, \cdots N - 1, \qquad (4.175)$$

along with the boundary conditions (4.141):

$$\sum_{j=1}^{N} \mathcal{F}_{g_c}^j \, T(N, j) = 6 a_{2,2}^n + \frac{5}{6} \left((p_0'(\tau^n))^2 - p_0(\tau^n) p_0''(\tau^n) \right). \qquad (4.176)$$

Given $\mathcal{F}_{g_c}^j$ we evaluate

$$g_i^n = \sum_{j=1}^{N} \mathcal{F}_{g_c}^j \, T(i, j), \qquad i = 1, \cdots N. \qquad (4.177)$$

- The next step is computation of

$$a_i^n \equiv a_c(\tau^n, \rho_i), \qquad (4.178)$$

168

using (4.136). Remarkably, this can be achieved analytically, given $\mathcal{F}_{g_c}^j$. Indeed, note that

$$
\begin{aligned}
a_c(\tau, \rho) &= \sum_{j=1}^{\infty} \mathcal{F}_{g_c}^j(\tau) \int_0^{\rho} \frac{dx}{x^2} \left[\int_0^x dy\, y^2 T_{j-1}\left(\frac{2y}{L_\rho} - 1 \right) \right] \\
&= \left(\frac{L_\rho}{2} \right)^2 \sum_{j=1}^{\infty} \mathcal{F}_{g_c}^j(\tau) \int_{-1}^{2\rho/L_\rho - 1} \frac{dx}{(1+x)^2} \left[\int_{-1}^x (1+y)^2 T_{j-1}(y) \right],
\end{aligned}
\tag{4.179}
$$

where in the second line we changed the integration variables

$$
y \to \frac{L_\rho}{2}(1+y), \qquad x \to \frac{L_\rho}{2}(1+x).
\tag{4.180}
$$

Furthermore,

$$
\int_{-1}^z \frac{dx}{(1+x)^2} \left[\int_{-1}^x (1+y)^2 T_{j-1}(y) \right] = \sum_{s=1}^{j+2} \mathcal{C}_{j,s}\, T_{s-1}(z).
\tag{4.181}
$$

where the rational coefficients $\mathcal{C}_{j,s}$ can be computed using the orthonormality properties of the Chebyshev polynomials. The first several coefficient sets are:

$$
\begin{aligned}
\mathcal{C}_{1,s} &= \left\{ \frac{1}{4},\, \frac{1}{3},\, \frac{1}{12} \right\}, \\
\mathcal{C}_{2,s} &= \left\{ -\frac{1}{24},\, -\frac{1}{48},\, \frac{1}{24},\, \frac{1}{48} \right\}, \\
\mathcal{C}_{3,s} &= \left\{ -\frac{7}{48},\, -\frac{13}{60},\, -\frac{1}{15},\, \frac{1}{60},\, \frac{1}{80} \right\},
\end{aligned}
\tag{4.182}
$$

$$
\cdots .
$$

Thus,

$$
a_c(\tau, \rho) = \left(\frac{L_\rho}{2} \right)^2 \sum_{j=1}^{\infty} \mathcal{F}_{g_c}^j(\tau) \left[\sum_{s=1}^{j+2} \mathcal{C}_{j,s}\, T_{s-1}\left(\frac{2\rho}{L_\rho} - 1 \right) \right],
\tag{4.183}
$$

and (truncating the Chebyshev modes to order $(N-2)$)

$$
a_i^n = \left(\frac{L_\rho}{2} \right)^2 \sum_{j=1}^{N-2} \sum_{s=1}^{j+2} \mathcal{F}_{g_c}^j\, \mathcal{C}_{j,s}\, T(i, s).
\tag{4.184}
$$

- Finally, we identify

$$
\left\{ \tau^n,\, p_2^n,\, a_{2,2}^n \,;\, \phi_i^n,\, b_i^n,\, a_i^n \right\} \qquad \to \qquad \left\{ \tau^o,\, p_2^o,\, a_{2,2}^o \,;\, \phi_i^o,\, b_i^o,\, a_i^o \right\},
\tag{4.185}
$$

and repeat the whole process from (4.150).

4.7.3 Convergence tests

All our simulations were performed with $N = 40$ collocation points. In this section we discuss the convergence of the simulations as the number of collocation points is varied, and also the accuracy of solving the constraint equations (4.127), (4.128), and (4.134).

As a representation test of the code convergence behaviour, we consider $\alpha = 1$ and different number of collocation points: $N = N_{i=1,\cdots 4} = \{10, 20, 40, 60\}$. We monitor the ($L_2$ norm of the) difference of solutions with successive values of N_i, defined as

$$
\begin{aligned}
e^{\phi_c}_{N_i}(\tau) &= || \, \phi_c[N_i] - \phi_c[N_{i-1}] \, ||_2, \\
e^{b_c}_{N_i}(\tau) &= || \, b_c[N_i] - b_c[N_{i-1}] \, ||_2, \\
e^{\hat{a}}_{N_i}(\tau) &= || \, \hat{a}[N_i] - \hat{a}[N_{i-1}] \, ||_2.
\end{aligned}
\tag{4.186}
$$

Additionally, given spectral coefficients $\mathcal{F}^i_{\pi_c}$, we can verify the accuracy of constraint (4.127) defining

$$
\mathrm{const}_{\pi_c}(\tau, \rho) \equiv J_\pi + \partial_\rho(\pi_{log}) - \frac{1}{2\rho}\pi_{log} + \sum_{j=1}^{N} \mathcal{F}^j_{\pi_c}(\tau) \, \left(\partial_\rho - \frac{1}{2\rho} \right) T_{j-1}\left(\frac{2\rho}{L_\rho} - 1 \right),
\tag{4.187}
$$

$$
\mathrm{error}[\pi_c](\tau) = ||\mathrm{const}_{\pi_c}(\tau, \rho)||_2.
$$

Likewise, for (4.128),

$$
\mathrm{const}_{b_c}(\tau, \rho) \equiv J_b + \partial_\rho^2 b_{log} + \sum_{j=1}^{N} \mathcal{F}^j_{b_c}(\tau) \, \partial_\rho^2 T_{j-1}\left(\frac{2\rho}{L_\rho} - 1 \right),
\tag{4.188}
$$

$$
\mathrm{error}[b_c](\tau) = ||\mathrm{const}_{b_c}(\tau, \rho)||_2,
$$

and, for (4.134),

$$
\mathrm{const}_{g_c}(\tau, \rho) \equiv J_{g_c} + \sum_{j=1}^{N} \mathcal{F}^j_{g_c}(\tau) \, \partial_\rho T_{j-1}\left(\frac{2\rho}{L_\rho} - 1 \right),
\tag{4.189}
$$

$$
\mathrm{error}[g_c](\tau) = ||\mathrm{const}_{g_c}(\tau, \rho)||_2.
$$

Results are shown in figures 4.22-4.24. The left panels illustrate how e_N decreases as the resolution is improved, while the right panels present the accuracy of solving constraints (4.187)-(4.189).

Figure 4.22: (Left panel) Convergence of ϕ_c for different number of collocation points as a function of τ, see (4.186). (Right panel) Residuals of the constraint (4.127), see (4.187).

Figure 4.23: (Left panel) Convergence of b_c for different number of collocation points as a function of τ, see (4.186). (Right panel) Residuals of the constraint (4.128), see (4.188).
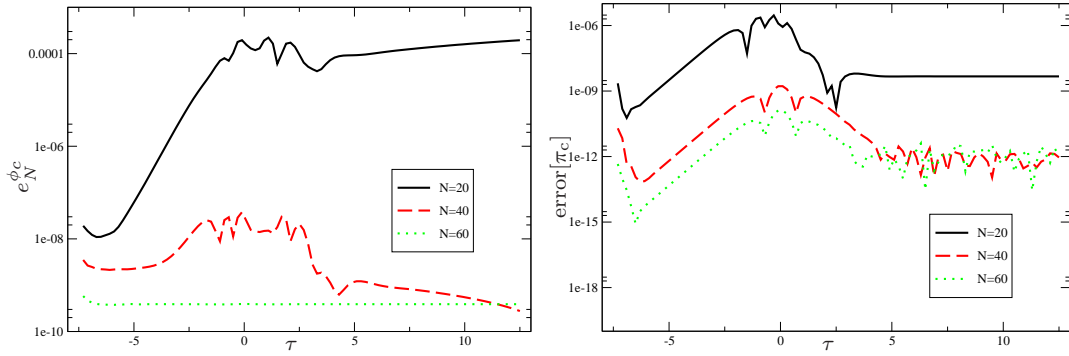
Figure 4.24: (Left panel) Convergence of $\hat{a}$ for different number of collocation points as a function of τ, see (4.186). (Right panel) Residuals of the constraint (4.134), see (4.189).
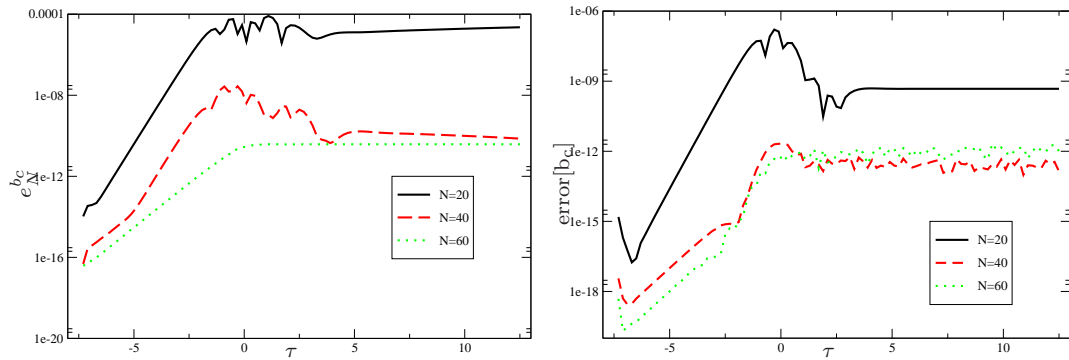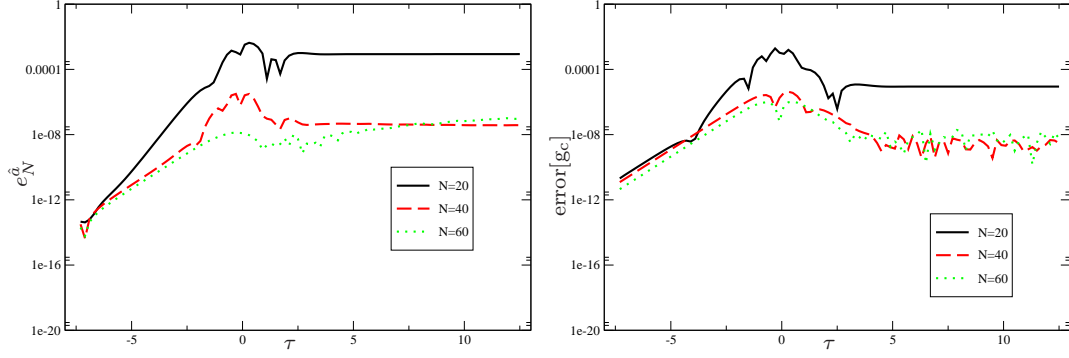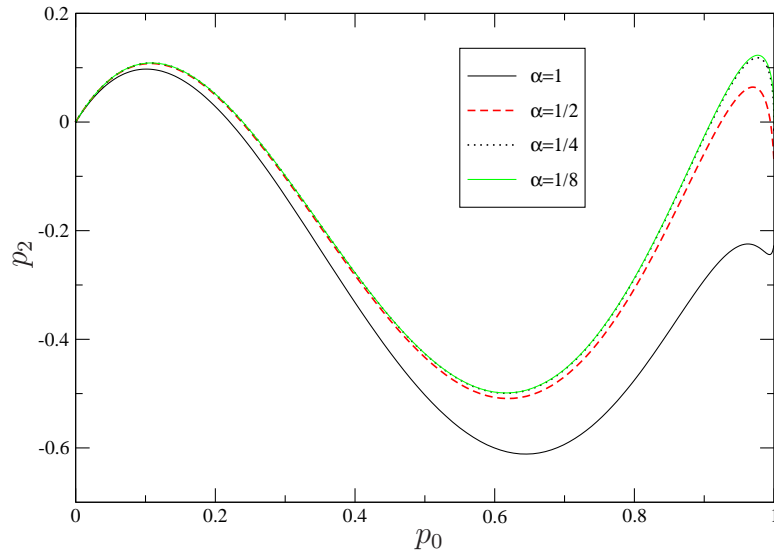

Figure 4.25: Response $p_2 = p_2(p_0)$ for fast quenches. The universal regime of abrupt quenches is achieved for $\alpha \gtrsim \frac{1}{4}$.

4.7.4 Limit of abrupt quenches

Quantum quenches have two scaling regimes: the adiabatic one ($\alpha \gg 1$), and the regime of the abrupt quenches ($\alpha \ll 1$). The former one represents an expected slow, hydrodynamic response of the system to external forcing [48]. It was observed in [48] (and further studied in [54]) that within a holographic framework a QFT exhibits a scaling response in the limit of abrupt quenches as well. The same scaling was observed outside of holography in a CFT deformed by a relevant operator [79]. Our code is ideally suited to study fast quenches since we use the α-rescaled scalar and metric variables [54]. Figure 4.25 illustrates the response function p_2 for fast quenches, $\{\alpha = 1, \frac{1}{2}, \frac{1}{4}, \frac{1}{8}\}$. Note that the response becomes almost indistinguishable between $\alpha = \frac{1}{4}$ and $\alpha = \frac{1}{8}$ quenches. We take $\alpha = \frac{1}{8}$ to correspond to *abrupt quench*.

Chapter 5

Conclusion

In this thesis we strove to understand quantum quenches in strongly coupled field theory systems with the aid of the holographic duality. We have been able to learn many interesting characteristics of such systems, both in terms of the theory of the response, as well as of different methods of solving such systems in different limits. While in these systems we have made approximations that were convenient for the particular approaches — a perturbative backreaction of the scalar in the numerical studies, and the limit of infinitely fast (or slow) quenches in the analytic studies — we now find ourselves in a position where it is possible to go forward without these restrictions. Our numerical technique developed in chapter 4 can be adapted study the backreaction of the scalar field in the bulk background nonperturbatively, and for quenches of any rate.

In chapter 2, we studied the quench of $\mathcal{N} = 4$ super Yang-Mills (SYM) in $d = 4$ Minkowski space by a relevant operator $\mathcal{O}_\Delta$ of arbitrary dimension $2 < \Delta \leq 4$. The operator was switched on by exciting the coupling $\lambda(\tau)$ in the additional term $\lambda \mathcal{O}_\Delta$ in the Lagrangian. We chose the coupling to be a smooth function of the boundary time as in (2.89):

$$\lambda(\tau) = \lambda_f \left(\frac{1}{2} + \frac{1}{2} \tanh \left(\frac{\tau}{\alpha} \right) \right), \tag{5.1}$$

which is initially zero at $\tau = -\infty$, and λ_f at time $\tau = \infty$. In particular, this function was chosen to have a tanh-profile, such that in the limit of $\alpha \to 0$ (instantaneous quenches), the change in λ becomes arbitrarily fast and it tends to a step function. By introducing the quench with a scalar operator in this way, we were able to imitate the controlled fashion in which experimentalists can switch on potentials in cold atom experiments, such as those described in section 1.3.3.

This work was a follow-up project on [48], in which quenches of the same system were considered by operators with dimension $\Delta = 2$ and $\Delta = 3$, corresponding to mass-terms of a scalar and fermion in the boundary field theory, respectively. In these two cases, my collaborators were able to find hints of universal behaviour in the scaling and equilibration of the expectation values of the operator $\mathcal{O}_\Delta$, as well as the energy density and pressure of the field theory, both in the limit of fast (limiting to instantaneous), and slow (limiting to adiabatic) quenches. In this chapter, published in [52], we sought to confirm the observed scaling behaviour hinted at in the previous work, by investigating quenches by operators of arbitrary dimension $\Delta = 7/3, 8/3, 10/3$ and $11/3$. These values for Δ were chosen so as to be evenly spread between the upper and lower bounds of 2 and 4, but also to avoid integer and half-integer values of the operator dimension for which the asymptotic expansions of the fields obtain logarithmic corrections in our coordinate system, leading to anomalous scaling.

To study the effect of the quench on the field theory system, we described the system by its holographic dual: a (tachyonic) scalar field of mass-squared $\Delta(\Delta - 4)$ backreacting on an asymptotically AdS$_5$ spacetime containing a planar black hole. This black hole is assumed to be large, such that the scalar field backreacts only perturbatively on the spacetime, thereby linearizing and scalar field equation, and making it much easier to solve. In the dual field theory, this limit is equivalent to taking the field theory to be initially in a high temperature state, such that switching on the operator is only a perturbation to the state. In the gravity dual, we then numerically evolved the scalar field using a finite difference procedure described in the appendix 2.14. By fitting the first few terms in the asymptotic expansion of the scalar field near the AdS boundary, we were able to determine its normalizable mode $p_{2\Delta-4}$, which is proportional to the expectation value $\langle \mathcal{O}_\Delta \rangle$, and from which we could calculate the changes to the field theory stress-energy, temperature and entropy density. We did this in both the fast quench and slow quench limits.

The less challenging situation addressed in chapter 2, was that of slow quenches. In this limit, it is in fact possible to solve the perturbative response analytically as first suggested in [48], by expanding it in an inverse power series in α, since α is now large, and since the subleading contribution to $p_{2\Delta-4}$ in $1/\alpha$ is proportional to $\dot{p}_0$ — see section 2.8 and appendix 2.15 for more details. We found that in this adiabatic limit, quench in the field theory is reversible. That is, the change in the stress-energy, temperature and entropy density are respectively equal and opposite in forward and backward quenches, *i.e.,* if we evolve the source as $p_0(\tau)$ the change in these quantities is minus the change if we evolve it as $p_0(-\tau)$.

We analytically determined the normalizable mode of the metric backreaction in its asymptotic expansion, $a_{2,4}$, in equation (2.31) and the dependence of the thermodynamic

175

quantities namely the change in temperature, energy density and pressure on $a_{2,4}$, and the dependence of the operator expectation value $\langle \mathcal{O}_\Delta \rangle$ on $p_{2\Delta-4}$. In the limit of fast quenches, we found numerically that both $p_{2\Delta-4}$ and $a_{2,4}$ scale as $\alpha^{4-2\Delta}$. These quantities grow without bound as we make the quenching time α arbitrarily small. Therefore there is no limit to the amount of energy that can be pumped into the field theory system for short enough quenches. This, of course, came with the caveat that the analysis was only a perturbative one, and that for a full nonperturbative quench these universal scalings might be violated. The question of the validity of this scaling beyond perturbation theory was addressed in chapter 3.

Another universal feature of fast quenches observed was the excitation and equilibration of the normalizable mode of the scalar field. We found that its excitation beyond the arbitrary threshold of 5% of its final value scales as $(\Delta - 2)\,\alpha \log \alpha$, *i.e.,* that it vanishes as α becomes small. Although we saw this scaling of the excitation time for a threshold of 5%, we believe it to be generally true for any fixed threshold that is small enough (*i.e.,* the excitation time must be defined for the given threshold). This is not surprising, since the limit of $\alpha \to 0$ is equivalent to the source becoming a step function around $\tau = 0$. The response of the scalar field cannot be excited before the source is switched on, thus in the limit where the source is a step function, the response must be excited at $\tau = 0$. The equilibration time of the scalar's normalizable mode has a more interesting behaviour during fast quenches, namely that it becomes independent of α or Δ, seeming to indicate that its late-time behaviour becomes dominated by the thermal timescale $\tau_{th} \propto 1/T$. An intuitive explanation for this behaviour in the thermal field theory picture is that the energy injected into the system due to an abrupt quench, will be redistributed through the various energy scales of the system. This redistribution should occur in roughly the thermal timescale, as long as the change in temperature remains small. This picture seems to only apply to local observables, since in chapter 4, it was found that nonlocal correlations can be distinguished for distances/times longer than the thermal scale. In the limit of nonperturbative quenches, it would be interesting to see how the thermalization of local quantities depends on the temperature of the system, since the high temperature approximation would no longer hold. However, within this perturbative regime, it would also be interesting to have a derivation of this universal thermalization behaviour of the scalar field, rather than just numerical evidence and heuristic arguments.

In chapter 3, we analytically addressed the limit of very fast quenches, by abruptly switching on the source of the boundary operator. The situation was more general than the discussion in chapter 2, since we addressed a quenching operator of general mass dimension Δ in a strongly coupled CFT living in d-dimensional Minkowski spacetime. An important difference between the source in chapter 2 and the source in chapter 3 was that the source

in chapter 3 was abruptly switched on at time $t = 0$, and held constant again after $t = \delta t$, while in chapter 2 the source was a smooth function from time $-\infty$ to $+\infty$. A final restriction of this study, which first appeared in [54], was that only operator dimensions were considered that did not lead to logarithmic terms in the asymptotic expansion of the scalar field in the dual AdS spacetime.

In this setup, after the source of the scalar field is switched on at time zero, the scalar field propagates into the bulk geometry from the asymptotic boundary as a shock wave. The scalar field is then zero at all points in the spacetime that falls outside of the lightcone emanating from the boundary at time $t = 0$ (see figure 3.1). We took the limit of a very short quench, *i.e.,* we kept the source constant after time $t = \delta t$, and took the limit $\delta t \to 0$. All energy pumped into the AdS geometry can be viewed as contained in the scalar field living in a spacetime very close to the AdS boundary. In this limit therefore, the scalar field evolves according to the linearized equations of motion of a scalar in pure Poincaré-AdS, which can be seen from higher-order terms in its equation scaling with higher powers of δt. Its short-time evolution is then oblivious of details of the full bulk theory, such as whether it contains a black hole, or of higher order terms in the action, due to this linearization coming from the scaling with δt. In the dual field theory picture, this means that the short-time response of the field theory does not depend on whether or not the field theory is initially in a thermal state, or on details of the scalar operator $\mathcal{O}_\Delta$ other than its dimension Δ and the dimension of the spacetime d. We found that, given the constraint that the scalar field vanishes on the light cone (*i.e.,* $\phi(\tau = \rho, \rho) = 0$), we could find the scaling of the normalizable mode $p_{2\Delta-d}$ in terms of the quenching time δt as well as the amplitude of the non-normalizable mode δp. We found that $p_{2\Delta-d}$ has exactly the same dependence on δt as in chapter 2, namely that it scales as $\delta t^{2\Delta-d}$. Furthermore, assuming that p_0 is a monomial in t, we were able to calculate the exact time dependence of $p_{2\Delta-d}$ during the time $0 < t < \delta t$.

Of course, this solution of the normalizable mode breaks down for longer times, since then the scalar field will be sensitive to infrared (IR) details of the spacetime. However, we were still able to calculate the change in energy density due to the quench. This is possible because $\Delta\mathcal{E}$ is proportional to an integral of $p_{2\Delta-d}$ times the time derivative of the source $\dot{p}_0$. Since the source is kept constant at times later than $t = \delta t$, $\dot{p}_0$ vanishes and the energy density of the dual field theory stops changing, even though the response of the scalar field keeps evolving in time. We therefore found that $\Delta\mathcal{E}$ has the same scaling in δt as the scalar field response, namely $\delta t^{2\Delta-d}$, while scaling as the amplitude of the scalar source-squared, *i.e.,* δp^2. To keep the change in energy density from diverging, we can scale δp as $\delta t^{\frac{d}{2}-\Delta}$. An explanation of the universal scalings's independence on the state of the system, is that the ultraviolet (UV) energy scale corresponding to the very short

timescale of the quench, dominates all other scales in the system, and therefore cannot be influenced by other energy scales in the theory. This work focused only on relevant quenching operators with dimension $\frac{d}{2} < \Delta < d$, chosen such that the solution of the dual scalar field does not contain logarithmic terms, and therefore avoids the anomalous scaling observed in [48]. A natural next step for future work would be to consider precisely such operators, with integer dimension Δ for even d, and half-integer dimension for odd d. The goal would then be to derive analytically the anomalous logarithmic scaling with δt of the response, and in thermodynamic quantities, such as the changes in energy and entropy density. Another future direction would be to calculate the short-time response for a quenching operator with dimension $\frac{d}{2} - 1 < \Delta < \frac{d}{2}$ in the alternative quantization scheme of Klebanov and Witten [19] in which $p_{2\Delta - d}$ is the source and p_0 is the response. We would then have covered the full range of allowed dimensions for relevant operators.

In chapter 4, we again specialized to the same system as in chapter 2, namely a thermal $\mathcal{N} = 4$ SYM in four spacetime dimensions perturbatively quenched by a relevant operator. In this case we chose the operator to be a fermionic mass term $m_f \mathcal{O}_3$ in the field theory Lagrangian. The operator therefore has mass dimension $\Delta = 3$; one of the cases considered in the original quenches paper by my collaborators in [48]. The mass of a fermionic operator is then switched on in the same time-dependent manner of chapter 2, *i.e.,* we perform a global thermal quench, with the same holographic dual of a scalar field collapsing onto a large black hole in asymptotically AdS$_5$ spacetime. Here we incorporated a new numerical method for solving the linearized field equations of the dual bulk spacetime using Chebyshev pseudo-spectral methods. This involves discretizing the spacetime in the radial direction from the asymptotic boundary up to some depth inside the event horizon of the black hole. Using Chebyshev polynomials to approximate the metric fields $\hat{a}$ and b, as well as the scalar field $\hat{\phi}$, we then optimized the coefficients of the polynomials at each order to closely interpolate the values of the fields at each spacetime point. The fields were then evolved in time using a fourth-order Runge-Kutta method, which amounted to finding the time-dependence of the Chebyshev coefficients. Unlike the numerical results of chapter 2, we were able by this method to obtain the time-dependent radial profiles of the metric coefficients in addition to the scalar field profile. This gave us the capability to calculate spacetime-dependent quantities in the bulk theory. In particular, focusing our efforts on fast quenches and following the example of [53], we calculated the evolution of the respective perturbations of the black hole's apparent and event horizons, the equal-time two-point function of a very high-dimension operator in the boundary theory and the entanglement entropy of an infinite strip in the four-dimensional boundary theory. We compared the time-evolution of each of these in turn with the evolution of the response of the scalar field p_2. This gave us the ability to probe the thermalization of the field the-

ory system at different length scales, set by the separation of the points in the two-point function and the width of the strip in the entanglement entropy, and compare the results of different measures.

The evolution of the perturbations on the area density of the black hole horizons served as a good test of our numerics. As physically expected, the event horizon showed only a monotonic increase in area density, and the apparent horizon was at all times contained inside the radius of the event horizon while converging to the position of the event horizon. The event horizon must increase monotonically, since it is a global property of the spacetime, namely the position from which a light ray cannot escape to infinity. If it were to decrease for some period of time, then that same light ray can escape to infinity, which is a contradiction. While a light ray at the position of the event horizon can still move radially outward from the black hole, it becomes static when it is located at the position of the apparent horizon. Since this is also the property of a static event horizon, we would expect the apparent horizon to be located inside the event horizon, and catch up with the event horizon at late times, which is what we observed.

The apparent horizon did show an interesting behaviour for fast quenches, namely that its growth was non-monotonic around time $\tau = 0$, when the derivative of the source p_0 was at its highest. This is interesting, since it has been proposed that the area density of the apparent horizon is dual to the time-dependent entropy of the field theory [94], and one would naively expect this growth to be monotonic. This behaviour is not well understood, and it would be interesting to investigate it further. The equilibration of the horizons' area densities was calculated using the scheme where the perturbation is within 2% of its final value, and found that it typically equilibrates much faster than the normalizable mode of the scalar field p_2. In fact, while the equilibration of p_2 becomes constant for fast quenches, the horizons' equilibration times τ_{eq} scale approximately as α. This behaviour seems to indicate that although the horizon is typically related to the thermal timescale, its perturbations are more sensitive to the normalizable mode of the scalar field, which also equilibrates as α.

We also calculated the evolution of the two-point function of an operator with high dimension Δ in the boundary theory using the geodesic approximation discussed in the introduction of this thesis, as well as the entanglement entropy of an infinite strip in the boundary theory using the Ryu-Takayanagi minimal surface prescription [95, 96]. Like the event horizon, such a geodesic or surface is static to leading order in the perturbation, and the perturbation of its length or area is calculated from the time evolution of the metric perturbations. Because the metric evolves with time, the shapes of the geodesic and minimal surface also depend on time, but are only expected to affect the perturbations in length and area at a higher order in perturbation theory, and not to influence our calculations.

179

We were, therefore surprised that the perturbations on the shape of the minimal surface *do* cause perturbations of the entanglement entropy at the calculated perturbative order, through a boundary term in the integral shown in section 4.4.3. For the strip, it only contributes a small finite amount to the perturbation of the entanglement entropy (EE), while for a spherical entangling surface it contributes an additional logarithmic divergence in the UV cut-off. While this result is surprising, it is perhaps a remnant of our regularization scheme for the EE when using time-dependent counterterms, and a better way of dealing with divergent EE is "renormalizing" it by taking the derivative with respect to the width of the surface, as described in [99, 100]. Nonetheless, we believe that the observed thermalization behaviour is not greatly affected by the absence of such a scheme. Regarding the thermalization times of the two-point correlator and EE, we calculated it using the same 2% criterion as mentioned above, for various separations in the boundary of the spacetime. We found similar behaviour to the literature on Vaidya metrics [47], namely that probes with small separations thermalized the fastest, and in fact had the same thermalization profile as the square of the source of the scalar field, p_0^2. Meanwhile, the wider probes thermalized more slowly, apparently without an upper bound on the thermalization time τ_{th}. The thermalization time τ_{th} also had a linear dependence on the boundary separation y_m in limit of wide surfaces. The widest separations considered were roughly twice the thermal length scale, and arguably not long enough to conclude that such a linear relationship holds true for very wide boundary separations.

We considered the reason why the wider probes thermalized slowest. It was concluded that because the minimal surfaces and geodesics have profiles in in time as well as in the radial direction of AdS (in Eddington-Finkelstein coordinates), and because it stretches back in time, such surfaces and geodesics can probe regions of the spacetime far back in the past, or from the opposite point of view, can be sensitive to the quench arbitrarily far in the future, for arbitrarily wide boundary separations. This behaviour can be further explained by the fact that the part of the probe closest to the black hole horizon contributes most to the perturbation of its surface or length. This linear behaviour agrees with that seen in free field theories and Vaidya studies (see for example [34] and [44]), and might be explained by the fact that opposite ends of the probe in the field theory take time to come into causal contact. The growth of the probe then only slows after causal contact is established, as proposed in other studies [34]. It would be interesting to see if this linear behaviour continues indefinitely, either by using much wider probes than used in this study, or by an analytical investigation. If it does, it would be puzzling, since wide enough probes have a characteristic energy scale that is smaller than the thermal energy scale, which should dominate the low-energy regime. Analytically, there is the opportunity to find evolution regimes of the EE and two-point function at different times during the

quench, as found in [87].

Future directions in this research program should include the numerical evolution of the response of the system in the nonperturbative regime, as mentioned above. This would be a natural extension of the research in the high temperature regime considered in our numerical studies thus far, and is well within the capabilities of the Chebyshev method developed for our system in chapter 4. While we have been able to analytically confirm the scaling of certain quantities nonperturbatively in the fast-quench limit, the thermalization behaviour of both the expectation value of the quenching operator as well as the nonlocal probes is an open question. Furthermore it would be interesting to see if there are more universal behaviours that can be discovered by considering quenches by operators in a range of dimensions, rather than just dimension 3 as in chapter 4. Looking further ahead, it would be of interest to consider local quenches in the field theory, with the aim of addressing the field theory's response to anisotropic disturbances. This would, of course be significantly more challenging, since our numerical method is designed to solve a system in $1 + 1$ effective dimensions, but should nevertheless be an eventual goal in the field of holographic quenches.

References

[1] J. D. Bekenstein, "Black holes and entropy," Phys. Rev. D **7**, 2333 (1973);
S. W. Hawking, "Particle Creation by Black Holes," Commun. Math. Phys. **43**, 199
(1975) [Erratum-ibid. **46**, 206 (1976)].

[2] G. 't Hooft, "Dimensional reduction in quantum gravity," Salamfest 1993:0284-296
[gr-qc/9310026].

[3] L. Susskind, "The World as a hologram," J. Math. Phys. **36**, 6377 (1995) [hep-th/9409089].

[4] G. 't Hooft, "A Planar Diagram Theory for Strong Interactions," Nucl. Phys. B **72**,
461 (1974).

[5] O. Aharony, S. S. Gubser, J. M. Maldacena, H. Ooguri and Y. Oz, "Large N field
theories, string theory and gravity," Phys. Rept. **323**, 183 (2000) [hep-th/9905111].

[6] J. M. Maldacena, "The Large N limit of superconformal field theories and supergravity," Int. J. Theor. Phys. **38**, 1113 (1999) [Adv. Theor. Math. Phys. **2**, 231 (1998)]
[hep-th/9711200].

[7] N. Itzhaki, J. M. Maldacena, J. Sonnenschein and S. Yankielowicz, "Supergravity and
the large N limit of theories with sixteen supercharges," Phys. Rev. D **58**, 046004
(1998) [hep-th/9802042].

[8] S. S. Gubser, I. R. Klebanov and A. M. Polyakov, "Gauge theory correlators from
noncritical string theory," Phys. Lett. B **428**, 105 (1998) [hep-th/9802109].

[9] E. Witten, "Anti-de Sitter space and holography," Adv. Theor. Math. Phys. **2**, 253
(1998) [hep-th/9802150].

[10] J. McGreevy, 8.821 String Theory, Fall 2008. (MIT OpenCourseWare: Massachusetts Institute of Technology).

[11] D. Z. Freedman and A. Van Proeyen, "Supergravity," Cambridge, UK: Cambridge Univ. Pr. (2012) 607 p

[12] J. M. Bardeen, B. Carter and S. W. Hawking, "The four laws of black hole mechanics," Commun. Math. Phys. **31**, 161-170 (1973).

[13] E. Witten, "Anti-de Sitter space, thermal phase transition, and confinement in gauge theories," Adv. Theor. Math. Phys. **2**, 505 (1998) [hep-th/9803131].

[14] S. W. Hawking and D. N. Page, "Thermodynamics of black holes in anti-de Sitter space," Commun. Math. Phys. **87**, 577-588 (1983).

[15] J. McGreevy, "Holographic duality with a view toward many-body physics," Adv. High Energy Phys. **2010**, 723105 (2010) [arXiv:0909.0518 [hep-th]].

[16] M. Henningson and K. Skenderis, "The Holographic Weyl anomaly," JHEP **9807**, 023 (1998) [hep-th/9806087];
See also:
M. Bianchi, D. Z. Freedman and K. Skenderis, "How to go with an RG flow," JHEP **0108**, 041 (2001) [hep-th/0105276];
M. Bianchi, D. Z. Freedman and K. Skenderis, "Holographic renormalization," Nucl. Phys. B **631**, 159 (2002) [hep-th/0112119].

[17] V. Balasubramanian and S. F. Ross, "Holographic particle detection," Phys. Rev. D **61**, 044007 (2000) [hep-th/9906226];
J. Louko, D. Marolf and S. F. Ross, "On geodesic propagators and black hole holography," Phys. Rev. D **62**, 044041 (2000) [hep-th/0002111].

[18] P. Breitenlohner and D. Z. Freedman, "Positive Energy In Anti-De Sitter Backgrounds And Gauged Extended Supergravity," Phys. Lett. B **115**, 197 (1982);
P. Breitenlohner and D. Z. Freedman, "Stability In Gauged Extended Supergravity," Annals Phys. **144**, 249 (1982);
L. Mezincescu and P. K. Townsend, "Stability At A Local Maximum In Higher Dimensional Anti-De Sitter Space And Applications To Supergravity," Annals Phys. **160**, 406 (1985).

[19] I. R. Klebanov and E. Witten, "AdS/CFT correspondence and symmetry breaking," Nucl. Phys. B **556**, 89 (1999) [arXiv:hep-th/9905104].

[20] T. Banks, M. R. Douglas, G. T. Horowitz and E. J. Martinec, "AdS dynamics from conformal field theory," hep-th/9808016.

[21] S. Sotiriadis and J. Cardy, "Quantum quench in interacting field theory: A Self-consistent approximation," Phys. Rev. B **81**, 134305 (2010) [arXiv:1002.0167 [quant-ph]].

[22] A. Peres, "Stability of quantum motion in chaotic and regular systems," Phys. Rev. A **30**, 1610 (1984).

[23] N. Armesto, N. Borghini, S. Jeon, U. A. Wiedemann, S. Abreu, V. Akkelin, J. Alam and J. L. Albacete *et al.*, "Heavy Ion Collisions at the LHC - Last Call for Predictions," J. Phys. G **35**, 054001 (2008) [arXiv:0711.0974 [hep-ph]].

[24] E. Shuryak, "Why does the quark gluon plasma at RHIC behave as a nearly ideal fluid?," Prog. Part. Nucl. Phys. **53**, 273 (2004) [hep-ph/0312227];
E. V. Shuryak, "What RHIC experiments and theory tell us about properties of quark-gluon plasma?," Nucl. Phys. A **750**, 64 (2005) [hep-ph/0405066].

[25] U. W. Heinz, "Thermalization at RHIC," AIP Conf. Proc. **739**, 163 (2005) [nucl-th/0407067].

[26] D. Teaney, "The Effects of viscosity on spectra, elliptic flow, and HBT radii," Phys. Rev. C **68**, 034913 (2003) [nucl-th/0301099].

[27] See for example:
K. H. Ackermann *et al.* [STAR Collaboration], "Elliptic flow in Au + Au collisions at (S(NN))**(1/2) = 130 GeV," Phys. Rev. Lett. **86**, 402 (2001) [nucl-ex/0009011];
K. Adcox *et al.* [PHENIX Collaboration], "Flow measurements via two particle azimuthal correlations in Au+Au collisions at s(NN)**(1/2) = 130-GeV," Phys. Rev. Lett. **89**, 212301 (2002) [nucl-ex/0204005];
B. B. Back *et al.* [PHOBOS Collaboration], "Pseudorapidity and centrality dependence of the collective flow of charged particles in Au+Au collisions at s(NN)**(1/2) = 130-GeV," Phys. Rev. Lett. **89**, 222301 (2002) [nucl-ex/0205021].

[28] P. Kovtun, D. T. Son and A. O. Starinets, "Viscosity in strongly interacting quantum field theories from black hole physics," Phys. Rev. Lett. **94**, 111601 (2005) [hep-th/0405231].

[29] A. Buchel, R. C. Myers and A. Sinha, "Beyond eta/s = 1/4 pi," JHEP **0903**, 084 (2009) [arXiv:0812.2521 [hep-th]].

[30] T. Kinoshita, T. Wenger1 and D. S. Weiss, "A quantum Newton's cradle," Nature **440**, 900 (2006).

[31] S. Hofferberth, I. Lesanovsky, B. Fischer, T. Schumm and J. Schmiedmayer, "Non-equilibrium coherence dynamics in one-dimensional Bose gases," Nature **449**, 324 (2007).

[32] S. Trotzky, Y-A. Chen, A. Flesch, I. P. McCulloch, U. Schollwöck, J. Eisert and I. Bloch, "Probing the relaxation towards equilibrium in an isolated strongly correlated one-dimensional Bose gas," Nature Physics **8**, 325 (2012).

[33] A. A. Burkov, M. D. Lukin and E. Demler, "Decoherence dynamics in low-dimensional cold atom interferometers," Phys. Rev. Lett. **98**, 200404 (2007) [arxiv:cond-mat/0701058].

[34] P. Calabrese and J. L. Cardy, "Evolution of entanglement entropy in one-dimensional systems," J. Stat. Mech. **0504**, P04010 (2005) [cond-mat/0503393].

[35] P. Calabrese and J. Cardy, "Quantum Quenches in Extended Systems," J. Stat. Mech. **0706**, P06008 (2007) [arXiv:0704.1880 [cond-mat.stat-mech]]

[36] L. -Y. Hung, M. Smolkin and E. Sorkin, "Modification of late time phase structure by quantum quenches," Phys. Rev. Lett. **109**, 155702 (2012) [arXiv:1206.2685 [cond-mat.str-el]].

[37] L. -Y. Hung, M. Smolkin and E. Sorkin, "Modification of late time phase structure by quantum quenches," JHEP **1312**, 022 (2013) [arXiv:1307.0376 [cond-mat.str-el]].

[38] See also
S. R. Das and K. Sengupta, "Non-equilibrium Dynamics of O(N) Nonlinear Sigma models: a Large-N approach," JHEP **1209**, 072 (2012) [arXiv:1202.2458 [hep-th]];
A. Chandran, A. Erez, S. S. Gubser and S. L. Sondhi, "Kibble-Zurek problem: Universality and the scaling limit," Phys. Rev. B **86**, 064304 (2012) [arXiv:1202.5277 [cond-mat.stat-mech]];
A. Chandran, A. Nanduri, S. S. Gubser and S. L. Sondhi, "On equilibration and coarsening in the quantum O(N) model at infinite N," Phys. Rev. B **88** 024306 (2013) [arXiv:1304.2402 [cond-mat.stat-mech]].

[39] P. C. Vaidya, "The external field of a radiating star in general relativity," Curr. Sci. **12** 183 (1943).

[40] S. Bhattacharyya and S. Minwalla, "Weak Field Black Hole Formation in Asymptotically AdS Spacetimes," JHEP **0909**, 034 (2009) [arXiv:0904.0464 [hep-th]].

[41] J. Abajo-Arrastia, J. Aparicio and E. Lopez, "Holographic Evolution of Entanglement Entropy," JHEP **1011**, 149 (2010) [arXiv:1006.4090 [hep-th]].

[42] E. Poisson, "A Relativist's Toolkit," Cambridge University Press (2004).

[43] S. R. Das, T. Nishioka and T. Takayanagi, "Probe Branes, Time-dependent Couplings and Thermalization in AdS/CFT," JHEP **1007**, 071 (2010) [arXiv:1005.3348 [hep-th]].

[44] V. Balasubramanian, A. Bernamonti, J. de Boer, N. Copland, B. Craps, E. Keski-Vakkuri, B. Muller and A. Schafer *et al.*, "Thermalization of Strongly Coupled Field Theories," Phys. Rev. Lett. **106**, 191601 (2011) [arXiv:1012.4753 [hep-th]].

[45] T. Albash and C. V. Johnson, "Evolution of Holographic Entanglement Entropy after Thermal and Electromagnetic Quenches," New J. Phys. **13**, 045017 (2011) [arXiv:1008.3027 [hep-th]];
V. Balasubramanian *et al.*, "Thermalization of Strongly Coupled Field Theories," Phys. Rev. Lett. **106**, 191601 (2011) [arXiv:1012.4753 [hep-th]].

[46] V. Balasubramanian *et al.*, "Holographic Thermalization," Phys. Rev. D **84**, 026010 (2011) [arXiv:1103.2683 [hep-th]].

[47] H. Ebrahim and M. Headrick, "Instantaneous Thermalization in Holographic Plasmas," arXiv:1010.5443 [hep-th];
V. Balasubramanian, A. Bernamonti, N. Copland, B. Craps and F. Galli, "Thermalization of mutual and tripartite information in strongly coupled two dimensional conformal field theories," Phys. Rev. D **84**, 105017 (2011) [arXiv:1110.0488 [hep-th]];
J. Aparicio and E. Lopez, "Evolution of Two-Point Functions from Holography," JHEP **1112**, 082 (2011) [arXiv:1109.3571 [hep-th]];
A. Allais and E. Tonni, "Holographic evolution of the mutual information," JHEP **1201**, 102 (2012) [arXiv:1110.1607 [hep-th]];
V. Keranen, E. Keski-Vakkuri and L. Thorlacius, "Thermalization and entanglement following a non-relativistic holographic quench," Phys. Rev. D **85**, 026005 (2012) [arXiv:1110.5035 [hep-th]];
D. Galante and M. Schvellinger, "Thermalization with a chemical potential from AdS spaces," JHEP **1207**, 096 (2012) [arXiv:1205.1548 [hep-th]];
E. Caceres and A. Kundu, "Holographic Thermalization with Chemical Potential," JHEP **1209**, 055 (2012) [arXiv:1205.2354 [hep-th]];

I. Y. .Arefeva and I. V. Volovich, "On Holographic Thermalization and Dethermal-ization of Quark-Gluon Plasma," arXiv:1211.6041 [hep-th];

W. H. Baron, D. Galante and M. Schvellinger, "Dynamics of holographic thermaliza-tion," arXiv:1212.5234 [hep-th];

V. Balasubramanian, A. Bernamonti, J. de Boer, B. Craps, L. Franti, F. Galli, E. Keski-Vakkuri and B. Müller *et al.*, "Inhomogeneous holographic thermalization," JHEP **1310**, 082 (2013) [arXiv:1307.7086];

P. Fonda, L. Franti, V. Keränen, E. Keski-Vakkuri, L. Thorlacius and E. Tonni, "Holo-graphic thermalization with Lifshitz scaling and hyperscaling violation," JHEP **1408**, 051 (2014) [arXiv:1401.6088 [hep-th]];

X. X. Zeng, X. M. Liu and W. B. Liu, "Holographic thermalization in noncommuta-tive geometry," arXiv:1407.5262 [hep-th];

X. X. Zeng, D. Y. Chen and L. F. Li, "Holographic thermalization and gravitational collapse in the spacetime dominated by quintessence dark energy," arXiv:1408.6632 [hep-th].

[48] A. Buchel, L. Lehner and R.C. Myers, "Thermal quenches in N=2* plasmas," JHEP **1208**, 049 (2012) [arXiv:1206.6785 [hep-th]].

[49] P.M. Chesler and L.G. Yaffe, "Horizon formation and far-from-equilibrium isotropiza-tion in supersymmetric Yang-Mills plasma," Phys. Rev. Lett. **102**, 211601 (2009). [arXiv:0812.2053 [hep-th]];

P. M. Chesler and L. G. Yaffe, "Boost invariant flow, black hole formation, and far-from-equilibrium dynamics in N = 4 supersymmetric Yang-Mills theory," Phys. Rev. D **82**, 026006 (2010) [arXiv:0906.4426 [hep-th]].

[50] See for example:

P. M. Chesler and L. G. Yaffe, "Holography and colliding gravitational shock waves in asymptotically AdS$_5$ spacetime," Phys. Rev. Lett. **106**, 021601 (2011) [arXiv:1011.3562 [hep-th]];

W. van der Schee, P. Romatschke and S. Pratt, "Fully Dynamical Simulation of Cen-tral Nuclear Collisions," Phys. Rev. Lett. **111**, no. 22, 222302 (2013) [arXiv:1307.2539];

J. Casalderrey-Solana, M. P. Heller, D. Mateos and W. van der Schee, "Longitudinal Coherence in a Holographic Model of p-Pb Collisions," Phys. Rev. Lett. **112**, 221602 (2014) [arXiv:1312.2956 [hep-th]];

D. Fernández, "Towards Collisions of Inhomogeneous Shockwaves in AdS," arXiv:1407.5628 [hep-th].

[51] D. Garfinkle and L. A. Pando Zayas, "Rapid Thermalization in Field Theory from Gravitational Collapse," Phys. Rev. D **84**, 066006 (2011) [arXiv:1106.2339 [hep-th]]; D. Garfinkle, L. A. Pando Zayas and D. Reichmann, "On Field Theory Thermalization from Gravitational Collapse," JHEP **1202**, 119 (2012) [arXiv:1110.5823 [hep-th]].

[52] A. Buchel, L. Lehner, R.C. Myers and A. van Niekerk, "Quantum quenches of holographic plasmas," JHEP **1305**, 067 (2013) [arXiv:1302.2924 [hep-th]].

[53] R. Auzzi, S. Elitzur, S. B. Gudnason and E. Rabinovici, "On periodically driven AdS/CFT," arXiv:1308.2132 [hep-th].

[54] A. Buchel, R. C. Myers and A. van Niekerk, "Universality of Abrupt Holographic Quenches," Phys. Rev. Lett. **111**, 201602 (2013) [arXiv:1307.4740 [hep-th]].

[55] A. Buchel, R. C. Myers and A. van Niekerk, "Nonlocal probes of thermalization in holographic quenches with spectral methods," arXiv:1410.6201 [hep-th].

[56] For example, see the following reviews:
S. Mondal, D. Sen and K. Sengupta, "Non-equilibrium dynamics of quantum systems: order parameter evolution, defect generation, and qubit transfer," *Quantum Quenching, Anealing and Computation*, Lecture notes in Physics, Volume 802, Page 21, 2010 [arXiv:0908.2922[cond-mat.stat-mech]];
J. Dziarmaga, "Dynamics of a quantum phase transition and relaxation to a steady state," Adv. Phys. **59**, 1063 (2010) [arXiv:0912.4034 [cond-mat.quant-gas]];
A. Polkovnikov, K. Sengupta, A. Silva and M. Vengalattore, "Nonequilibrium dynamics of closed interacting quantum systems," Rev. Mod. Phys. **83**, 863 (2011) [arXiv:1007.5331 [cond-mat.stat-mech]];
A. Lamacraft and J.E. Moore, "Potential insights into non-equilibrium behavior from atomic physics," Chapter forthcoming in *Ultracold Bosonic and Fermionic Gases*, Contemporary Concepts in Condensed Matter Science, Elsevier (Editors: A. Fletcher, K. Levin and D. Stamper-Kurn) [arXiv:1106.3567[cond-mat.quant-gas]].

[57] L. D. Landau and E. M. Lifshitz, *Quantum Mechanics*, Course of Theoretical Physics, Volume 3, 1989.

[58] P. Calabrese and J. L. Cardy, "Time-dependence of correlation functions following a quantum quench," Phys. Rev. Lett. **96**, 136801 (2006) [cond-mat/0601225];
S. Sotiriadis and J. Cardy, "Inhomogeneous Quantum Quenches," J. Stat. Mech. P11003 (2008) [arXiv:0808.0116 [cond-mat.stat-mech]];

S. Sotiriadis, P. Calabrese and J. Cardy, "Quantum quench from a thermal initial state," EPL **87**, 20002 (2009) [arXiv:0903.0895v2 [cond-mat.stat-mech]].

[59] M. Rigol, V. Dunjko, V. Yurovsky, and M. Olshanii, "Relaxation in a completely integrable many-body quantum system: An ab initio study of the dynamics of the highly excited states of lattice hard-core bosons", Phys. Rev. Lett. **98** (2006), no. 5 4 [arXiv:cond-mat/0604476];
C. Kollath, A. Laeuchli, and E. Altman, "Quench dynamics and nonequilibrium phase diagram of the bose-hubbard model", Phys. Rev. Lett. **98** (2006), no. 18 180601;
S. R. Manmana, S. Wessel, R. M. Noack, and A. Muramatsu, "Strongly correlated fermions after a quantum quench", Phys. Rev. Lett. **98** (2006), no. 21 4.

[60] P. Basu and S. R. Das, "Quantum Quench across a Holographic Critical Point," JHEP **1201**, 103 (2012) [arXiv:1109.3909 [hep-th]];
S. R. Das, "Holographic Quantum Quench," J. Phys. Conf. Ser. **343**, 012027 (2012) [arXiv:1111.7275 [hep-th]];
P. Basu, D. Das, S. R. Das and T. Nishioka, "Quantum Quench Across a Zero Temperature Holographic Superfluid Transition," arXiv:1211.7076 [hep-th].

[61] U. H. Danielsson, E. Keski-Vakkuri and M. Kruczenski, "Spherically collapsing matter in AdS, holography, and shellons," Nucl. Phys. B **563**, 279 (1999) [hep-th/9905227];
U.H. Danielsson, E. Keski-Vakkuri and M. Kruczenski, "Black hole formation in AdS and thermalization on the boundary," JHEP **0002**, 039 (2000) [hep-th/9912209];
S.B. Giddings and S.F. Ross, "D3-brane shells to black branes on the Coulomb branch," Phys. Rev. D **61**, 024036 (2000) [hep-th/9907204];
S. B. Giddings and A. Nudelman, "Gravitational collapse and its boundary description in AdS," JHEP **0202**, 003 (2002) [hep-th/0112099];
R. A. Janik and R. B. Peschanski, "Gauge/gravity duality and thermalization of a boost-invariant perfect fluid," Phys. Rev. D **74**, 046007 (2006) [hep-th/0606149];
R. A. Janik, "Viscous plasma evolution from gravity using AdS/CFT," Phys. Rev. Lett. **98**, 022302 (2007) [hep-th/0610144];
S. Lin and E. Shuryak, "Toward the AdS/CFT Gravity Dual for High Energy Collisions. 3. Gravitationally Collapsing Shell and Quasiequilibrium," Phys. Rev. D **78**, 125018 (2008) [arXiv:0808.0910 [hep-th]].

[62] H. Bantilan, F. Pretorius and S. S. Gubser, "Simulation of Asymptotically AdS5 Spacetimes with a Generalized Harmonic Evolution Scheme," Phys. Rev. D **85**, 084038 (2012) [arXiv:1201.2132 [hep-th]];
M. P. Heller, D. Mateos, W. van der Schee and D. Trancanelli, "Strong Coupling

Isotropization of Non-Abelian Plasmas Simplified," Phys. Rev. Lett. **108**, 191601 (2012) [arXiv:1202.0981 [hep-th]];

M. P. Heller, R. A. Janik and P. Witaszczyk, "A numerical relativity approach to the initial value problem in asymptotically Anti-de Sitter spacetime for plasma thermalization – an ADM formulation," Phys. Rev. D **85**, 126002 (2012) [arXiv:1203.0755 [hep-th]];

M. J. Bhaseen, J. P. Gauntlett, B. D. Simons, J. Sonner and T. Wiseman, "Holographic Superfluids and the Dynamics of Symmetry Breaking," Phys. Rev. Lett. **110**, 015301 (2013) [arXiv:1207.4194 [hep-th]];

B. Wu, "On holographic thermalization and gravitational collapse of massless scalar fields," JHEP **1210**, 133 (2012) [arXiv:1208.1393 [hep-th]];

B. Wu, "On holographic thermalization and gravitational collapse of tachyonic scalar fields," arXiv:1301.3796 [hep-th].

[63] V. Cardoso, L. Gualtieri, C. Herdeiro, U. Sperhake, P. M. Chesler, L. Lehner, S. C. Park, H. S. Reall *et al.*, "NR/HEP: roadmap for the future," Class. Quant. Grav. **29**, 244001 (2012). [arXiv:1201.5118 [hep-th]].

[64] A. Buchel, J. Escobedo, R. C. Myers, M. F. Paulos, A. Sinha and M. Smolkin, "Holographic GB gravity in arbitrary dimensions," JHEP **1003**, 111 (2010) [arXiv:0911.4257 [hep-th]].

[65] S. Bhattacharyya, V. E. Hubeny, S. Minwalla and M. Rangamani, "Nonlinear Fluid Dynamics from Gravity," JHEP **0802**, 045 (2008) [arXiv:0712.2456 [hep-th]];

V. E. Hubeny, S. Minwalla and M. Rangamani, "The fluid/gravity correspondence," Chapter in *Black holes in Higher Dimensions*, To be published by Cambridge University Press (Editor: G. Horowitz) [arXiv:1107.5780 [hep-th]].

[66] R. Emparan, C. V. Johnson and R. C. Myers, "Surface terms as counterterms in the AdS/CFT correspondence," Phys. Rev. D **60**, 104001 (1999) [hep-th/9903238].

[67] C. Fefferman and C. R. Graham, "Conformal Invariants," in Elie Cartan et les Mathématiques d'aujourd hui (Astérisque, 1985) 95;

C. Fefferman and C. R. Graham, "The Ambient Metric," arXiv:0710.0919 [math.DG].

[68] L.-Y. Hung, R. C. Myers and M. Smolkin, "Some Calculable Contributions to Holographic Entanglement Entropy," JHEP **1108**, 039 (2011) [arXiv:1105.6055 [hep-th]].

[69] O. Aharony, A. Buchel and A. Yarom, "Holographic renormalization of cascading gauge theories," Phys. Rev. D **72**, 066003 (2005) [hep-th/0506002].

[70] I. Papadimitriou, "Holographic Renormalization of general dilaton-axion gravity," JHEP **1108**, 119 (2011) [arXiv:1106.4826 [hep-th]].

[71] A. Buchel, "N=2* hydrodynamics," Nucl. Phys. B **708**, 451 (2005) [hep-th/0406200].

[72] A. Buchel and J. T. Liu, "Thermodynamics of the N=2* flow," JHEP **0311**, 031 (2003) [hep-th/0305064].

[73] P. M. Hohler and M. A. Stephanov, "Holography and the speed of sound at high temperatures," Phys. Rev. D **80**, 066002 (2009) [arXiv:0905.0900 [hep-th]].

[74] R. A. Isaacson, J. S. Welling and J. Winicour, "Null Cone Computation Of Gravitational Radiation," J. Math. Phys. **24**, 1824 (1983).

[75] L. Lehner, "A Dissipative algorithm for wave - like equations in the characteristic formulation," J. Comput. Phys. **149**, 1 (1999) [gr-qc/9811095].

[76] A. Buchel, L. Lehner, R. C. Myers and A. van Niekerk, unpublished.

[77] V. Balasubramanian, A. Bernamonti, J. de Boer, B. Craps, L. Franti, F. Galli, E. Keski-Vakkuri and B. Mller *et al.*, "Inhomogeneous thermalization in strongly coupled field theories," Phys. Rev. Lett. **111**, 231602 (2013) [arXiv:1307.1487 [hep-th]].

[78] M.P. Heller, D. Mateos, W. van der Schee and D. Trancanelli, "Strong Coupling Isotropization of Non-Abelian Plasmas Simplified," Phys. Rev. Lett. **108**, 191601 (2012) [arXiv:1202.0981 [hep-th]].

[79] S. R. Das, D. A. Galante and R. C. Myers, "Universal scaling in fast quantum quenches," Phys. Rev. Lett. **112**, 171601 (2014) arXiv:1401.0560 [hep-th].

[80] See for example:
M. Greiner, O. Mandel, T. W. Hänsch and I. Bloch, Nature **419** 51-54 (2002);
S. Will, T. Best, U. Schneider, L. Hackermüller, D-S. Lühmann and I. Bloch, "Time-resolved observation of coherent multi-body interactions in quantum phase revivals," Nature **465** 197-201 (2010).

[81] P. Calabrese, C. Hagendorf and P. Le Doussal, "Time evolution of 1D gapless models from a domain-wall initial state: SLE continued?" J. Stat. Mech. P07013 (2008) [arXiv:0804.2431 [cond-mat.stat-mech]].

[82] M. Cramer, C. M. Dawson, J. Eisert, T. J. Osborne, "Exact relaxation in a class of non-equilibrium quantum lattice systems," Phys. Rev. Lett. **100**, 030602 (2008) [arXiv:cond-mat/0703314];
G. Roux, "Quenches in quantum many-body systems: One-dimensional Bose-Hubbard model reexamined," Phys. Rev. A. **79**, 021608 (2009) [arXiv:cond-mat.str-el/0810.3720].

[83] M. Rigol, V. Dunjko and M. Olshanii, "Thermalization and its mechanism for generic isolated quantum systems," Nature, **452** (7189):854-858 (2008) [arXiv:cond-mat/0708.1324];
P. Calabrese, F. H. L. Essler, and M. Fagotti, "Quantum Quench in the Transverse Field Ising Chain," Phys. Rev. Lett. **106**, 227203 (2011) [arXiv:cond-mat.str-el/1104.0154].

[84] M. Nozaki, T. Numasawa and T. Takayanagi, "Holographic Local Quenches and Entanglement Density," JHEP **1305**, 080 (2013) [arXiv:1302.5703 [hep-th]].

[85] T. Hartman and J. Maldacena, "Time Evolution of Entanglement Entropy from Black Hole Interiors," JHEP **1305**, 014 (2013) [arXiv:1303.1080 [hep-th]];
N. Engelhardt and G. T. Horowitz, "Entanglement Entropy Near Cosmological Singularities," JHEP **1306**, 041 (2013) [arXiv:1303.4442 [hep-th]];
P. Basu and A. Ghosh, "Dissipative Nonlinear Dynamics in Holography," Phys. Rev. D **89**, 046004 (2014) [arXiv:1304.6349 [hep-th]];
W. J. Li, Y. Tian and H. b. Zhang, "Periodically Driven Holographic Superconductor," JHEP **1307**, 030 (2013) [arXiv:1305.1600 [hep-th]];
Y. Z. Li, S. F. Wu, Y. Q. Wang and G. H. Yang, "Linear growth of entanglement entropy in holographic thermalization captured by horizon interiors and mutual information," JHEP **1309**, 057 (2013) [arXiv:1306.0210 [hep-th]];
K. Hashimoto and T. Oka, "Vacuum Instability in Electric Fields via AdS/CFT: Euler-Heisenberg Lagrangian and Planckian Thermalization," JHEP **1310**, 116 (2013) [arXiv:1307.7423].

[86] P. Basu, D. Das, S. R. Das and K. Sengupta, "Quantum Quench and Double Trace Couplings," JHEP **1312**, 070 (2013) [arXiv:1308.4061 [hep-th]];
P. M. Chesler and L. G. Yaffe, "Numerical solution of gravitational dynamics in asymptotically anti-de Sitter spacetimes," JHEP **1407**, 086 (2014) [arXiv:1309.1439 [hep-th]];
X. X. Zeng, X. M. Liu and W. B. Liu, "Holographic thermalization with a chemical

192

potential in Gauss-Bonnet gravity," JHEP **1403**, 031 (2014) [arXiv:1311.0718 [hep-th]];

T. Ugajin, "Two dimensional quantum quenches and holography," arXiv:1311.2562 [hep-th];

X. O. Camanho, J. D. Edelstein, G. Giribet and A. Gomberoff, "Generalized phase transitions in Lovelock gravity," arXiv:1311.6768 [hep-th];

J. F. Pedraza, "Evolution of nonlocal observables in an expanding boost-invariant plasma," Phys. Rev. D **90**, 046010 (2014) [arXiv:1405.1724 [hep-th]];

X. Bai, B. H. Lee, M. Park and K. Sunly, "Dynamical Condensation in a Holographic Superconductor Model with Anisotropy," JHEP **1409**, 054 (2014) [arXiv:1405.1806 [hep-th]];

A. F. Astaneh and A. E. Mosaffa, "Quantum Local Quench, AdS/BCFT and Yo-Yo String," arXiv:1405.5469 [hep-th];

M. Nozaki, "Notes on Quantum Entanglement of Local Operators," arXiv:1405.5875 [hep-th];

D. Berenstein and A. Miller, "Conformal perturbation theory, dimensional regularization and AdS/CFT," arXiv:1406.4142 [hep-th];

K. Hashimoto, S. Kinoshita, K. Murata and T. Oka, "Electric Field Quench in AdS/CFT," arXiv:1407.0798 [hep-th];

V. Cardoso, L. Gualtieri, C. Herdeiro and U. Sperhake, "Exploring New Physics Frontiers Through Numerical Relativity," arXiv:1409.0014 [gr-qc].

[87] H. Liu and S. J. Suh, "Entanglement Tsunami: Universal Scaling in Holographic Thermalization," Phys. Rev. Lett. **112**, 011601 (2014) [arXiv:1305.7244 [hep-th]];
H. Liu and S. J. Suh, "Entanglement growth during thermalization in holographic systems," Phys. Rev. D **89**, 066012 (2014) [arXiv:1311.1200 [hep-th]].

[88] A. Cherman and A. Nellore, "Universal relations of transport coefficients from holography," Phys. Rev. D **80**, 066006 (2009) [arXiv:0905.2969 [hep-th]].

[89] For example, see: J.P. Boyd, "Chebyshev and Fourier Spectral Methods," Second Edition, Dover Publications Inc. (2000).

[90] K. Pilch and N. P. Warner, "N=2 supersymmetric RG flows and the IIB dilaton," Nucl. Phys. B **594**, 209 (2001) [hep-th/0004063];
A. Khavaev, K. Pilch and N. P. Warner, "New vacua of gauged N=8 supergravity in five-dimensions," Phys. Lett. B **487**, 14 (2000) [hep-th/9812035].

[91] A. Buchel, A.W. Peet and J. Polchinski, "Gauge dual and noncommutative extension of an N = 2 supergravity solution," Phys. Rev. D **63**, 044009 (2001) [arXiv:hep-th/0008076].

[92] N.J. Evans, C.V. Johnson and M. Petrini, "The Enhancon and N=2 gauge theory: Gravity RG flows," JHEP **0010**, 022 (2000) [hep-th/0008081].

[93] E. D'Hoker and D. Z. Freedman, "Supersymmetric gauge theories and the AdS / CFT correspondence," hep-th/0201253.

[94] V. E. Hubeny, M. Rangamani and T. Takayanagi, "A Covariant holographic entanglement entropy proposal," JHEP **0707**, 062 (2007) [arXiv:0705.0016 [hep-th]]. S. Bhattacharyya, V. E. Hubeny, R. Loganayagam, G. Mandal, S. Minwalla, T. Morita, M. Rangamani and H. S. Reall, "Local Fluid Dynamical Entropy from Gravity," JHEP **0806**, 055 (2008) [arXiv:0803.2526 [hep-th]].

[95] S. Ryu and T. Takayanagi, "Holographic derivation of entanglement entropy from AdS/CFT," Phys. Rev. Lett. **96**, 181602 (2006) [hep-th/0603001].

[96] S. Ryu and T. Takayanagi, "Aspects of Holographic Entanglement Entropy," JHEP **0608**, 045 (2006) [hep-th/0605073].

[97] V. E. Hubeny, M. Rangamani and T. Takayanagi, "A Covariant holographic entanglement entropy proposal," JHEP **0707**, 062 (2007) [arXiv:0705.0016 [hep-th]].

[98] A. Lewkowycz, R. C. Myers and M. Smolkin, "Observations on entanglement entropy in massive QFT's," JHEP **1304**, 017 (2013) [arXiv:1210.6858 [hep-th]].

[99] H. Liu and M. Mezei, "A Refinement of entanglement entropy and the number of degrees of freedom," JHEP **1304**, 162 (2013) [arXiv:1202.2070 [hep-th]].

[100] R. C. Myers and A. Singh, "Comments on Holographic Entanglement Entropy and RG Flows," JHEP **1204**, 122 (2012) [arXiv:1202.2068 [hep-th]].

[101] T. Nishioka, S. Ryu and T. Takayanagi, "Holographic Entanglement Entropy: An Overview," J. Phys. A **42**, 504008 (2009) [arXiv:0905.0932 [hep-th]].

[102] L. Lehner, "Numerical relativity: A Review," Class. Quant. Grav. **18**, R25 (2001) [gr-qc/0106072].

[103] H. P. Pfeiffer, L. E. Kidder, M. A. Scheel and S. A. Teukolsky, "A Multidomain spectral method for solving elliptic equations," Comput. Phys. Commun. **152**, 253 (2003) [gr-qc/0202096].